NASA Contractor
Report No. 66519

Research and Development Program for a Combined Carbon Dioxide Removal and Reduction System

N68-18142 (ACCESSION NUMBER) (THRU)
373 (PAGES) 1 (CODE)
CR-66519 (NASA CR OR TMX OR AD NUMBER) 05 (CATEGORY)
FACILITY FORM 602

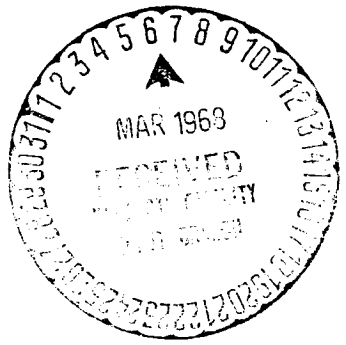
GPO PRICE $ _____

CFSTI PRICE(S) $ _____

Hard copy (HC) 3.00

Microfiche (MF) .65

ff 653 July 65



Contract No. NAS 1-4154
Final Report - Phase II A
November 1967 HSER 4908

Hamilton Standard
DIVISION OF UNITED AIRCRAFT CORPORATION

Hamilton Standard
DIVISION OF UNITED AIRCRAFT CORPORATION

NASA Contractor
Report No. 66519

RESEARCH and
DEVELOPMENT
PROGRAM for a

COMBINED
CARBON DIOXIDE
REMOVAL AND REDUCTION SYSTEM

Distribution of this Report is provided in the interest of information exchange. Responsibility of the contents resides in the author or organization that prepared it.

Contract NAS 1-4154
Final Report - Phase IIA.
HSER 4908

November 1967

PRECEDING PAGE BLANK NOT FILMED.

FOREWORD

Hamilton Standard, a Division of United Aircraft Corporation, began company-funded research in the electrochemistry of fused salts in 1963 with a series of experiments directed toward the simultaneous removal and reduction of carbon dioxide through the electrolysis of a molten alkali carbonate. Favorable results and new insights were achieved. The significance of the basic process in achieving a single-step carbon dioxide removal and reduction system for aerospace environmental control systems was recognized. In September 1964, the Langley Research Center of the National Aeronautics and Space Administration (NASA-LRC) gave support to the research and development program through issuance of contract NAS 1-4154. Based upon the technological progress during the initial fourteen months (Phase I), Phase IIA of NAS 1-4154 was awarded in September 1966 for continuing research and engineering efforts associated with the fused salt electrochemical process and initiating investigation of practical engineering problems.

This is the final report of Phase IIA of NAS 1-4154 and covers progress made in the fourteen month period between September 1966 and November 1967.* Mr. C.R. Russell was Project Manager, serving also as Technical Director of Engineering Activity. Mr. W. E. Arnoldi was Technical Director of the Research Activity, serving also to monitor specific activities done under this contract by the United Aircraft Research Laboratory (UARL). The following individuals contributed significantly to Phase IIA of this contract:

Dr. P. J. Birbara
**Dr. C. T. Brown
**Dr. G. L. M. Christopher
Mr. J. Cohen
Mr. D. Leickhardt
Mr. K. Michaels
Mr. R. Riethof
**Mr. R. Roback
Mr. S. Russell

**United Aircraft Research Laboratories

*A Contract Change Notice (CCN #2) to Phase IIA of NAS 1-4154, dated 28 August 1967, directs Hamilton Standard to monitor and administer an experimental study, to establish certain physical properties of electrolyte mixtures, being done by the University of Pennsylvania Electrochemistry Laboratory. The Phase IIA Final Report will document the results of this extended effort, following its completion on 9-1-68, through an Addendum to the report.

SUMMARY

This final report concerning contractor activities and progress during Phase IIA of NAS 1-4154 is divided into two parts. Part I presents an account of the research program conducted to extend basic understanding of the electrochemical processes applicable to the direct removal and reduction of carbon dioxide through the electrolysis of a fused salt. Part II presents an account of engineering design and development activities directed toward the selection of a practical electrolytic cell configuration and the identification of related engineering problems.

RESEARCH

The primary research objective in Phase IIA was to extend and refine the understanding of the three basic functions inherent in the fused carbonate CO_2 reduction cell: the oxygen-producing anode, the carbon-collecting cathode, and the CO_2 absorbing scrubber. Alternatively, the performance of the system can be discussed in terms of three problem areas: the composition and properties of the electrolyte, processes at the electrodes and their control, and the susceptibility of various materials to chemical attack by liquid and gaseous reactants involved in the cell. The significant accomplishments of Phase I included the establishment of the characteristics required in the electrolyte, development of working hypotheses for the electrode processes, and preliminary demonstrations of the feasibility of simple electrode configurations. In Phase IIA each of these was delineated in more detail, and important process interrelationships were explored in laboratory experiments directed toward support of engineering design concepts. Several cathode configurations were demonstrated and conditions established for controlling high quality carbon deposition at higher current densities than seemed feasible at an earlier date. The anode was shown to be primarily a materials and configuration problem, and, although gratifying progress was made in achieving anode durability, the basis for an ultimate solution was established in terms of strongly supported hypotheses. Effective scrubbing of carbon dioxide was demonstrated in practical configurations.

ENGINEERING

As directed by contract, a Laboratory Demonstration Model (LDM #2) was designed, fabricated, and delivered to NASA - LRC early in this phase. The LDM's activation will allow this facility to perform independent CO_2 removal-reduction experiments on a model which can be modified to test alternative concepts.

Twenty seven cell performance tests plus material corrosion tests were performed using facilities built during Phase IIA. Information from the first nine cell performance tests, together with analytical studies, resulted in concepting several candidate 1/6 g cell configurations. The oscillating electrolyte concept was selected from those considered as the configuration to be pursued in the four-man cell complex

designs required by the Phase IIA contract. Simplicity and growth potential to zero gravity environments were the two main reasons for the selection. Subsequent tests of this configuration yielded cathode efficiency and carbon purity values of approximately 100% and 75 to 85%, respectively, and to a considerable degree gave further substantiation to the selection. The cell complex description and expected performance features are given in the text of this report. The detail drawings are being forwarded separately.

In a similar manner, and as required by contract, a preliminary system specification for a zero gravity CO_2 removal and reduction system was prepared during this phase and is being forwarded separately. When finalized, the specification will provide the basis for the detailed system design to be accomplished in Part IIB of this contract.

RECOMMENDATIONS

Analyses of competitive CO_2 removal and reduction systems continue to indicate the unique advantages of the fused salt electrolytic process which is able to accomplish both functions in a single operation. Aside from the simplicity of the technique, which implies an inherent reliability not achievable in more complex systems, studies have shown a significant equivalent weight advantage over the nearest competing approach.

Considerable progress was made in the thirteen-month working period of Phase IIA of this contract. Research activities have made significant progress oriented to a fuller and more quantitative understanding of the electrolytic process. Engineering tests and analyses have complemented the research gains by deriving a concept for a practical configuration, verifying through test the workability of the concept, and identifying specific and potential problem areas associated with the 1/6 g design to be fabricated during the follow-on phase (Part IIB) of this contract.

Recommendations regarding research and engineering activities to be pursued during the early part of the follow-on phase include:

RESEARCH

1. Further refinement and definition of the electrochemical reactions and the completeness and coefficients of the significant reactions in the context of the total electrolytic process,

2. Further experimentation regarding the influence of the varieties of contaminants that are anticipated to concentrate within the electrolyte,

3. Further investigation into process indices which can be employed for adequate control of cell performance under normal operating conditions, i.e., influent moisture level, CO_2 nominal and adverse pressure, electric power variations, etc.

4. Further analysis and investigation of the feasibility of achieving a satisfactory cathode deposit through purely passive measures without the need of imposing rotation, dipping, vibration, etc.

5. A continuation of fundamental CO_2 scrubber investigations initiated in Phase IIA, with the objective of establishing mass transfer versus configuration versus surface area versus flow mechanics considerations.

ENGINEERING

1. A continuation and expansion of the materials area to pursue, in order of preference:

(a) A single metal or alloy capable of withstanding the ullage gas and fused salt environment.

(b) A non-metallic coating which can be sprayed or otherwise affixed to a base metal and capable of withstanding the ullage gas and fused salt environment.

(c) A metal or non-metal which can be clad or otherwise bonded to a base metal capable of withstanding the ullage gas and fused salt environment.

2. A materials screening and life testing program directed at achieving anode electrical and structural stability.

3. An early evaluation of the 1/6 g half-cell as designed to permit a meaningful assessment of electrolyte current density loading, anode polarization, scrubbing efficiency, etc. for the design configuration.

4. An early evaluation of the effect upon carbon purity (and current efficiency) of variations in melt CO_2 and H_2O partial pressures, to confirm the hypotheses resulting from Phase IIA engineering tests.

5. An early evaluation of the detailed design of the oscillating electrolyte level control, to ascertain the basic reliability, repeatability, and accuracy of the fluidic technique.

6. An early evaluation of cathode deposit thickness versus electrode height to establish nominal deposit operational life, together with an evaluation of the effectiveness of various measures to extend this life.

CONTENTS

Section		Page
	PART I - BASIC PROCESS STUDIES	
1.0	INTRODUCTION TO RESEARCH STUDIES	1
2.0	SUMMARY	2
3.0	CONCLUSIONS	5
4.0	RECOMMENDATIONS	7
5.0	PROCESS EXPERIMENTS	8
	5.1 Anode Processes	8
	5.2 Cathode Processes	30
	5.3 Scrubber: CO_2 Absorption Processes	62
6.0	SUPPORTING STUDIES (UARL)	73
	6.1 Carbonate Decomposition Characteristics	73
	6.2 Thermodynamic Equilibrium Carbonate Melts	121
	6.3 Electrolyte Carry-Over Investigations	134
	PART II - DESIGN/ENGINEERING ACTIVITIES	
7.0	INTRODUCTION TO ENGINEERING ACTIVITIES	150
8.0	ENGINEERING AND DEVELOPMENTAL CONCLUSIONS	151
	8.1 General Conclusions	151
	8.2 Specific Conclusions	152
9.0	RECOMMENDATIONS	154
10.0	RESULTS OF ENGINEERING TESTS	157
	10.1 Performance Tests	157
	10.2 Materials Tests	265
11.0	RESULTS OF ANALYSIS AND STUDY	281
	11.1 Reduced Gravity Considerations Applicable to 1/6 g Design	281
	11.2 Oxygen Bubble Terminal Velocity as a Function of g Level	287
	11.3 Analytical Model of CO_2 Scrubber Applicable to the Fused Salt Program	293

CONTENTS

(Continued)

Section		Page
12.0	ONE-SIXTH GRAVITY CONCEPT SELECTION CRITERIA	304
	12.1 Introduction	304
	12.2 Basic Objectives of the 1/6 g Cell Complex to be Designed in Phase IIA	304
	12.3 Specific Guide-Lines Pertinent to the Selection of a 1/6 g Configuration	305
13.0	DESCRIPTION OF a 1/6 G CONCEPT SELECTED FOR DESIGN/FABRICATION	307
	13.1 Description	307
	13.2 Considerations and Discussion of Description	320
	13.3 Expected Performance	323
	13.4 Possible Problem Areas Associated with the One-Sixth Gravity/Four Man Design	324
APPENDIX A	DEFINITIONS	326
APPENDIX B	PROCEDURES	330
APPENDIX C	CONFIGURATION OF TEST HARDWARE	341

ILLUSTRATIONS

Figure		Page
5-1	Tafel Plot of Anode Current-Voltage Relationships	9
5-2	Test Configuration: Anode Dissolution Studies and Polarograms	11
5-3	Effect of Current Density on Anode Dissolution at Various Temperatures	12
5-4	Anode Dissolution Rates for Gold-Nickel Alloys	15
5-5	Anode Tafel Slopes for Assorted Metals	16
5-6	Effect of Chloride Concentration on Anode Dissolution Rate	17
5-7	Effect of Current Density on Anode Dissolution Rate for Various Oxide Concentrations	18
5-8	Anode Polarograms with Increasing Oxide Ion Concentration	20
5-9	Effect of Chloride Concentration on Oxygen Purity	21
5-10	Schematic: Anode Assembly; Tube Bundle Sponge Retainer	24
5-11	Photograph: Anode Assembly; Tube Bundle Sponge Retainer	25
5-12	Gold-Gold Sponge Electrode	27
5-13	Schematic: Anode Assembly; Vortex Retention of Sponge	28
5-14	Tafel Plot of Cathode Current-Voltage Relationships	31
5-15	Potential-Log pCO_2 Relationships between Carbon Electrodes	33
5-16	Carbon Deposit on Axially Oscillated Cathode	36
5-17	Carbon Deposit on Rotating Vertical Disc	37
5-18	Schematic: Gas Lift Pump Cathode Assembly	39
5-19	Carbon Deposit on S Shape Spinning Cathode	40
5-20	Carbon Plate on Spectrographic Carbon Electrode	42
5-21	Influence of Temperature on Carbon Purity and Current Efficiency	44
5-22	Influence of Current Density on Carbon Purity and Current Efficiency	45
5-23	Effect of Gas Phase pCO_2 on Carbon Purity and Current Efficiency	46
5-24	Carbon Purity and Current Efficiency vs. Current Density for Spinning Cathode	48
5-25	Carbon Purity and Current Efficiency vs. Cathode Spin Rate	49
5-26	Effect of Halide Concentration on Carbon Purity and Current Efficiency	52

ILLUSTRATIONS
(Continued)

Figure		Page
5-27	Carbon Purity vs Current Efficiency for Rotating and Axially Oscillating Cathodes	53
5-28	Cell Mass Balance Study: Net CO_2 in; O_2 Out	54
5-29	Cell Mass Balance Study: CO Out; H_2O Out; H_2O In	55
5-30	Composite Cathode Polarogram	60
5-31	Schematic of CO_2 Absorption Apparatus	63
5-32	Influence of Flow Rate on CO_2 Absorbed at Constant pCO_2	66
5-33	Effect of Inlet pCO_2 on CO_2 Absorbed	67
5-34	CO_2 Absorbed on Screen vs Sheet Stock at Various Cycle Times	68
5-35	CO_2 Absorbed vs Cycle Time	69
6-1	Thermogravimetric Apparatus for Carbonate Decomposition Studies	75
6-2	Thermogravimetric Balance Assembly	76
6-3	Equilibrium Constants for the Decomposition of $CaCO_3$ as a Function of Temperature	81
6-4	Equilibrium Constants for the Decomposition of Li_2CO_3 as a Function of Temperature	90
6-5	Equilibrium Constants for the Decomposition of Li_2CO_3 in the Li_2CO_3-LiCl Eutectic Melt as a Function of Temperature	99
6-6	LiCl Evaporation Rates in the Li_2CO_3-LiCl Eutectic Melt	104
6-7	Equilibrium Constants for the Decomposition of $LiCO_3$ in the Li_2CO_3-LiF Melt as a Function of Temperature	109
6-8	Equilibrium Constants for the Decomposition of Li_2CO_3 in the Pure State and in Mixtures with LiCl and LiF as a Function of Temperature	115
6-9	Theoretical Positions of Ions in the Li_2CO_3-LiCl & Li_2CO_3-LiF Eutectic Melts	117
6-10	Regions of Possible Combinations of Three Condensed Phases in Carbonate Melts	126
6-11	Partial Pressures of Gases Above a Melt Containing 60% LiCl - 40% Li_2CO_3 by Weight	129
6-12	Partial Pressures of Gases Above a Melt Containing 35% Li_2CO_3 - 65% K_2CO_3 by Weight	130
6-13	Partial Pressures of Gases Above a Melt Containing 58 Moles LiCl - 42 Moles KCl - 1.5 Moles Li_2CO_3	131
6-14	Partial Pressures of Gases Above a Melt Containing 8 Moles Li_2CO_3 - 6 Moles K_2CO_3 - 6 Moles Na_2CO_3	132

ILLUSTRATIONS

(Continued)

Figure		Page
6-15	Partial Pressures of Gases Above a Melt Containing $LiCl - Li_2CO_3 - C$	133
6-16	Schematic: Melt Loss Apparatus	135
6-17	Melt Container	136
6-18	Melt Loss Apparatus	137
10-1	Test Tabulation, Phase IIA	159
10-2	Molten Carbonate Cell, Control Panel and Power Control System	161
10-3	Instrumentation and Calibration Gases	162
10-4	Oscillating Electrolyte Test Article	163
10-5	Engineering Test Facility. Flow Schematic	165
10-6	Tabulation of Significant Events Associated with Oscillating Electrolyte Configuration	168
10-7	Rotating Anode Used in Test 7	181
10-8	Cathode Deposit From Test 9	187
10-9	Deposit From Cathodes in Test 12	193
10-10	X-Ray Photograph of Cathodes from Test 14	197
10-11	Cathode 1 (Configuration No. 8B) Following Test 14	198
10-12	Cathode 2 (Configuration No. 10) Following Test 14	199
10-13	X-Ray Photograph of Cathodes 1 and 2 from Test 15	202
10-14	Cathode 1 Following Test 15	203
10-15	Cathode 2 Following Test 15	204
10-16	Cathode 1 Following Test 16	207
10-17	Cathode 2 Following Test 16	208
10-18	X-Ray of Cathode 1 (Configuration No. 12) Following Test 17	210
10-19	Anode (Configuration No. 7) As Removed From Test Article Following Test 21	218
10-20	Cathode 2 (Configuration No. 13) Following Test 21	219
10-21	Average Ratio CO_2/H_2O Versus Carbon Purity	233
10-22	CO_2 and H_2O Partial Pressures In Electrolyte Versus Carbon Purity	236
10-23	Weight Penalty as Function of Carbon Purity	240
10-24	Light Photomicrograph of the Three Types of Regions Observed	250
10-25	Light Photomicrograph of the Three Types of Regions Observed	251
10-26	Spectral Pattern Obtained from an Oxide Particle Similar to those Indicated in Figure 10-25	253
10-27	Aluminum and Nickel Distributions Across a Normal Area of the Anode	254

ILLUSTRATIONS
(Continued)

Figure		Page
10-28	Gold and Nickel Distributions Across a Normal Area of the Anode	255
10-29	Degussa Al 23 Alumina Samples Exposed to the Eutectic for the Times Shown	271
10-30	McDanel 997 Alumina Samples Exposed to the Eutectic for the Times Shown	272
10-31	Hastelloy N Nickel Alloy Samples Exposed to the Eutectic for the Times Shown	273
10-32	Tantalum Electrocladded Copper Sample (Left) and Titanium A70 Sample Exposed to the Eutectic for the Times Shown	274
10-33	Nickel 201 Samples Exposed to the Eutectic for the Times Shown	275
10-34	Cross-Section of Tantalum Electrocladded Copper Sample After 120 Hours Exposure to the Eutectic Etch NH_4OH Solution 200X	276
10-35	Cross-Section of Hastelloy N Sample After 240 Hours Exposure to the Eutectic	277
10-36	Container Made of Welded Hastelloy N Sheets After Having Been Heated to 1300°F with Molten Salt for the Second Time	279
11-1	Schematic Representative 1/6 g Cell	283
11-2	Hypothetical Geometry of Bubble on Verticle Anode	286
11-3	Break-Away O_2 Bubble Diameter at Anode Versus Gravity Level and Direction of Electrolyte Movement	288
11-4	Critical Bubble Diameter Versus Stream Velocity In a 1 g Field Where Drag and Adhesion Forces are (-) While the Buoyancy Force is (+)	289
11-5	Critical Bubble Diameter Versus Stream Velocity In a 1 g Field Where Drag and Buoyancy Forces are (+) While the Adhesion Force is (-)	290
11-6	Critical Bubble Diameter Versus Stream Velocity In a 1/6 g Field Drag and Adhesion Forces are (-) While the Buoyancy Force is (+)	291
11-7	Critical Bubble Diameter Versus Stream Velocity In a 1/6 g Field Where Drag and Buoyancy Forces are (+) While the Adhesion Force is (-)	292
11-8	Concentration as a Function of Distance Through Gas Liquid Interfacial Film	295
11-9	Hypothetical Equilibrium Curves for CO_2	299
11-10	Concentration Variation in Scrubber of Length L	302
13-1	Cell Complex, CO_2 Removal Mod. II	309
13-2	Typical Cell (18 Reqd)	313

ILLUSTRATIONS
(Continued)

Figure		Page
13-3	Anode	315
13-4	Cover and Bus-bar	316
13-5	Typical Inlet	318
13-6	Typical Outlet	319

TABLES

Table		Page
5-I	Anode Dissolution Rates For Selected Materials	14
5-II	Results of Statistical Study of Four Variables on Absorption Rate	70
6-I	$CaCO_3$ Decomposition Pressures	80
6-II	Equilibrium Constants for the Decomposition of Li_2CO_3 at 749°C	83
6-III	Equilibrium Constants for the Decomposition of Li_2CO_3 at 770°C	84
6-IV	Equilibrium Constants for the Decomposition of Li_2CO_3 at 790°C	85
6-V	Equilibrium Constants for the Decomposition of Li_2CO_3 at 813°C	86
6-VI	Equilibrium Constants for the Decomposition of Li_2CO_3 at 830°C	87
6-VII	Thermodynamic Data for the Decomposition of Li_2CO_3	89
6-VIII	Equilibrium Constants for the Decomposition of Li_2CO_3-LiCl Eutectic at 557°C	92
6-IX	Equilibrium Constants for the Decomposition of Li_2CO_3-LiCl Eutectic at 574°C	93
6-X	Equilibrium Constants for the Decomposition of Li_2CO_3-LiCl Eutectic at 588°C	94
6-XI	Equilibrium Constants for the Decomposition of Li_2CO_3-LiCl Eutectic at 606.5°C	95
6-XII	Equilibrium Constants for the Decomposition of Li_2CO_3-LiCl Eutectic at 643°C	96
6-XIII	Equilibrium Constants and Thermodynamic Data For the Li_2CO_3-LiCl Eutectic Mixture	98
6-XIV	Extrapolated Thermodynamic Data For Pure Li_2CO_3 (Supercooled)	100
6-XV	Activity Coefficients and Activities for Li_2CO_3 In the Li_2CO_3-LiCl Eutectic Melt	101
6-XVI	Evaporation Rates for LiCl From the Li_2CO_3-LiCl Eutectic Melt In the Experimental System of Figure 6-6	103
6-XVII	Equilibrium Constants for the Decomposition of Li_2CO_3-LiF Eutectic at 675°C	107
6-XVIII	Equilibrium Constants for the Decomposition of Li_2CO_3-LiF Eutectic at 697°C	107
6-XIX	Equilibrium Constants for the Decomposition of Li_2CO_3-LiF Eutectic at 725°C	108

TABLES
(Continued)

Table		Page
6-XX	Equilibrium Constants for the Decomposition of Li_2CO_3-LiF Eutectic at 749°C	110
6-XXI	Equilibrium Constants and Thermodynamic Data for Li_2CO_3-LiF Eutectic Mixture	111
6-XXII	Extrapolated Thermodynamic Data for Pure Li_2CO_3	111
6-XXIII	Activity Coefficients and Activities for Li_2CO_3 In the Li_2CO_3-LiF Eutectic Mixture	112
6-XXIV	Summary of Equilibrium Constants and Thermodynamic Data	113
6-XXV	Summary of Thermodynamic Mixing Data	114
6-XXVI	Total Pressure Above Carbonate Melts Containing Three Condensed Phases	124
6-XXVII	Loss of Melt Components From LiCl-Li_2CO_3 Eutectic at 670°C	141
6-XXVIII	Rates of Evaporation of LiCl From LiCl-Li_2CO_3 Eutectic Melt at 670°C	143
6-XXIX	Calculated Pressures of LiCl Vapor over LiCl-Li_2CO_3 Eutectic at 670°C	145
6-XXX	LiCl Vapor Pressure Versus Temperature	145
10-I	Results of Cathode Deposit Chemical Analysis In Tests 20 to 26	237
10-II	Differences in Environment for Three Configurations Tested	261
10-III	Likely Effects of Variables Upon Favorable Cathode Current Efficiency	262
10-IV	Free Energy of Formation of Certain Metal Oxides and Chlorides at 637°C	266
10-V	Test Results for CO_2 Reduction Container Material	269

1.0 INTRODUCTION TO RESEARCH STUDIES

Part I of this report is a presentation of continued theoretical and experimental research into a process for reclaiming oxygen from exhaled carbon dioxide by electrolysis of fused, alkali carbonate base, carbon dioxide absorbents. Process goals include the production of pure oxygen gas at the anode and the deposition of dense, high purity, solid carbon at the cathode at high current efficiency, while carbon dioxide in dilute concentrations is continuously absorbed from the atmospheric mixture fed to the electrolyte.

The research program has been divided into three separate areas of study - the anode process, the cathode process, and the CO_2 scrubbing process - and is herein reported according to that breakdown, although in actual practice all the processes are thoroughly interdependent. Supporting studies have included both theoretical and experimental investigations of electrolyte thermodynamic equilibria, carbonate dissociation pressures in systems with and without halide diluents, and determinations of system vapor pressures with special attention toward quantification of electrolyte carryover in processed air. These are reported under separate headings, although cross references are frequently made when appropriate.

The research program has been conducted, as in Phase I, by two research teams using independent test facilities, primary responsibility being vested in the Product Research Group at Hamilton Standard, with supporting studies carried out by the Chemical Sciences Section at the United Aircraft Research Laboratories. As in Phase I, the research activities have been directed toward providing a sound theoretical basis for understanding of electrode and electrolyte processes within the limitations of time and manpower, and in recognition of the ultimate engineering objective of developing a reliable, working device.

2.0 SUMMARY

Some time ago it was demonstrated that pure oxygen was obtained from the anode compartment when a fused lithium carbonate-lithium halide mixture was electrolyzed under appropriately controlled circumstances. It was shown also that anode current efficiencies close to 100% were readily attained. However, every anode metal which was experimentally evaluated was adversely affected by the electrolyte or by electrolysis so as to permit usage only for a limited life.

The problems of anode dissolution, oxygen purity, and anodic current efficiency have continued to be studied from the aspects of electrode material, electrolyte composition, and electrolysis conditions, and now a considerable amount of information has been accumulated on the nature of the anodic processes and the various process restrictions.

Anode materials have been discovered (among these are gold, gold-nickel alloy, and iridium) which when operated in specific electrode configurations provide significantly extended life. The effects of electrolyte oxide ion activity, carbonate to halide dilution ratio, and other general composition variables, on anode performance have been thoroughly investigated, and anode process theory has been sufficiently sharpened to define best conditions for electrode operation. Polarographic electrolyte monitoring techniques have been developed which permit in-process checks on oxide ion activity and, in turn, good predictability of anode dissolution rate, oxygen purity, and current efficiency.

Relative to the cathode, it has been possible theoretically to deduce and prepare an electrolyte composition with respect to carbonate, hydroxide, and oxide ion concentrations (with corresponding partial pressures of carbon dioxide, water vapor, and other gases in accord with equilibria considerations) which favors the deposition of carbon rather than some competing cathode process (reference 1). However, it has proved difficult to sustain a suitable composition in the vicinity of the cathode once electrolysis is initiated, owing to inappropriately balanced ionic and gaseous diffusion rates.

To overcome the limitations imposed by system intrinsic diffusion rates, two experimental techniques have been developed which enable the achievement of high carbon purity and current efficiency. The first of these involves periodic exposure of the electrolyte at the cathode interface to a gaseous atmosphere that is carefully controlled with respect to carbon dioxide and water vapor pressure and acts to re-establish proper catholyte equilibria. This is accomplished alternatively by 1) cyclically withdrawing the cathode from the electrolyte into the controlled gas phase above while electrolyzing, or 2) slowly rotating a vertical disc of which only the bottom portion remains submerged in the electrolyte, or 3) by continuously cascading a thin film of electrolyte over a cathode which is held stationary in the gas phase above the bulk electrolyte with provision to sustain an ionic conduction path.

2.0 (Continued)

The other technique involves the high speed movement of fresh electrolyte past the cathode during electrolysis, either by rapidly spinning the cathode itself or by flowing the electrolyte swiftly past a stationary cathode.

Carbon purity and cathode current efficiency have been determined under the alternative modes of operation and show that cathodic current densities considerably greater than expected at the end of Phase I are possible.

The role of halide diluent in achieving high carbon purity has been clearly demonstrated, as well as the detrimental effects of relatively low concentrations of hydroxide in the electrolyte. Chloride has proved most satisfactory of the halide diluents, although its high corrosive action on normal anode materials prompted an unsuccessful search for a substitute nonhalide diluent. Significant progress has been made toward identification of ionic species and processes occurring at the cathode through inspection and interpretation of cell current-voltage relationships and by chemical analysis of deposits.

In carbon dioxide absorption studies, an experimental baseline for effect of gas flow rate to scrubber surface area, electrolyte replenishment rate, electrolyte constitution, and temperature has been established. Effective scrubbing of carbon dioxide on a sustained basis by passing the process air over intermittently wetted surfaces has been demonstrated, and the direction of experimental work to achieve improved scrubber configurations has been defined.

Studies of carbonate dissociation rates in the presence and absence of halide diluents have shown that such diluents are not inert; rather, they strongly affect carbon dioxide-oxide ion equilibria in the electrolyte and, in turn, the electrode processes. Both fluoride and chloride diluents have been found to increase the extent of carbonate decomposition, although the effect of chloride is by far the greater. This has proved a beneficial effect because it makes the electrolyte system less sensitive to small oxide concentration changes, and also because it permits finer control over carbon dioxide transport rates.

Thermodynamic calculations begun in Phase I to ascertain thermodynamically possible chemical species in pertinent electrolyte systems have now been further extended in Phase IIA to new systems and to incorporate latest available data. These data have continued to provide guidelines for theoretical speculations. They have indicated that only two product combinations are possible in which solid carbon can co-exist with lithium carbonate. These are systems in which either alkali oxide or alkali metal is the third constituent. This has proved thoroughly consistent with experimental results.

2.0 (Continued)

The quantity of electrolyte carry-over as a result of the finite vapor pressures of electrolyte components was examined, utilizing lithium carbonate diluted with lithium chloride at the eutectic composition. These studies show that lithium chloride was the principal component lost from the electrolyte and that the amount was in reasonable agreement with published vapor pressure data. It was also shown that a small amount of electrolyte may be lost in the form of particulate matter when electrolyte agitation is sufficiently violent. Percentage of total electrolyte lost was generally negligible, reaffirming that the principal concern will be design consideration in preventing the clogging of small ports with condensed vapors.

3.0 CONCLUSIONS

3.1 The successful operation of fused alkali carbonate base electrolytic cells can be repeatably demonstrated. These cells absorb carbon dioxide at low concentrations from an air stream and decompose it to produce essentially pure oxygen gas at the anode and high-purity coherent carbon at the cathode.

3.2 Sustained performance of these cells requires control within the following process constraints:

3.2.1 For most successful anode performance, the anode should comprise a noble metal such as gold or iridium, or gold-nickel alloy (18 wt. % Ni) and should be so constructed as to entrain any anode sludge formed during operation. Such sludge consists chiefly of fine particles of the electrode base material, arising from temporary solution followed by precipitation into a spongy agglomerate that is highly electrically conductive, and upon recontact with the main electrode body continuously renews it.

3.2.2 Minimum anode dissolution and sponge formation is achieved when oxide ion activity in the electrolyte is highest. An increasing dilution of carbonate with halide results in greater anode dissolution, and, under extreme dilution, if oxide activity is not maintained sufficiently high, the metal of the anode will be plated on the cathode.

3.2.3 Oxide ion activity and therefore an estimation of anode life can be made from observations of anodic current-voltage behavior of the electrode. Oxide ion activity is controllable by appropriate regulation of input carbon dioxide rate and/or cathodic current density.

3.2.4 For successful cathode performance, oxide ion activity in the catholyte must be sufficiently high (low carbon dioxide partial pressure) to preclude a chemical reaction of gaseous carbon dioxide with the deposited carbon, resulting in carbon monoxide production; yet, the oxide must not be permitted to reach saturation and thus result in an occluded salt in the carbon deposit.

3.2.5 Carbon dioxide transport rate to the cathode must be balanced to the rate of alkali metal production at the cathode. This may be accomplished by altering the concentration of carbonate in the electrolyte, by adjusting the operating oxide ion activity, or by otherwise changing electrolyte constitution so as to alter carbonate decomposition rate.

3.2.6 For maximum oxide solubility it is necessary to employ an electrolyte diluent. Only the alkali halides have thus far been satisfactory for this purpose.

3.2.7 The requirement for high oxide ion activity at both the anode and cathode is consistent with a similar requirement for the scrubber, in order to absorb CO_2 from the influent air down to a sufficiently low partial pressure. The lower limit of pCO_2 achievable in the scrubber is established by the requirement that bulk electrolyte oxide concentration be adequately below saturation level to prevent precipitation of oxide at the cathode with the depositing carbon. For most systems studied this pCO_2 limit has been about 0.01 vol. % (0.076 mm Hg.).

3.2.8 Intrinsic electrolyte diffusion limitations can be overcome by operating the electrodes in modes which selectively enrich or deplete, as required, carbonate, oxide, and diluent; these include electrolysis, utilizing thin catholyte films and gas phase phenomena, and forced circulation of electrolyte.

3.2.9 Acceptable combinations of carbon purity and oxygen purity at high current efficiency are achieved at cathode current densities up to 200 ma/cm^2 and anode current density on the order of 25 ma/cm^2. With improved process control, it is expected that substantially higher current densities will be feasible.

3.2.10 Temperature limits for cell operation are constrained by the need to prevent freezing of the electrolyte surrounding each electrode as local composition changes occur due to electrolytically induced concentration gradients, and at the higher limit by the requirement to limit system vapor pressures and to minimize formation of carbon monoxide gas at the cathode. An operating temperature of 640C ± 40C has been generally found to be satisfactory.

3.3 Scrubbing of influent air containing 3.8 to 7.6 mm. Hg carbon dioxide down to 0.038 to 0.10 mm. Hg is readily achieved.

3.3.1 The dew point temperature of influent air to the system should be maintained below about -15°F to keep the hydroxide level in the electrolyte sufficiently low so as not to interfere with the cathode carbon deposition process. When this is not done hydrogen, methane, and carbon monoxide are gaseous by-products which disrupt the orderly deposition of carbon.

3.3.2 Carbon dioxide can be effectively absorbed from the air stream if it is passed over scrubber surfaces which are cyclically wetted by electrolyte. Under these conditions electrolyte foaming and carry-over are minimal.

3.4 Because a finite amount of electrolyte will be carried out in vapor form, system design will have to preclude the clogging of small ports by condensed vapors.

4.0 RECOMMENDATIONS

4.1 Experimental research should be continued toward further improving cell performance and component life, with special attention to the following operational details:

4.1.1 The ability to relate steady-state cell performance to anodic and cathodic polarographic behavior should continue to be improved.

4.1.2 The capacity to control electrode processes, as reflected in cell polarographic behavior, by modifications in electrolyte composition, particularly with respect to cation and anion substitutes and diluent concentration, should be strengthened.

4.1.3 Work should be continued to develop an automatic process controlling device based upon polarographic sensors.

4.1.4 Further efforts should be made to define cell operating modes which would permit use of static electrode systems rather than moving electrodes or electrolyte.

4.1.5 Other metal oxides (noble metal combinations in addition to nickel oxide-gold) should be investigated as a means for extension of anode life. These should include cobalt oxide, manganese oxide, gold, and iridium in various composites.

4.1.6 Carbon dioxide absorption tests should be continued toward defining scrubber requirements for optimum performance, and to investigate the effects of simultaneously using the scrubber as the anode.

4.1.7 The decomposition studies of lithium carbonate in halide diluted systems should be extended to include compositions more varied in halide concentration, in search for greater control over system oxide solubility and transport phenomena.

4.1.8 Because volume changes on mixing carbonate and halide should give an indication as to extent of carbonate dissociation and oxide ion "stability", electrolyte density determinations should be made as a function of composition for correlation with thermodynamic measurements to help predict optimum operating conditions.

4.1.9 Kinetic data, available from present and future thermogravimetric studies, should be evaluated to determine whether reaction rates might be calculated and, in turn, mechanisms for carbonate decomposition and recombination deduced. The rate constants should then be compared to those rates imposed by the electrolysis to predict dynamic equilibrium oxide concentrations in the electrolyte.

4.1.10 Precise measurement of halide diluent vapor pressure should be made at a number of temperatures and for a number of electrolyte compositions to determine halide activity in these systems and conditions for minimizing carry-over. Halide activity measurements should be confirmed, if possible, by electrochemical techniques using a halide sensing electrode.

5.0 PROCESS EXPERIMENTS

5.1 Anode Processes

5.1.1 Anode Electrochemistry

Anode current-voltage relationships plotted as Tafel lines (log current density against anode potential) give insight to the fundamental processes occurring at the anode, reference 2. The Tafel theory indicates that a linear relationship should be obtained when a single electrochemical process is occurring at an electrode and that the slope of this line is determined by the number of electrons being transferred as a unit. To illustrate, if oxide ions, each with a valence of minus 2, were being electrochemically oxidized to oxygen gas, and if this were occurring exclusively, then a linear plot would be obtained with a slope reflecting a two electron transfer process.

A Tafel plot taken with a gold anode in a molten lithium carbonate-lithium chloride electrolyte, suitably prepared and controlled to plate high density carbon at the cathode, typically shows three characteristic slopes for three regimes of anode current density. This is illustrated in figure 5-1. A slope reflecting a one electron process is observed at high current density, a two electron slope in an intermediate range, and a three electron slope at low current density. The latter slope appears uncertain at times, being three or somewhat greater than three. The uncertainty is believed due to the limitations of present instrumentation and experimental technique in the low current density range.

An appropriate hypothesis to cover these experimental results is that the unit slope at high current density corresponds to the electrochemical oxidation of chloride ions to chlorine gas. This occurs because oxide and carbonate ions become depleted at the electrode surface. Chlorine gas in turn chemically oxidizes oxide ions or carbonate ions a short distance away from the electrode surface, in accord with thermodynamic principles, to release oxygen gas, and in so doing returns to ionic form. This second chemical reaction would not be directly reflected in the Tafel plot. The two slope at the intermediate current density represents the direct discharge of oxide or carbonate ions to produce oxygen gas. The three electron slope denotes electrochemical oxidation of the gold anode to plus three valence gold ions. The gold ions subsequently acquire electrons from oxide or carbonate ions in a secondary chemical reaction, releasing oxygen gas and returning to the atomic form. The unit slope chloride process also involves the secondary chemical oxidation of the gold anode by the nascent chlorine to produce gold ions, which, as before by further chemical reaction with the electrolyte, produce oxygen gas and revert to metallic gold. Gold dissolution is most severe under this last circumstance.

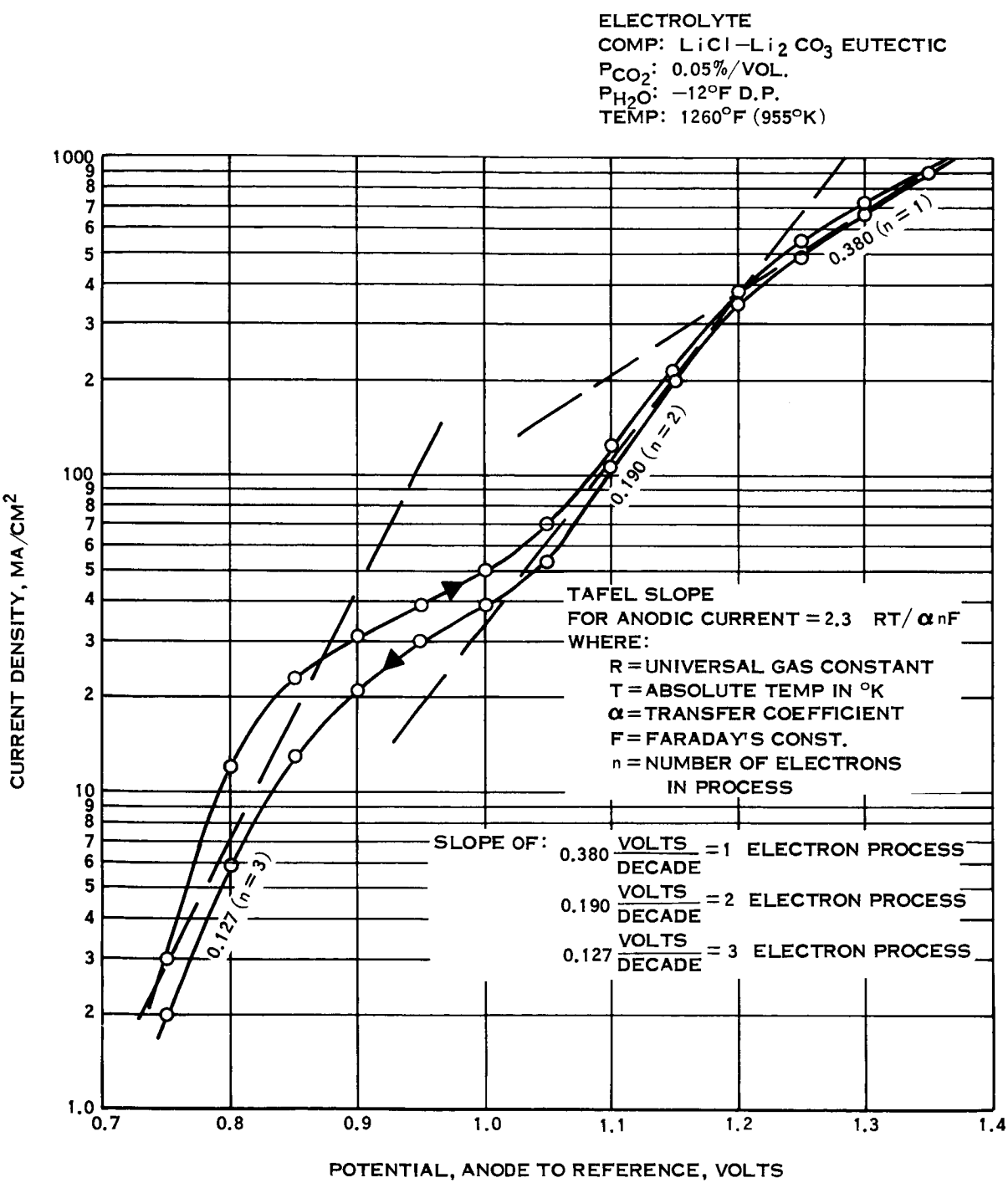


FIGURE 5–1. TAFEL PLOT OF ANODE CURRENT – VOLTAGE RELATIONSHIPS

5.1.1 (Continued)

Additional credence is lent the above hypothesis by the formation of a gold sponge at the anode during cell operation, and the achievement of near 100% current efficiency in oxygen production under all modes of anode operation. It would be expected from the above that gold dissolution might be minimized by anode operation at intermediate current density or by appropriate adjustments in electrolyte constitution such that direct oxide or carbonate discharge is the predominating electrochemical process (two electron slope), but in practice anode dissolution has been least when the three electron slope (gold ion intermediate to oxygen production) has predominated.

5.1.2 Electrode Dissolution Rates

5.1.2.1 Electrode Materials

A wide assortment of metals has been experimentally evaluated for use as anodes. These have included gold, gold-nickel alloy, gold-palladium, platinum, iridium, nickel, iron, cobalt, aluminum, molybdenum, tungsten, zirconium, Hastelloy X, copper, and silver. All materials tested have lost stock during anodic operation. In some cases the lost stock has reappeared as a metal sponge a short distance from the electrode; in other cases the electrolyte has become contaminated with metal ions and the carbon plating process at the cathode undermined. Important among the sponge formers have been gold base materials, platinum, silver, and iridium.

Quantitative data have been obtained on rate of stock lost from gold as a function of operating temperature, current density, electrolyte oxide ion activity, and electrolyte halide to carbonate ratio. Appropriate weight loss data for comparison have been obtained for iridium, gold-nickel alloy, and pure nickel at selected check points. During the taking of this data the constitution of the electrolyte has been carefully monitored with respect to CO_2 and water vapor pressure, with anode current-voltage relationship determinations (polarograms) before and after each run. In time it became possible to predict the expected electrode weight loss by examination of the polarographic information, as will be described presently.

The test configuration used for taking polarographic data and for running anode dissolution determinations is shown in figure 5-2. In both cases, 0.5 cm^2 of anode surface area was exposed to the electrolyte. The alumina shield which isolated the anode from the cathode and reference electrodes was kept relatively large so as not to hinder ionic transport, which proved to be a problem in the lower conductivity halide-free electrolytes.

Weight loss data obtained for gold over a range of temperatures and current densities are graphically shown in figure 5-3. The data are presented as the weight of gold actually lost from the anode divided by the weight of gold that would be lost if all the current were being used to convert the gold to plus three gold ions, expressed as

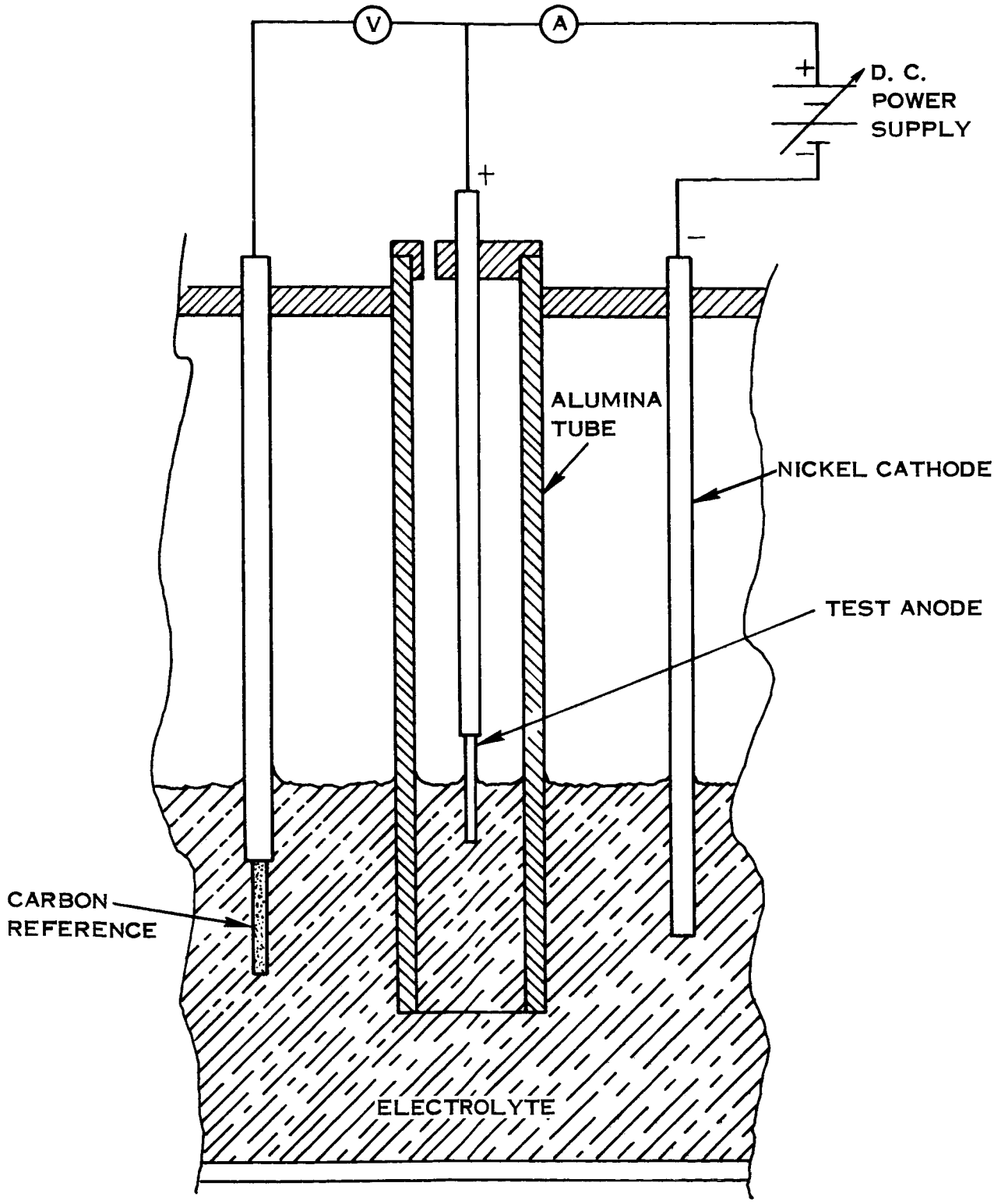


FIGURE 5–2. TEST CONFIGURATION : ANODE DISSOLUTION STUDIES & POLAROGRAMS

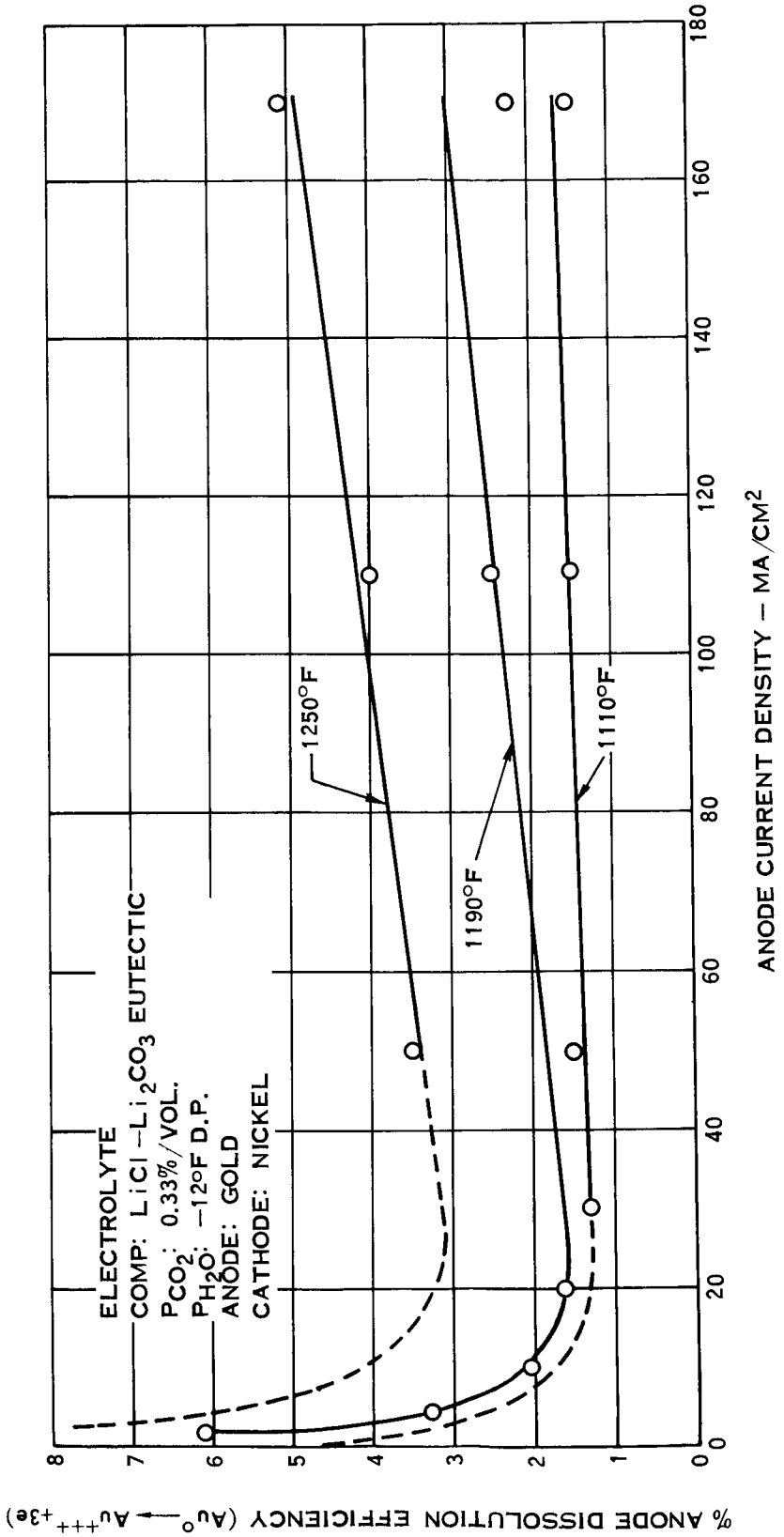


FIGURE 5–3. EFFECT OF CURRENT DENSITY ON ANODE DISSOLUTION FOR VARIOUS TEMPERATURES

5.1.2.1 (Continued)

percent. It therefore represents that percent of the anode current involved in removing gold stock. The result has been called the anode dissolution efficiency - the lower the percent at any selected current, the less stock being lost from the electrode. It will be noted in the figure that dissolution efficiency increases with increasing temperature (greater dissolution). It appears to go through a minimum at about 20 ma/cm^2.

A tabulation of comparative weight losses for the more promising anode metals is found in table 5-1. In this series a gold dissolution test was run before and after testing each of the other materials, so that a change in electrolyte composition would not be in question. The gold-nickel alloy and iridium look particularly attractive, the loss being less than that of pure gold.

The observed low dissolution rate for gold-nickel alloy prompted a study of a number of alloy compositions containing from 2 to 18 weight percent nickel. The greater the nickel content, the lower was the observed dissolution rate, as can be seen from figure 5-4. Microscopic examination of the test specimens indicated a preferential depletion of nickel from the alloy when nickel was present in low concentrations, but a conversion to nickel oxide when it was present in higher concentrations.

In the course of the program a brief study was made of pure nickel with a lithiated nickel oxide surface treatment, but this failed to show any significant advantage over the untreated material. It should be noted that none of the above data have been taken in electrolytes which have been rigorously optimized as to composition for minimum anode dissolution, as discussed in the following sections.

It is also interesting to note that the Tafel plots of the polarographic data, figure 5-5, show only minor differences among metals at current densities above 10 ma/cm^2 and indicate that similar electrochemical processes are occurring. Below 10 ma/cm^2 a difference between nickel and the other metals, which can be related to stable oxide formation on the nickel surface, can be readily discerned.

5.1.2.2 Electrolyte Composition

Gold dissolution efficiency as a function of the mole ratio of lithium chloride to lithium carbonate is shown in figure 5-6. Anode dissolution increases markedly as the chloride to carbonate ratio is increased beyond about 4 to 1. This is commensurate with an increase in operating voltage and a shift toward the unit slope chloride ion discharge process which, as we have already noted, results in most severe anode attack.

Figure 5-7 illustrates the effect of varied oxide ion activity in the electrolyte on gold dissolution. As oxide ion activity is increased, anode dissolution is decreased. For example, at 110 ma/cm^2 a newly mixed electrolyte, curve 1, showing high CO_2 and

TABLE 5-I ANODE DISSOLUTION RATES FOR SELECTED MATERIALS

(pCO_2 = 0.17%/vol, Dew Point = -15 F, T = 1290 F)

Run No.	Material	Electrolyte Mole Ratio LiCl : Li_2CO_3	Metal Ion	Time of Test (hrs)	Dissolution Efficiency, % Anode Wt. Loss / Theor. Wt. Loss for Current Passed X100		
					(50 ma/cm^2)	(110 ma/cm^2)	(170 ma/cm^2)
101	Gold	2.7:1	Au^{+3}	16	-	2.34	-
102	Iridium	"	Ir^{+3}	"	-	No Measurable Wt. Loss	-
103	Gold	"	Au^{+3}	"	-	2.27	-
104	Iridium	"	Ir^{+3}	64	-	0.321	-
105	Gold	"	Au^{+3}	16	1.31	1.75	1.87
201	Gold	6.45:1	Au^{+3}	"	4.1	4.82	5.53
202	Gold-Nickel Alloy 82-18 Wt. %	"	Au^{+3}-Ni^{+3}	"	1.02	0.415	0.318
203	Gold	"	Au^{+3}	"	3.4	5.0	5.38
204	Nickel	"	Ni^{+3}	"	17.7	6.9	6.88

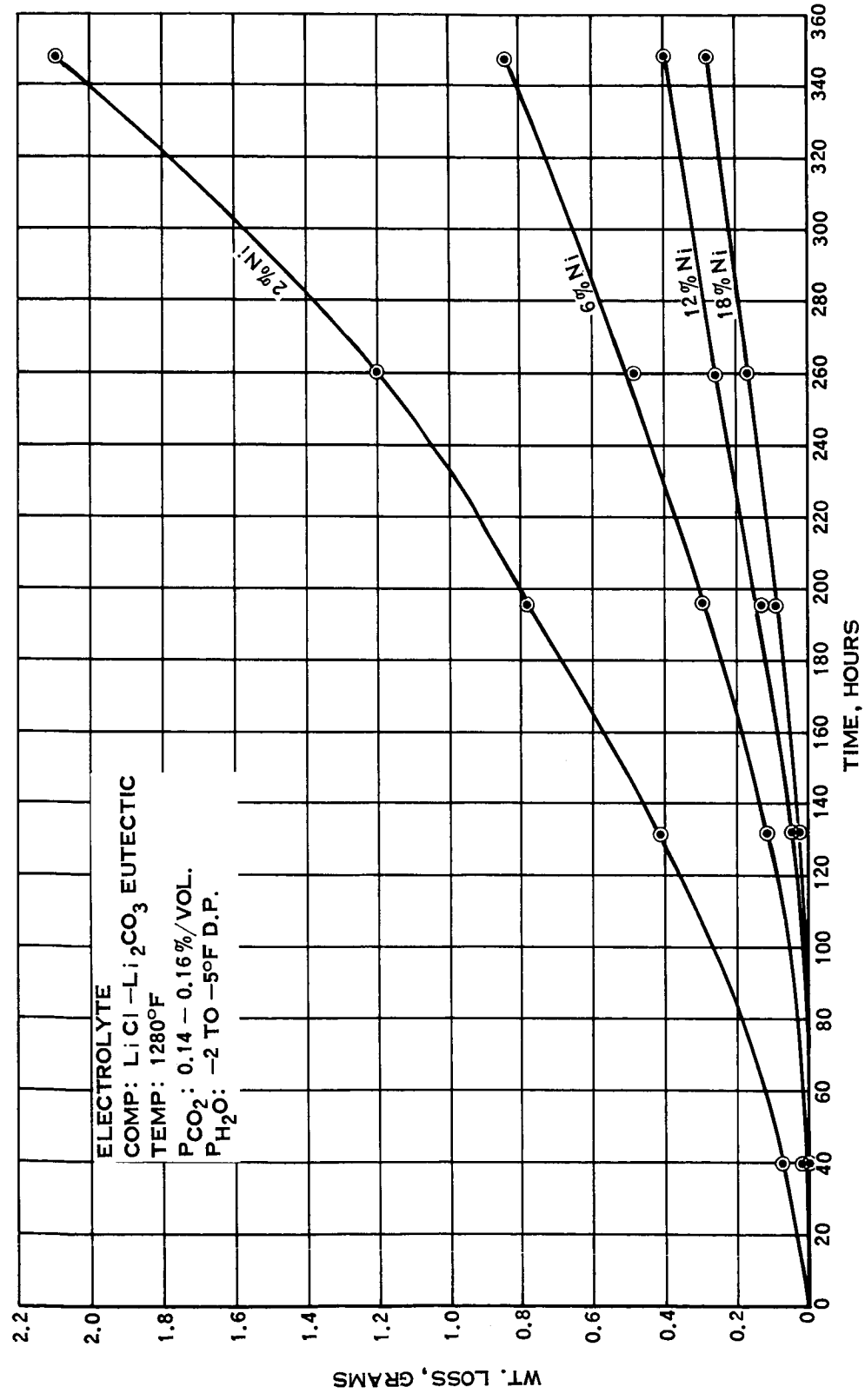


FIGURE 5–4. ANODE DISSOLUTION RATES FOR GOLD–NICKEL ALLOYS

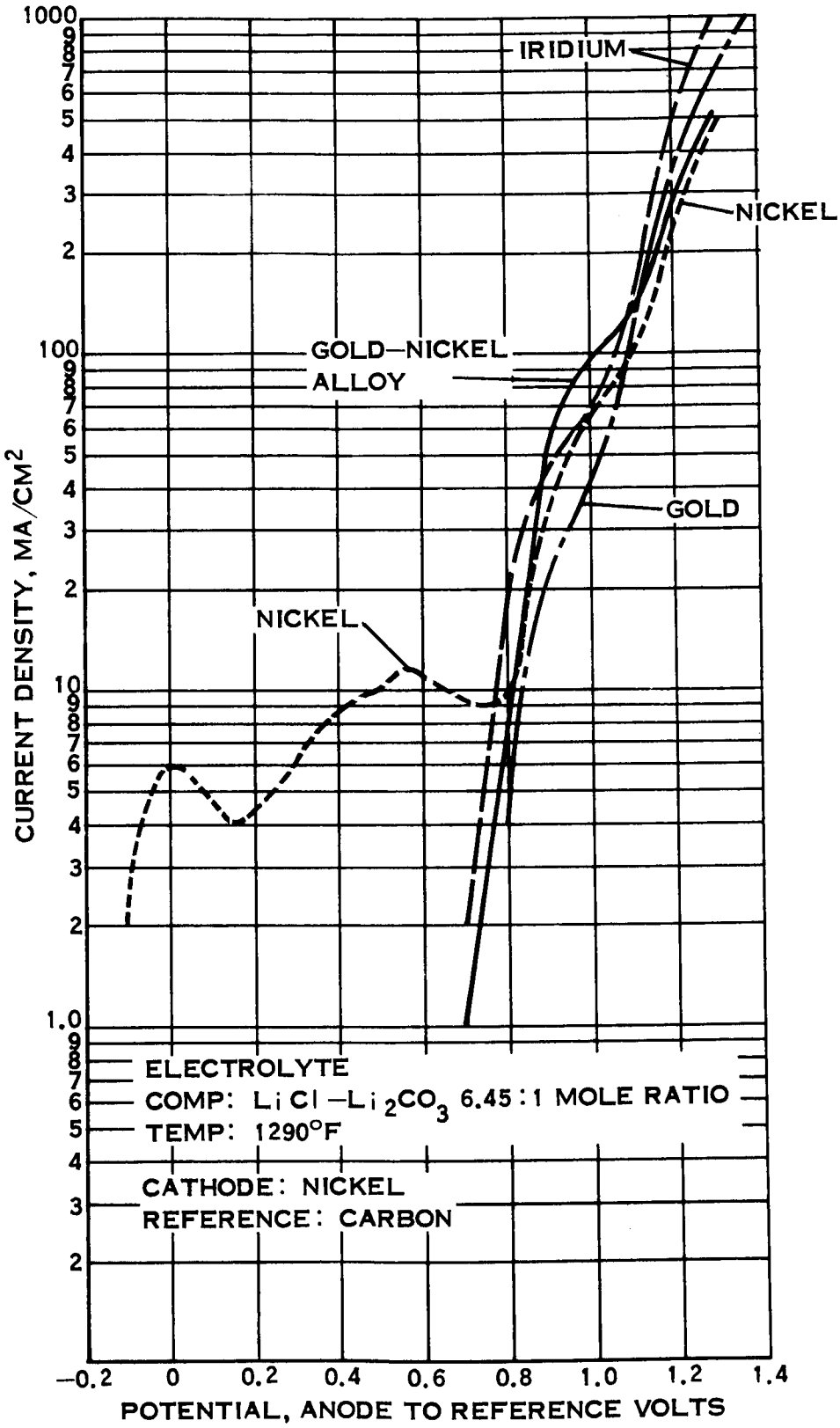


FIGURE 5—5. ANODE TAFEL SLOPES FOR ASSORTED METALS

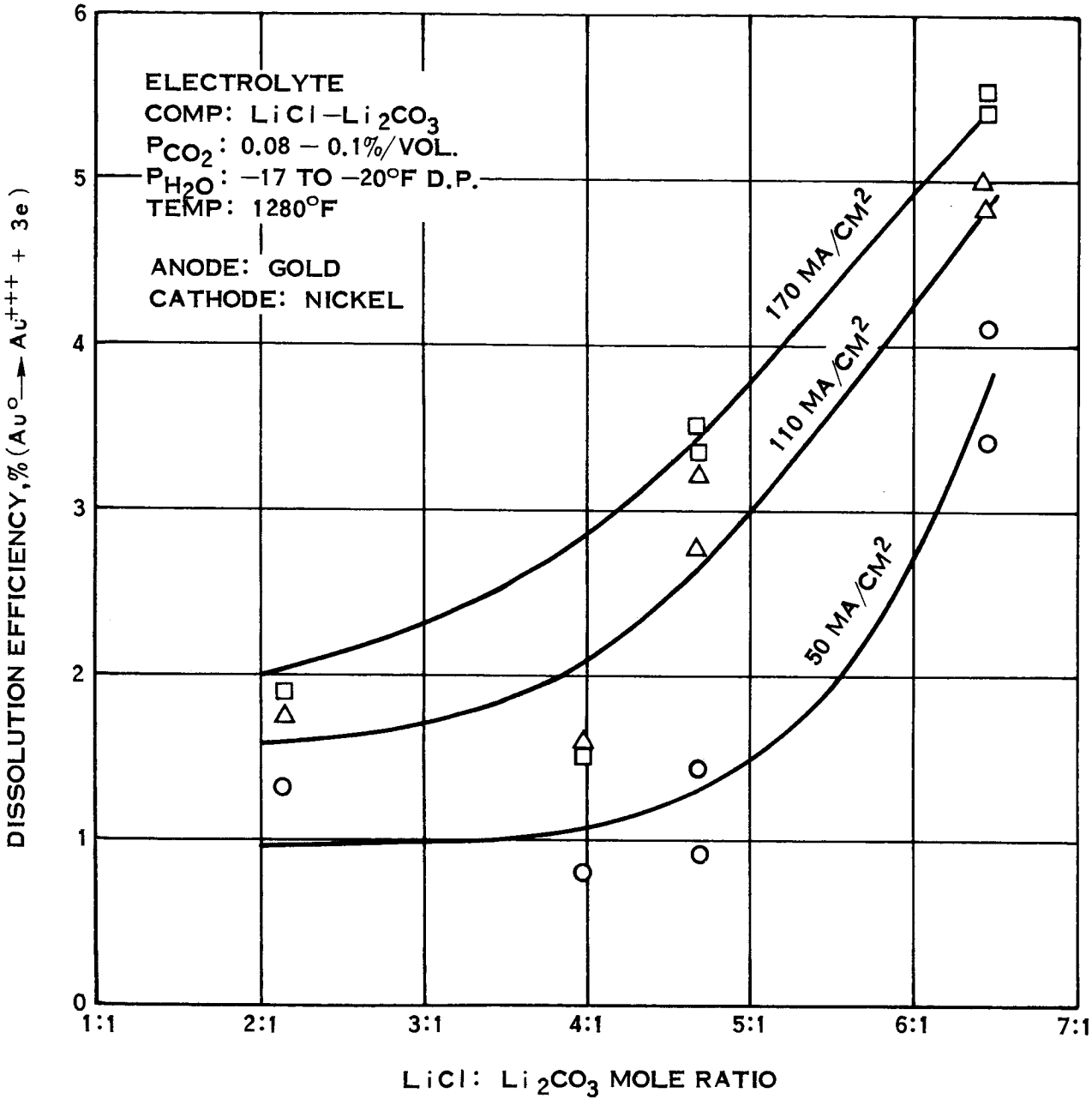


FIGURE 5–6. EFFECT OF CHLORIDE CONCENTRATION ON ANODE DISSOLUTION RATE

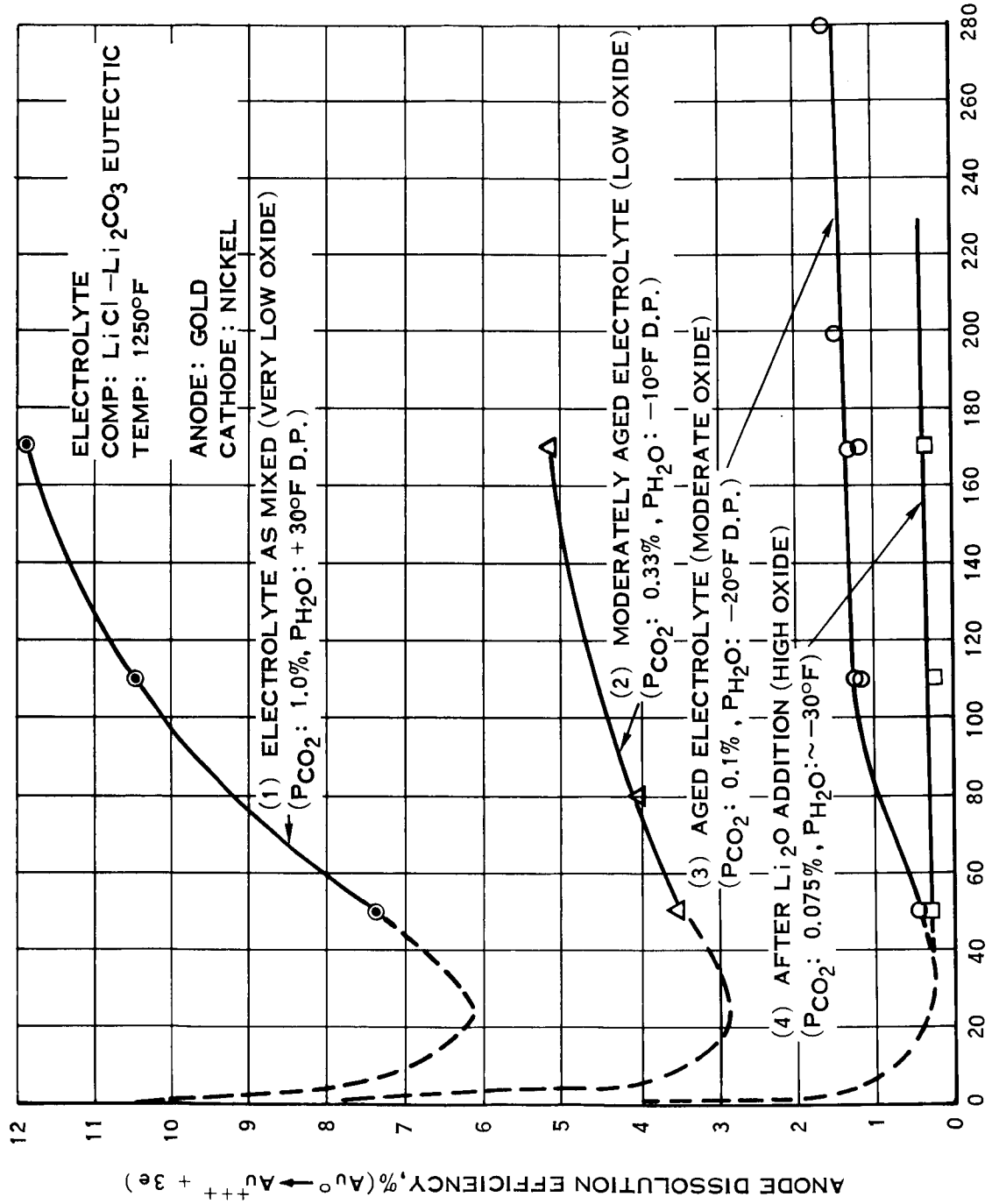


FIGURE 5–7. EFFECT OF CURRENT DENSITY ON ANODE DISSOLUTION RATE FOR VARIOUS OXIDE ION CONCENTRATIONS

PAGES 19 AND 20
ARE MISSING FROM
ORIGINAL DOCUMENT

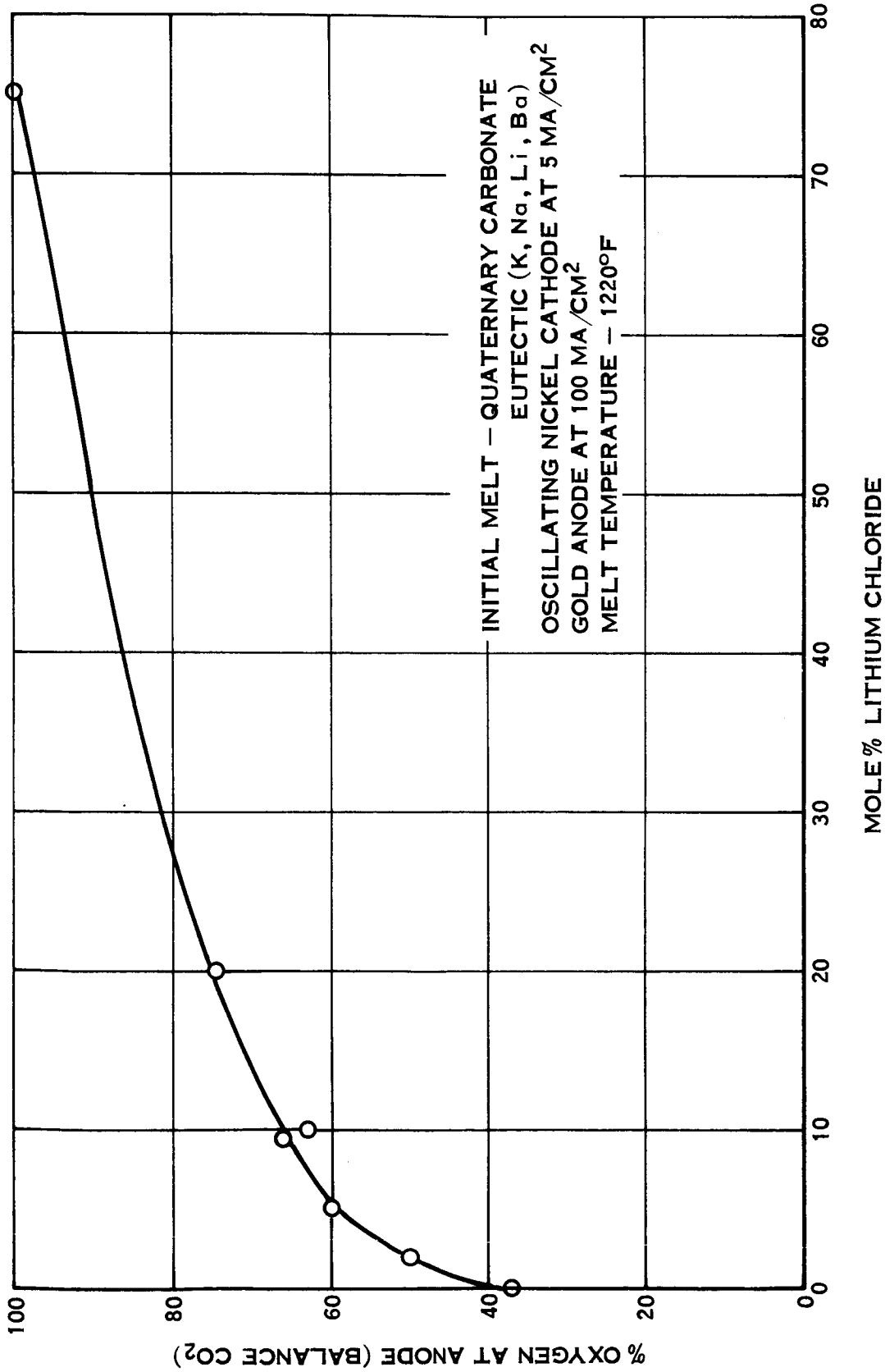


FIGURE 5–9. EFFECT OF CHLORIDE CONCENTRATION ON OXYGEN PURITY

5.1.3 (Continued)

case, resulting from a greater solubility of lithium oxide in the halide. The presence of halide therefore appears necessary even at the expense of somewhat increased anode dissolution, not only for the cathode process but also for the closely interrelated oxygen delivery and system CO_2 scrubbing functions.

Oxygen with acceptably low carbon dioxide content has also been obtained when the carbonate is diluted with hydroxide. Here the contaminant is water vapor. The scrubbing function also persists as long as sufficient hydroxide is present in the electrolyte for reaction with CO_2, water being displaced in the process. As has been noted, however, high density carbon is not plated at the cathode. Instead, predominantly hydrogen gas, along with CO and CH_4, is discharged.

With regard to oxygen purity as affected by anode current density, pure oxygen has been obtained in a lithium carbonate-chloride eutectic at current densities below 100 ma/cm^2 for periods of several days without change. Above 300 ma/cm^2 pure oxygen has been obtained for periods up to a few hours before CO_2 content rose rapidly. The limitation here appears to be the rate of oxide availability from the cathode. In the high current density runs described, oxide was accumulated at the cathode. The use of a larger cathode at lower current density would be expected to permit anode operation at higher current density within the restrictions of anode dissolution rate.

5.1.4 Current Efficiency

Anodic current efficiency is defined as the actual volume of oxygen obtained over a chosen time interval from the anode compartment, divided by the theoretically expected volume for that time in accordance with Faraday's law, expressed in percent. This definition would take into account any oxygen lost to solubility in the electrolyte, or by leakage. When gold is utilized as an anode, near 100% current efficiency is generally obtained under all modes of anode operation, at all current densities, and in all carbonate base electrolytes investigated. This is so because all secondary chemical reactions result in oxygen production, as does the direct discharge of oxide ions. Only at high halide dilution, where the gold ions are more stable, would any deviations be expected. The same would be true for iridium and the other platinum metals. The high efficiencies obtained negate the possibility of any significant oxygen solubility in the electrolyte.

When other metals are employed as anodes, current efficiencies vary in accord with the stability of metal ions and/or metal oxides formed. Such is the case with metals like tungsten or iron which form stable ions, and zirconium and aluminum which form stable oxides before conductivity is eventually lost. In these cases current efficiency is low.

5.1.4 (Continued)

Under normal circumstances favorable to the cathode process, ready achievement of high current efficiencies is expected with selection of an appropriate anode material.

5.1.5 Anode Assembly Design

Because all metals lose stock when utilized as anodes, it has proved advantageous to select for system use those where the lost stock is recovered as a sponge. Of these latter materials, gold has been the most intensively studied. Other supporting hardware requirements for a completed anode assembly include a gas impermeable shield around the electrode, which serves to capture the oxygen bubbles, keeps them separated from the carbon depositing at the cathode, and permits delivery of the oxygen to other systems through an appropriate outlet port. The shield is generally immersed sufficiently deep in the electrolyte to sustain a slight positive pressure of gas above the electrolyte without emptying the shield. The positive pressure is useful in preventing back leakage of atmospheric gases and facilitates oxygen delivery to analysis and other systems. Of practical note, when operating at close to ambient pressure, it has been found necessary to assure that the shield cap is thoroughly impermeable to air. It should be made of such material as laminated silicone plastic, rather than transite, which has proved permeable to air and has allowed back diffusion into the anode compartment.

A further hardware requirement is for a suitable retainment system for the metal sponge which is formed. This should be designed to cause the sponge to re-establish electrical contact with the anode proper, and in so doing result in an eventual steady-state in the rate of stock removal from the anode and return as sponge to constitute a self-healing electrode. The sponge retainment system must also allow free passage of oxide ions to the anode for continuous generation of pure oxygen.

A representative anode assembly is illustrated in figure 5-10. The electrode is a slug of gold carefully fused around an alumina tube to prevent localized anodic action at possibly thinner connecting joints. It rests in a small alumina crucible which serves as a receptacle for the gold sponge which is formed. The shield is fashioned from high purity alumina. It has been found advisable to surround the alumina shield with a nickel sleeve, since the operation of the anode at high oxygen generation rates has on occasion resulted in the formation of an electrolyte foam which rises in the smaller diameter shields. The metal sleeve distributes heat sufficiently high in the shield to allow foam collapse before solidification. Sponge retainment while allowing ionic transport in the illustrated assembly is accomplished by means of a fence consisting of small diameter alumina tubes which, though touching, permit passage electrolyte. This is apparent from figure 5-11b, where the fence is lighted from within.

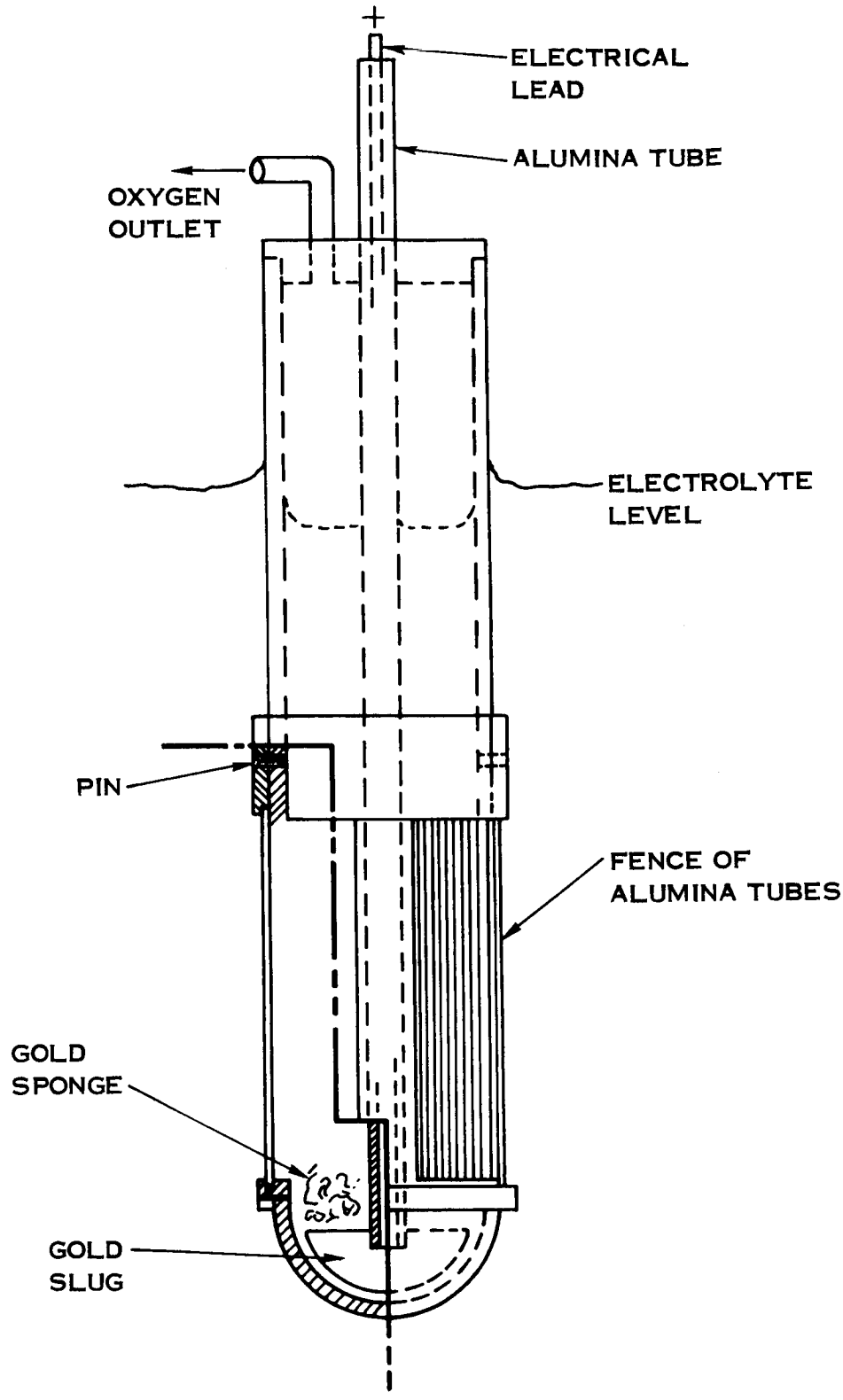
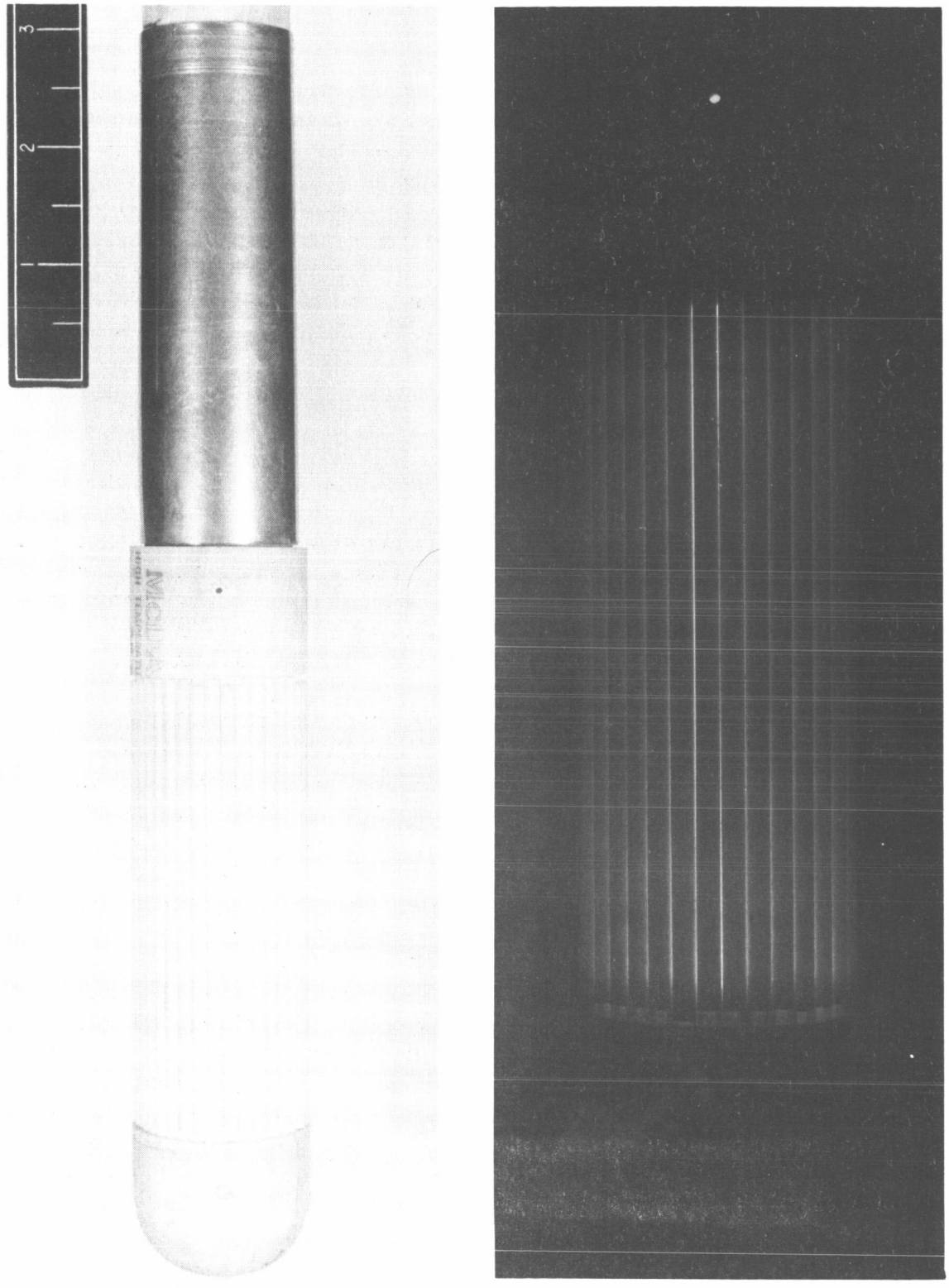


FIGURE 5–10. SCHEMATIC: ANODE ASSEMBLY: TUBE BUNDLE SPONGE RETAINER



A B

FIGURE 5–11. ANODE ASSEMBLY ; TUBE BUNDLE SPONGE RETAINER

5.1.5 (Continued)

Anode assemblies such as this one have been operated for periods up to several weeks while producing high purity oxygen. Figure 5-12 shows a gold electrode with sponge at the end of such a period. Two shortcomings have been encountered. First, a fair amount of gold sponge is found outside the shield, and second, the electrolyte within the fence in time becomes depleted of oxide ions, eventually leading to substantial increases of CO_2 partial pressure in the oxygen gas. The two phenomena are interrelated in that depletion of oxide ion enhances gold dissolution and increases the chance of gold ions passing through the fence before being reduced. Accumulation of gold at the fence further restricts ionic migration, so that the condition is self aggravating.

Porous alumina and magnesia cups have been evaluated as alternatives to the fence structure. Both types of cups physically pass electrolyte, and no gold sponge has been found to pass through them. All cups tested, however, have reacted with the electrolyte to evolve a high CO_2 pressure, as in the case of the porous alumina, or to disintegrate with time as has been the case with the magnesia, except one sample pretreated by firing to cone 35. Current-voltage studies using the magnesia cup, however, indicate that the rate of ionic transport through this type of structure is severely limited. Thinner walled test pieces might eventually prove more satisfactory if the problem of compatability with the electrolyte can be completely resolved.

A third approach to the problem of gold retention while preserving ionic transport utilized an electrolyte vortex created by a spinning cathode to keep the gold sponge close to the anode. (The spinning cathode has been demonstrated to produce high density carbon.) No physical barrier around the anode was employed, so that ionic transport was not inhibited, figure 5-13. Electrode dissolution at minimum rate was possible, and sponge formation tended to occur close to the electrode. However, small gold particles that strayed from the anode region were found to adhere to the spinning cathode, where they contaminated the carbon deposit.

Three other anode configurations have been studied. The first of these employed alumina and zirconia wicks dipping into the electrolyte to deliver a thin film of electrolyte to metal wire and screen electrodes wrapped around the ceramic materials and operated in the gas phase. The configuration is not gravity dependent and was therefore of particular interest. However, oxide transport rate through the wicks proved to be too slow, so that a 2 to 1 ratio of CO_2 to oxygen was obtained under almost all electrolysis conditions with tests conducted in a lithium carbonate-chloride eutectic. Pure nickel was used most commonly as electrode material and consistently showed severe dissolution.

A second anode configuration employed solid membranes of zirconium oxide stabilized with yttrium and calcium oxides to form a non-porous cup around the electrode that passed only oxide ions. In one technique the internal surface of the cup was coated

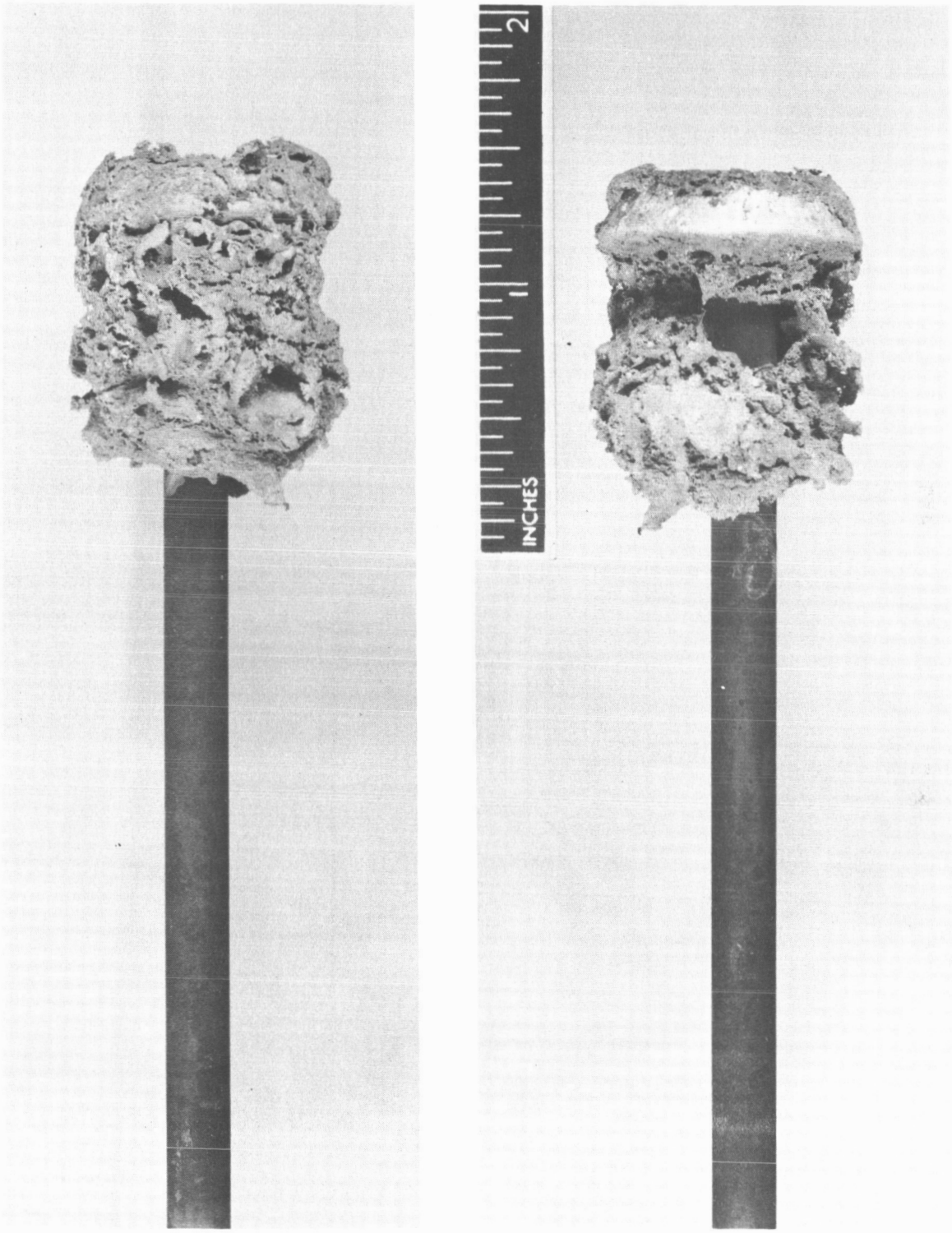


FIGURE 5—12. GOLD—GOLD SPONGE ELECTRODE

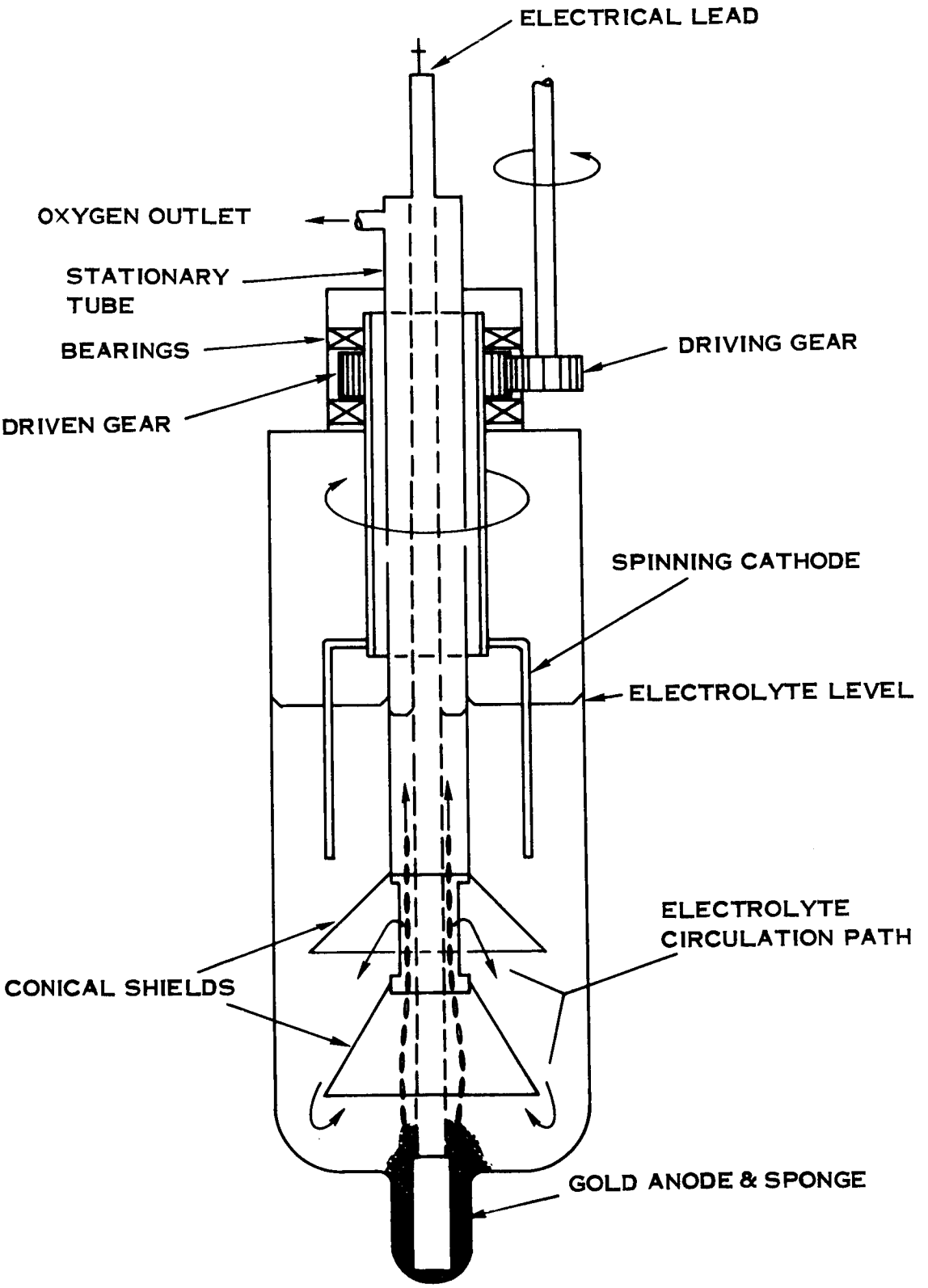


FIGURE 5–13. SCHEMATIC: ANODE ASSEMBLY; VORTEX RETENTION OF SPONGE

5.1.5 (Continued)

with porous platinum metal, which served as anode. The cup was dipped half way into the electrolyte so as to leave the inside platinum-coated surface dry, and electrolysis was carried out using the dry platinum as anode and an external nickel cathode. In another technique a separate electrolyte was contained within a partially submerged cup (with no platinum coating) and a conventional gold electrode was used as an anode in the center. Since the anolyte was separated from the catholyte by the membrane, lithium hydroxide alone was used as anolyte to eliminate CO_2 contamination of the oxygen and to assure negligible electrode dissolution. The feasibility of both configurations was experimentally demonstrated; however, the service life of the membranes could not be extended beyond a few days.

Finally, a brief look was taken at the possibility of spinning a gold anode in such a fashion as to insure continued washing with fresh electrolyte. It has been suggested that if the layer of electrolyte next to the electrode is not allowed to become depleted of oxide, dissolution rates might remain acceptably low. A single attempt at this, in an electrolyte where gold dissolution was high under usual circumstances of anode operation, showed even higher dissolution rates for spun specimens. A repeat test must be made in a low dissolution rate electrolyte before a final judgment is made.

5.1.6 Long Term Testing

An endurance test was run on a woven anode of 15-mil-diameter gold-nickel alloy wire, (18 wt. % nickel), suspended within an open-bottom alumina shield in a Li_2CO_3-LiCl electrolyte. A total of 800 hours operating time was accumulated with high oxygen purity at high current efficiency when fracture of the supporting portion of the wire occurred. Examination of the electrode at that time showed extensive conversion of the nickel to nickel oxide, which served to entrain the gold. In the process, the electrode was severely embrittled, as witness the fracture of the supporting lead wire.

In this and in other extended tests of gold and gold-nickel alloy anodes, a fine powder, varying in color from white to blue to green, was observed to be occluded with the nickel oxide and/or gold sponge forming on the anode surface. This powder was identified by x-ray diffraction as aluminum oxide in various combinations with nickel oxide. In subsequent experimentation, a magnesia shield was used in place of the alumina shield and no powder accumulation was observed. These observations are consistent with general experience in this program, which indicates that although alumina is highly resistant to attack by lithium carbonate-chloride electrolyte systems, very slow surface deterioration does occur. It is speculated that aluminate ions formed in the electrolyte are discharged at the anode to release oxygen gas, with alumina remaining behind as a precipitate. Magnesium oxide, when fired under appropriate conditions ($\sim$3500 F), warrants further consideration when a ceramic material is required.

5.1.7 Future Anode Study

The combination of nickel with gold, whether in alloy form or as nickel screen surrounding a gold core, or nickel oxide powder incorporated into a porous well enclosing a gold electrode, has experimentally provided the most effective and prolonged anode operation to date. It is presently believed that the nickel oxide formed at the anode serves a catalytic function, buffering the oxide ion activity at the anode so as to facilitate oxide discharge as well as serving as a retention device for gold sponge that may be formed. As has been noted already, nickel when used alone severely deteriorates and oxide penetration causes successive delaminations.

Using 100 mesh gold-nickel alloy powder (18 wt % Ni), a single attempt has thus far been made to preoxidize the nickel before sintering the powder to fashion an anode. The resultant structure showed a considerable reduction in electrical conductivity, as well as some continued leaching of residual nickel metal from the gold when used as anode. Much work remains to be done in this area which should lead to great improvements in anode life. This work should include investigation of other oxide-precious metal combinations as well. The most obvious candidate materials among these are cobalt oxide, manganese oxide, and iridium. Utilization of the anode surfaces to scrub carbon dioxide from the air stream while electrolyzing also requires demonstration.

5.2 Cathode Processes

5.2.1 Cathode Electrochemistry

As was the case in anode studies, it is possible to gain insight into the fundamental processes occurring at the cathode by examining cathode current-voltage relationships plotted as Tafel lines (log current density against cathode potential). A linear relationship should be obtained when a single electrochemical process is occurring at the electrode, and the slope of this line is proportional to the number of electrons being transferred as a unit. A Tafel plot taken with a carbon or nickel cathode in a molten lithium carbonate-lithium chloride electrolyte typically shows only one characteristic slope - that of a single electron process, figure 5-14.

This experimental evidence convincingly affirms the proposition that the alkali metal cation is initially reduced to atomic form at the cathode, and the alkali metal in turn reduces carbon from carbonate or carbon dioxide in a secondary chemical reaction, as in Equations 1 and 2 for the electrolyte cited.

1) $4\ Li^{+} + 4\ e \longrightarrow 4\ Li^{\circ}$

2) $CO_2 + 4\ Li^{\circ} \longrightarrow C + 2\ Li_2O$

(or $CO_3^{=} + 4\ Li^{\circ} \longrightarrow C + 4\ Li^{+} + 3\ O^{=}$)

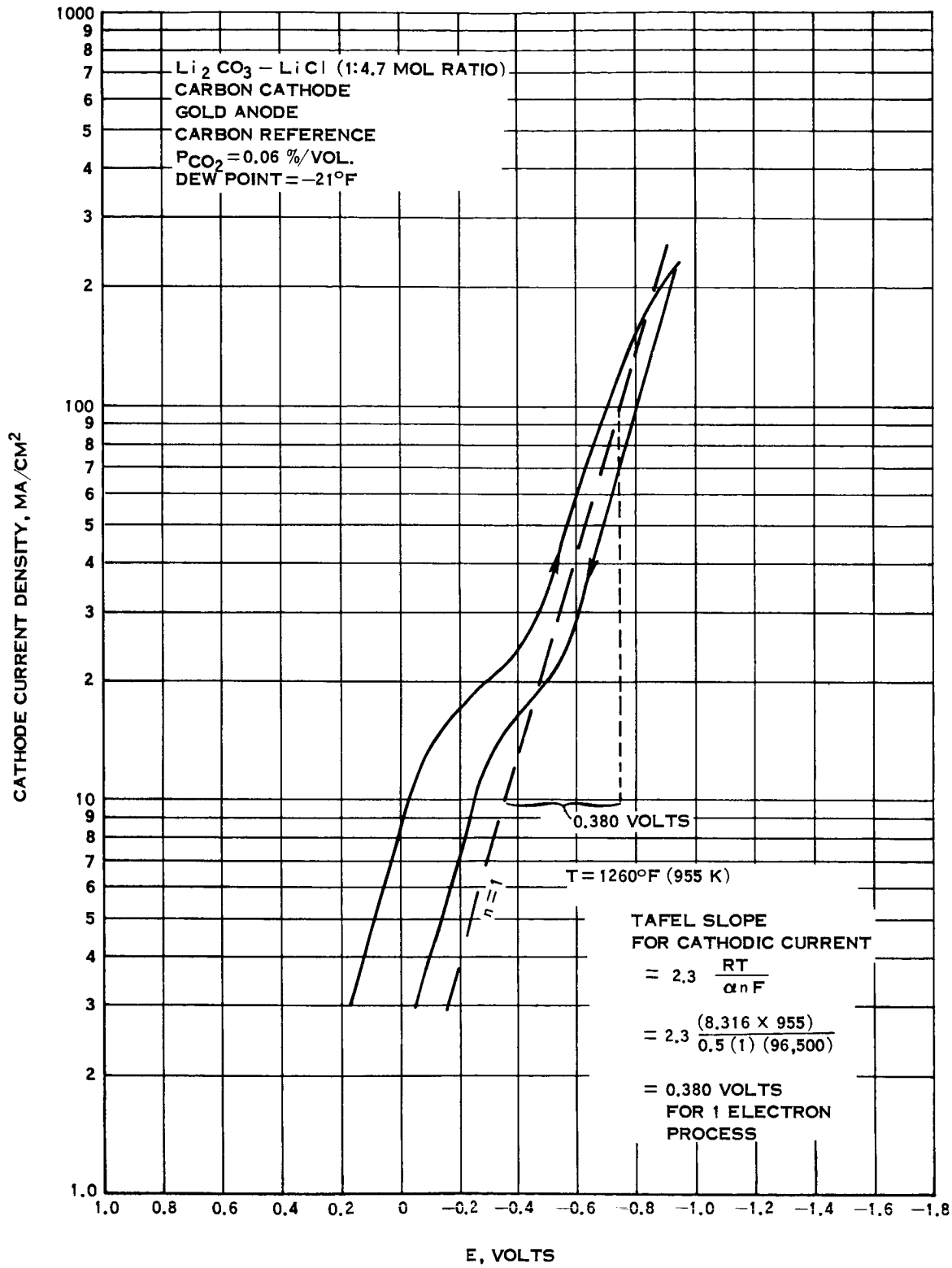


FIGURE 5–14. TAFEL PLOT OF CATHODE CURRENT – VOLTAGE RELATIONSHIPS

5.2.1 (Continued)

The plateau occurring between 15 and 20 ma/cm^2 on figure 5-14 has been related to electrolyte oxide ion concentration (height inversely proportional to concentration) and is believed to represent the limit in oxide solubility at the cathode. Unit slopes predominate both before and after the plateau.

An understanding of basic ion-gas equilibria necessary to achieve high quality carbon at the cathode has been gained by considering an equilibrium condition at the carbon coated cathode, based upon reversible reduction of carbon from the carbonate ion, as in the equation,

$$CO_3^{=} + 4\,e \longrightarrow C + 3\,O^{=}$$

The Nernst equation for the potential difference between such an electrode (open circuit) and a carbon electrode reference can be written as

$$E_R - E_C = -\frac{RT}{4F} \ln \frac{(O^{=3})_R}{(O^{=3})_C} \frac{(CO_3^{=})_C}{(CO_3^{=})_R}$$

where R and C subscripts refer to reference and cathode - both carbon electrodes. Since we are concerned with oxide ion concentrations which are extremely low relative to carbonate, the equilibrium constant for decomposition of lithium carbonate to lithium oxide and CO_2 being of the order 10^{-5}, oxide ion activity is inversely proportional to CO_2 partial pressure, p, and carbonate ion activity is substantially constant, therefore

$$E_R - E_C = -\frac{3RT}{4F} \ln p_C/p_R$$

A plot of potential difference against log CO_2 pressure at the cathode (open circuit) (semilog paper) should be a straight line with a slope of 3RT/4F. This slope would indicate no oxide precipitation and would apply so long as the equilibrium of carbon with various gases, including carbon dioxide, carbon monoxide, water, hydrogen and methane, is satisfied, and is therefore believed to be a necessary condition for the growth of high purity carbon. When conditions incompatible with such equilibrium are enforced, one or more of these gases may be generated on a continuous basis, and interfere with the orderly deposition of carbon.

With appropriate electrolyte composition control, a 3RT/4F slope is indeed observed experimentally when pCO_2 is varied at a carbon electrode, figure 5-15. With other electrolyte compositions, continued experiments have shown at least two additional characteristic potential difference - log pCO_2 slopes. These correspond to RT/4F and 4RT/4F. The former has been both theoretically and experimentally related to the presence of moisture in the electrolyte. The original 3RT/4F slope was theoretically derived for the case where the carbonate-oxide equilibrium is the predominant

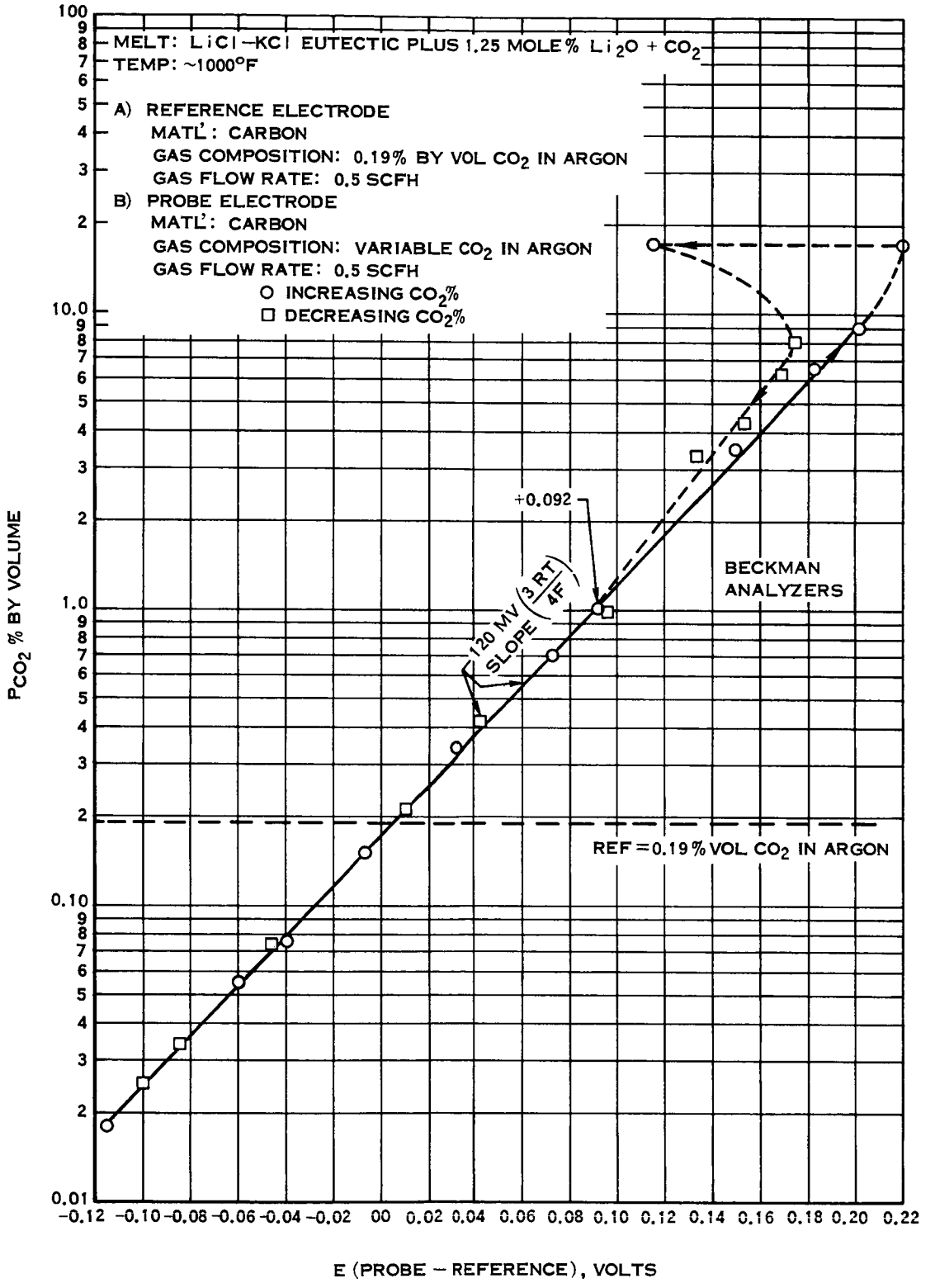


FIGURE 5–15. POTENTIAL – LOG P_{CO_2} RELATIONSHIPS BETWEEN CARBON ELECTRODES

5.2.1 (Continued)

electrolyte reaction when pCO_2 is varied. It can be shown that when moisture is present in such quantity as to make the relationship

$$O^{=} + H_2O \longrightarrow 2\ OH^{-}$$

predominate, or in other words, to make oxide ion concentration relatively independent of carbon dioxide pressure, a voltage coefficient of RT/4F is deduced. Thus, for a given water vapor pressure, the potential difference between carbon electrodes tends to be linearly proportional to the logarithm of the CO_2 pressure ratio with the RT/4F slope at low CO_2 pressure but changes to the 3RT/4F slope at higher pressures.

Reproducible slopes of 4RT/4F have been consistently obtained over a wide range in a freshly prepared LiCl-LiF-Li_2CO_3 electrolyte when CO_2 pressure at one carbon electrode was varied from 0.05% to 100% by volume. When this system was purged with CO_2 and dry argon, and then lithium oxide added until both moisture and CO_2 pressures were substantially lowered, the 3RT/4F slope was once again obtained. It is believed that the 4RT/4F slope is characteristic when gas evolution is occurring at the variable pCO_2 electrode, but adequate theoretical justification has not been established.

Thus it is inferred that the ratio of carbonate to hydroxide ions at the cathode determines whether pure carbon deposition is favored, or whether gas evolution or other interfering process prevails. It is also inferred that the ratios of carbonate and hydroxide ions to oxide ions, reflecting absolute partial pressures of carbon dioxide and water, determine whether cathodic gas pressures will be sufficiently high to generate gas bubbles. Accordingly carbon reference and variable pCO_2 electrodes have been employed to set electrolyte composition and conditions to favor carbon deposition, as indicated by exhibition of an appropriate slope before and during electrolysis, and to monitor conditions prevailing at the cathode.

5.2.2 Electrode Materials

Early experiments showed that under similar electrolysis conditions, graphitic carbon coatings could be obtained on nickel, on AISI stainless steel, on cast iron, on cobalt, and on manganese, while no coatings or non-adherent coatings were obtained in attempts to deposit on titanium, tungsten, copper, silver, platinum, gold, and carbon. Similarities in the crystal form of the carbides of each of the successful substrates, all of which were geometrically compatible with the graphite structure and involved low heats of formation (readily reversible reactions) suggested an associated catalytic action. Since that time, however, graphitic carbon has been obtained in repeat runs on tungsten and graphite substrates when greater control was exercised over electrolyte composition, pCO_2, and pH_2O. It would appear that the original successful substrates more likely owed their successful performance to a capacity to buffer oxide, carbonate, and hydroxide ions in a proper relationship.

5.2.2 (Continued)

Furthermore, as soon as these substrates became coated with carbon, such capacity was lost and interfering processes such as gas formation prevailed. In any event, at this time, nickel and carbon are considered preferred cathode substrates, since these have shown the least tendency to contaminate the electrolyte and interfere with the deposition process.

A comparison of nickel pretreatment procedures showed no major variation among acid etch only, an anodic alkali treatment (aqueous bath) followed by an acid etch, vapor blast, or a brief anodic etch period in the electrolyte itself. Deposits on both hard and soft nickel (electroplated in aqueous plating baths) whereby an altered surface nickel orientation was anticipated, displayed no noticeable difference in carbon plating pattern or adhesion. Any reasonably clean nickel or carbon surface appears to suffice.

5.2.3 Electrode Configurations

Catholyte composition control to achieve high quality carbon has been achieved by exposure of the catholyte, in a thin film adhering to the electrode, to a gas phase with carefully regulated carbon dioxide and water vapor pressures. The initial technique for doing this involved axially oscillating the electrode while electrolyzing, so that the submergence depth was periodically altered. That portion of the electrode remaining in the electrolyte at all times generally exhibited a carbon purity of about 25 wt %, whereas that portion periodically exposed to the gas phase reached purities well over 90%, depending on the constitution of the gas phase.

The oscillating cathode inherently requires that the tip be submerged in the electrolyte at all times to conduct the current. This results in a substantially lower purity carbon deposit at the tip, figure 5-16. This difficulty was later overcome through the use of a cathode in the form of a rotating vertical disc, where any selected portion of the disc was immersed in the electrolyte for a small faction of the rotation cycle, figure 5-17. Various gear and chain driven rotating disc configurations were tried; all had a high seizure rate due to buildup of electrolyte salts in the area of the rotating shaft supporting the disc. The salt buildup is believed due to the excessive heat loss through the drive mechanisms tried, which cooled the shaft sufficiently to freeze the salt. Improved designs are believed feasible but have not been tested.

Diminution of the bulbous tip deposit has been achieved alternatively by a technique making use of cyclic complete withdrawal of the electrode from the electrolyte, so that the electrolysis occurs only when the electrode is in the submerged position. This is accomplished by oscillating either the electrode or the electrolyte periodically to cover and uncover the entire electrode surface. Two separate cathodes, cycled out of phase, are employed so as to sustain a constant cell current. This system is reported on further in Part II of this report, and has thus far demonstrated highly favorable carbon purities and current efficiencies.

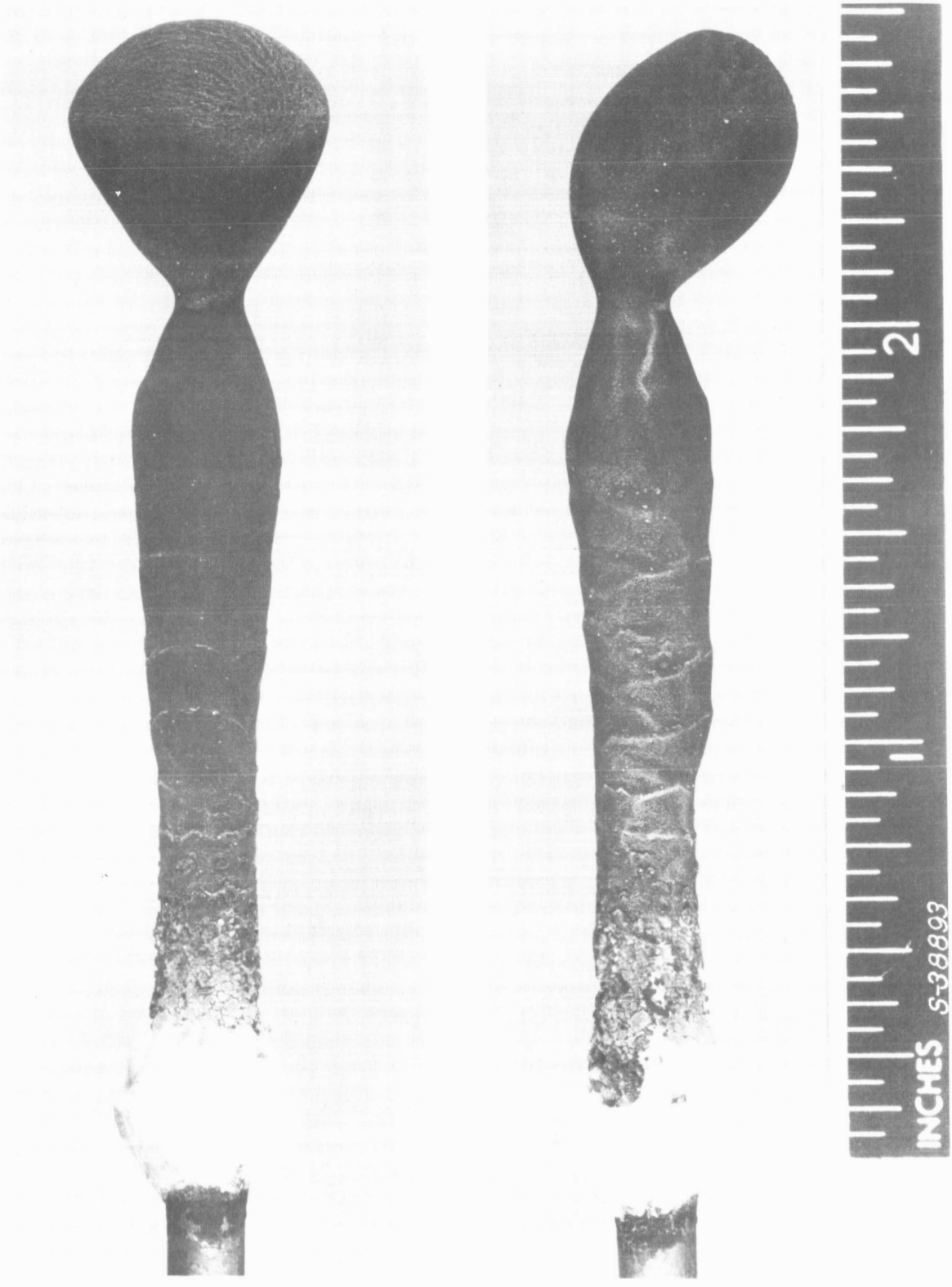


FIGURE 5–16. CARBON DEPOSIT ON AXIALLY OSCILLATED CATHODE

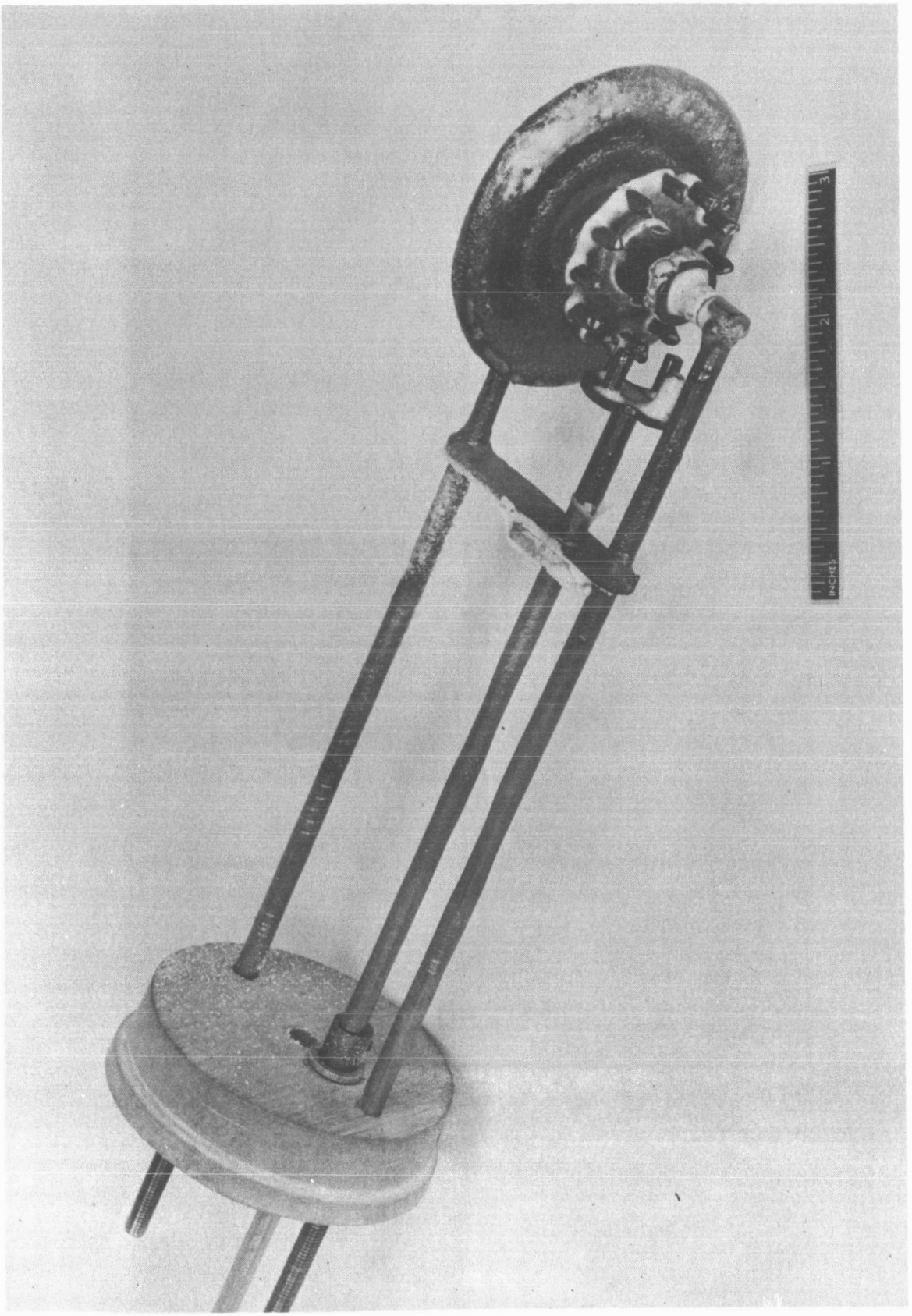


FIGURE 5–17. CARBON DEPOSIT ON ROTATING VERTICAL DISC

5.2.3 (Continued)

Another cathode configuration utilized the principle of the gas lift pump to deliver and circulate electrolyte as a thin film over a suspended electrode. The device, diagramatically illustrated in figure 5-18, delivered electrolyte up an annular space inside an alumina tube to cascade as a thin film over a cathode fixed to the outer wall of the tube above the bulk electrolyte. Voltages required for operation of this configuration were higher than those observed with oscillating or rotating electrodes. Uniform deposits were not achieved because it was too difficult to avoid electrolyte channeling along the cathode. Also great difficulty was encountered in the tendency for carbon to bridge across the alumina and contact the electrolyte below.

Most recently, high speed rotation of completely immersed cathodes has been evaluated for effect on carbon purity and current efficiency. Among cathode configurations evaluated have been nickel rods bent into rectangular, T bar, S, and helical shapes, flat nickel plates, airfoil contoured plates, and cylindrical drums. An S-shaped cathode is shown in figure 5-19. Spin speeds were varied from zero to 700 rpm. Effect of rapid rotational oscillation through a 110-degree angle was also studied. Additional experiments were carried out wherein an impeller was utilized to rotate electrolyte rapidly within a cylindrical cathode which was tightly fitted into an open-bottom alumina shield.

In the following discussions, differentiation among the various cathode modes of operation will be indicated by the terminology: stationary (complete submergence); gas phase deposition (thin film-periodic submergence); and spinning (complete submerger

5.2.4 Carbon Purity and Efficiency

Carbon deposited on a stationary electrode (simply immersed in the electrolyte) at 100 ma/cm^2 in a carefully conditioned electrolyte exhibits a purity of only a few percent, although current efficiency is measured at near 100%. Under identical electrolyte conditions, a gas phase deposit exhibits a purity of 82%; however, with a current efficiency reduction to 90%. A spinning electrode (450 rpm) under similar circumstances produces carbon that is at least 93% pure but with efficiency just above 50%. The purities and efficiencies obtained in all cases are amenable to control by adjustments in deposition current density, electrolyte temperature, spin rates, and so on, so that the major portion of our recent cathode studies has involved optimizing conditions for concurrent maximum purity and maximum efficiency. Since it has not been possible to improve the overall purity of reasonably thick stationary cathode deposits (a mil or so of dense carbon can be achieved at the cathode surface) to much over 15 or 20%, the data which will now be presented cover only gas phase and spinning cathode deposits.

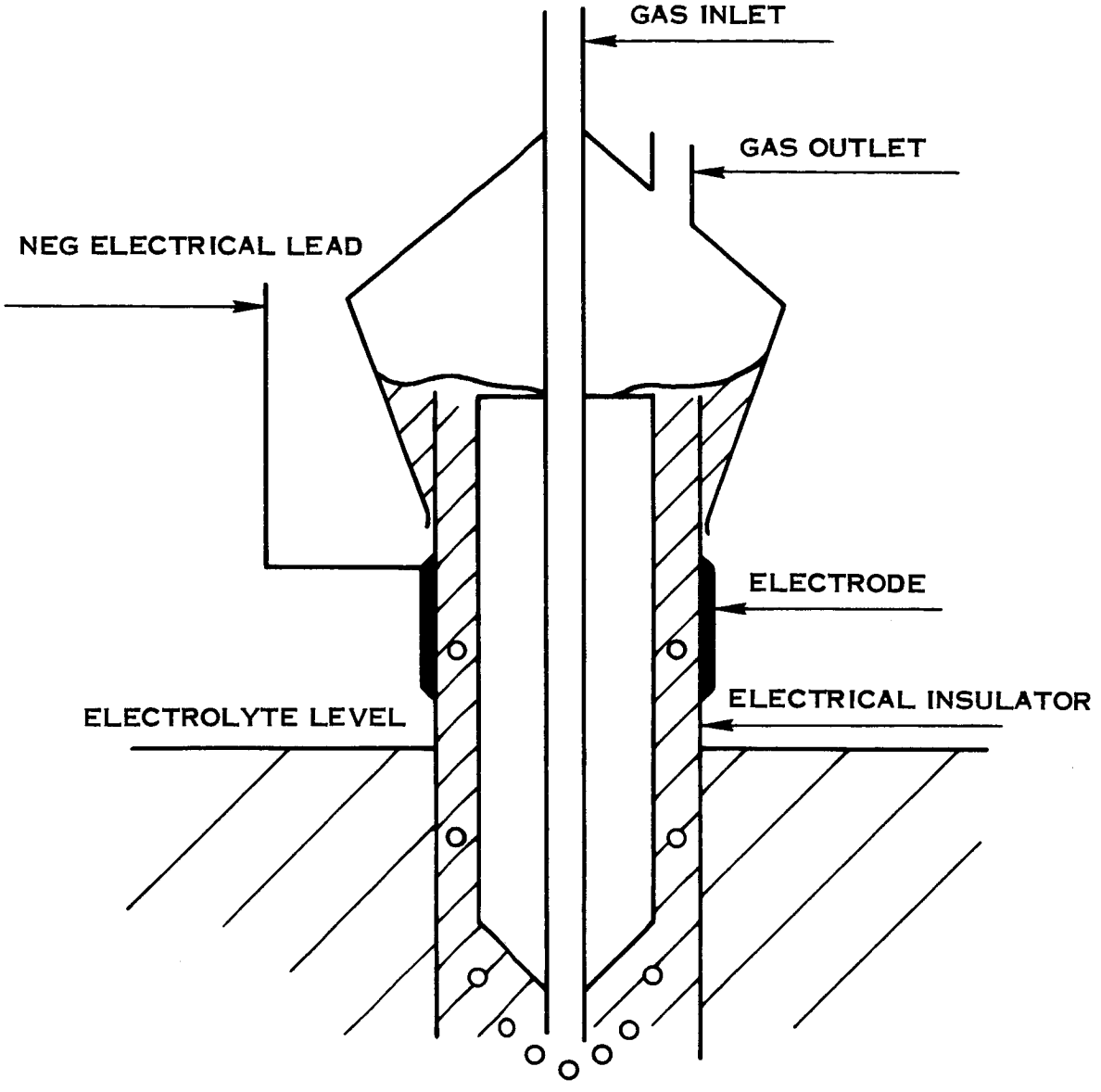


FIGURE 5–18. SCHEMATIC : GAS LIFT PUMP CATHODE ASSEMBLY

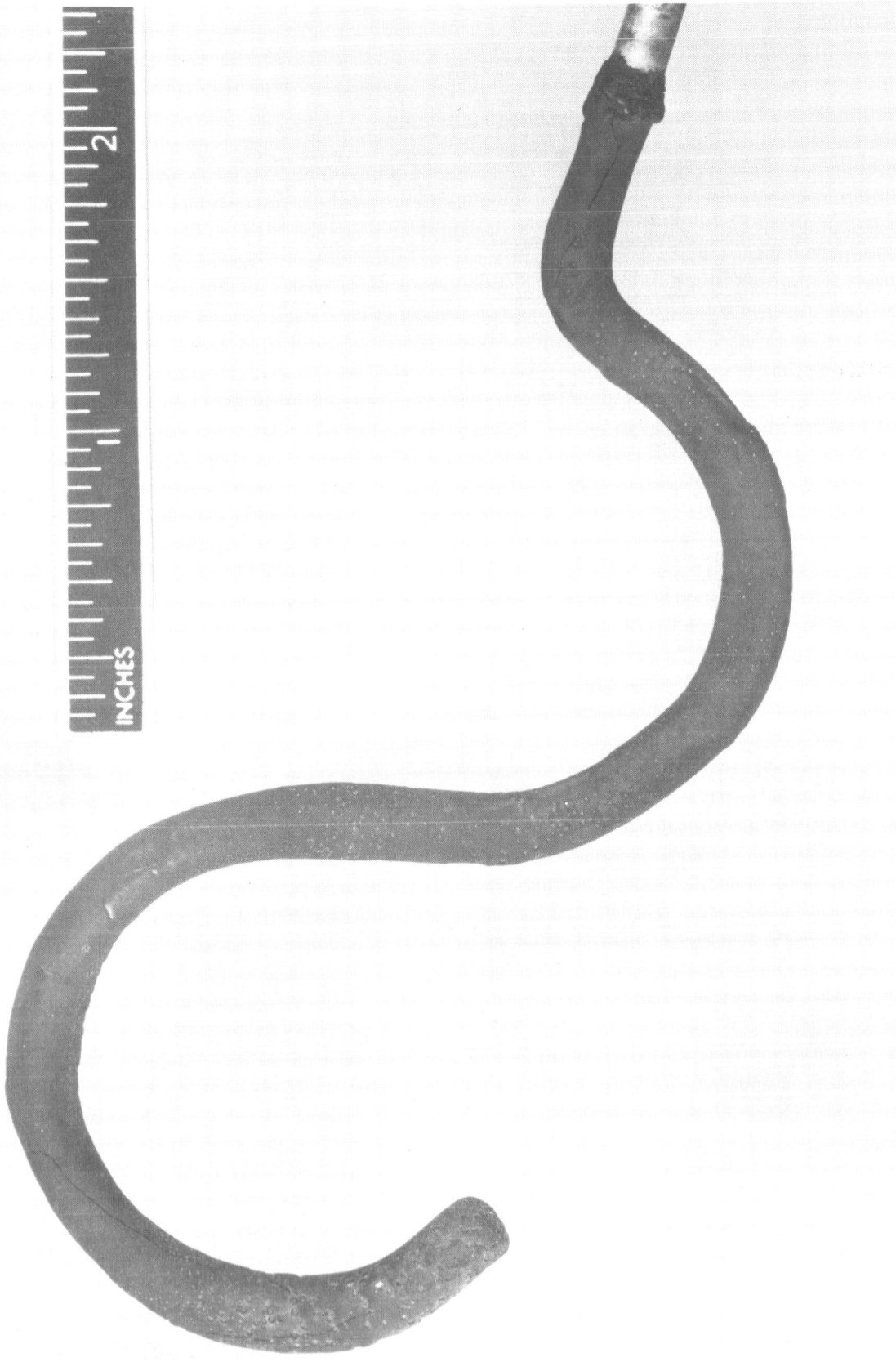


FIGURE 5—19. CARBON DEPOSIT ON S SHAPE SPINNING CATHODE

5.2.4.1 Gas Phase Deposits

The bulk of the data on gas phase carbon deposits has been obtained utilizing an axially oscillating nickel rod where only the extreme end (sharpened to a point) is in contact with the electrolyte reservoir at all times. Results with the partially submerged rotating disc duplicated those with the oscillating electrode in the limited number of test runs made. Rapid growth of carbon along the alumina in gas lift pump cathode devices resulted in forming a conductive path to the main electrolyte, where carbon growth was controlled, so that valid data were not obtained from that type of system.

Axial oscillation of the cathode has inherent in it the probability for accompanying periodic fluctuations in temperature. Such temperature cycling has been experimentally studied as a function of electrode oscillation rate (cycles per minute) and altered dwell patterns (percent of cycle out of the electrolyte), to ascertain actual gas phase electrode temperatures and breadth of fluctuations.

Over the range of cathode oscillating rates (1 cycle per minute to 7 cycles per minute), oscillating patterns (50% to 80% of the cycle in the up position), and bulk electrolyte temperatures (1080 to 1220°F), the temperature variation in the gas phase electroplating zone, measured on the cathode, was found as a rule to be about $\pm$ 15 degrees F, and the average temperature was generally within 15 to 20 degrees F of the bulk electrolyte temperature. Therefore temperatures, which will be noted in subsequent sections of this report when pertaining to gas phase deposits, are bulk electrolyte temperatures but closely represent that of the gas phase portion of the electrode.

Carbon purity and current efficiency determinations on gas phase electrodeposits have been made as a function of electrolyte temperature, cathode current density, and gas phase pCO_2 and pH_2O. Purity determinations of the cathodic carbon were made simply by crushing the deposits and boiling them in a solution of 4 parts HCl (37% wt) to 1 part distilled water for a period shown to produce no weight change in successive boilings when samples were dried and weighed. In order to obtain current efficiency data for such a system as this, where oscillation of one of the electrodes might readily result in current-voltage fluctuations (in practice these prove slight), it was necessary to employ an in-line coulometer to measure the time integral of current.

The quality of carbon obtained on a dipping electrode is illustrated in figure 5-20. This photograph was taken after boiling the cathode section in the HCl solution. The lighter grey portion is the electro-deposited carbon. It is generally smoother and more uniform looking than spectrographic grade carbon such as was used as a plating substrate for the sample shown. However, both spectrographic carbon and the electrodeposited carbon exhibit a specific gravity of about 1.8. The purity of gas phase plated carbon varied widely in these series of tests, up to a maximum of 97% by weight.

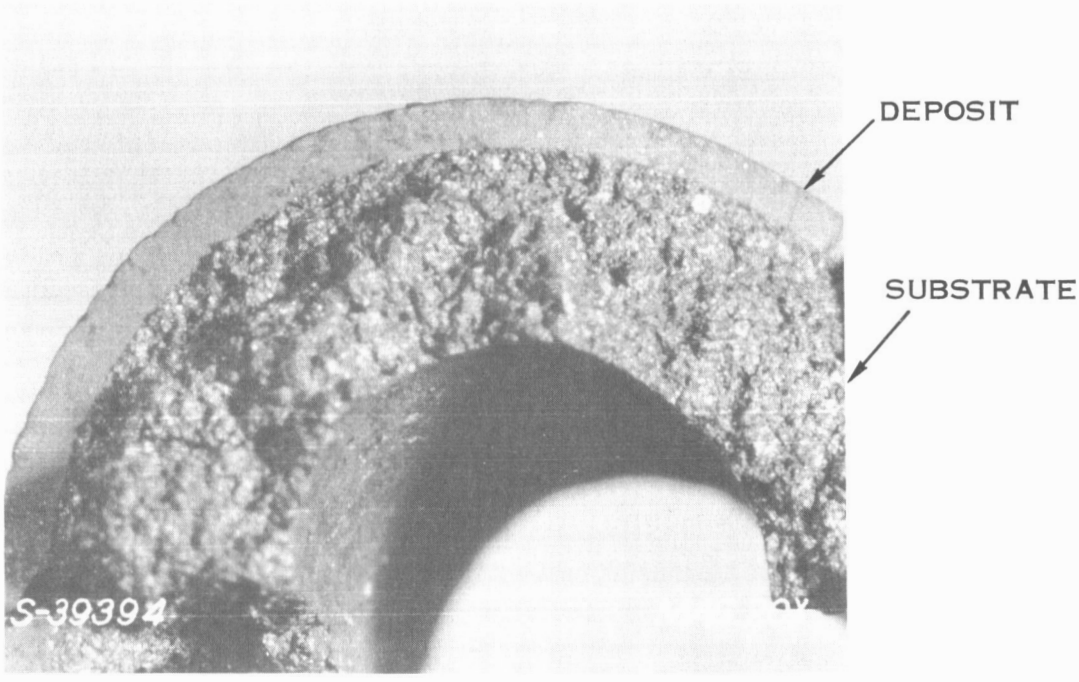


FIGURE 5–20. CARBON PLATE ON SPECTROGRAPHIC CARBON ELECTRODE

5.2.4.1.1 Effect of Temperature

Over the range of temperatures studied, 1050 - 1220 degrees F, carbon purity increased with temperature, figure 5-21. This is believed due largely to the reduction in viscosity of the electrolyte, which decreases salt inclusion in the deposit by permitting greater drainage. Improved oxide solubility would also be anticipated. It is possible also that the thickness of adhering film exposed to the gas phase is considerably lessened so that equilibria are more readily achieved. Current efficiency decreased with increasing temperature, reflecting an increase in cathode CO formation and carbon spalling.

5.2.4.1.2 Effect of Current Density

Determinations of carbon purity and current efficiency as a function of cathode current density showed a drop-off in carbon purity at current densities over 200 ma/cm^2 and at the same time an increase in current efficiency to 100%, figure 5-22. These results are believed due to the accumulation of lithium oxide in the deposit at the higher current densities. This lowers purity but at the same time depresses catholyte pCO_2, which in turn decreases the loss of carbon through CO formation and spalling, resulting in increased efficiency.

5.2.4.1.3 Gas Phase CO_2 and Water Vapor Pressure

Carbon purity has been found to increase as system CO_2 pressure is increased; at the same time current efficiency tapers off only slightly, with increased CO formation evident, figure 5-23. Initial increases in water vapor pressure, from -40 degrees F up to -5 degrees F dew point, showed no significant effect on carbon purity or current efficiency. When dew point was raised above zero degrees F, attrition and flaking of the deposit became so considerable as to render deposit analyses unreliable. After exposing the system to the higher humidities for slightly over one week's testing, it was not possible to return directly to adherent deposits by simple water vapor pressure reduction to about the -5 degrees F dew point, as was achieved previously. A chemical analysis of the electrolyte at that time indicated a buildup in hydroxide ion concentration to somewhat under 2 wt. %.

There was some indication of a minor improvement in carbon quality when current density was increased - perhaps owing to a local increase in oxide and corresponding reduction in pH_2O in the vicinity of the cathode. Lithium oxide additions to the electrolyte failed to produce further significant improvements in the carbon deposit. The general failure to produce acceptable deposits with oxide addition was attributed to a simultaneous depression of electrolyte pCO_2 so that the ratio of pH_2O and pCO_2 was still inappropriate for achieving a high quality deposit.

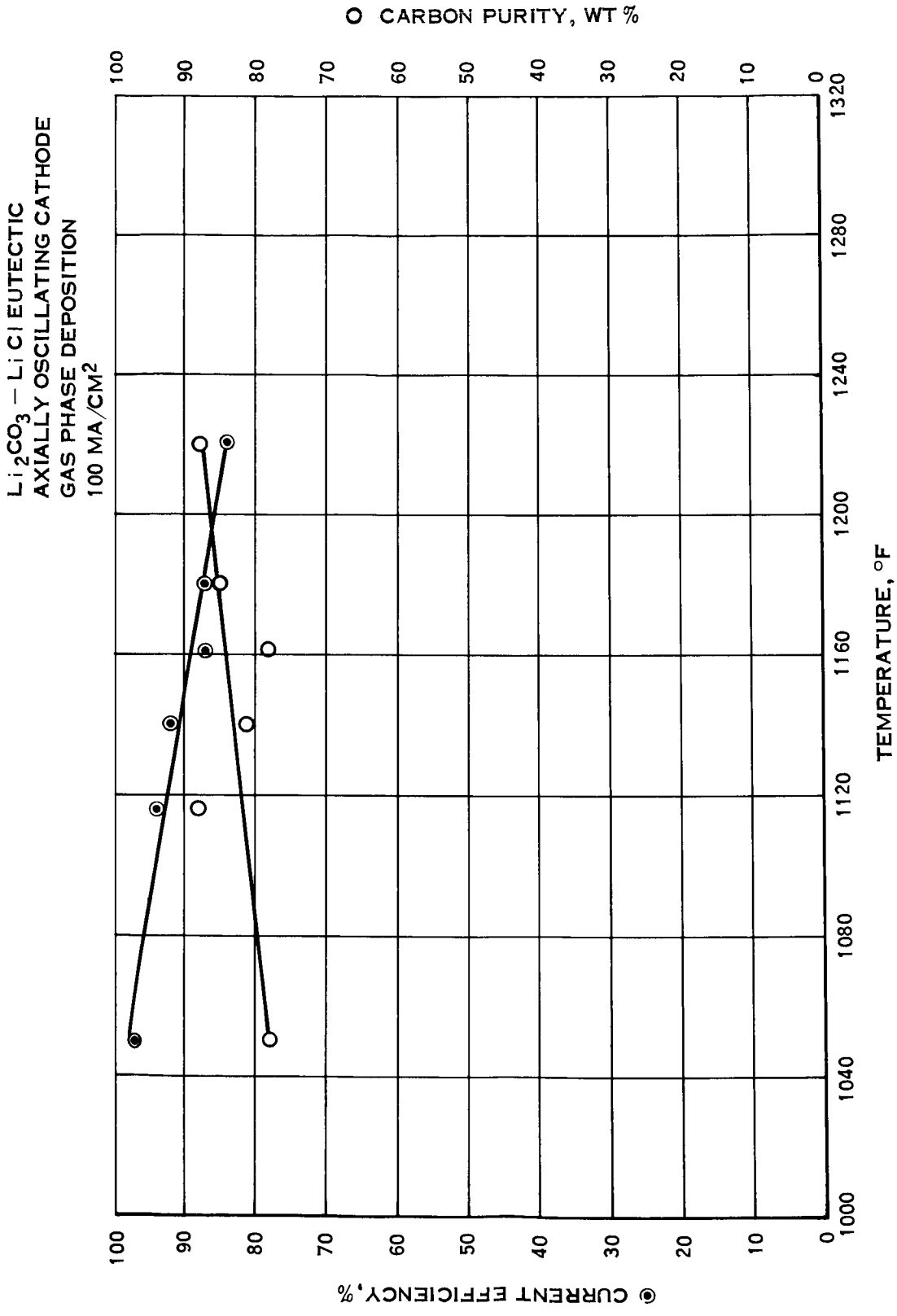


FIGURE 5–21. INFLUENCE OF TEMPERATURE ON CARBON PURITY & CURRENT EFFICIENCY

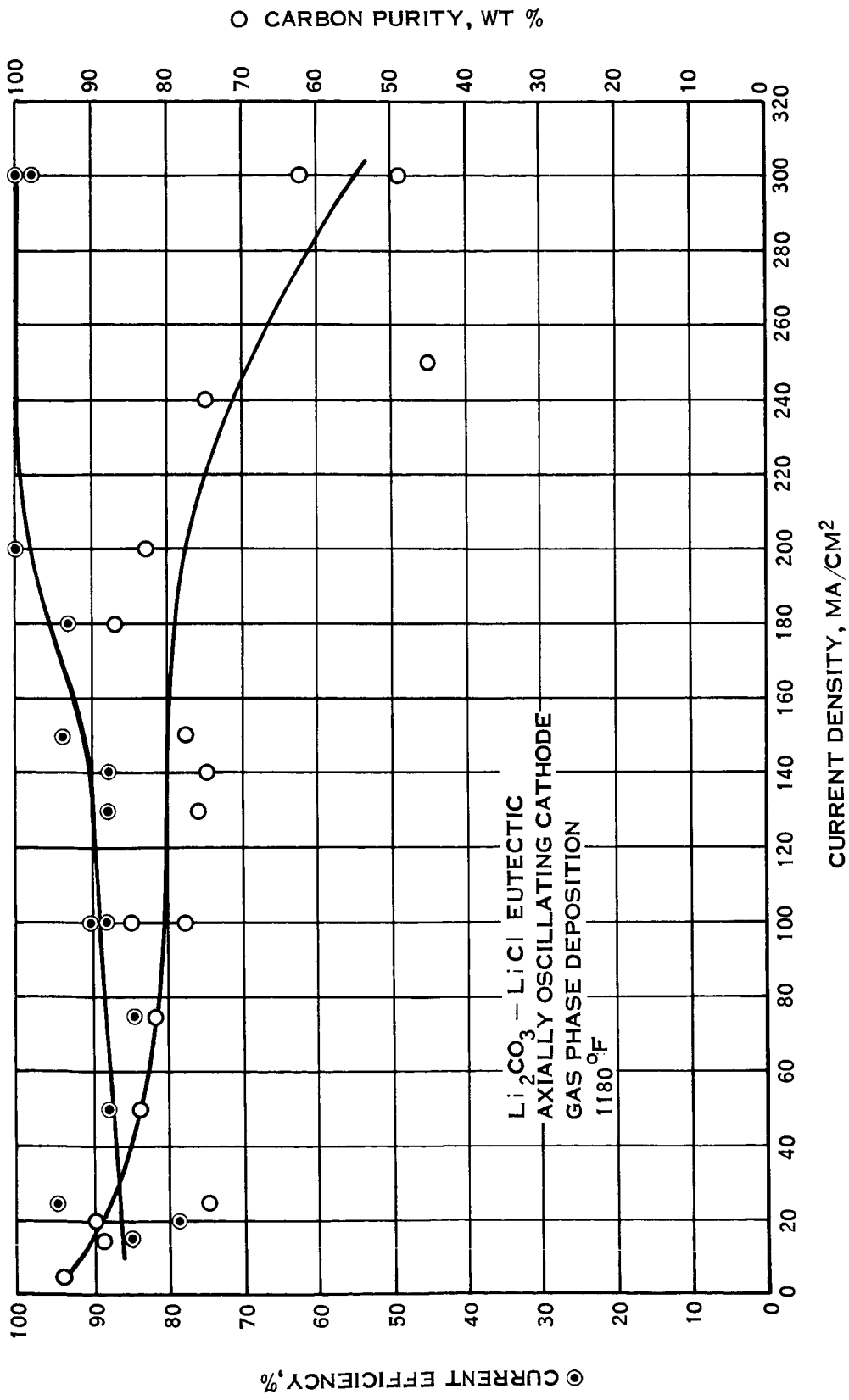


FIGURE 5–22. INFLUENCE OF CURRENT DENSITY ON CARBON PURITY & CURRENT EFFICIENCY

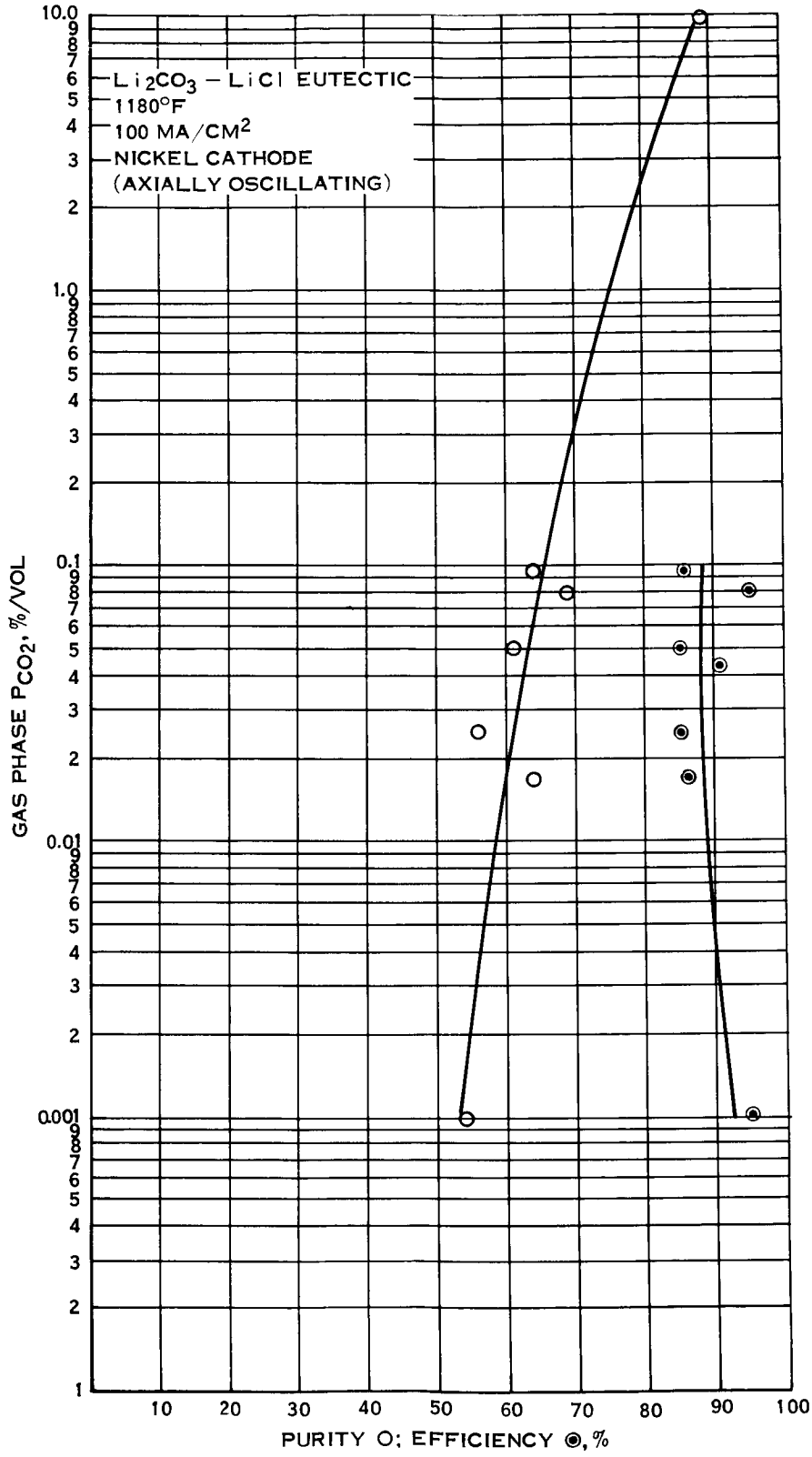


FIGURE 5–23. EFFECT OF GAS PHASE P_{CO_2} ON CARBON PURITY & CURRENT EFFICIENCY

5.2.4.1.3 (Continued)

In a complementary line of investigation, pH_2O was maintained constant at a selected low dew point (about -20 F) while simultaneous additions of lithium hydroxide and lithium oxide were made to the system. In this case flaky carbon deposits became evident when electrolyte hydroxide concentration reached just above 0.5 wt %. Again such increase in hydroxide and oxide resulted in greatly suppressed electrolyte pCO_2. As a result of this work, subsequent experimental work has involved a strict limitation of catholyte hydroxide ion concentration in order to work at the lower carbon dioxide pressures (0.01 to 0.05 vol %), which are of current interest for the system scrubbing function.

5.2.4.2 Spinning Cathodes

A systematic study has been made of cathode spin rate and current density as these affect carbon purity and current efficiency. In preliminary runs, carbon quality was shown to be as critically dependent upon electrolyte constitution (reflected in equilibrium carbon dioxide and water vapor pressures) as were previous gas phase deposits (same range of pressures required). At higher than optimum CO_2 partial pressure (greater than 0.05%/vol), a loose deposit formed, part of which flaked off during deposition to form soot in the electrolyte. At optimum CO_2 (between 0.01 and 0.05%) a dense deposit was obtained (over 90%/wt purity). Thus current successes in obtaining high purity carbon by spinning the cathode, when compared to failure to do so much earlier in the program, are confirmed to result from selection of a more optimum electrolyte enabled by a greater understanding of electrolyte equilibria.

At a cathode spin rate of 470 rpm, current density was varied from 10 ma/cm^2 to 1200 ma/cm^2. The results are shown in figure 5-24. From 10 to 50 ma/cm^2, purity increased from 27 wt % to above 90% and stayed at this level beyond 200 ma/cm^2, when it gradually tapered off to 72% at 1200 ma/cm^2. Current efficiencies, however, were only about 50% at the lower current densities, owing in good part to attrition of deposited carbon in the spinning process. Above 300 ma/cm^2 current efficiency rose steadily till it reached 80% at 1200 ma/cm^2.

At the same current density of 200 ma/cm^2, when spin rate was varied from 600 rpm to 100 rpm, efficiency increased from 40% to 100%. At the same time, however, purity decreased from 96% at 600 rpm to 67% at 100 rpm. These results are shown in figure 5-25.

It has not yet been possible to couple satisfactorily high current efficiency with the high carbon purities obtainable using spinning electrodes (over 96%). The bulk of the difficulty appears to be due to the attrition of carbon at the cathode surface and/or the diffusion of electrodeposited lithium away from the electrode to react with carbonate to produce isolated carbon particles. It has been possible to retain much

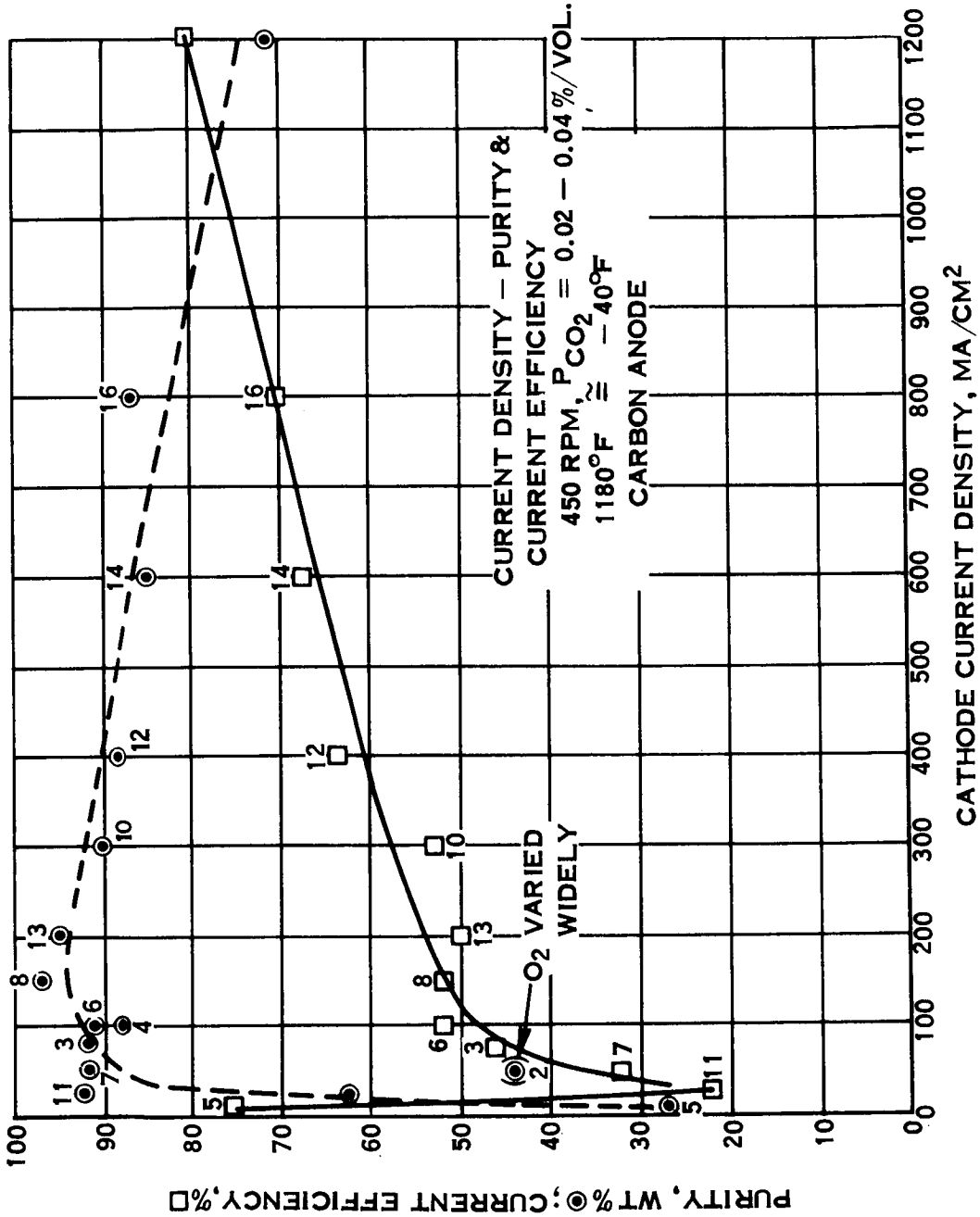


FIGURE 5-24. CARBON PURITY & CURRENT EFFICIENCY VS CURRENT DENSITY FOR SPINNING CATHODE

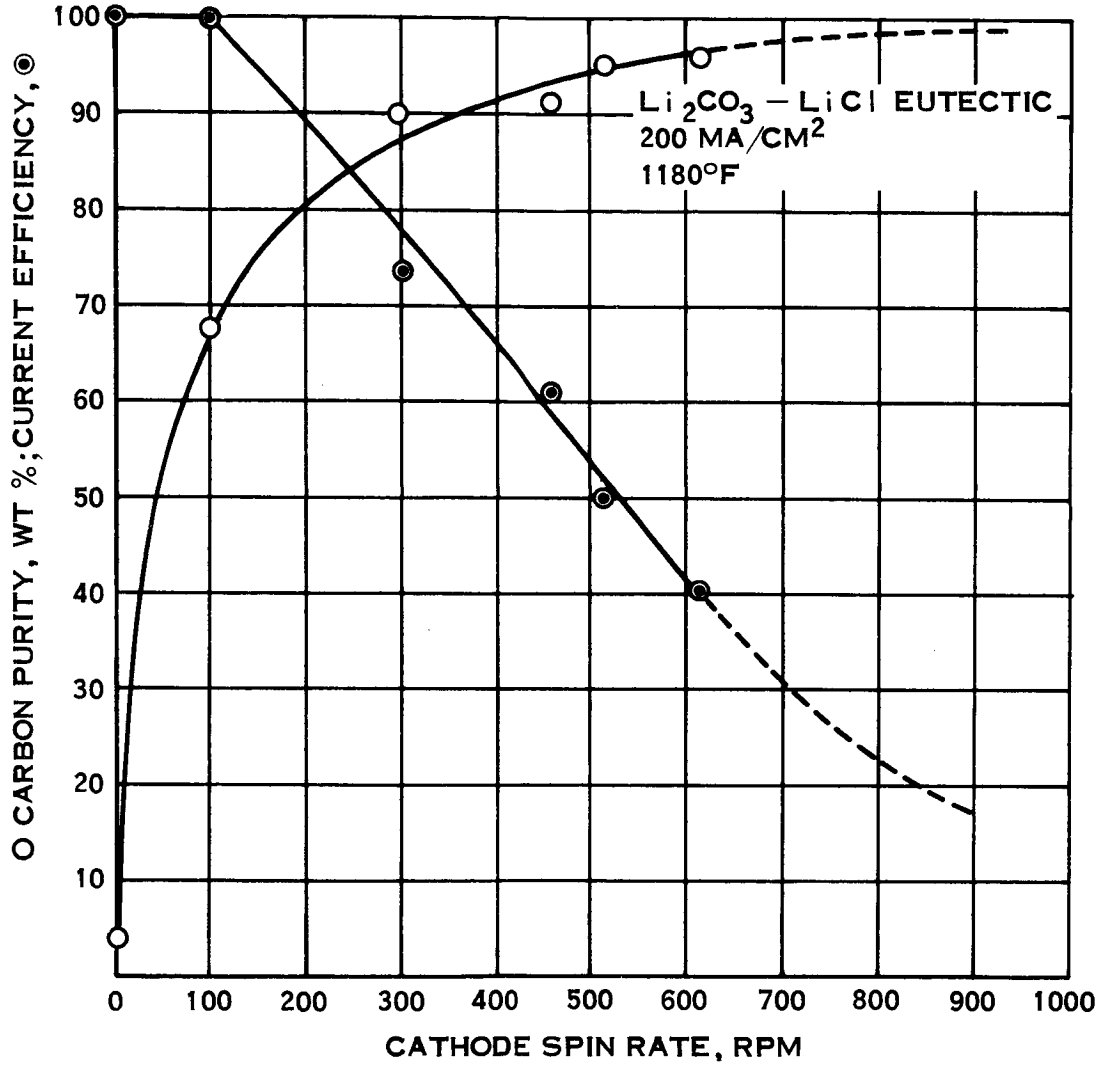


FIGURE 5–25. CARBON PURITY & CURRENT EFFICIENCY VS CATHODE SPIN RATE

5.2.4.2 (Continued)

of this loose carbon in a fine mesh nickel basket surrounding the cathode, but this does not seem practical for a working system. Aside from electrolyte salts which would be entrained and lost when discarding such loosely packed carbon, the screen would shortly become clogged with carbon and prevent adequate electrolyte circulation to the cathode.

A single test run has been made to investigate the quality of carbon obtained by circulating electrolyte past a stationary cathode. This was accomplished by spinning the electrolyte contained in an open-bottom nickel tube cathode, using an electrically driven impeller. The external surface of the nickel tube was shielded from the electrolyte by a close fitting alumina jacket. A dense carbon deposit began to grow on the inner wall of the nickel tube but soon spread over the alumina shield and eventually resulted in overall low quality growth.

5.2.4.2.1 Electrolyte Additives

Oxide formed at the cathode as carbon is deposited must be dissolved away in one form or another or it occludes with the carbon. A simple conversion to carbonate by reaction with carbon dioxide results in three carbonate ions where there was one originally; two excess carbonate ions must be transported away if the system contains anions other than carbonate, or continuous catholyte composition change occurs. When a mixture of alkali carbonates comprises the electrolyte (with or without halide), the smaller more mobile cations collect at the cathode and thereby change electrolyte constitution. For these reasons, various electrolyte diluents and oxide ion buffers which might favor the solubility and transport of oxide from the cathode have been studied. These tests were run using rotating cathodes primarily, with controlled pCO_2 and pH_2O.

5.2.4.2.1.1 Halide Diluents

Of the halides only chloride and fluoride have been tested extensively. Bromide had been only briefly put into test when noxious vapors leaving the electrolyte made further testing unattractive. Similar disagreeable vapors would be expected from the iodide, so this has not been evaluated at all. Under comparable conditions of electrolysis, higher purity carbon deposits were consistently achieved with the chloride diluent than with the fluoride (e.g. 90% compared to 40%). Purity in mixed fluoride and chloride systems fell somewhere between. Analyses indicate the impurity to be oxide rich electrolyte.

.2.4.2.1.1 (Continued)

Chloride Systems

A plot of carbon purity and current efficiency as carbonate-to-chloride ratio is varied is shown in figure 5-26 where a spinning cathode was utilized. Note the improvement in both carbon purity and efficiency with increasing halide dilution until alkali metal begins to accumulate and both purity and efficiency begin to fall off. The low purity at higher carbonate concentration is due to decreased oxide solubility and deviations from eutectic composition in the catholyte resulting in "freeze-out". The low current efficiency is in great part due to carbon attrition as was already described, although it was not possible in selected tests of this particular series to achieve a reasonable materials balance when attempts were made to trap lost carbon. There is always the possibility that the missing efficiency may result from some other reduction process occurring at the cathode, not leading to carbon formation, although no spurious reactions have been recognized, and it has not been possible to identify any new chemical species in the electrolyte after sustained electrolysis.

The problem of reduced current efficiency has been much more severe with rotating cathodes than with dipping cathodes. This is evident from figure 5-27 which compares deposits from each type cathode. Deposits closest to the upper right-hand corner best approach targets requirements. It will be noted that dipping cathode deposits more closely approach this corner.

Cell Mass Balance

Cell mass balance studies were carried out over continuous periods of electrolysis extending from 6 to 14 days to determine whether or not rotating cathode current efficiency varies with time, and whether missing carbon might be accounted for in system gaseous outputs. Accumulated data are presented graphically in figures 5-28 and 5-29 which represent a typical 14-day test. In these runs, using a lithium carbonate - lithium chloride eutectic electrolyte, carbon purity varied between 75 and 85 wt. %, and current efficiencies were of about the same order, 75 to 85%. No significant changes were apparent with time.

It is seen from figure 5-28 that oxygen gas was being produced at the anode at near 100% current efficiency for the bulk of the test period. Early inefficiencies were due to oxidation of nickel contained in the new gold-nickel anode being used. Also evident from figure 5-28 is that the net carbon dioxide fed to the cell to sustain conditions during the test (input to the cell minus total output) was less than stoichiometric for oxygen produced. This discrepancy, coupled with low cathodic efficiency, indicates that an unidentified reduction process not resulting in solid carbon formation nor perhaps even involving carbon dioxide was competing with the main process.

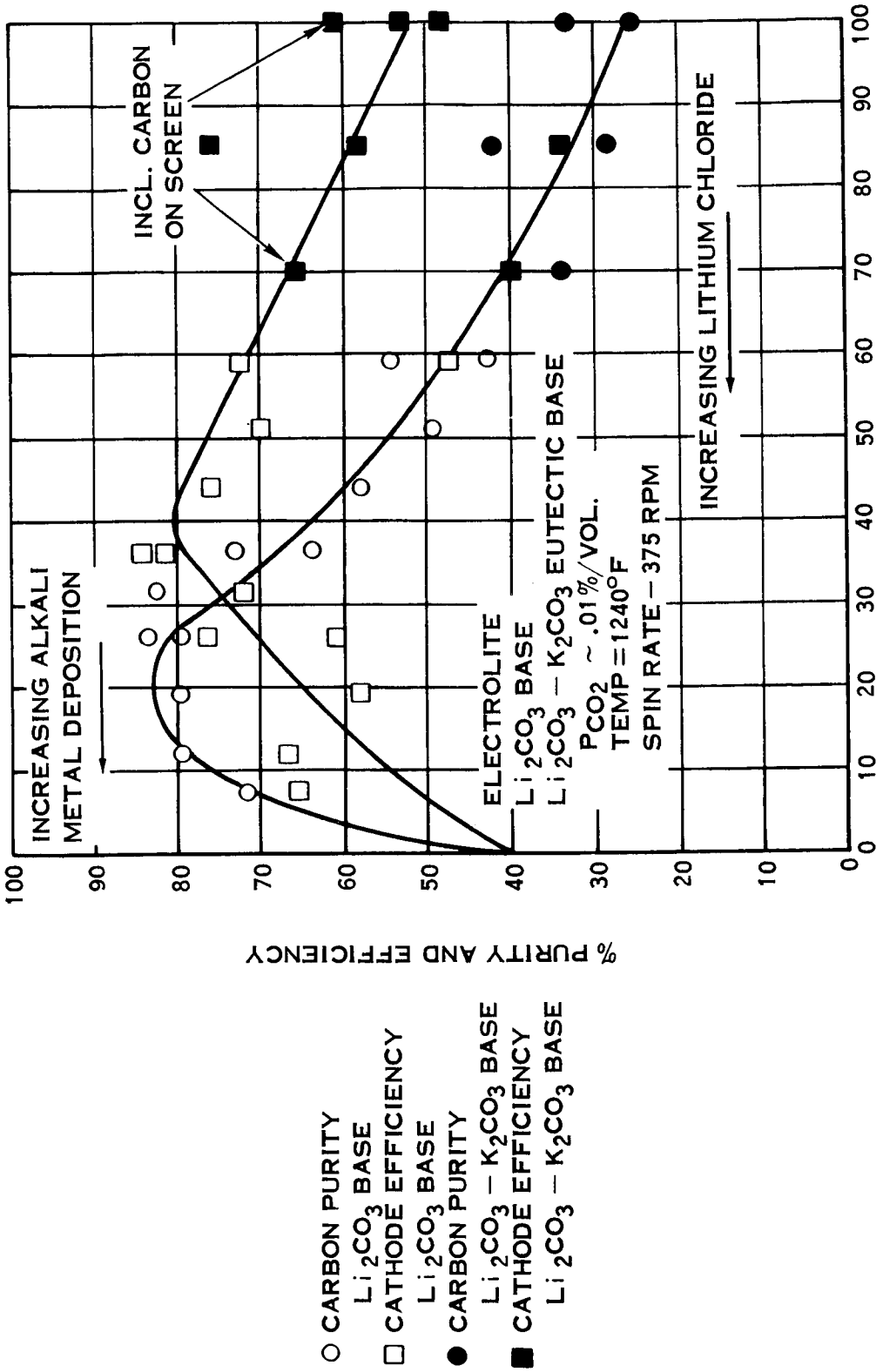


FIGURE 5–26. EFFECT OF HALIDE CONCENTRATION ON CARBON PURITY AND CURRENT EFFICIENCY

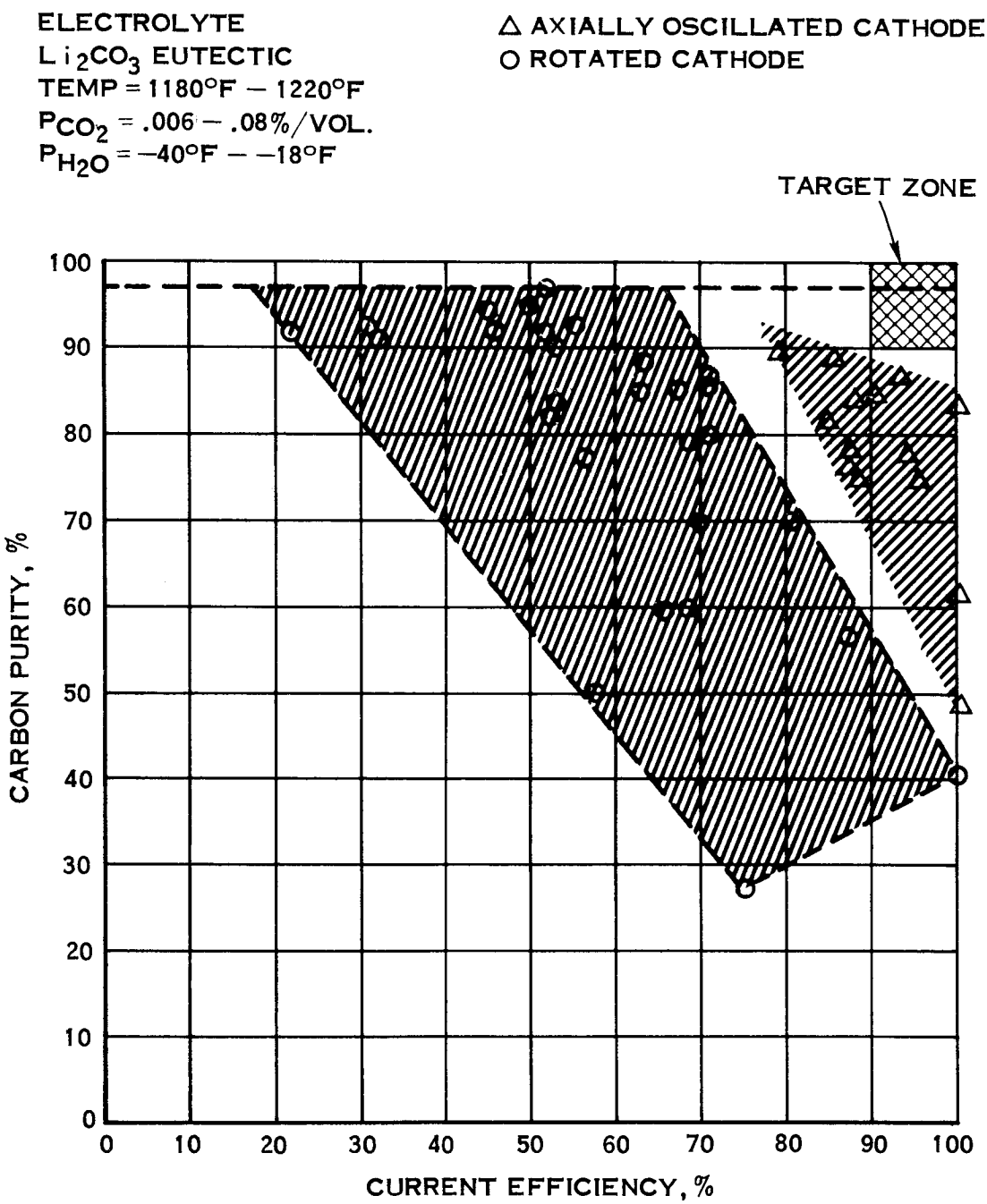


FIGURE 5–27. CARBON PURITY VS CURRENT EFFICIENCY FOR ROTATING AND AXIALLY OSCILLATING CATHODES

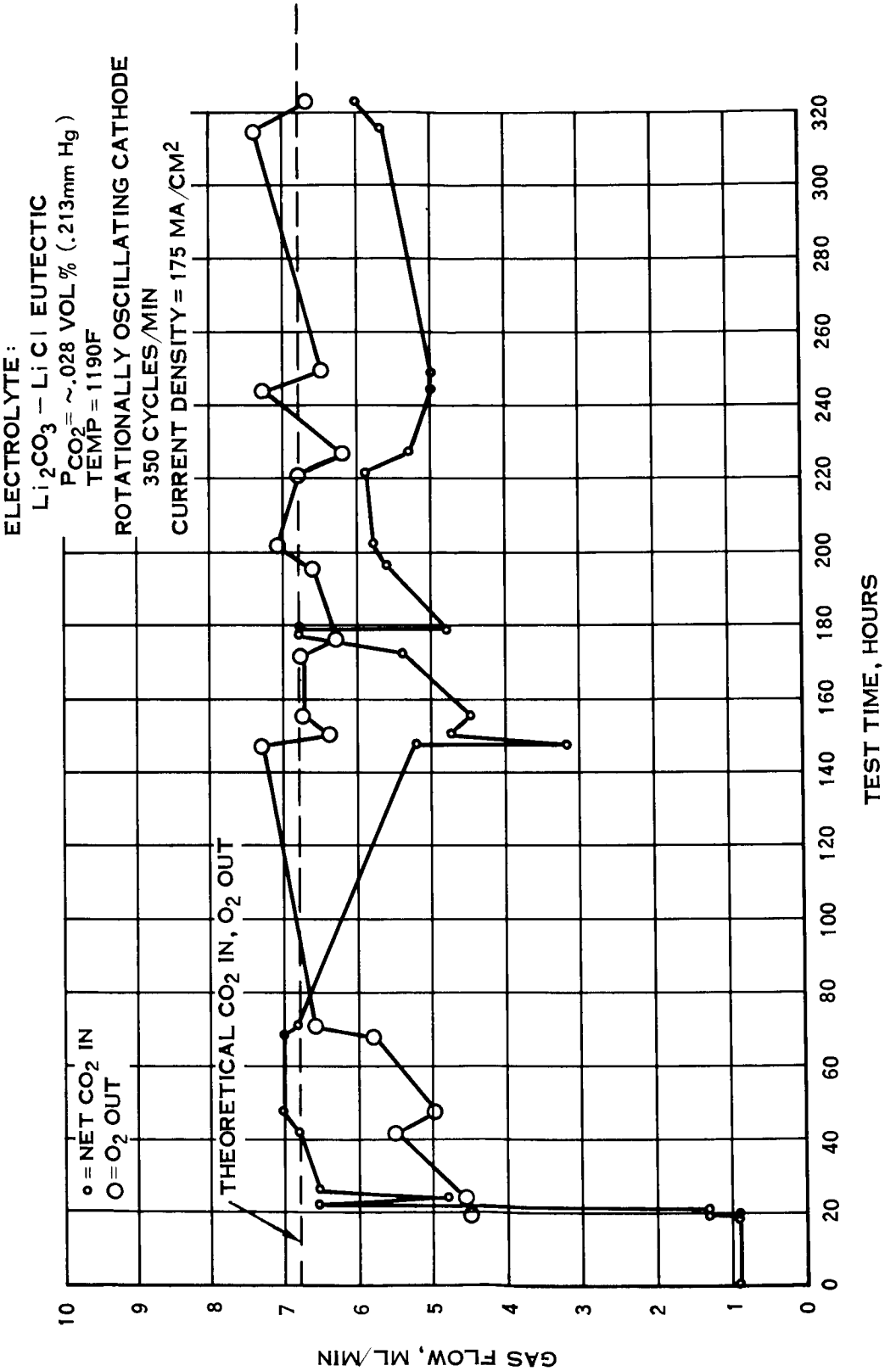


FIGURE 5–28. CELL MASS BALANCE STUDY
NET CO_2 IN ; O_2 OUT

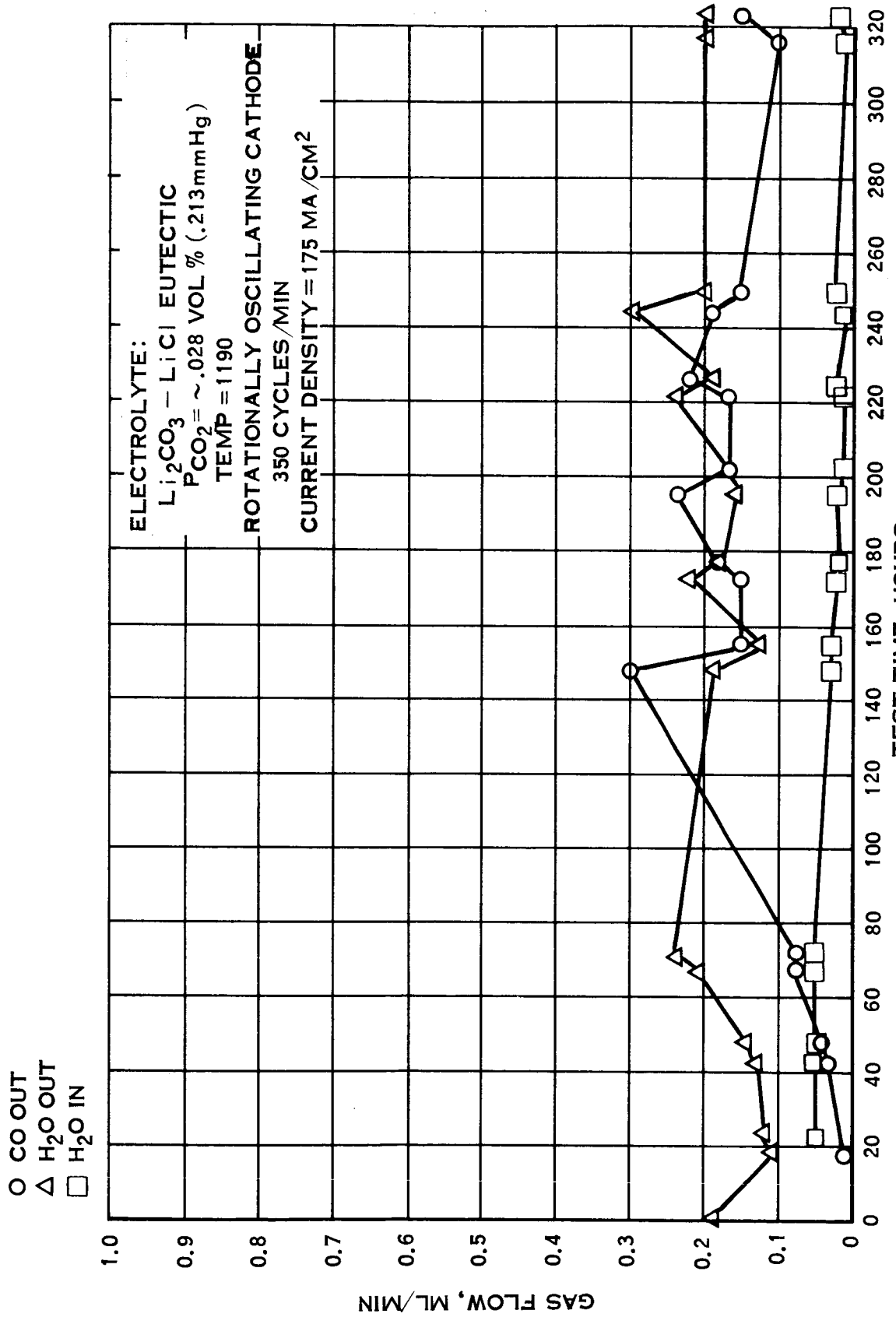


FIGURE 5–29. CELL MASS BALANCE STUDY: CO OUT; H_2O OUT; H_2O IN

5.2.4.2.1.1 (Continued)

Prolonged electrolysis, using X-ray diffraction, infrared spectroscopy, and chemical analysis techniques, failed to identify any new soluble carbon-containing species in the electrolyte and also failed to physically trap insoluble species. These failures reinforce the above preposition and suggest that the competing process might involve foreign species perhaps originating from cell materials of construction. This would also confirm the observation that under similar electrolysis conditions utilizing thin film-gas phase phenomena (where selective enrichment of the catholyte in carbon dioxide through preferential transport via the gas phase favors the carbon producing process) deposits are obtained at high efficiency. Finally, the most likely source for the balance of anodic oxygen, if not input carbon dioxide, would be ceramic materials.

The quantity of water vapor leaving the cell in the outlet gas stream, figure 5-29, exceeded the amount in the inlet stream for the entire period of the test and showed no indications of diminishing with time. The outlet moisture was not indicated to be dependent on electrolysis; however, its presence could also be related in some as yet unknown manner with the competing cathode process.

In this test, argon was used as a carrier gas for the carbon dioxide feed in order to permit scrubbing within a carbon container, a matter of convenience. The reaction between carbon and CO_2 yielded a small amount of carbon monoxide, shown as a constituent of the outlet gas in figure 5-29. Since this circumstance was peculiar to the scrubber configuration, it is not significant to the mass balance question, and, if air had been used as the carrier gas in a metal or ceramic container, no measurable level of carbon monoxide would have been produced. During this test the cathode region was sealed off but connected to a glycol manometer which confirmed that no gas was formed at the cathode, hence the CO observed was uniquely associated with the scrubber. The absence of gas craters and porosity in the carbon deposits also confirmed this explanation. In any event the quantity of CO observed would account for only a small fraction (1/10) of the carbon not found at the cathode.

Although a precise explanation of factors contributing to greater inefficiencies with rotating electrodes under certain circumstances cannot be given, it must be remembered that other electrolysis conditions and techniques are known which do provide high current efficiencies, so that in the present instance it is a case of satisfactory theory lagging somewhat behind the art.

5.2.4.2.1.2 Non-Halide Diluents

Since the presence of halide ions in the electrolyte detrimentally affects common anode materials (and therefore anode current efficiency and system life) electrolytes consisting only of carbonates or carbonate diluted with salts other than halides were more completely evaluated for quality of carbon deposited. As has already been

5.2.4.2.1.2 (Continued)

noted, electrolysis of a halide-free lithium and potassium carbonate electrolyte produced carbon deposits of less than 25 wt % purity. Two factors were shown to contribute to the occluded salt. First, there was a selective accumulation of lithium ions at the cathode (owing to a greater mobility than potassium ions) which raised the melting point of the catholyte so that there was local solidification, and second, the accumulation of oxide ions likewise raised the melting point and resulted in freeze-out. These factors were readily confirmed by chemical analysis. Behavior was similar in ternary and quaternary carbonate systems. Changes in other process variables such as current density, temperature, agitation, and so on, did not significantly increase carbon purity.

It is therefore believed that a major role for the halide diluent, when present, is to sustain a low melting point catholyte with high oxide solubility, hence a series of alternative melting point depressants were studied. Cathode deposits were obtained using eutectic or near-eutectic mixtures of these with lithium carbonate. Results of this study may be summarized as follows:

Lithium Molybdate - This salt formed a eutectic with lithium carbonate at about 50 mole % with a melting point of 600°C. The cathode deposit contained a mixture of molybdenum and carbon.

Lithium Vanadate (Vanadium Pentoxide) - An excessive amount of vanadium pentoxide was required to depress the system melting point to below 700°C. Under these circumstances practically all the CO_2 appeared to be displaced from the carbonate. Vanadium metal was electrolytically deposited at the cathode.

Lithium Phosphate (Ortho) - Lithium phosphate formed a eutectic (670°C) at 10 mole % lithium carbonate. Cathode deposits were of low carbon purity and could not be improved.

Lithium Borate (Meta) - A eutectic was formed at 50 mole % borate (660°C). As was the case with the phosphate, carbon purity was very low and could not be improved.

Lithium Nitrate - Electrolysis was carried out at just under 400°C in lithium nitrate with 5 mole % lithium carbonate added. An unidentified brown-black coating was obtained on a nickel cathode. Nitrogen oxides were evolved at the anode, hence this activity was curtailed as an unattractive direction of investigation.

It is worth a brief digression to discuss the "buffering" behavior of the above oxyanion diluents in regulating oxide-carbonate ratio by fixing excess oxide in the form of soluble compounds - phosphates, borates, etc. - capable of subsequent displacement by a finite CO_2 pressure to reform carbonate.

5.2.4.2.1.2 (Continued)

The previously noted effect of water vapor partial pressure on oxide ion concentration is an example of such a phenomenon which, by loose analogy with means for hydrogen ion control in aqueous solutions, has been considered a buffering action in fused carbonate systems. At a sufficiently high water vapor pressure, formation of hydroxide ions effectively limits the concentration of oxide ions achievable. However, although this effect may be viewed as a means for limiting oxide ion concentration at the cathode so as to prevent the tendency to exceed solubility limits (low melting point hydroxide formed), cathodic gas formation when hydroxide is present precludes effective use of water as a buffer. On the other hand, the same principle may be applied to other oxyanion forming species. The buffer need not be a volatile constituent, such as water. The primary requirement is only that a suitably stable anion be formed by combination with the oxide ion. One possibility is boric oxide (B_2O_3), which is highly soluble in the electrolytes under consideration and has been observed to react with the carbonate to release carbon dioxide. The oxide ion-boric oxide equilibrium may be represented as:

$$O^{=} + B_2O_3 \leftrightharpoons 2\,BO_2^{-}$$

It can be theoretically deduced that, as was the case with water, for high CO_2 partial pressure, or very low oxide ion concentration, the oxide ion concentration is inversely proportional to CO_2 pressure. At low pCO_2, the limiting value for oxide ion concentration is more greatly dependent upon the oxide ion-borate relationship.

Similarly, other additives may be considered as potential buffers - aluminum oxide forms an aluminate ion, silicon dioxide forms a silicate ion, nickel oxide forms a nickelate ion, and so on. However, no buffer, in the sense here discussed, has yet been found, as evidenced by the results noted above, which performs the desired function without undesirable side effects. Borate and phosphate result in low purity carbon deposits. Aluminate and silicate are insufficiently soluble except in fluoride electrolytes, where the respective oxides are ultimately occluded with carbon at the cathode. With all, CO_2-oxide buffering does not appear to occur at an appropriate CO_2 pressure level for an optimum carbon deposit or for system CO_2 scrubbing functions.

5.2.5 Cathode Assembly Design

Currently the alternative modes of cathode operation, i.e. gas phase (thin film electrolyte), fast spinning electrode, or fast circulating electrolyte, all remain as potential candidates for further development depending upon which best fits the overall cell concept with respect to anode and scrubbing functions. One requirement common to all these cathode types is a means for protecting the depositing

5.2.5 (Continued)

carbon from burning by oxygen gas either generated at the anode or introduced via the CO_2 scrubber. Experimental evidence to date indicates that a simple gas bubble barrier is sufficient, oxygen solubility and transport as solute in the electrolyte being too low to cause significant carbon deficiency. A second problem is cathodically generated gases such as CO which, although at low partial pressures, (50-200 ppm) must be reckoned with. It is possible to join cathodically produced gases with oxygen from the anode or scrubber in a sufficiently hot zone to reconvert them to CO_2 and H_2O. This would represent only a very small electrolytic inefficiency since the gas produced at the cathode represents only a small fraction of the current going to carbon production. Alternatively, if provisions were made to allow the catholyte to reach an equilibrium with the cathodic gases by entrapping (no net flow of gas is experimentally observed under these circumstances), or by closed circulation of the gases in the cathode area, rather than continually sweeping them away as in the case first described, then current efficiency lost to gas production could be made negligible.

Most uniform carbon coatings have thus far been obtained on the rotating vertical discs partially submerged in the electrolyte. Vertically oscillated electrodes show greater thickness and correspondingly less purity with increasing exposure of a given part of the electrode to the bulk electrolyte, resulting in a pear-shaped deposit. Cathode configurations used in spinning tests show a wide variation in carbon thickness between leading and trailing edges with a thinner and denser coating at the leading edge and extremely thick, slightly less pure growths along the axis of rotation. Since these are evidently related to fluid flow patterns and attendant variations in catholyte composition, cathode shapes more suitable to uniform flow patterns and deposits should be possible although these have not yet been demonstrated. As was noted above, the possibilities offered by a stationary electrode and circulating electrolyte have not yet been pursued experimentally.

5.2.6 Process Monitoring and Control

Considerable success has been achieved in relating cell polarographic information to processes occurring at the cathode. It has been consistently possible to distinguish, on current-voltage curves, the start of alkali metal accumulation, and there is very convincing evidence that the point at which oxide precipitation begins can also be discerned.

A composite cathode polarogram is illustrated in figure 5-30. The uppermost curve can be interpreted in the following manner. As cathode voltage is increased, the first rise in current results from the reduction of carbon dioxide. The exact starting reduction potential is dependent on the partial pressure of carbon dioxide in the electrolyte as described earlier. As long as this partial pressure is sustained at the cathode via appropriately fast diffusion rates, current continues to increase

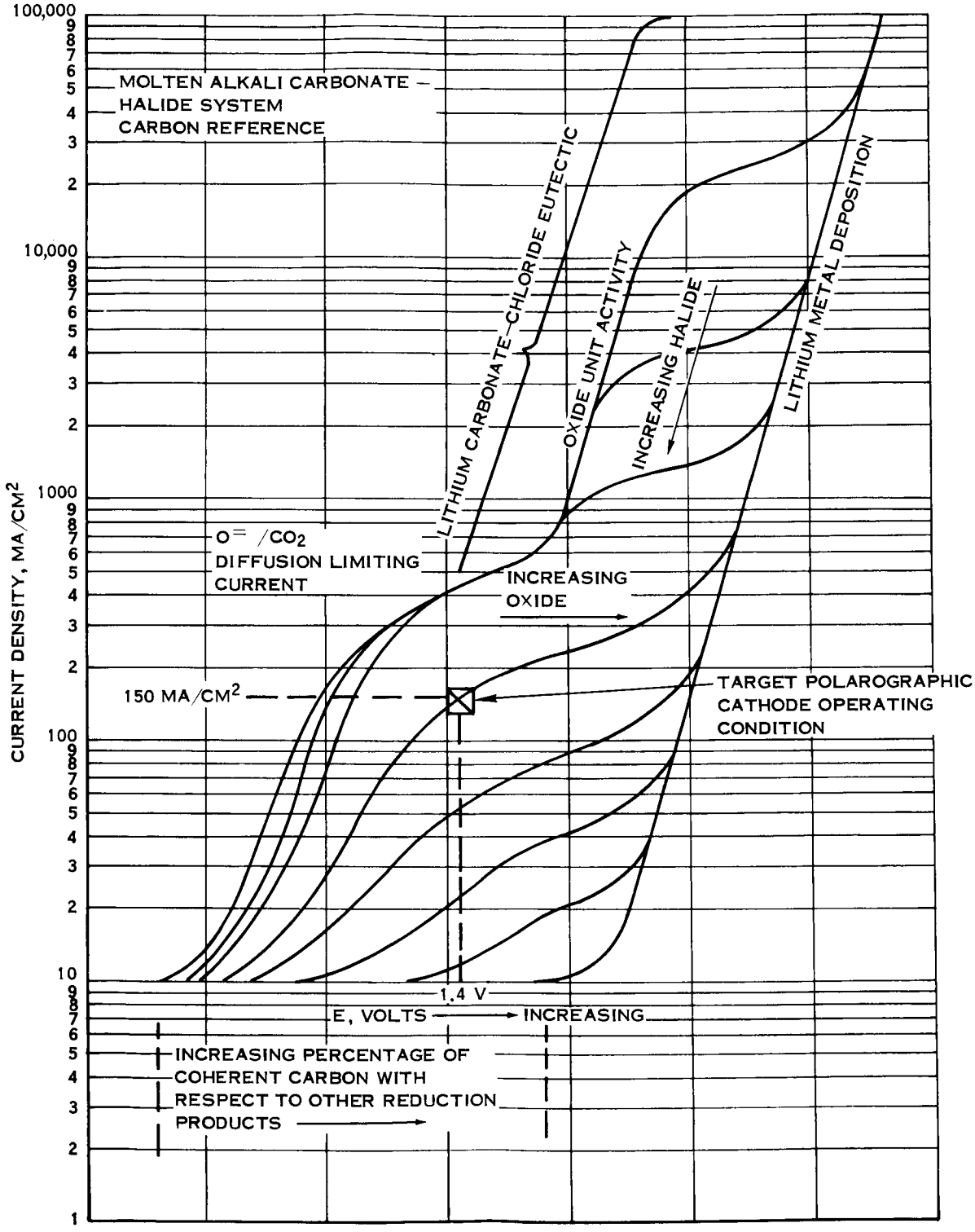


FIGURE 5–30. COMPOSITE CATHODE POLAROGRAM

5.2.6 (Continued)

as voltage is increased. At length a current is reached where oxide ion concentration begins to increase rapidly and carbon dioxide reduction potential increases accordingly. This condition is recognized as a first plateau on the polarogram. When the oxide ion reaches constant activity (the limit of oxide solubility) increasing potential results in a second rise in current until the point is reached where the carbon dioxide available at the cathode becomes depleted (second plateau) and alkali metal begins to accumulate with a third current rise.

Empirical data indicate that best cathode deposits are achieved when carbonate concentration is controlled (lower curves representing less carbonate) so that carbon dioxide depletion begins to occur (approaching alkali metal deposition) before the oxide solubility limit is reached. It is theorized that a suitable stoichiometry between carbon dioxide and alkali metal reducing agent must be sustained in order to accomplish a complete reduction. When carbon dioxide is too high, partial reductions occur; when it is too low, alkali metal accumulates.

The ability to identify various cathodic processes with easily obtained polarographic data offers the possibility for using this type sensing for process monitoring and control purpose. Intermittent checks might be made and appropriate systems corrections carried out when called for. Or, it has been suggested that an alternating current might be superimposed upon the direct carbon depositing current, and the slope of accompanying voltage changes be used to identify a specific area on the polarographic curve. If the monitored slope changes, a feedback system would adjust current density or other appropriate system variable to bring it back in line. A target polarographic operating condition is indicated in figure 5-30.

5.2.7 Future Cathode Study

Cathodes utilizing periodic gas phase exposure and completely submerged spinning cathodes have been adequately characterized by experimentation to define specific problem areas. Either technique appears amenable to further experimental development to achieve a combination of high carbon purity and high current efficiency. Of the two, the spinning cathode perhaps requires the somewhat greater effort to satisfactorily overcome the carbon attrition difficulty. The stationary cathode with circulating electrolyte has not yet been characterized adequately to represent a solid practical alternative to the first two cathode types. Further cathode research study will be directed toward solving the carbon attrition problem with the spinning cathode, and experimentally studying the stationary cathode-circulating electrolyte concept, subject to the priority of most quickly integrating any suitable one of these cathode configurations with concurrently developing anode and scrubber assemblies and overall cell concepts.

5.2.7 (Continued)

The capacity to relate cathode performance to cell polarographic behavior will be improved, using stationary electrode-electrolyte systems as well as dynamic ones. The utilization of polarography to help study the effect of electrolyte composition, particularly with regard to cation and anion substitutes and diluent concentration on carbon quality, will be expanded. The development of automatic cathode process monitoring and control devices based upon polarography will be initiated.

5.3 Scrubber: CO_2 Absorption Processes

Scrubbing tests have been performed at essentially atmospheric pressure to relate carbon dioxide absorption characteristics to electrolyte composition, scrubber configuration, air flow rate, carbon dioxide concentration, and other pertinent parameters. Basically, the tests have involved passing air containing carbon dioxide over assorted surfaces of known area which are cyclically wetted by electrolyte under carefully controlled circumstances. The partial pressure of carbon dioxide in the inlet air has normally been maintained at about 3.8 mm. Hg (0.5 vol. %) although higher and lower pressures have been examined. Outlet partial pressure has varied, depending on absorption efficiency, down to 0.076 mm. Hg (0.01 vol%), which was the lowest bulk electrolyte carbon dioxide partial pressure studied.

5.3.1 Test Configuration

The basic experimental test configuration has consisted of two separate scrubbing chambers which are used alternately. While carbon dioxide absorption is taking place on the wetted surfaces of one scrubber, the other is being rinsed with fresh electrolyte, thereby permitting a continuous scrubbing process. The half cycles of absorption or electrolyte replenishment are accomplished by appropriate valving and regulation of process air pressure.

Operation of the scrubber units is schematically illustrated in figure 5-31 where scrubber #1 is shown in the absorption mode and scrubber #2 in the electrolyte replenishment mode. Inlet air is predried by passing it through an in-line molecular sieve bed. Downstream of the drier, carbon dioxide is fed into the system to maintain a desired inlet partial pressure. This is monitored by an infrared type gas analyzer. The mixture is passed through a flowmeter into a valving arrangement shown schematically as a one piece valve. In practice, it comprises three separate three-way solenoid valves which are controlled simultaneously by tandem timers.

As the air - carbon dioxide mixture passes into scrubber #1, it displaces the electrolyte downward to bare the scrubbing surfaces. When the surfaces have been uncovered, the flow directed down a centrally located tube exits below the scrubbing elements, whence it passes up over the wetted surfaces to an exhaust port and subsequently to

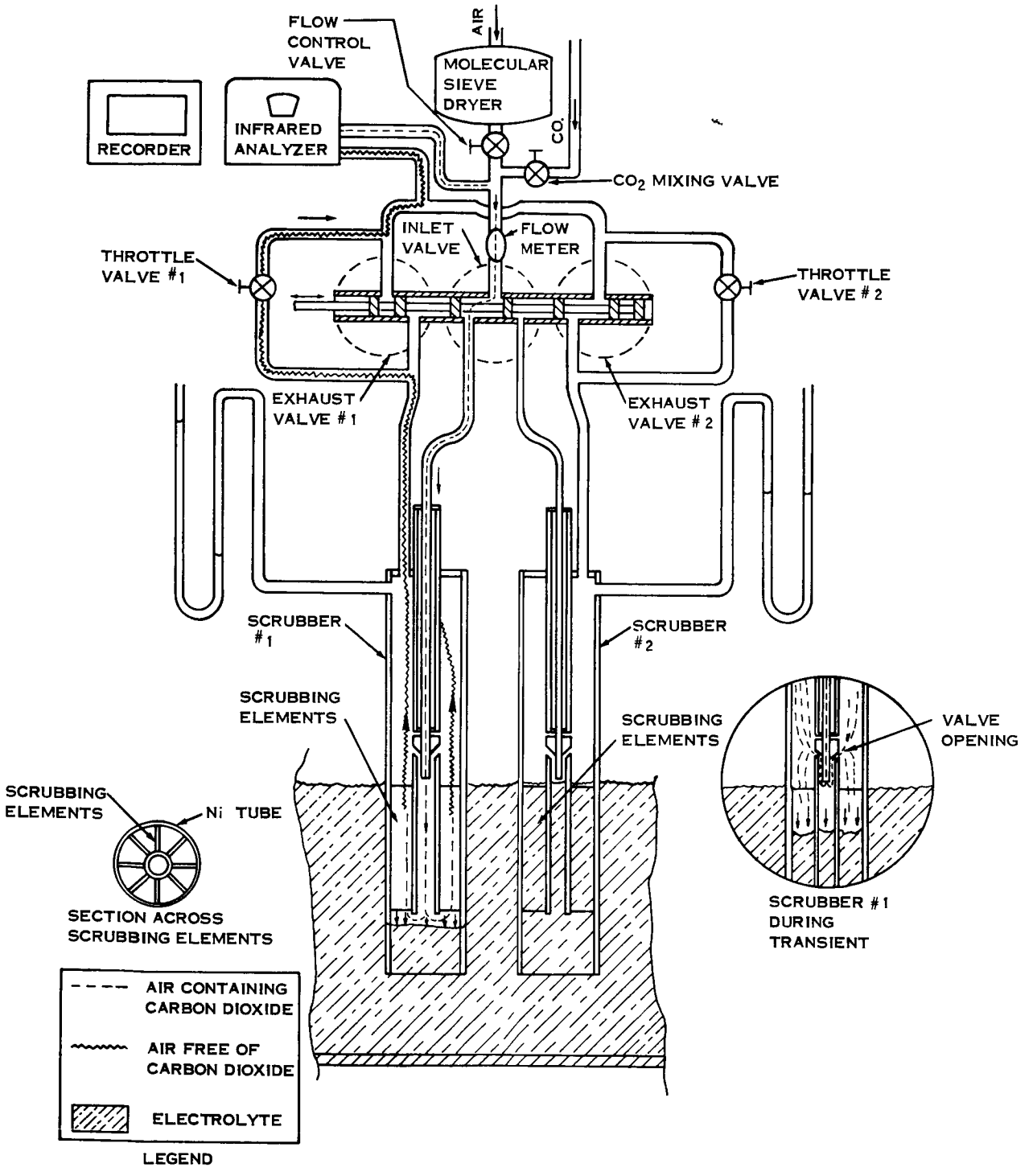


FIGURE 5–31. SCHEMATIC OF CO_2 ABSORPTION APPARATUS

5.3.1 (Continued)

an outlet CO_2 analyzer. The depth of electrolyte displacement is controlled by means of the back pressure afforded by a throttling valve in the exhaust line. Depth of displacement is ascertained by visual observation of an interconnected glycol manometer, and throttling adjustments in the exhaust valve are made accordingly. Once the throttling valve has been set to provide a desired displacement depth the system remains exceptionally stable over a great many cycles.

With the start of carbon dioxide scrubbing in scrubber #1, air flow to scrubber #2 is shut off. The scrubber #2 exhaust throttling valve is simultaneously bypassed so that the chamber is vented with little restriction. The bypass is utilized to effect greater speed in restoring the chamber to atmospheric pressure. This is necessary to accommodate very short cycle times. When this happens, the electrolyte rises to cover the scrubber plates. The tandem timers which control the valving sequence are of such a design that half cycle times for absorption or electrolyte replenishment may be varied from a few seconds up to several minutes each.

It has seemed desirable in these studies to introduce the air to be processed at the base of the scrubber to ensure that all of it must pass over the wetted surfaces before being exhausted. Also, in this circumstance, it has seemed desirable to use the process gas itself to effect the pressurization and displacement of electrolyte to cover and uncover the scrubber surfaces. Thus it has proved useful to employ an inlet air nozzle of the configuration shown in the figure 5-31 insert. This nozzle permits electrolyte pressurization and displacement without bubbling, but once the scrubber surfaces are cleared, the flow is channeled down the central tube to circulate back up through the scrubber plates. Fine control is provided by altering the distance between the tapered collar on the nozzle and the central tube, although this has not proved very critical. In operation, melt displacement is rapid and clean, and in development studies a slight tendency was also noted for the configuration to aspirate a portion of the exhaust gases back into the central tube, thereby giving good indication that esentially all of the air is being passed over the scrubbing surfaces.

5.3.2 Experimental Results

Although thus far testing has been primarily of a baseline and statistical nature to sort out and partially quantify the more important parameters, the collection and interpretation of data have been straightforward and indicate that assembly of reasonably thorough design information should be possible within a short time period. The data below are presented to illustrate the effects of various parameters on carbon dioxide absorption and give indication of our current understanding of the process. Adequate design data have not yet been accumulated to prescribe a preferred scrubber configuration, and therefore, the data are presented from the aspect of comparing volume of carbon dioxide scrubbed by a selected surface area and volume of electrolyte under varied circumstances, rather than in terms of scrubbing efficiency for a specific scrubber design.

5.3.2 (Continued)

It will be seen from the data presented in figure 5-32 that at constant carbon dioxide partial pressure, process air flow rate can be varied over a wide range while the absolute quantity of carbon dioxide absorbed remains nearly unchanged. That is, the quantity of carbon dioxide absorbed depends on its partial pressure in the air being processed and not on its rate of supply. This is further supported by the data presented in figure 5-33 where rate of carbon dioxide supply has been kept constant but partial pressure varied. The collected data show that carbon dioxide absorbed increases in a nearly linear relationship to its partial pressure.

In another test series, the results of which are reported in figure 5-34, carbon dioxide rate of supply and partial pressure were both held constant, as was surface area, but volume of electrolyte entrained on the plates was increased. This was accomplished by using nickel screen rather than sheet stock in one of the scrubber units. A 50% increase in amount of entrained electrolyte is achieved using the screen. Carbon dioxide absorbed was greater in the case of the screen, increasing markedly as cycle time was lengthened and reaching the condition where about twice as much carbon dioxide was being absorbed on the screen as on the nickel sheet. Since the electrolyte is found also to be more uniformly distributed on the nickel screen it is possible that this, in addition, contributes to the marked improvement.

Generally, the faster the rate of electrolyte replenishment (shorter cycle time), the greater the quantity of carbon dioxide absorbed on a continuous basis. Figure 5-35 illustrates one of many similar type curves showing this. Zero cycle time as plotted in figure 5-35 represents a special condition where no electrolyte displacement was allowed and the gas was continuously bubbled through the electrolyte using a continous tube inserted below the scrubber plates. At this condition, absorption has been greatest but it should be added that surface scrubbing configurations have not been optimum to date and bubbling through the electrolyte generally has led to foaming and increased electrolyte carryover. It is interesting to note that when cycling is occurring and cycle time gets very short, a slight fall-off in scrubbing performance has been noted in several instances. This may be related to an incomplete renewal of the entrained electrolyte, but this needs further consideration.

Results of some electrolyte compositional changes on scrubber performance, when statistically selected test combinations were investigated, are shown in table 5-II. This table summarizes the results when four system variables were examined. These variables included three associated with the electrolyte temperature, pCO_2, and pH_2O; the fourth variable was pCO_2 of the air stream. The two selected conditions for each variable represent limits in electrolyte variations which might commonly be encountered in a working cell. For each combination of variables tested, the quantity of carbon dioxide absorbed is shown to the right.

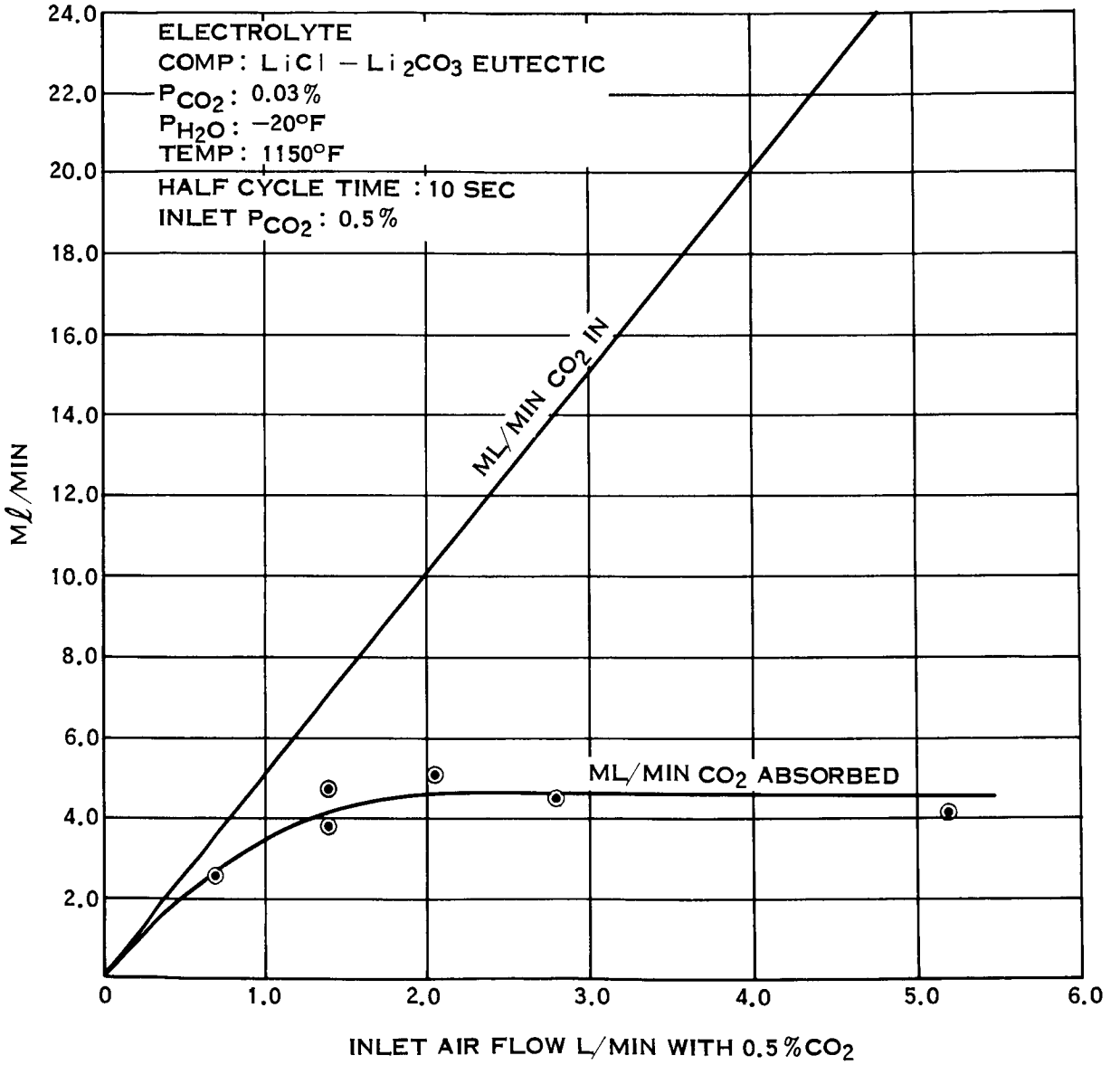


FIGURE 5–32. INFLUENCE OF FLOW RATE ON CO_2 ABSORBED AT CONSTANT P_{CO_2}

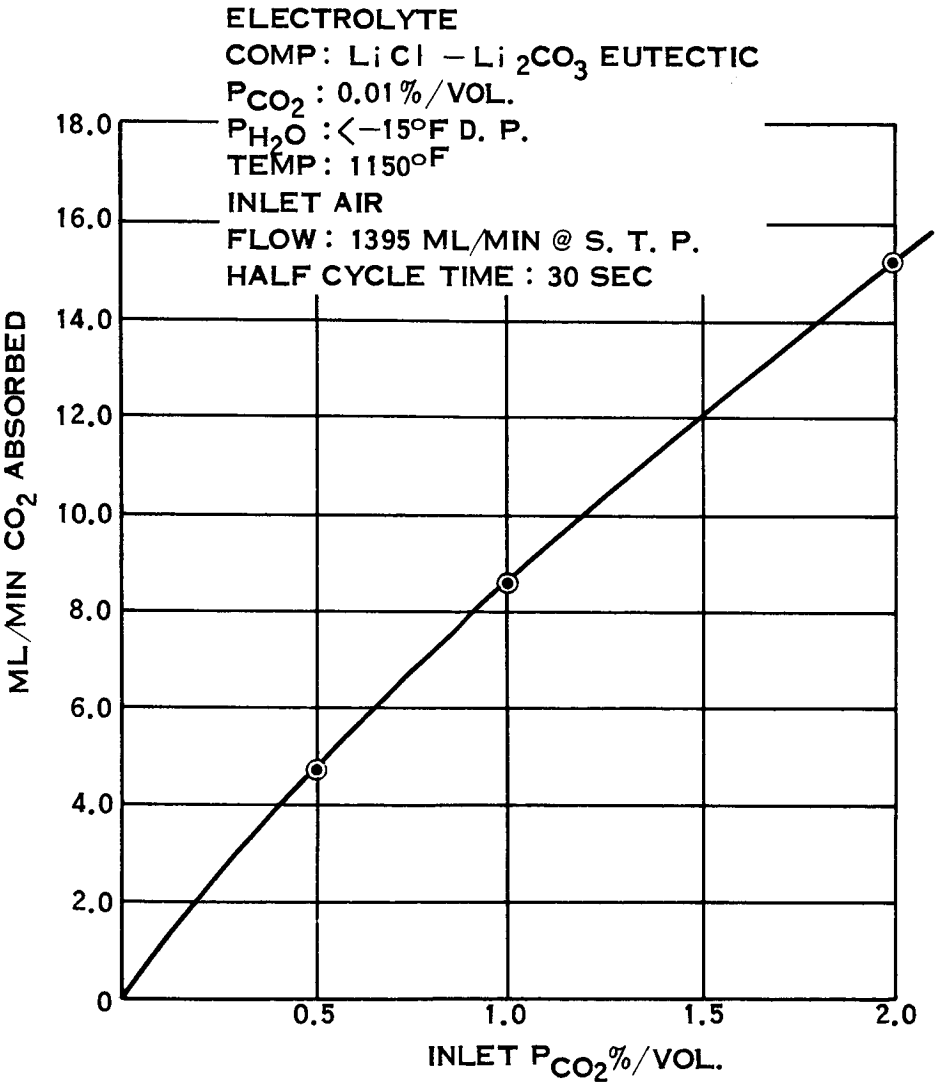


FIGURE 5–33. EFFECT OF INLET P_{CO_2} ON CO_2 ABSORBED

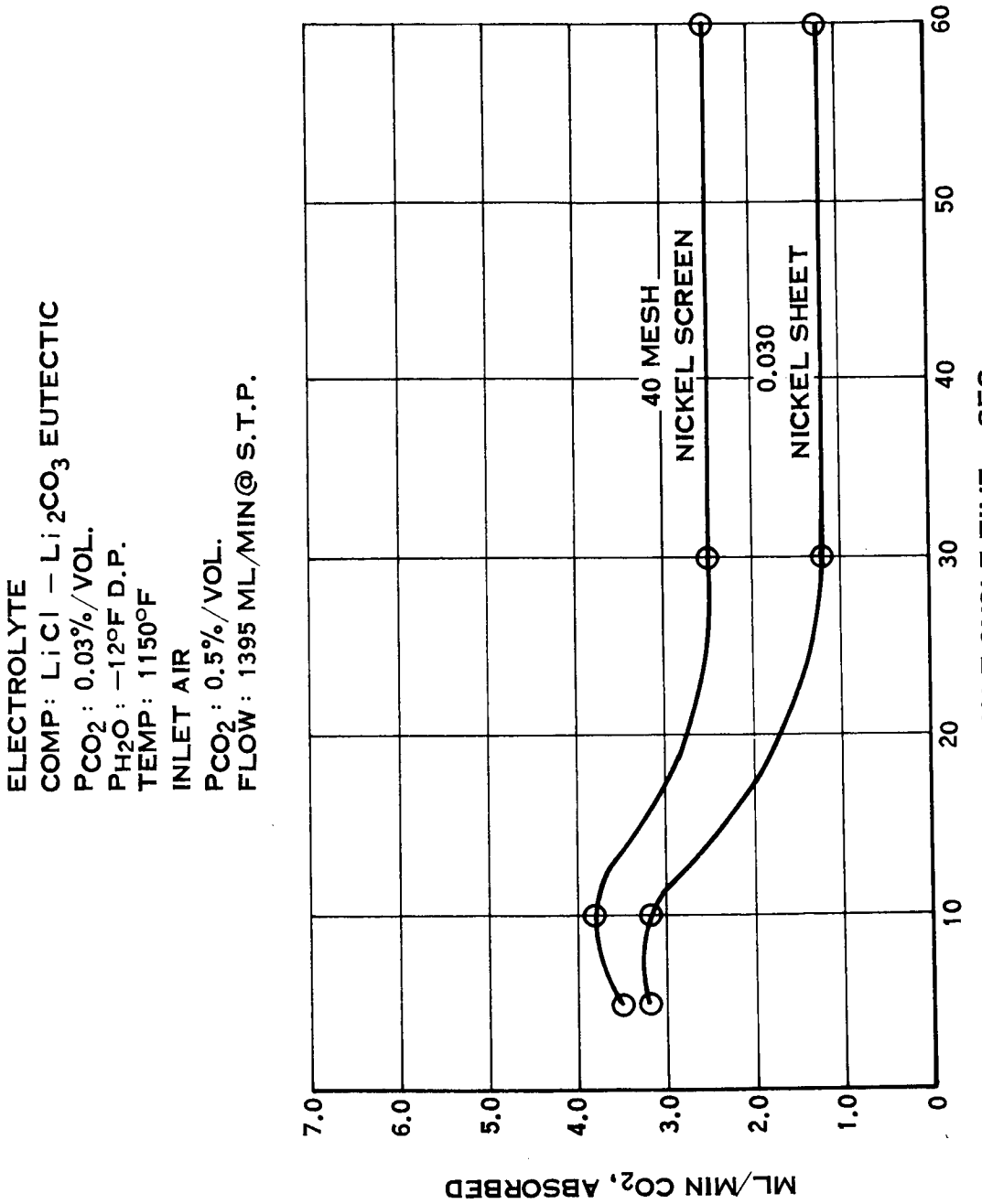


FIGURE 5–34. CO_2 ABSORBED ON SCREEN VS SHEET STOCK AT VARIOUS CYCLE TIMES

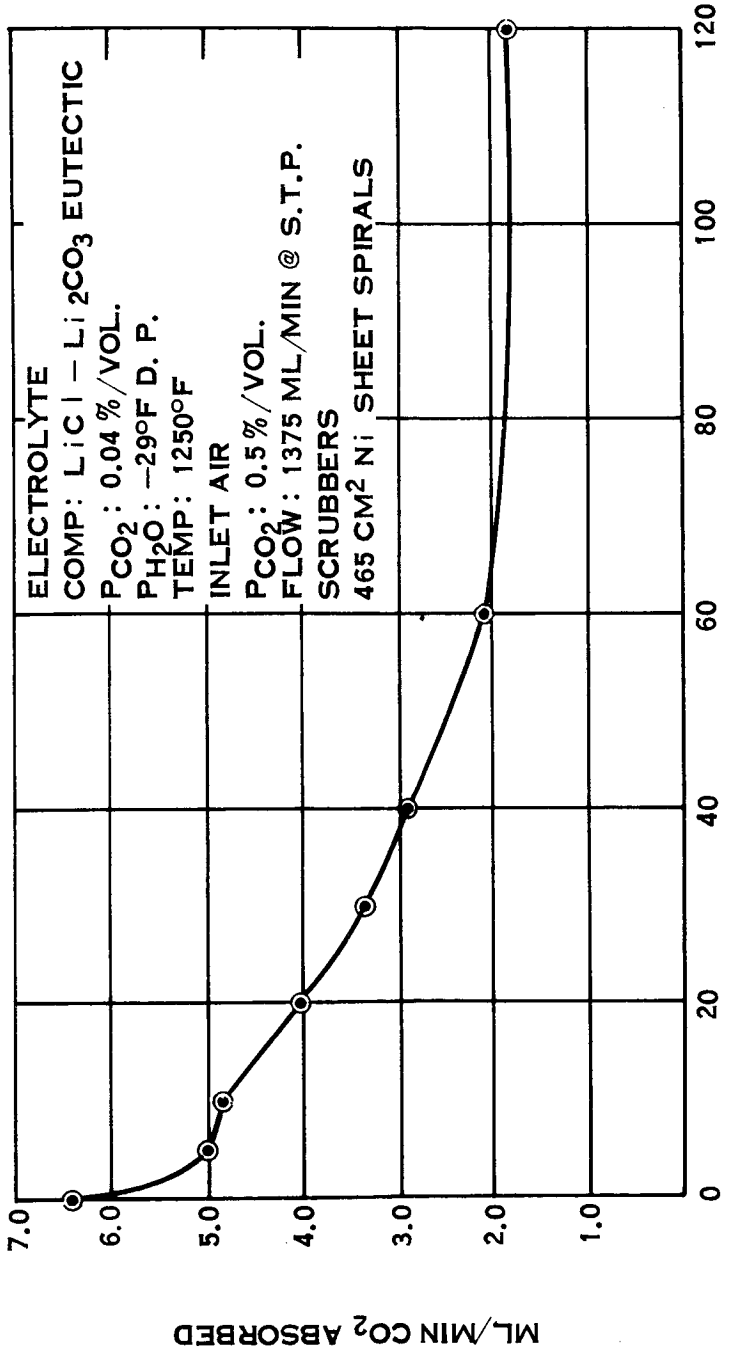


FIGURE 5–35. CO_2 ABSORBED VS CYCLE TIME

TABLE 5-II. RESULTS OF STATISTICAL STUDY OF FOUR VARIABLES ON ABSORPTION RATE

		+	-
1.	Inlet CO_2 Concentration	0.5%/vol. @ 1395 ml/min	1.0/vol @ 698 ml/min
2.	Electrolyte Dew Point	$<-20°F$	$-10°F$
3.	Electrolyte Temperature	1250°F	1150°F
4.	Electrolyte P_{CO_2}	0.03-0.06%/vol.	0.08-0.15%/vol.

Run #	Variables				CO_2 Absorbed, ml/min (stp)
	1	2	3	4	
1	+	-	-	-	3.3
2	-	-	-	-	5.6
3	+	+	-	-	4.5
4	-	+	-	-	5.3
5	+	-	+	-	4.6
6	-	-	+	-	5.9
7	+	+	+	+	5.3
8	-	+	+	+	6.3
9	+	+	-	+	4.5
10	-	+	-	+	6.0

Feed Rate: 7.0 cc/min
Half Cycle Time: 10 sec.

5.3.2 (Continued)

The large effect of carbon dioxide pressure in the air stream is evident by the manner in which the pattern of CO_2 absorbed rigidly follows the pressure variation (variable 1). Runs 8 and 10, which combine the higher gas CO_2 pressure with the lower electrolyte CO_2 pressure, provided the best scrubbing. Electrolyte dew point and temperature effects were not particularly significant over the limited range studied.

All of the above data have been collected by passing the air through vertical parallel nickel plates. Horizontal, baffled plates are only just being put into test. These will provide for a longer flow path and a slightly more turbulent flow using the same scrubber surface area. More complete data on the effect of varied surface area must still be obtained. It is of particular interest to note that although marked oxidation of the nickel surfaces was anticipated, the scrubbing elements after a reasonable period of use continued to appear little affected. We must presume that under the mode of operation used, the nickel is protected by the electrolyte film. Oxygen gas, having such low solubility in the electrolyte, does not penetrate to the metal.

5.3.3 Future Scrubber Study

Although it is unrealistic to attempt to extrapolate from our present state of knowledge of absorption characteristics to the final design of a prototype scrubber, some comment in this direction is in order. The use of vertical parallel plates as absorption surfaces has proved completely satisfactory in sorting out the effects of film replenishment rate, film thickness, surface area, and so on, but when results are projected in accord with current complete cell design concepts, these are only about 40% effective at the air flow rate to scrubber surface being considered. This is not surprising and actually it is very gratifying to experience such a relatively large amount of scrubbing without detailed attention to scrubber configuration. It is expected that, as we place experimental emphasis on scrubber physical design with regard to air flow path and electrolyte film control, essentially 100% efficiency should be readily achieved.

REFERENCES

1. Phase 1. Final Report: Research and Development Program for a Combined Carbon Dioxide Removal and Reduction System. Hamilton Standard Report HSER 3732, pp 7-48. (October 1965)

2. Kelly, Eugene J., Tafel Lines, Encyclopedia of Electrochemistry, Reinhold Publishing Co., pp. 1097-1100 (1964)

6.0 SUPPORTING STUDIES (UARL)

6.1 Carbonate Decomposition Characteristics

6.1.1 Introduction

The research and development of a molten salt electrolysis system for the simultaneous removal of CO_2 and production of O_2 in environmental control systems has shown that proper control of CO_2 partial pressure and thus oxide ion concentration in the melt is essential to the production of dense, adherent carbon at the cathode and pure oxygen at the anode, (ref. 1). Although the mechanisms of the reactions in the cell have not been definitely established, it is probable that they proceed in such a manner that oxide ions are produced at the cathode as a product of the reduction of CO_2 to carbon by the action of lithium metal and that these oxide ions are then consumed at the anode to form oxygen. During electrolysis the rate of production and consumption of oxide ions is determined by the amount of electricity passed. However, in the melt itself the carbonate decomposition equilibrium determines the concentration of oxide ions in the bulk of the melt and tries to act as a buffer to maintain the oxide ion concentrations dictated by the operating temperature and the inherent thermodynamics of the molten system as a whole.

In the final analysis, the kinetics of the carbonate decomposition reaction compared with the imposed kinetics of electrolysis will determine the dynamic equilibrium oxide ion concentration in the melt. However, the values of the equilibrium constant for the carbonate decomposition reaction in the system of interest would serve as valuable basic information relative to the irreversible kinetic behavior in a dynamic system.

A survey of the literature showed that no reliable experimental work had been done on the decomposition of Li_2CO_3 or related mixtures of carbonates and halides. Therefore an experimental program was initiated to determine the equilibrium behavior of Li_2CO_3 and the eutectic mixtures of Li_2CO_3-LiF and Li_2CO_3-LiCl. Combinations of these compounds have comprised the most satisfactory electrolytes for the CO_2 reduction system.

A thermogravimetric system was used for these experiments to provide data on the weight loss of samples as a function of pressure, temperature, and time. Theoretical evaluation of the thermodynamic properties of these systems was undertaken as a basis for correlation of experimental data.

6.1.2 Experimental Details

6.1.2.1 Description of Technique

The decomposition studies were carried out using a weight loss technique. With this technique a carbonate-containing sample of known initial composition is heated at various temperatures and pressures and the amount of CO_2 evolved is determined from the decrease in weight of the sample during the test.

6.1.2.1 (Continued)

The weight losses observed in a typical run using "pure" Li_2CO_3 varied from 0.1 mg to as much as 7.6 mg. Since the weight loss at each pressure was due to evolved CO_2, these weights may be converted to moles CO_2 lost, which are in turn equivalent to the moles of Li_2O formed according to the decomposition equilibrium expression:

$$Li_2CO_3(\ell) = Li_2O(\ell) + CO_2(g) \qquad (1)$$

For every mole of CO_2 formed, a mole of Li_2CO_3 is lost. The difference between the initial moles of Li_2CO_3 dried sample weight and the moles of CO_2, yields the moles of Li_2CO_3 remaining at any given partial pressure of CO_2 (P_{CO2}). These two values are then used to calculate the $O^{=}/CO_3^{=}$ ratio which is multiplied by P_{CO2} in atmospheres to obtain K_{eq} in atmospheres.

Thus the equilibrium constant may be expressed in ionic terms as:

$$K_{eq} = \frac{\left[O^{=}\right]}{\left[CO_3^{=}\right]} P_{CO_2} \qquad (2)$$

where $\left[O^{=}\right]$ is the concentration of oxide ions equivalent to the CO_2 loss; $\left[CO_3^{=}\right]$ is the concentration of carbonate ions remaining in the sample; and P_{CO_2} is the partial pressure of CO_2 in atmospheres.

This ionic expression for K_{eq} is identical to that for the molecular equation (1) since both Li_2O and Li_2CO_3 are completely ionized in their molten state. The concept of complete ionization of alkali metal compounds has been verified by many investigators as referenced in a review text on molten salts edited by Blander (ref. 2). Thus, in this particular case, one mole of oxide ion is equivalent to one mole of Li_2O and one mole of carbonate ions is equivalent to one mole of Li_2CO_3.

When other volatile species are present in the melt, appropriate corrections to the weights loss to account for this volatility must be made.

6.1.2.2 Apparatus

The decomposition studies were carried out using a weight-loss technique in a Cahn Model RH Vacuum Electrobalance shown in figures 6-1 and 6-2. The balance has a capacity of 100 grams and an ultimate sensitivity of ± 2 micrograms. In the present experiments the balance was used with a total load of about 50 grams. Most of this weight is tared using a small crucible and calibrated weights on the right-hand arm of the balance (B in figure 6-2), and the remainder is balanced electrically by means of the control unit (3 in figure 6-1). A small unbalance is left in the control unit and this final weight difference is fed into a Varian Model G11A 10 mv Recorder (5 in

1 VACUUM BALANCE
2 FURNACE
3 BALANCE CONTROL UNIT
4 MICROVOLT AMPLIFIER
5 WEIGHT RECORDER
6 POTENTIOMETER
7 BALANCE MANIFOLD & MANOMETER
8 MOISTURE MONITOR
9 VALVING SYSTEM

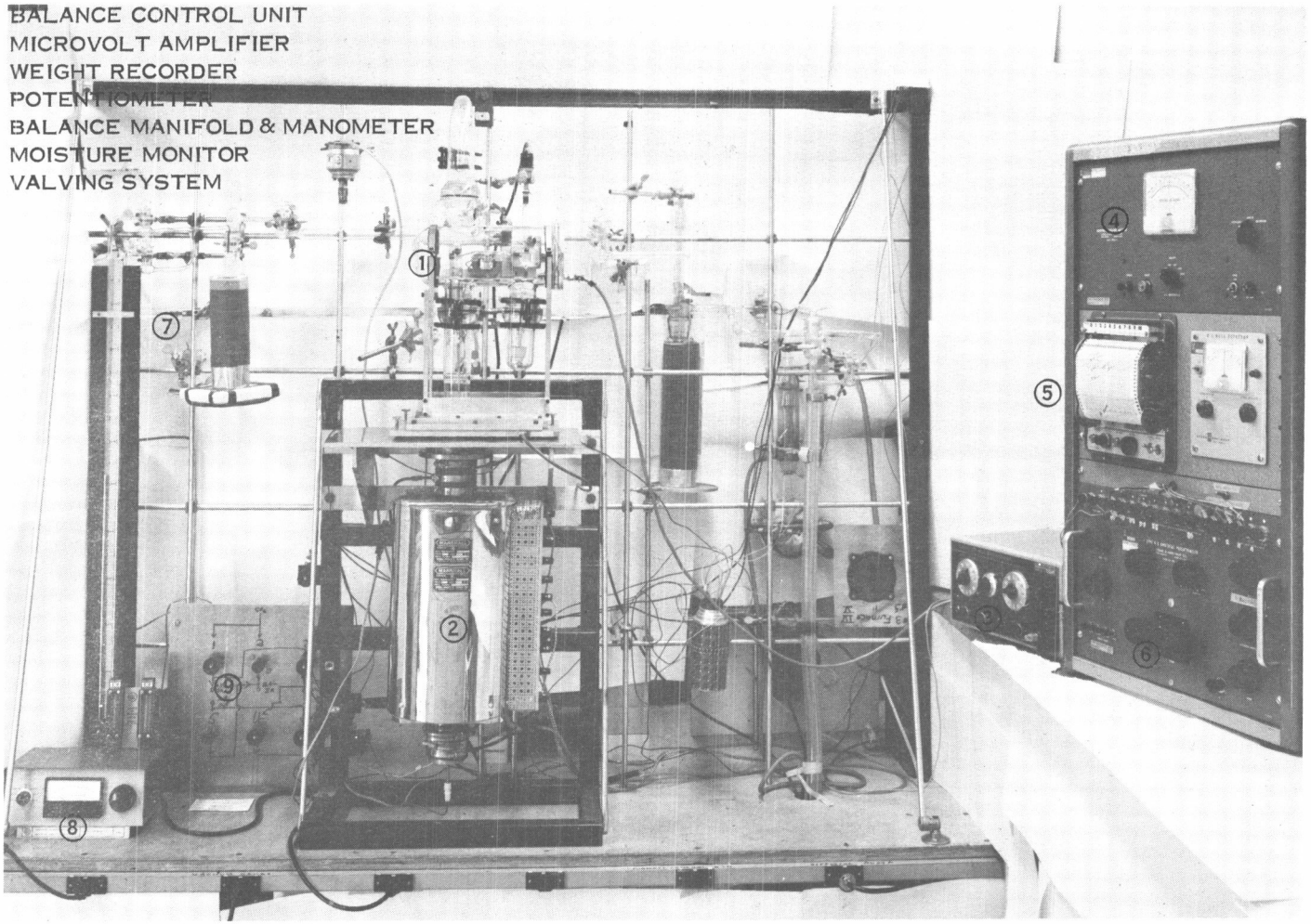
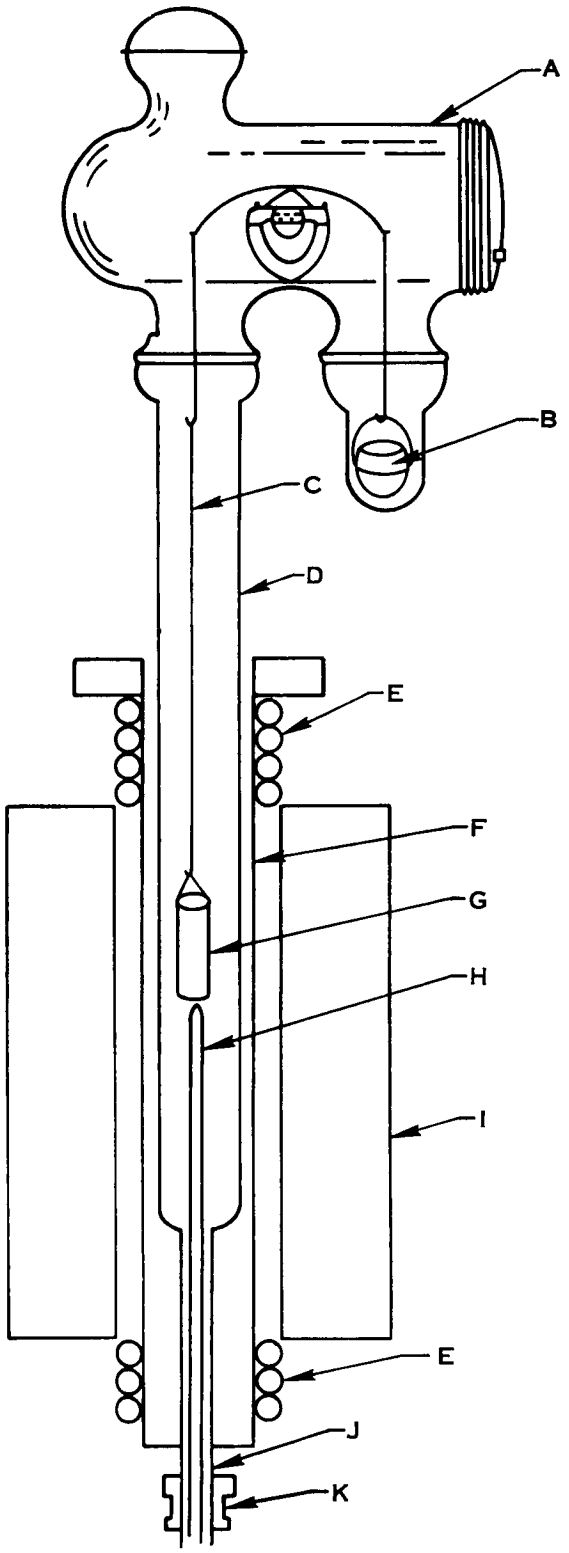


FIGURE 6—1. THERMOGRAVIMETRIC APPARATUS FOR CARBONATE DECOMPOSITION STUDIES



A – VACUUM BALANCE
B – PORCELAIN CRUCIBLE AND WEIGHTS
C – IRIDIUM HANG–DOWN WIRE
D – QUARTZ HANG–DOWN TUBE
E – COOLING COILS
F – INCONEL LINER
G – Au-Pd CRUCIBLE & SAMPLE
H – THERMOCOUPLE WELL
I – FURNACE
J – THERMOCOUPLE INLET TUBE
K – NYLON SWAGELOK FITTING

FIGURE 6–2, THERMOGRAVIMETRIC BALANCE ASSEMBLY

6.1.2.2 (Continued)

figure 6-1). The total weight of the sample is determined from the weight in the balance, the control unit setting and the recorder reading. The recorder is set at a sensitivity equal to 10 mg full scale or 0.1 mg/div. The accuracy of the readings is ± 50 micrograms.

The sample (usually about 10 grams) is contained in an 80 percent gold-20 percent palladium crucible one inch in diameter and 2.5 inches deep (G in figure 6-2), suspended from the left hand arm of the balance by means of a 20 mil iridium wire (C in figure 6-2). Iridium was found to be the only material that would neither fatigue nor oxidize in the CO_2 atmosphere at temperatures of 600-900° C under the 50 gram load used in these experiments. Nichrome, platinum, and gold-palladium wires all failed after 7-10 days of operation.

The hang-down tube (D in figure 6-2) which contains the sample and crucible is constructed of quartz and is terminated in a special glass-to-Kovar seal (J) at its lower end.

Nylon swagelok fittings (K) are connected to the Kovar to hold either a gas inlet tube or a quartz thermocouple sheath (A). When the thermocouple is used, the end of the sheath is positioned about 1/9 in. below the bottom of the gold-palladium crucible.

The crucible is positioned in the center zone of a 16-in long Marshall tube furnace (I in figure 6-2). An inconel liner (F) fitted with copper cooling coils, (E), is inserted in the 3-1/2 in. diameter furnace. The cooling water is also circulated through the base of the balance support and serves to keep the balance mechanism near room temperature. The center 4-in. zone of the furnace has an axial temperature variation of less than 2° C. Temperature control is maintained with a Barber-Colman Proportional Controller (not shown) which regulates to ± 2° C. The control thermocouple is positioned in the center zone of the furnace lining opposite the center of the gold-palladium crucible.

The measuring thermocouple is platinum, platinum-13% rhodium with a zero degree ice bath reference junction. The temperature is measured using a Leeds and Northrup Model K potentiometer (6 in figure 6-1), a Model 9385-B microvolt amplifier (4 in figure 6-1) and a Beckman strip chart recorder (not shown). Most of the thermocouple EMF is cancelled by the potentiometer setting and the remainder is amplified and fed to the recorder so that a full scale deflection is equivalent to 10° C. The temperature is read to an accuracy of ± 0.1 °C, but since the thermocouple calibration is ± 0.5°C, the temperatures are reported only to the least accurate value.

The vacuum balance assembly is attached to the vacuum system, shown in figure 6-1, through a 10 mm bore stopcock. The balance manifold (7 in figure 6-1) includes a dry ice trap, mercury manometer and stopcocks which connect it to either the main pumping system or to a gas inlet manifold. By proper manipulation of the stopcocks the pressure of the system may be regulated to ± 0.5 mm Hg.

6.1.2.2 (Continued)

The CO_2 used in the measurement is Matheson "Bone Dry" grade and is used without further drying. The moisture level of the gas is 30 ppm as determined by means of a Consolidated Electrodynamics Model 203-1 Moisture Monitor (8 in figure 6-1). A valving system is constructed so that the CO_2 may be introduced directly into the balance manifold and/or passed through the balance system, exiting at the lower end of the hangdown tube. The Moisture Monitor may be bypassed or connected to the inlet or outlet gas stream by means of the same valving system.

6.1.2.3 Preparation and Drying of Samples

All salts used in the experiments were pre-dried under vacuum and stored in sealed bottles in a drybox. The drybox moisture level was $\leq$300 pmm. LiCl and LiF were dried at a maximum temperature of 500°C and Li_2CO_3 was dried at a maximum temperature of 400°C.

The crucible was charged with the sample in the drybox and was immediately transferred to the balance assembly. Subsequent drying was accomplished in situ and low temperature weight loss under vacuum recorded on the balance was used as the final drying criterion. At temperatures above the decomposition point of the samples, drying was effected with a CO_2 gas flow through the cell. The dry state was considered to have been reached when the inlet and outlet gas streams both indicated a residual gas moisture content of 30 ppm.

6.1.2.4 Operational Procedures

After a sample had been dried, as outlined above, the sample was heated to the desired operating temperature under a partial pressure of CO_2 on the order of 300 to 400 mm. The minimum CO_2 partial pressure necessary to prevent carbonate decomposition at any given temperature was determined by raising the pressure in 50 mm steps until no further weight loss was observed. At the highest operating temperature for Li_2CO_3 (825°C), it was necessary to raise the pressure to 550 mm to insure that no decomposition occurred. The pressure was then reduced by partially evacuating the balance manifold, and the weight loss was observed until a new equilibrium weight was obtained. In most cases the pressures studied were arbitrary. During the experiments on pure Li_2CO_3 the CO_2 in the balance and balance manifold was expanded into the rest of the vacuum system with the pumping part of the system closed off. In this manner the CO_2 pressure was reduced in successive steps until some arbitrary low pressure was reached which resulted in a total CO_2 loss not exceeding 10 mg. The CO_2 pressure was then increased to the original value and the weight gain of the sample due to reaction with CO_2 was observed until equilibium was achieved. When Li_2CO_3 was studied the total weight loss was completely recovered after re-pressurizing the system. In the case of the Li_2CO_3-LiF and particularly the Li_2CO_3-LiCl runs it was necessary to raise the pressure back to the original value after each lower pressure run in order to correct for losses due to LiF and LiCl volatility.

6.1.2.4 (Continued)

During these experiments the CO_2 pressure was reduced by pumping on the system. CO_2 pressures of 300 mm for the Li_2CO_3-LiCl system and 400 mm for the Li_2CO_3-LiF system were used as the starting points and equilibrium constants were determined at values of 300 mm (in the case where the starting pressure was 400 mm), 200 mm, 100 mm, 50 mm and 25 mm. At the lowest temperatures 10 mm was used for the Li_2CO_3-LiCl system.

In all runs it was necessary to correct for temperature and pressure buoyancy effects on the sample. All weights were corrected to room temperature and vacuum.

The volume of the balance and balance manifold system was 5.8 liters. It was found that a 12 mg loss of CO_2 was necessary to change the system pressure 1 mm so total weight losses were kept below a maximum of 10 mg CO_2. Thus the equilibrium system was operating under essentially constant pressure and volume conditions. The calculated equilibrium constants were expressed in atmospheres according to equation (2).

6.1.3 Test Results

6.1.3.1 $CaCO_3$

The balance assembly and weight loss procedure for the determination of the decomposition of carbonates was tested by measuring the decomposition pressures of solid $CaCO_3$ and comparing the data with several literature values (ref. 3-5).

Since both $CaCO_3$ and CaO were in the solid state over the temperature range studied, and therefore their activities were unity, Eq. (1) reduced to $K_{eq} = P_{CO_2}$. In this case the CO_2 pressure was simply lowered to the point where a weight loss was noted and K_{eq} was thus determined. Table 6-I and figure 6-3 summarize the data obtained in this manner. Values of ΔH°, the standard heat associated with the decomposition reaction in Kcal/mole, were determined from the slopes of a plot of log P_{CO_2} versus 1/T according to the equation:

$$\frac{d \ln K_{eq}}{d (T)} = \frac{\Delta H^\circ}{RT^2} \qquad (3)$$

Since in this case ln K_{eq} was equivalent to ln P_{CO_2}, equation (3) reduces to:

$$\log \frac{P_{CO_2\ (1)}}{P_{CO_2\ (2)}} = \frac{\Delta H^\circ}{4.576} \times \frac{T_2 - T_1}{T_1 T_2} \qquad (4)$$

where the subscripts (1) and (2) refer to P_{CO_2} at temperature T_1 and temperature T_2 respectively and the constant 4.576 is the product of R in cal/°/mole and the factor for converting from natural logs to the base 10 log scale. The slope of the log P_{CO_2} versus 1/T plot is $-\Delta H^\circ/4.576$.

6.1.3.1 (Continued)

TABLE 6-I

$CaCO_3$ DECOMPOSITION PRESSURES

Partial Pressure of CO_2 (mm)

Temp. (°K)	This Work	Hill & Winter[2]	Johnston[3]	Smyth & Adams[4]
1023	52	68	68	63
973	21.5	25	25	22
923	8	8	9	7
ΔH^o (Kcal/mole)	35.4	40.0	39.4	42.8

The data obtained were in agreement with the literature at the lower temperatures but at 750°C were somewhat lower. However, a straight line was obtained using raw data, which implies a constant heat of decomposition over the temperature range studied. In view of the reproducibility of the data, it was felt that any errors incurred in this experiment were no larger than those of the other investigators referenced. The agreement was felt to be sufficient to warrant the use of a weight loss method in the Li_2CO_3 investigations.

6.1.3.2 Li_2CO_3

Decomposition data for molten Li_2CO_3 were obtained over a wide range of pressures at 750, 770, 790, 810, and 830°C. At least seven CO_2 pressures were used at each temperature, and equilibrium constants were calculated at each pressure in order to obtain an average value for K_{eq} at each temperature.

The pre-dried Li_2CO_3 sample was heated to constant weight under vacuum. The sample lost weight in the 400-500°C range very rapidly (it was pre-dried to 400°C under 1 atm. of CO_2) and then more slowly in the 500-550°C range.

At 550°C CO_2 was introduced into the system and the sample gained weight equivalent to the observed weight loss above 500°C. On cooling the sample to 400°C the weight remained constant even after the system was pumped down to a pressure less than 1 micron. Thus the higher temperature weight loss was due to carbonate decomposition at a temperature almost 200°C below the melting point of Li_2CO_3. The unrecovered weight loss is attributed to moisture or other volatile impurities and amounted to 8.8 mg in a ten gram sample (880 ppm).

The decomposition runs were made starting at the lowest temperature. It was found that a partial pressure of CO_2 on the order of 300 mm was sufficient to obtain a constant sample weight identical to that of the original dried sample weight after each decomposition run. At the highest operating temperature (830°C), it was necessary

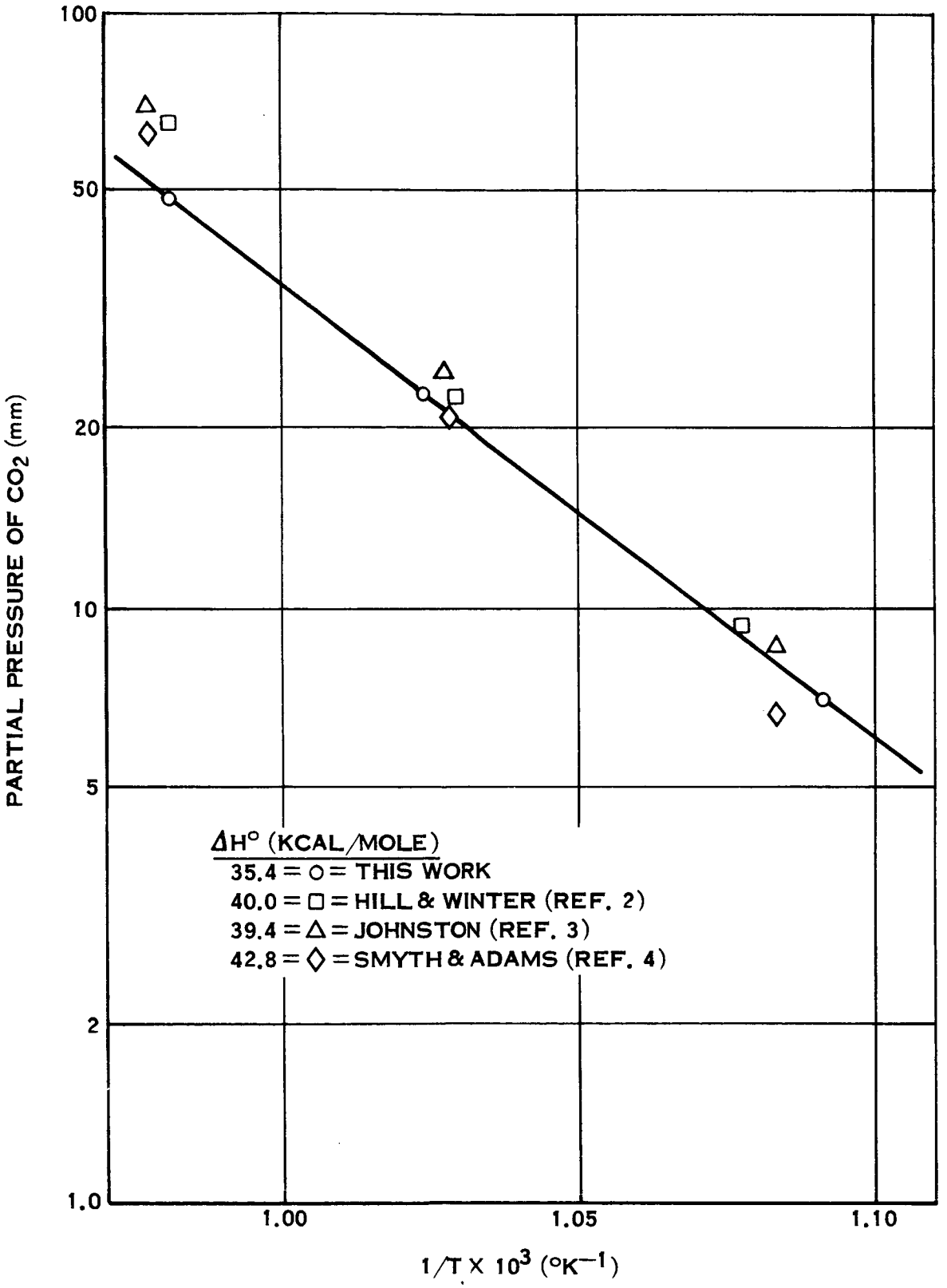


FIGURE 6–3. EQUILIBRIUM CONSTANTS FOR THE DECOMPOSITION OF C CO_3 AS A FUNCTION OF TEMPERATURE

6.1.3.2 (Continued)

to raise the CO_2 pressure to 550 mm before the original sample weight was obtained. An increase in weight of < 0.1 mg was observed when the CO_2 pressure was raised above 300 mm at the lower temperatures and 500 mm at 830°C. These weight differences are on the order of the $\pm$ 50 microgram uncertainty in the weight measurements. The fact that the original sample weight was regained after each run indicates that no problem exists due to volatilization of the Li_2CO_3, and hydrolysis impurities such as LiOH were probably absent.

The data for the five temperatures calculated in the manner described above are summarized in tables 6-II through 6-VI. In most cases the equilibrium constants calculated on the basis of small weight losses at high pressures are considerably lower than those obtained at lower pressures and thus higher weight losses. These high pressure values were excluded when the average K_{eq} was calculated.

Plots of K_{eq} versus P_{CO_2} show that K_{eq} increases as pressure is reduced from the higher pressures and then levels off at the lower pressures. In most cases the majority of the points fell in the flat region of the curves; however, in at least one case (830°C) the values of K_{eq} did not level off within the range of the data and only the last two points were used to calculate K_{eq}. All indicated deviations in the average values of K_{eq} are average deviations.

The low values of K_{eq} may be attributed to the presence of residual oxide in the melt after heating and treatment with CO_2 to stabilize the melt composition. The amount of residual oxide required to make most of the data for K_{eq} of Li_2CO_3 melts consistent would be generally on the order of 10^{-6} moles and in no case would have been greater than 10^{-4} moles. This small amount of Li_2O would not be detectable in Li_2CO_3 mixtures using any available methods of chemical analysis. Other methods for correcting the data are available but the corrections that would be introduced are small enough that the general conclusions of this study would not be significantly affected.

The standard free energy (ΔF°) for the carbonate decomposition reaction may be calculated from the K_{eq} according to the equation:

$$\Delta F^\circ = -RT \ln K_{eq} \qquad (5)$$

As noted previously, K_{eq} is also related to ΔH° (the standard enthalpy of the reaction) by

$$\frac{d \ln K}{d (T)} = \frac{\Delta H^\circ}{RT^2} \qquad (3)$$

TABLE 6-II

EQUILIBRIUM CONSTANTS FOR THE DECOMPOSITION OF Li_2CO_3 at 749°C

(1022°K) ($1/T = 0.975 \times 10^{-3}$°K^{-1})

PCO_2 (atm)	Wt. Loss CO_2 (mg)	Moles CO_2 Lost	Moles Li_2CO_3	$O^{=}/CO_3^{=}$	K_{eq}(atm)
0.4105	----	----	0.13780	----	----
0.3289	0.11	2.55×10^{-6}	0.13778	1.814×10^{-5}	5.968×10^{-6}
0.2460	0.63	1.432×10^{-5}	0.13766	1.040×10^{-4}	2.559×10^{-5}
0.1618	1.28	2.909×10^{-5}	0.13751	2.116×10^{-4}	3.423×10^{-5}
0.1316	1.58	3.591×10^{-5}	0.13744	2.613×10^{-4}	3.438×10^{-5}
0.1066	2.18	4.954×10^{-5}	0.13730	3.608×10^{-4}	3.847×10^{-5}
0.0882	2.75	6.250×10^{-5}	0.13718	4.556×10^{-4}	4.017×10^{-5}
0.0724	3.51	7.977×10^{-5}	0.13700	5.823×10^{-4}	4.214×10^{-5}
0.0592	4.10	9.318×10^{-5}	0.13687	6.808×10^{-4}	4.031×10^{-5}
0.0474	4.76	1.082×10^{-4}	0.13672	7.912×10^{-4}	3.748×10^{-5}
0.0316	7.61	1.729×10^{-4}	0.13607	1.271×10^{-3}	4.014×10^{-5}

K_{eq} (ave) $= 3.98 \pm 0.12 \times 10^{-5}$ (Based on last 6 values of K_{eq})

$\log K_{eq} = -4.4001$

$\Delta F^{\circ} = -4.5761\ (1022)\ (-4.4001)$

$\Delta F^{\circ} = 20.58$ K cal/mole

TABLE 6-III

EQUILIBRIUM CONSTANTS FOR THE DECOMPOSITION OF Li_2CO_3 at 770°C

(1043°K) (1/T = 0.958 x 10^{-3} °K^{-1})

P_{CO_2} (atm)	Wt. Loss CO_2 (mg)	Moles CO_2 Lost	Moles Li_2CO_3	$O^{=}/CO_3^{=}$	K_{eq} (atm)
0.4105	----	----	0.13780	----	----
0.3329	0.20	6.8181×10^{-6}	0.13779	4.948×10^{-5}	1.647×10^{-5}
0.2184	1.20	2.7272×10^{-5}	0.13776	6.980×10^{-4}	4.324×10^{-5}
0.1763	1.80	4.0909×10^{-5}	0.13772	2.970×10^{-4}	5.236×10^{-5}
0.1434	2.50	5.6818×10^{-5}	0.13766	4.127×10^{-4}	5.918×10^{-5}
0.1171	3.20	7.2727×10^{-5}	0.13759	5.286×10^{-4}	6.190×10^{-5}
0.09605	4.00	9.0909×10^{-5}	0.13750	6.610×10^{-4}	6.349×10^{-5}
0.07237	5.70	1.2954×10^{-4}	0.13737	9.430×10^{-4}	6.824×10^{-5}
0.05526	7.70	1.7500×10^{-4}	0.13719	1.276×10^{-3}	7.051×10^{-5}

K_{eq} (ave) = $6.47 \pm 0.38 \times 10^{-5}$ (Based on last 5 values of K_{eq})

$\log K_{eq}$ = -4.1891

ΔF° = -4.5761 (1043) (-4.1891)

ΔF° = 20.00 K cal/mole

TABLE 6-IV

EQUILIBRIUM CONSTANTS FOR THE DECOMPOSITION OF Li_2CO_3 at 790°C
(1063°K) ($1/T = 0.940 \times 10^{-3}$°$K^{-1}$)

P_{CO_2} (atm)	Wt. Loss CO_2 (mg)	Moles CO_2 Lost	Moles Li_2CO_3	$O^{=}/CO_3^{=}$	K_{eq} (atm)
0.4105	----	----	0.13780	----	----
0.3789	0.40	9.0909×10^{-6}	0.13779	6.598×10^{-5}	2.500×10^{-5}
0.3487	0.60	1.3636×10^{-5}	0.13778	9.897×10^{-5}	3.451×10^{-5}
0.3342	1.00	2.2727×10^{-5}	0.13776	1.650×10^{-4}	5.514×10^{-5}
0.2947	1.00	2.2727×10^{-5}	0.13774	1.650×10^{-4}	4.862×10^{-5}
0.2710	1.20	2.7272×10^{-5}	0.13771	1.980×10^{-4}	5.366×10^{-5}
0.2066	2.40	5.4545×10^{-5}	0.13766	3.962×10^{-4}	8.185×10^{-5}
0.1434	3.60	8.1818×10^{-5}	0.13758	5.947×10^{-4}	8.528×10^{-5}
0.1224	4.60	1.0454×10^{-4}	0.13747	7.604×10^{-4}	9.307×10^{-5}

K_{eq} (ave) = $8.67 \pm 0.42 \times 10^{-5}$ (based on last 3 values of K_{eq})
$\log K_{eq}$ = -4.0620
ΔF° = -4.5761 (1063) (-4.0620)
ΔF° = 19.76 K cal/mole

TABLE 6-V

EQUILIBRIUM CONSTANTS FOR THE DECOMPOSITION OF Li_2CO_3 at 813°C
(1085°K) (1/T = 0.922 x 10^{-3} °K^{-1})

P_{CO_2} (atm)	Wt. Loss CO_2 (mg)	Moles CO_2 Lost	Moles Li_2CO_3	$O^{=}/CO_3^{=}$	K_{eq}(atm)
0.4158	0.90	2.0454×10^{-5}	0.13778	1.484×10^{-4}	6.170×10^{-5}
0.4539	0.80	1.8182×10^{-5}	0.13776	1.320×10^{-4}	5.991×10^{-5}
0.4184	1.00	2.2727×10^{-5}	0.13774	1.650×10^{-4}	6.904×10^{-5}
0.3381	1.80	4.0909×10^{-5}	0.13770	2.971×10^{-4}	1.004×10^{-4}
0.2631	2.80	6.3636×10^{-5}	0.13764	4.623×10^{-4}	1.216×10^{-4}
0.2434	3.20	7.2727×10^{-5}	0.13757	5.286×10^{-4}	1.287×10^{-4}
0.2237	3.50	7.9545×10^{-5}	0.13749	5.785×10^{-4}	1.294×10^{-4}

K_{eq} (ave) = $1.20 \pm 0.10 \times 10^{-4}$ (Based on last 4 values of K_{eq})
$\log K_{eq}$ = -3.9208
$\Delta F°$ = -4.5761 (1085) (-3.9208)
$\Delta F°$ = 19.47 K cal/mole

TABLE 6-VI

EQUILIBRIUM CONSTANTS FOR THE DECOMPOSITION OF Li_2CO_3 at 830°C
(1103°K) ($1/T = 0.905 \times 10^{-3}$ °K^{-1})

P_{CO_2} (atm)	Wt. Loss CO_2 (mg)	Moles CO_2 Lost	Moles Li_2CO_3	$O^{=}/CO_3^{=}$	K_{eq} (atm)
0.6737	----	----	0.13780	----	----
0.6224	0.20	4.5454×10^{-6}	0.13779	3.299×10^{-5}	2.053×10^{-5}
0.5724	0.60	1.3636×10^{-5}	0.13778	9.897×10^{-5}	5.665×10^{-5}
0.5276	0.90	2.0454×10^{-5}	0.13776	1.485×10^{-4}	7.835×10^{-5}
0.4842	1.20	2.7272×10^{-5}	0.13773	1.980×10^{-4}	9.587×10^{-5}
0.4447	1.50	3.4090×10^{-5}	0.13770	2.476×10^{-4}	1.101×10^{-4}
0.4105	1.80	4.0909×10^{-5}	0.13766	2.972×10^{-4}	1.220×10^{-4}
0.3776	2.20	5.0001×10^{-5}	0.13761	3.633×10^{-4}	1.372×10^{-4}
0.3053	3.50	7.9545×10^{-5}	0.13753	5.784×10^{-4}	1.766×10^{-4}
0.2474	5.00	1.1364×10^{-4}	0.13742	8.270×10^{-4}	2.046×10^{-4}

K_{eq} (ave) = $1.91 \pm 0.14 \times 10^{-4}$ (Based on last 2 values of K_{eq})
$\log K_{eq}$ = -3.7190
ΔF° = -4.5761 (1103) (-3.7190)
ΔF° = 18.77 K cal/mole

6.1.3.2 (Continued)

A plot of ln K_{eq} vs 1/T yields a slope of $-\Delta H^\circ/R$. Once ΔF° and ΔH° are known ΔS° can be calculated from the expression

$$\Delta F^\circ = \Delta H^\circ - T\Delta S^\circ \qquad (6)$$

the results of these calculations are summarized in Table 6-VII along with the data obtained from the JANAF tables (ref. 6). Plots of log K_{eq} vs 1/T for both sets of data are shown in figure 6-4 and, since they are a straight line, ΔH° is a constant for the temperature range studied and may be used in Eq. (6).

The values of K_{eq} obtained in this work are about a factor of two larger than the calculated values in the JANAF tables. The ΔH° value of 43.38 Kcal/mole is about 7 Kcal/mole lower than the calculated values (ΔH° from the JANAF data = 50.29 Kcal/mole). It should be pointed out that the JANAF data are based on derived thermodynamic values using data obtained by Brown and Latimer (ref. 7) for the reaction:

$$2Li^+(\infty H_2O) + (CO_3^=) \quad (\infty H_2O) \rightleftharpoons Li_2CO_3(c) \qquad (7)$$

and the data for

$$2Li(c) + 2H_2O(l) \rightleftharpoons 2Li^+(\infty H_2O) + 2OH^-(\infty H_2O) + H_2(g) \qquad (8)$$

obtained by Gunn and Green (ref. 8) and Messer et al. (ref. 9). Combining Equ. (7) and (8), the reaction,

$$2Li(c) + 2H_2O(l) + (CO_3)^= (\infty H_2O) \rightleftharpoons Li_2CO_3(c) + 2OH^-(\infty H_2O) + H_2(g) \qquad (9)$$

is obtained. Using values of ΔH_f for H_2O (l), $(CO_3)^=$ (∞H_2O) and OH^- (∞H_2O) by Wagman and Evans (ref. 10) a value of $\Delta H_f^= -290.64$ Kcal/mole is obtained for Li_2CO_3 in the crystalline state.

The values of ΔH_f for liquid Li_2CO_3 were then determined by adding the heat of fusion of 10.7 Kcal/mole for Li_2CO_3, as determined by Janz (ref. 19), to the value for Li_2CO_3(c) and correcting for temperature.

TABLE 6-VII

THERMODYNAMIC DATA FOR THE DECOMPOSITION OF Li_2CO_3
(UARL) ΔH° = 43.38 Kcal/mole

Temp. (°K)	K_{eq} (atm)	ΔF° (Kcal/mole)	ΔS° (cal/°/mole)
1022	3.98×10^{-5}	20.58	22.31
1043	6.47×10^{-5}	20.00	22.42
1063	8.67×10^{-5}	19.76	22.22
1085	1.20×10^{-4}	19.47	22.04
1103	1.91×10^{-4}	18.78	22.22

DECOMPOSITION OF Li_2CO_3 (JANAF TABLES)
ΔH° = 50.29 Kcal/mole

Temp. (°K)	K_{eq} (atm)	ΔF° (Kcal/mole)	ΔS° (cal/°/mole
900	4.39×10^{-7}	26.18	26.80
1000	8.08×10^{-6}	23.30	26.90
1100	8.47×10^{-5}	20.50	27.05
1200	5.84×10^{-4}	17.76	27.08

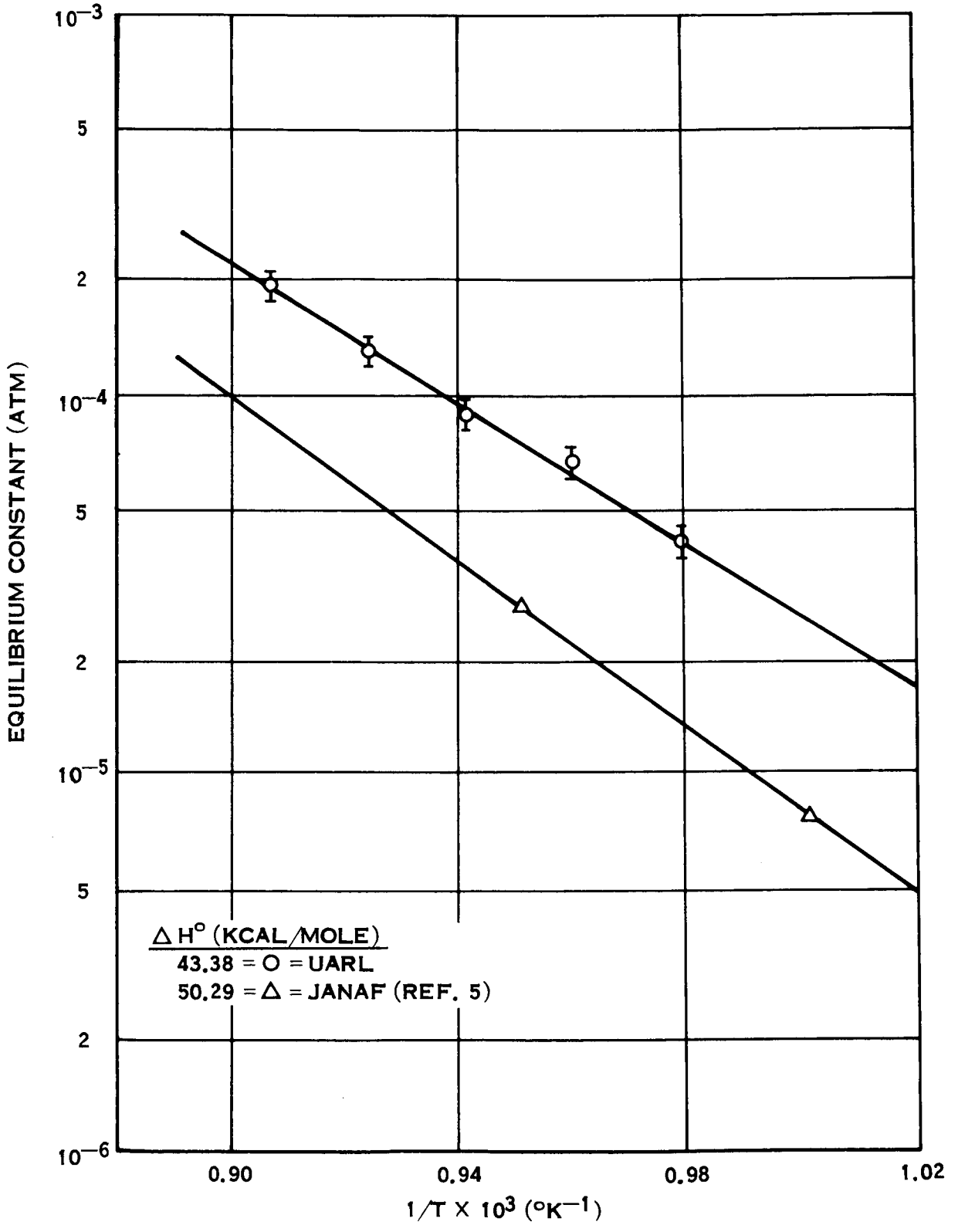


FIGURE 6–4. EQUILIBRIUM CONSTANTS FOR THE DECOMPOSITION OF Li_2CO_3 AS A FUNCTION OF TEMPERATURE

6.1.3.2 (Continued)

This was then used along with similarly derived values for Li_2O and known values for CO_2 to get the data shown in table 6-VII. The JANAF data are therefore subject to some uncertainty.

It is probable that better agreement between our results for ΔH° and the JANAF data would be achieved if corrections were made for the residual oxide in Li_2CO_3 melts. For example the data for two values of K_{eq} at 830°C (1103°K) were averaged to give a value $K_{eq} = 1.91 \times 10^{-4}$. A preliminary evaluation of residual oxide, however, suggests that the true value at this temperature may be closer to $K_{eq} = 2.9 \times 10^{-4}$. A similar but smaller correction could be made at 812°C (1085°K).

The effect of these changes would be to increase the slop of K_{eq} vs 1/T to a value nearer to JANAF value of 50.29 Kcal/mole without changing the fact that our values for K_{eq} are about twice those of the JANAF tables.

Dr. Stern of the National Bureau of Standards (ref. 11) has calculated a ΔH°_{1100} value for the decomposition of Li_2CO_3 using Kelley's (ref. 12) values of $H^\circ_{1100}-H^\circ_{298}$ for Li_2O and CO_2 and Janz's data for Li_2CO_3 (ref. 13) and gets $\Delta H^\circ_{1100} = 38.1$ Kcal/mole. This value is consistent with the UARL results reported herein and, as pointed out by Stern, contradicts the $\Delta H^\circ = 77.9$ Kcal/mole obtained from the slope of ln P_{CO_2} vs 1/T using Janz's data in ref. 13.

The present results are therefore believed to be essentially correct and indicate that valuable information can be obtained on molten salt mixtures containing Li_2CO_3 provided complications arising from volatilization of other components can be properly handled.

6.1.3.3 Li_2CO_3 - LiCl Eutectic Mixture

6.1.3.3.1 Decomposition

The decomposition measurements were extended to the Li_2CO_3 - LiCl eutectic mixture where the mole fraction of $Li_2CO_3 = 0.277$. Equilibrium constants were calculated for the decomposition reaction at 557, 575, 588, 610 and 643°C, tables 6-VIII - 6-XII, using the modified procedure, described in the experimental part of this report, in order to correct the data for LiCl evaporation. The LiCl evaporation was significant enough at temperatures above 600°C so that a white deposit was noted in the inside walls of the hang-down tube and on the hang-down wire. Corrections were made for LiCl evaporation at those temperatures to account for the LiCl on the wire, assuming uniform distribution and a wire/tube surface area ratio of 0.01.

Observations of the LiCl deposit show a thicker coat on the wire than on the tube and some error is introduced by assuming uniform distribution. The deposits on both the tube and the wire occurred between 2 and 3 inches above the top of the crucible.

TABLE 6-VIII

EQUILIBRIUM CONSTANTS FOR THE DECOMPOSITION OF Li_2CO_3 - LiCl EUTECTIC AT 557°C
(830°K) ($1/T = 1.205 \times 10^{-3}$ °K^{-1})

P_{CO_2} (atm)	Wt. Loss CO_2 (mg)	Moles CO_2 Lost	Moles Li_2CO_3	$O^{=}/CO_3^{=}$	K_{eq} (atm)
0.3921	----	----	0.056070	----	----
0.2605	0.07	1.590×10^{-6}	0.056068	2.837×10^{-5}	7.391×10^{-6}
0.1316	0.07	1.590×10^{-6}	0.056066	2.837×10^{-5}	3.733×10^{-6}
0.0618	0.30	6.817×10^{-6}	0.056059	1.216×10^{-4}	7.520×10^{-6}
0.0329	0.90	2.045×10^{-5}	0.056039	3.649×10^{-4}	1.200×10^{-5}
0.0118	2.04	4.635×10^{-5}	0.055993	8.278×10^{-4}	9.803×10^{-6}

K_{eq} (ave) = $9.18 \pm 1.09 \times 10^{-6}$ (Neglecting low value of K_{eq} at 0.1316 atm)
$\log K_{eq}$ = -5.0372
ΔF° = -4.5761 (830) (-5.0372)
ΔF° = 19.13 K cal/mole

TABLE 6-IX

EQUILIBRIUM CONSTANTS FOR THE DECOMPOSITION OF THE Li_2CO_3 - LiCl EUTECTIC AT 574°C (847°K) ($1/T = 0.181 \times 10^{-3}$ °K^{-1})

P_{CO_2} (atm)	Wt. Loss CO_2 (gm)	Moles CO_2 Lost	Moles Li_2CO_3	$O^{=}/CO_3^{=}$	K_{eq} (atm)
0.4158	----	----	0.506070	----	----
0.2684	----	----	0.056070	----	----
0.1303	0.24	5.453×10^{-6}	0.056065	9.727×10^{-5}	1.267×10^{-5}
0.0658	0.52	1.181×10^{-5}	0.056053	2.108×10^{-4}	1.387×10^{-5}
0.0355	0.93	2.113×10^{-5}	0.056032	3.771×10^{-4}	1.340×10^{-5}
0.0092	2.85	6.477×10^{-5}	0.056005	1.156×10^{-3}	1.065×10^{-5}

K_{eq} (ave) $= 1.26 \pm 0.10 \times 10^{-5}$ (Based on all values of K_{eq})

$\log K_{eq} = -4.8996$

$\Delta F^{\circ} = -4.5761\ (847)\ (-4.8996)$

$\Delta F^{\circ} = 18.99$ K cal/mole

TABLE 6-X

EQUILIBRIUM CONSTANTS FOR THE DECOMPOSITION OF THE Li_2CO_3 - LiCl EUTECTIC AT 588°C (861°K) ($1/T = 1.161 \times 10^{-3}\ ^oK^{-1}$)

P_{CO_2} (atm)	Wt. Loss CO_2 (mg)	Moles CO_2 Lost	Moles Li_2CO_3	$O^=/CO_3^=$	K_{eq} (atm)
0.4013	----	----	0.056205	----	----
0.2513	0.10	2.272×10^{-6}	0.056203	4.043×10^{-5}	1.016×10^{-5}
0.1342	0.40	9.089×10^{-6}	0.056194	1.617×10^{-4}	2.171×10^{-5}
0.0618	0.85	1.931×10^{-5}	0.056175	3.438×10^{-4}	2.126×10^{-5}
0.0342	1.50	3.408×10^{-5}	0.056141	6.071×10^{-4}	2.077×10^{-5}
0.0145	2.35	5.340×10^{-5}	0.056088	9.520×10^{-4}	1.378×10^{-5}

K_{eq} (ave) $= 1.94 \pm 0.28 \times 10^{-5}$ (Neglecting value of K_{eq} at 0.2513 atm)

$\log K_{eq} = -4.7122$

$\Delta F^\circ = -4.5761\ (861)\ (-47122)$

$\Delta F^\circ = 18.57$ K cal/mole

TABLE 6-XI

EQUILIBRIUM CONSTANTS FOR THE DECOMPOSITION OF THE Li_2CO_3 - LiCl EUTECTIC AT 606.5°C (879.5°K) ($1/T = 1.13 \times 10^{-3} °K^{-1}$)

P_{CO_2} (atm)	Wt. Loss CO_2 (mg)	Moles CO_2 Lost	Moles Li_2CO_3	$O^{=}/CO_3^{=}$	K_{eq} (atm)
0.3960	----	----	0.056070	----	----
0.2645	0.25	5.680×10^{-6}	0.056064	1.013×10^{-4}	2.680×10^{-5}
0.1316	0.35	7.953×10^{-6}	0.056056	1.419×10^{-4}	1.867×10^{-5}
0.0671	0.83	1.886×10^{-5}	0.056037	3.365×10^{-4}	2.258×10^{-5}
0.0329	2.09	4.749×10^{-5}	0.055990	8.482×10^{-4}	2.790×10^{-5}

K_{eq} (ave) $= 2.58 \pm 0.21 \times 10^{-5}$ (Neglecting value of K_{eq} at 0.1316 atm)
$\log K_{eq} = -4.5884$
$\Delta F^{\circ} = -4.5761\ (879.5)\ (-4.5884)$
$\Delta F^{\circ} = 18.47$ K cal/mole

TABLE 6-XII

EQUILIBRIUM CONSTANTS FOR THE DECOMPOSITION OF THE Li_2CO_3 - LiCl EUTECTIC AT 643°C (916°K) ($1/T = 1.091 \times 10^{-3}$ °K^{-1})

P_{CO_2} (atm)	Wt. Loss CO_2 (mg)	Moles CO_2 Lost	Moles Li_2CO_3	$O^{=}/CO_3^{=}$	K_{eq} (atm)
0.3947	----	----	0.056205	----	----
0.2460	0.22	4.999×10^{-6}	0.056200	8.895×10^{-5}	2.189×10^{-5}
0.1316	0.40	9.089×10^{-6}	0.056191	1.618×10^{-4}	2.128×10^{-5}
0.0592	1.78	4.044×10^{-5}	0.056151	7.203×10^{-4}	4.265×10^{-5}

K_{eq} (ave) = $2.86 \pm 0.94 \times 10^{-5}$ (Based on all values of K_{eq})
$\log K_{eq}$ = -4.5436
ΔF° = -4.5761 (916) (-4.5436)
ΔF° = 19.04 K cal/mole

6.1.3.3.1 (Continued)

The drying of the Li_2CO_3-LiCl mixture was accomplished in the same manner as before. In this case, a total irreversible weight loss on drying of about 54 mg (5400 ppm) was noted in a ten gram sample. A steady weight was obtained at 450°C but above this temperature (60° below the melting point) CO_2 loss was noted at a system pressure of 1 micron. The amount of moisture present in this system compared to pure Li_2CO_3 (8.8 mg volatile impurities in a 10 gram sample) is probably due to the affinity of LiCl for H_2O.

A summary of the LiCl-Li_2CO_3 eutectic data is shown in table 6-XIII. The values for ΔF were calculated using Eq. (5). A value for ΔH of 31.34 Kcal/mole was determined from the slope of the log K_{eq} versus 1/T plot, shown in figure 6-5.

In order to compare these data with that for the Li_2CO_3, melt, it was necessary to correct the ΔH and ΔF values for the mole fraction of Li_2CO_3 in the Li_2CO_3 - LiCl eutectic mixture. The mole fraction of Li_2CO_3 is 0.277 and is given the symbol, $X_{Li_2CO_3}$. The expressions

$$\Delta F' = \Delta F - RT \ln X_{Li_2CO_3} \quad (10)$$

$$\text{and } \Delta H' = \Delta H - RT \ln X_{Li_2CO_3} \quad (11)$$

were used for these calculations. The values for $\Delta S'$ were calculated from the $\Delta F'$ and $\Delta H'$ values using Eq. (6). The primed values for ΔH, ΔF, and ΔS are so designated since they correspond to the standard thermochemical quantities of ΔH°, ΔF° and ΔS° for Li_2CO_3 only in the case of ideal mixing. Since there is a difference between the primed and standard values, excess thermodynamic quantities of mixing are indicated.

A median temperature of 582°C was used for calculation of $\Delta H'$ since ΔH is essentially constant over the temperature range investigated. It will be noted that the point corresponding to 643°C was neglected in drawing the plot in figure 6-5, and thus the calculated thermodynamic values for this temperature are considerably different from the rest. This deletion was justified on the basis of statistics, but more so on the fact that the point was obtained under conditions of extreme LiCl volatility. A considerable amount of LiCl had deposited on the hang-down wire making it impossible to evaluate correctly the LiCl losses.

Using the above data, it is now possible to determine the degree of nonideality of the system by comparing them with the data for pure Li_2CO_3 at corresponding

TABLE 6-XIII

EQUILIBRIUM CONSTANTS AND THERMODYNAMIC DATA FOR THE Li_2CO_3-LiCl EUTECTIC MIXTURE (MOLE FRACTION Li_2CO_3 = 0.277) $\Delta H' = 33.53$ Kcal/mole

Temperature (°K)	K_{eq} (atm)	ΔF (Kcal/mole)	$\Delta F'$ (Kcal/mole)	$\Delta S'$ (Cal/°/mole)
916	2.86×10^{-5}	19.04	21.38	13.26
880	2.58×10^{-5}	18.47	20.72	14.55
861	1.94×10^{-5}	18.57	20.76	14.82
847	1.26×10^{-5}	18.99	21.15	14.61
830	9.18×10^{-6}	19.13	21.25	14.79

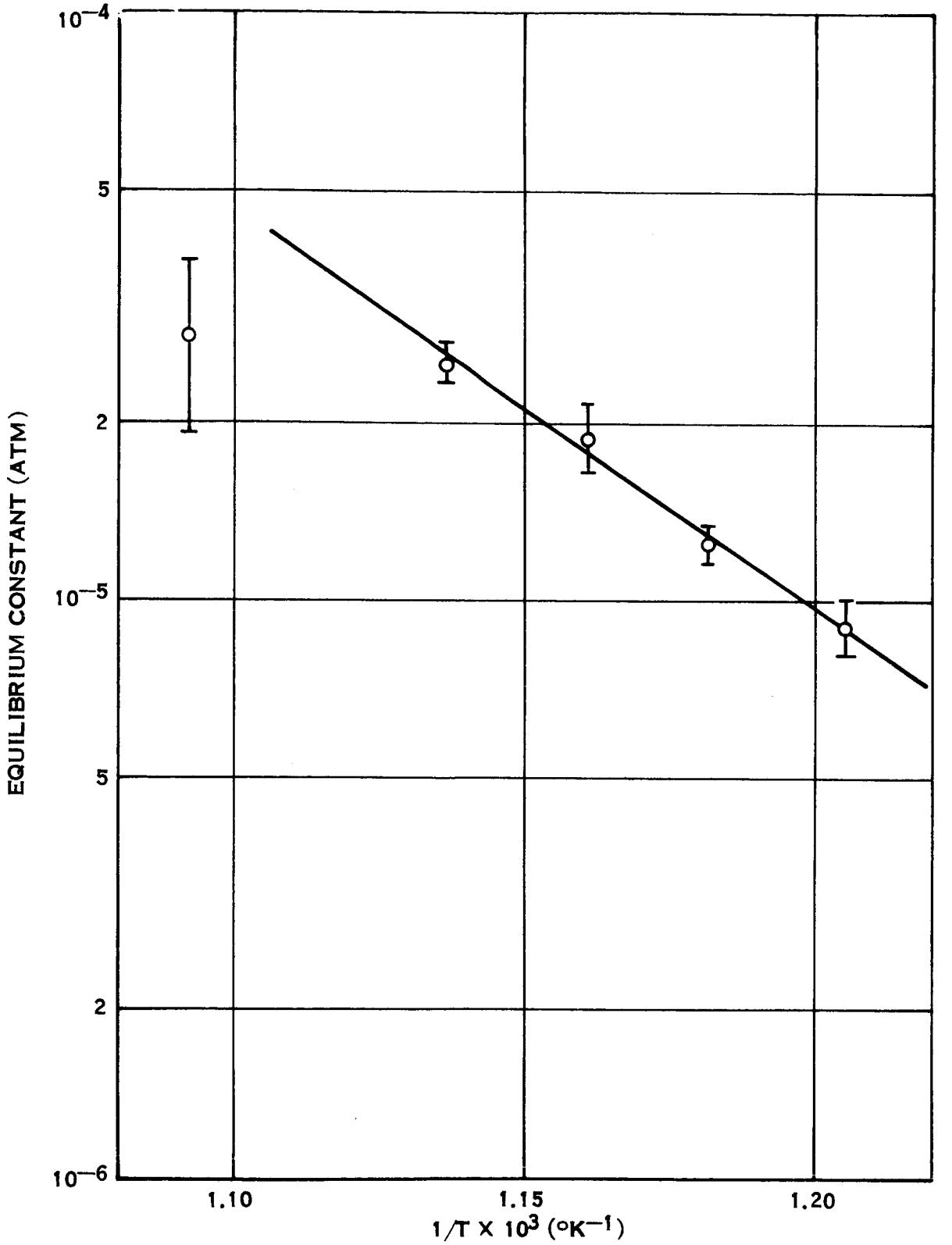


FIGURE 6–5. EQUILIBRIUM CONSTANTS FOR THE DECOMPOSITION OF Li_2CO_3 IN THE $Li_2CO_3 - LiCl$ EUTECTIC MELT AS A FUNCTION OF TEMPERATURE

6.1.3.3.1 (Continued)

temperatures. In order to do this, it is necessary to extrapolate the Li_2CO_3 data as a function of temperature to temperatures below the normal Li_2CO_3 melting point, thus treating the Li_2CO_3 as a supercooled liquid. The extrapolated data are summarized in table 6-XIV.

TABLE 6-XIV

EXTRAPOLATED THERMODYNAMIC DATA FOR PURE Li_2CO_3 (SUPERCOOLED)

Temperature (°K)	K_{eq} (atm)	$\Delta F°$ (Kcal/Mole)	$\Delta S°$ Cal/°/Mole	ΔF_{mix} (Kcal/Mole)	ΔS_{mix} (Cal/°/Mole)
916	3.55×10^{-6}	22.87	22.38	-1.49	-9.13
880	1.41×10^{-6}	23.57	22.50	-2.85	-7.95
861	8.20×10^{-7}	23.98	22.53	-3.21	-7.71
847	5.52×10^{-7}	24.29	22.50	-3.14	-7.89
830	3.41×10^{-7}	24.57	22.66	-3.32	-7.87

The values for ΔF_{mix} and ΔS_{mix} are the excess free energies and entropies as a result of non-ideal mixing. The value for ΔH_{mix} is -9.85 Kcal/mole, based on $\Delta H°$ for pure Li_2CO_3 of 43.38 Kcal/mole over the experimental temperature range.

Activity coefficients can be calculated from ΔF_{mix} using the equation,

$$\Delta F_{mix} = -RT \ln \gamma \qquad (12)$$

and thus activities corresponding to the mole fraction of Li_2CO_3 can be determined as a function of temperature. These data are summarized in table 6-XV.

Although these activities appear to be low, Baboian and Flengas (ref. 14) have shown that the activities of AgCl, RbCl and KCl in binary mixtures are on the order of 0.11 to 0.13 at mole fractions of 0.3, where the differences in ionic sizes are much less than those of the carbonate and chloride ions. In fact, the deviations from ideality for the AgCl-MCl systems expected from thermodynamic data are considerably less than those expected for the Li_2CO_3-LiCl system.

TABLE 6-XV

ACTIVITY COEFFICIENTS AND ACTIVITIES FOR Li_2CO_3 IN THE Li_2CO_3-LiCl EUTECTIC MELT ($X_{Li_2CO_3} = 0.277$)

Temp. (°K)	ΔF_{mix} (Kcal/mole)	γ	a(activity)*
916	-1.49	0.442	0.122
880	-2.85	0.196	0.054
861	-3.21	0.153	0.042
847	-3.14	0.155	0.043
830	-3.32	0.134	0.037

*activity (a) = activity coefficient (γ) x mole fraction (X)

6.1.3.3.1 (Continued)

Application of the excess free energies, enthalpy and entropies to structural interpretations, should be possible in the light of cation-anion attractive forces and anion-anion and cation-cation repulsive forces.

The role of ion pairs of differing ionic sizes and charges in the thermodynamics of molten salt mixtures are examined in the light of these results in the following section of this report.

6.1.3.3.2 LiCl Evaporation

LiCl evaporation rates were determined at each temperature as a function of total system pressure (in this case CO_2 pressure) by subtracting the CO_2 weight gain after repressurizing with CO_2, from the total weight loss over the period of the run at each temperature and pressure for the melt surface area of 5.07 cm^2. The data for these rates could be expressed as a log-log relationship which yielded a straight line. The data are summarized in table 6-XVI and plotted in figure 6-6.

The LiCl evaporation rates shown in figure 6-6 represent the net rate of removal of LiCl from one cm^2 surface area as a function of the CO_2 pressure over the melt (considered as an inert gas) and temperature. The slopes of these plots are summarized below and may be used to calculate rates at any pressure for a given temperature.

Temperature (°C)	Slope
557	-0.786
574	-0.843
588	-0.832
607	-0.691
643	-0.671

The slopes at the three lower temperatures are nearly constant at about -0.8. The two higher temperature plots have a lower slope on the order of -0.7. In the latter case, the amount of LiCl deposited on the hang-down wire was larger than at the lower pressures, yielding lower apparent evaporation rates and thus contributing to the lower slope.

The LiCl evaporation rates as determined here may serve as a guide to the degree of melt makeup necessary in actual cell operation and gas line clogging problems. It should be pointed out that all these measurements were made in a stagnant system, and gas flow would certainly compound the LiCl evaporation problem. In addition, the possible errors in evaporation rate measurements at the higher temperatures would yield low results.

TABLE 6-XVI

EVAPORATION RATES FOR LiCl
FROM THE Li_2CO_3-LiCl EUTECTIC MELT
IN THE EXPERIMENTAL SYSTEM OF FIGURE 6-6

643°C (916°K)		607°C (880°K)		588°C (861°K)	
Rate ($mg/hr/cm^2$)	Pressure (mm)	Rate ($mg/hr/cm^2$)	Pressure (mm)	Rate ($mg/hr/cm^2$)	Pressure (mm)
0.0659	187	0.0262	201	0.0114	191
0.0999	100	0.0361	100	0.0193	102
0.163	45	0.0619	51	0.0355	47
		0.0937	25	0.0720	26
				0.136	10

574°C (847°K)		557°C (830°K)	
Rate ($mg/hr/cm^2$)	Pressure (mm)	Rate ($mg/hr/cm^2$)	Pressure (mm)
0.0102	204	0.0082	198
0.0156	99	0.0110	100
0.0292	50	0.0203	47
0.0501	27	0.0302	25
0.162	7	0.0721	9

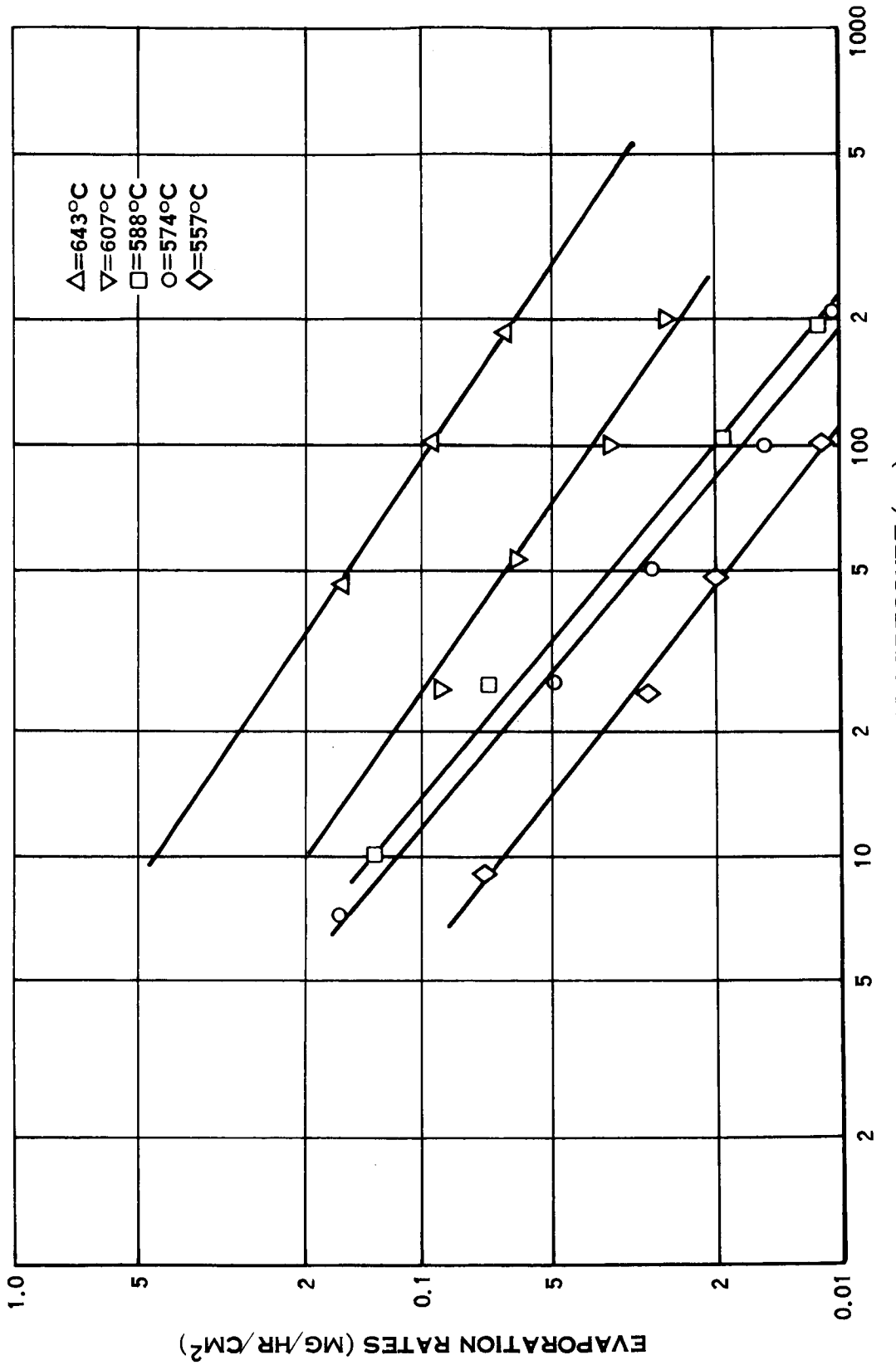


FIGURE 6–6. LiCl EVAPORATION RATES IN THE Li_2CO_3 – LiCl EUTECTIC MELT

6.1.3.3.2 (Continued)

If it can be assumed that the average values for the equilibrium constants at 607 and 643°C are in error due to errors in LiCl evaporation rate measurements, the slope of the log K_{eq} versus 1/T plot will yield a value for ΔH that is lower than would be expected. If only the three lower temperature values for K_{eq} are used, the slope of the plot would yield a value for $\Delta H'$ of 36 Kcal/mole as compared to the 33.5 Kcal/mole used in the above calculations. Since ΔH° for Li_2CO_3 = 43 Kcal/mole, ΔH_{mix} would be -7 Kcal/mole instead of the -10 Kcal/mole. The $\Delta F'$ values would be the same since they are based on K_{eq} but $\Delta S'$ would be 18 cal/°/mole as compared to 15 cal/°/mole and ΔS_{mix} would be -5 cal/°/mole.

6.1.3.4 Li_2CO_3-LiF Eutectic Mixture

The decomposition of Li_2CO_3 was also determined in the Li_2CO_3-LiF eutectic mixture in which the mole fraction of Li_2CO_3 was 0.514. This system was studied for two reasons: 1) it was a candidate as an electrolyte for the CO_2 reduction system, and 2) the LiF volatility was low, so the decomposition behavior should be simpler to handle than in the Li_2CO_3-LiCl system. The initial experiments on this system were carried out by simply lowering the pressure at a given temperature in successive steps as was done with pure Li_2CO_3. The Li_2CO_3-LiF system was dried in the same manner as before. The total irreversible weight loss was 9.8 mg in a 10 gram sample.

It was possible to heat the system to 500°C (100° below the melting point) under 1 micron pressure before CO_2 was lost. There were cases in which all the weight was not regained at the end of a run. Treatment of this apparent LiF loss in the same manner as was done with LiCl did not prove successful, since it was not possible to get straight line plots of the log of the evaporation rate versus the log of P_{CO_2}. These erratic results are attributed to the slower rates of carbonate decomposition in this system. Evidently in many cases, equilibrium had not been established at a given pressure before the pressure was changed. The time intervals allowed for this process, based on previous experience with Li_2CO_3 and the Li_2CO_3-LiCl system, were apparently inadequate.

Upon completion of the experiments, no salt deposits were noted anywhere in the system. In some cases more weight was gained than was lost. Several long term runs (72 hrs.) were made and it was found that much different results were obtained. The weight loss was completely regained in these cases confirming the premise that the rates of the carbonate decomposition in this system were much slower than in either pure Li_2CO_3 or in the Li_2CO_3-LiCl mixture.

What may be considered as fairly reliable data has been obtained (using long term runs at only a few pressures) at 750, 725, 700°C and 675°C. The data for those

6.1.3.4 (Continued)

temperatures are summarized in tables 6-XVII, 6-XIII, and 6-XIX. The thermodynamic data were calculated as outlined previously, and the symbols have the same significance as before.

The plot of log K_{eq} vs $\frac{1}{T}$ for the Li_2CO_3-LiF system is shown in figure 6-7. As can be seen from this plot, the highest temperature point was much lower than would be predicted from the data for the three lower temperatures and thus was neglected in determining the slope of the plot. Similar data was obtained with the Li_2CO_3-LiCl data and the highest temperature point was neglected in that case also.

ΔH for the slope shown in figure 6-7 is 39.36 Kcal/mole and $\Delta H'$ is 40.68 Kcal/mole. A comparison of these data with those for pure Li_2CO_3 is shown below in table 6-XX. In this case only, the lowest temperature points represents a super cooled liquid, since the melting point of pure Li_2CO_3 is 725°C. The corresponding ΔH_{mix} for this system is -2.70 Kcal/mole.

The activities of Li_2CO_3 in the mixture calculated from ΔF_{mix} according to Equation (12) are summarized in table 6-XXI.

The activity of Li_2CO_3 in this system approached that which would be expected if the Li_2CO_3 were merely diluted and still behaved as pure Li_2CO_3.

6.1.4 Discussion of Results

The results of the decomposition measurement for pure Li_2CO_3 and for Li_2CO_3 mixed with LiCl and LiF in eutectic proportions provide comparisons which help explain the differences in the behavior of melts containing carbonate and oxide as the only anions present and those containing carbonate, oxide and halide ions of varying size. In order to facilitate this comparison, the equilibrium constant data for the three melts has been plotted as a function of reciprocal temperature on one graph as shown in figure 6-8. The thermodynamic data for three systems, including the extrapolated Li_2CO_3 data, have also been summarized in tables 6-XXII through 6-XXV. It is immediately apparent that the presence of fluoride or chloride ions has increased the equilibrium constants to a considerable extent. If it were assumed that the plots can be linearly extrapolated, a convenient temperature for comparison is the point at 950°K or 677°C, which is in the range of interest for an operating CO_2 reduction system. At this point K_{eq} is 6.4×10^{-6}, 1.75×10^{-5} and 1.0×10^{-4} for Li_2CO_3, Li_2CO_3-LiF and Li_2CO_3-LiCl respectively. If it is further assumed that the partial pressure of CO_2 over the melts was that normally encountered in air (3×10^{-4} atm) the relative $O^{=}/CO_3^{=}$ ratios may be calculated from the equation

$$K_{eq} = (O^{=}/CO_3^{=})\ P_{CO_2} \qquad (2)$$

TABLE 6-XVII

EQUILIBRIUM CONSTANTS FOR THE DECOMPOSITION OF THE Li_2CO_3-LiF EUTECTIC AT 675°C (948°K) (1/T = 1.055x10^{-3}°K^{-1})

P_{CO_2} (atm)	Wt. Loss CO_2 (mg)	Moles CO_2 Lost	Moles Li_2CO_3	$O^{=}/CO_3^{=}$	K_{eq} (atm)
0.5263	--	--	0.10618	--	--
0.0513	1.70	$3.863X10^{-5}$	0.10614	$3.639X10^{-4}$	$1.868X10^{-5}$

K_{eq} = $1.87X10^{-5}$ (Only 1 point taken)
log K_{eq} = -4.7282
$\Delta F°$ = -4.5761 (948) (-4.7282)
$\Delta F°$ = 20.51 Kcal/mole

TABLE 6-XVIII

EQUILIBRIUM CONSTANTS FOR THE DECOMPOSITION OF THE Li_2CO_3-LiF EUTECTIC AT 697°C (970°K) (1/T = 1.031x10^{-3}°K-1)

P_{CO_2} (atm)	Wt. Loss CO_2 (mg)	Moles CO_2 Lost	Moles Li_2CO_3	$O^{=}/CO_3^{=}$	K_{eq} (atm)
0.5290	--	--	0.10618	--	--
0.1290	0.95	$2.159X10^{-5}$	1.10616	$2.033X10^{-4}$	$2.622X10^{-5}$
0.0632	2.10	$4.772X10^{-5}$	0.10611	$4.497X10^{-4}$	$2.840X10^{-5}$

K_{eq} (ave) = $2.73 \pm 0.11x10^{-5}$ (Based on both values of K_{eq})
log K_{eq} = -4.5638
$\Delta F°$ = -4.5761 (970) (-4.5638)
$\Delta F°$ = 20.24 Kcal/mole

TABLE 6-XIX

EQUILIBRIUM CONSTANTS FOR THE DECOMPOSITION OF THE Li_2CO_3-LiF EUTECTIC at 725°C (998°K) ($1/T = 1.001 \times 10^{-3}$ °K^{-1})

P_{CO_2} (atm)	Wt. Loss CO_2 (mg)	Moles CO_2 Lost	Moles Li_2CO_3	$O^{=}/CO_3^{=}$	K_{eq} (atm)
0.5224	--	--	0.10618	--	--
0.3855	0.20	4.544×10^{-6}	0.10617	4.280×10^{-5}	1.650×10^{-5}
0.2540	0.20	4.544×10^{-6}	0.10617	4.280×10^{-5}	1.087×10^{-5}
0.1303	1.95	4.431×10^{-5}	0.10613	4.175×10^{-4}	5.438×10^{-5}
0.0658	2.50	5.680×10^{-5}	0.10607	5.355×10^{-4}	3.523×10^{-5}

K_{eq} (ave) $= 4.48 \pm 0.96 \times 10^{-5}$ (Based on last 2 values of K_{eq})

$\log K_{eq} = -4.3487$

$\Delta F^{\circ} = -4.5761\ (998)\ (-4.3487)$

$\Delta F^{\circ} = 19.86$ K cal/mole

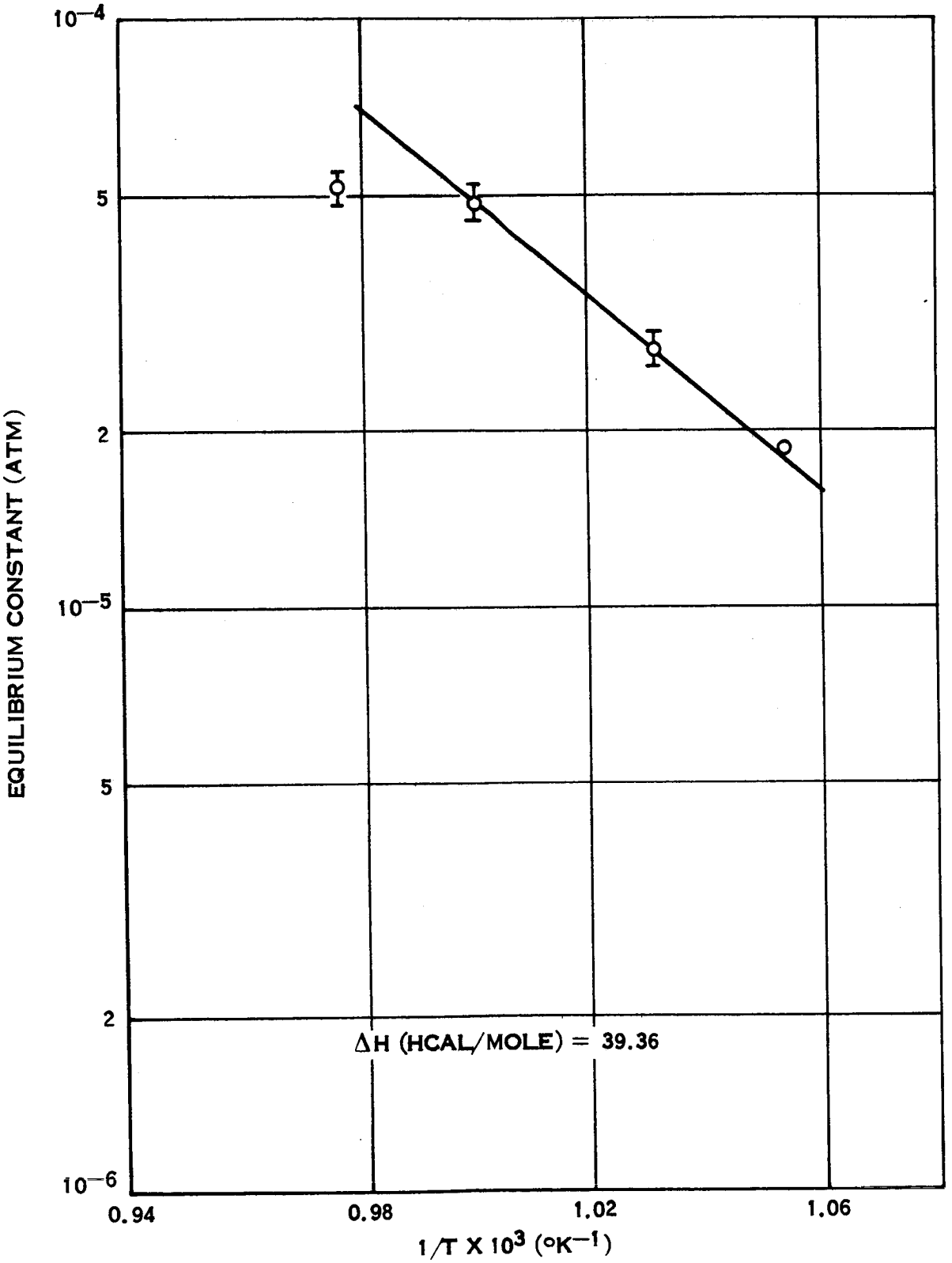


FIGURE 6–7. EQUILIBRIUM CONSTANTS FOR THE DECOMPOSITION OF Li_2CO_3 IN THE Li_2CO_3 – LiF EUTECTIC MELT AS A FUNCTION OF TEMPERATURE

TABLE 6-XX

EQUILIBRIUM CONSTANTS FOR THE DECOMPOSITION OF THE Li_2CO_3-LiF EUTECTIC at 749°C
(1022°K) (1/T = 0.975×10^{-3}°K^{-1})

P_{CO_2} (atm)	Wt. Loss CO_2 (mg)	Moles CO_2 Lost	Moles Li_2CO_3	$O^{=}/CO_3^{=}$	K_{eq} (atm)
0.5315	------	----	0.10618	----	----
0.2552	0.95	2.159×10^{-5}	0.10616	2.034×10^{-4}	5.190×10^{-5}
0.1023	2.30	5.226×10^{-5}	0.10611	4.925×10^{-4}	5.040×10^{-5}

K_{eq} (ave) = $5.12 \pm 0.08 \times 10^{-5}$ (Based on both values of K_{eq})
$\log K_{eq}$ = -4.2907
ΔF° = -4.5761 (1022) (-4.2907)
ΔF° = 20.07 K cal/mole

TABLE 6-XXI

EQUILIBRIUM CONSTANTS & THERMODYNAMIC DATA FOR THE Li_2CO_3-LiF EUTECTIC MIXTURE
(MOLE FRACTION Li_2CO_3 = 0.514)
$\Delta H'$ = 33.53 Kcal/mole

Temp (°K)	K_{eq} (atm)	ΔF (Kcal/mole)	$\Delta F'$ (Kcal/mole)	$\Delta S'$ (cal/°/mole)
1022	$5.12X10^{-5}$	20.07	21.42	18.84
998	$4.48X10^{-5}$	19.86	21.02	19.70
970	$2.73X10^{-5}$	20.24	21.52	19.75
948	$1.87X10^{-5}$	20.51	21.76	19.96

TABLE 6-XXII

EXTRAPOLATED THERMODYNAMIC DATA FOR PURE Li_2CO_3

Temp (°K)	K_{eq} (atm)	$\Delta F°$ (Kcal/mole)	$\Delta S°$ (cal/°/mole)	ΔF_{mix} (Kcal/mole)	ΔS_{mix} (cal/°/mole)
1022	$4.30X10^{-5}$	20.42	22.46	-1.00	-3.62
998	$2.44X10^{-5}$	21.06	22.36	-0.04	-2.66
970	$1.35X10^{-5}$	21.62	22.43	-0.10	-2.73
948	$8.10X10^{-6}$	22.09	22.46	-0.33	-2.50

TABLE 6-XXIII

ACTIVITY COEFFICIENTS & ACTIVITIES FOR Li_2CO_3 IN THE Li_2CO_3-LiF EUTECTIC MIXTURE ($X_{Li_2CO_3} = 0.514$)

Temp (°K)	ΔF_{mix} (Kcal/mole)	γ	a(activity)
1022	-1.00	0.611	0.314
998	-0.04	0.980	0.504
970	-0.10	0.948	0.487
948	-0.33	0.840	0.432

TABLE 6-XXIV

SUMMARY OF EQUILIBRIUM CONSTANTS & THERMODYNAMIC DATA

TEMP (° K)	Li_2CO_3 (ΔH° = 43.38 KCAL/MOLE)			Li_2CO_3–LiF ($\Delta H'$ = 40.68 KCAL/MOLE)			Li_2CO_3–LiCl ($\Delta H'$ = 33.53 KCAL/MOLE)		
	K_{EQ} (ATM)	ΔF° (KCAL/MOLE)	ΔS° (CAL/°/MOLE)	K_{EQ} (ATM)	$\Delta F'$ (KCAL/MOLE)	$\Delta S'$ (CAL/°/MOLE)	K_{EQ} (ATM)	$\Delta F'$ (KCAL/MOLE)	$\Delta S'$ (CAL/°/MOLE)
1103	$1.91X10^{-4}$	18.77	22.22						
1085	$1.20X10^{-4}$	19.47	22.04						
1063	$8.67X10^{-5}$	19.76	22.22						
1043	$6.47X10^{-5}$	20.00	22.42						
1022	$3.98X10^{-5}$	20.58	22.31	$5.12X10^{-5}$	21.42	18.84			
998	$2.44X10^{-5}$*	21.06*	22.36*	$4.88X10^{-5}$	21.02	19.70			
970	$1.35X10^{-5}$*	21.62*	22.43*	$2.73X10^{-5}$	21.52	19.75			
948	$8.10X10^{-6}$*	22.09*	22.46*	$1.87X10^{-5}$	21.76	19.96			
916	$3.55X10^{-6}$*	22.87*	22.38*				$2.86X10^{-5}$	21.38	13.26
880	$1.41X10^{-6}$*	23.57*	22.50*				$2.58X10^{-5}$	20.72	14.55
861	$8.20X10^{-7}$*	23.98*	22.53*				$1.94X10^{-5}$	20.76	14.82
847	$5.52X10^{-7}$*	24.29*	22.50*				$1.26X10^{-5}$	21.15	14.61
830	$3.41X10^{-7}$*	24.57*	22.66*				$9.18X10^{-6}$	21.25	14.79

* EXTRAPOLATED DATA

TABLE 6-XXV

SUMMARY OF THERMODYNAMIC MIXING DATA

	Li_2CO_3–LiF (ΔH_{MIX} = -2.70 KCAL/MOLE)		Li_2CO_3–LiC1 (ΔH_{MIX} = -9.85 KCAL/MOLE)	
TEMP. (°K)	ΔF_{MIX} (KCAL/MOLE)	ΔS_{MIX} (CAL/°/MOLE)	ΔF_{MIX} (KCAL/MOLE)	ΔS_{MIX} (CAL/°/MOLE)
1022	+1.00	-3.62		
998	-0.04	-2.66		
970	-0.10	-2.73		
948	-0.33	-2.50		
916			-1.49	-9.13
880			-2.85	-7.95
861			-3.21	-7.71
847			-3.14	-7.89
830			-3.32	-7.87

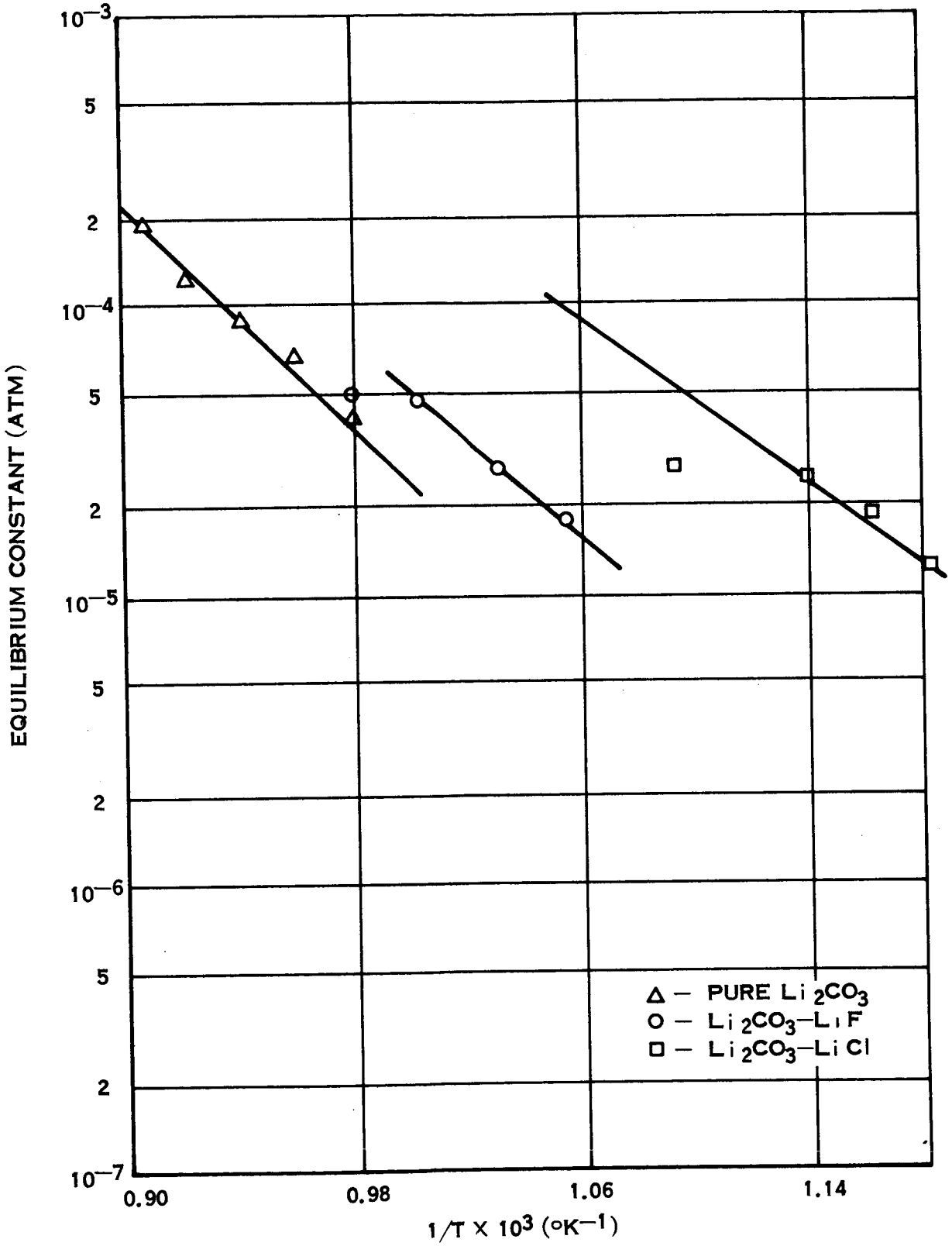


FIGURE 6–8. EQUILIBRIUM CONSTANTS FOR THE DECOMPOSITION OF Li_2CO_3 IN THE PURE STATE AND IN MIXTURES WITH LiCl AND LiF AS A FUNCTION OF TEMPERATURE

6.1.4 (Continued)

The ratio will then be 2.1×10^{-2}, 5.8×10^{-2} and 3.3×10^{-1} for Li_2CO_3, Li_2CO_3-LiF and Li_2CO_3-LiCl respectively. Thus, while the presence of LiF at the eutectic composition increases the equilibrium value for the $O^{=}/CO_3^{=}$ ratio over that for pure Li_2CO_3 by a factor of about 3, the presence of chloride ion at its eutectic composition increases the ratio by more than ten fold. The ratio of carbonate ion concentrations in the three systems is 1/0.514/0.277. By using the initial mole fractions of carbonate in each melt, it is possible to calculate the concentrations of oxide ions that would be present. For the three systems at equal temperatures and P_{CO_2} the oxide ion concentrations would be 2.0×10^{-2}, 2.8×10^{-2} and 6.9×10^{-2} moles for Li_2CO_3, Li_2CO_3-Li and Li_2CO_3-LiCl, respectively. Even on an absolute basis, therefore, the fluoride system slightly enhances the oxide ion concentration, but the oxide ion concentration in the chloride system is increased to about three times that expected for pure Li_2CO_3.

It is strongly suggested that this "stabilization" of oxide ions in the carbonate-chloride melt accounts for the observed superior CO_2 scrubbing ability of this electrolyte over that of an all carbonate or carbonate-fluoride mixture. The "stabilization" need not be due to the formation of complex ions but may be the result of changes in ionic attractions and repulsions in the melt, which are a function of the relative size and charge of the ions present.

Temkin, (ref 15) in his classical work on the theory of the structure of molten salts, has shown that a good theoretical model is obtained if it is assumed that all cations in the melt are surrounded by anions and all anions by cations, and that as first approximation the non-ideal behavior of the system is controlled by the coulombic forces between next-nearest neighbor ions without respect to charge. A model of the ionic configurations for the two mixed systems studied is shown in figure 6-9. The radii for these ions are as follows: CO_3 = 2.63Å, C^{-} = 1.82Å, $O^{=}$ = 1.40Å, F^{-} = 1.36Å, and Li^{+} = 0.60Å. The radii used here are ionic crystal radii with the exception of the carbonate ion. The latter value was taken from X-Ray diffraction by Zarzycki (ref. 16).

Molten salt solution behavior, such as deviations from ideality in mixtures, has been explained on the basis of differences in ionic sizes of the two melt constituents. The case for monovalent cations with a common anion is the only class of system that has been worked out mathematically to the extent where theoretical relationships fit experimental data for heats of mixing. Most of this work was done by Kleppa (ref. 16) for mixtures of alkali metal nitrates. Fluoride mixtures containing polyvalent cations have been studied by Cantor (ref. 18). Only qualitative information is available, but ionic size and charge does appear to have an effect on the magnitude of the heat of the mixing.

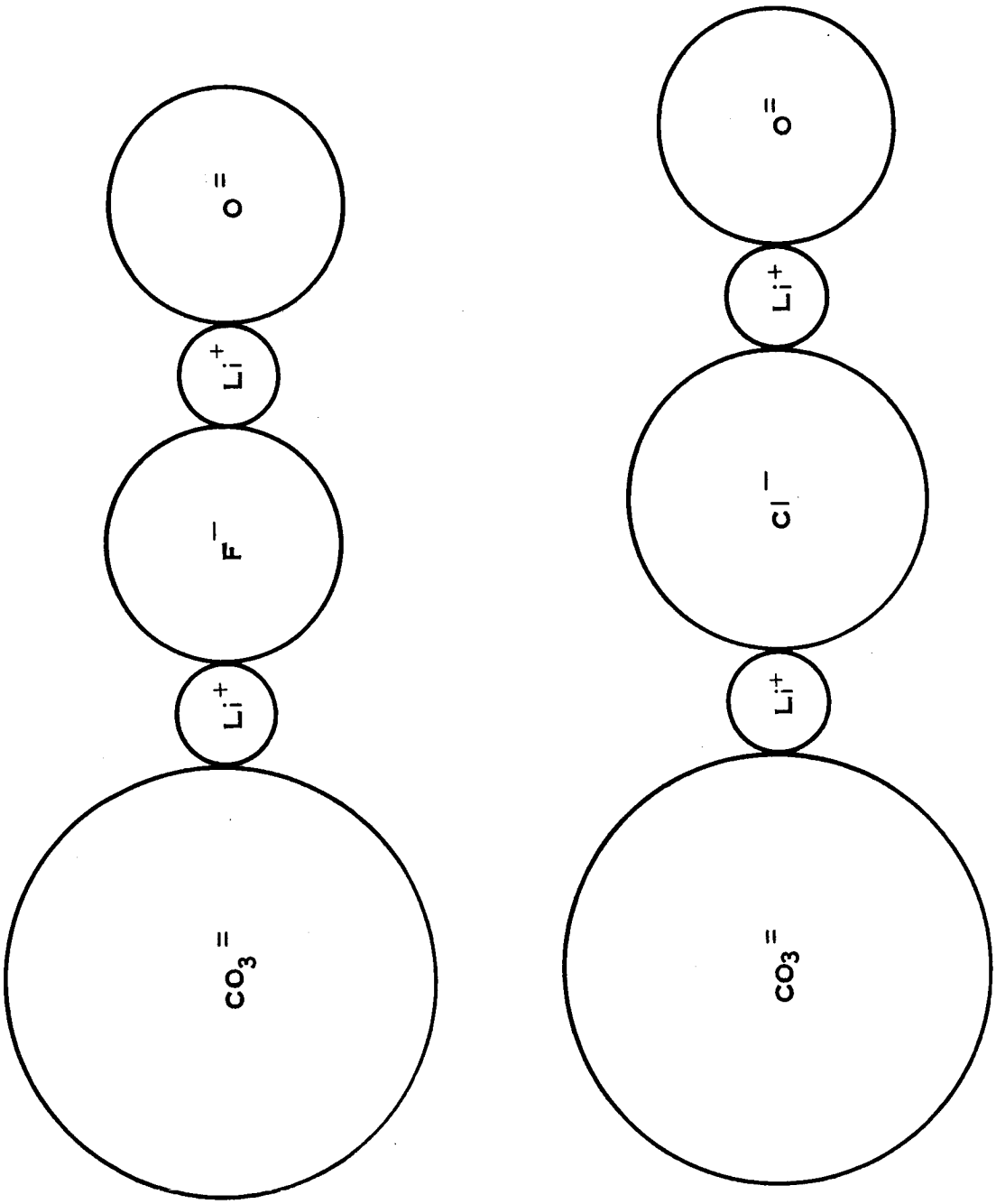


FIGURE 6–9. THEORETICAL POSITIONS OF IONS IN THE Li_2CO_3–LiCl & Li_2CO_3–LiF EUTECTIC MELTS

6.1.4 (Continued)

It should be pointed out that heats of mixing and other "excess" thermodynamic quantities are those which deviate from the values expected for a mixture to two or more components. For example, the heats of fusion of a mixture of component A and component B should lie between the values for pure A and pure B and be a linear function of the mole fractions of the components in any given mixture. If the heat of fusion of the mixture is greater than the value predicted on the basis of mole fractions, then the system is said to exhibit positive deviations from ideal behavior. If it is less than predicted, the system is said to exhibit negative deviations from ideal behavior. Almost without exception the highly ionic fused salt mixtures exhibit negative deviations from ideal behavior. For instance, in CaF_2-NaF mixtures the calcium ion is about the same size as the sodium ion, but the system shows negative deviations from ideality due to the difference in charge of the two ions. The BaF_2-NaF shows only slight deviations from ideality since the barium ion is larger than the sodium ion and this size difference partially makes up for the differences in charge.

No published experimental work has been found on mixtures with a common cation and mixtures of monovalent and divalent anions, but it is possible to make some conjectures on the behavior of this type of system on the basis of those discussed above.

In the case of pure Li_2CO_3, only one ionic configuration is possible; i.e. Li-CO_3 attractions are the only forces present in the system. When oxide ions are formed, the attractions between lithium and oxide ions are much greater than those between Li and CO_3 ions due to the similarity of their sizes. Thus, the oxide ion is stabilized to some extent. This is probably the reason that Li_2CO_3 is less stable than the corresponding sodium or potassium salts since the attraction forces between Na and oxide (γN_a = 0.95 Å) and K^+ and oxide (γK^+ = 1.33 Å) are less than those between Li and oxide (γLi^+ = 0.60 Å). During the decomposition process the carbonate ion concentration is essentially constant but the oxide ion concentration (in the experiments reported herein) increases from the minimum detectable amount of about 10^{-6} moles to as much as 10^{-4} moles at about 10^{-2} atm. CO_2. Thus, changes in the system when chloride or fluoride ions are added should be interpreted in terms of F-O or Cl-O interactions and Li-Cl or Li-F interactions rather than interactions involving the large carbonate ions. The results substantiate this premise since the difference in size between $CO_3^=$ and Cl^- is 0.81 Å while the difference in size between $CO_3^=$ and F^- is 1.27 Å and thus fluoride should have a greater effect than chloride. Since this is not the case, the differences in Cl-O and F-O must be the controlling factor; these differences being 0.42 Å and 0.04 Å for Cl-O and F-O respectively. Obviously the effects are not a direct result of ionic size differences, since a ten-fold difference in the relative thermodynamic quantities ratios would be noticed. As can be seen in table 6-XXIII, the ratios of ΔH_{mix}, ΔF_{mix} and ΔS_{mix} for the two systems are on the order of 3, 10, and 3 for the three quantities respectively. The ratio of charge densities for the chloride ion and the fluoride ion is about 2, so there seems to be a compromise between the closest point of approach of the ions and the charge densities of the ions.

6.1.4 (Continued)

It is postulated that the greater oxide ion concentration in the chloride system as compared to the fluoride system is due to the larger difference in size of the Cl^- and $O^=$, as compared to the F^- and $O^=$. It is further postulated that the smaller fluoride ion, which has relatively the same size as the oxide ion, has relatively little effect on the decomposition of Li_2CO_3. This premise is supported by the phase studies carried out in Phase I of the contract (ref. 1) where regular two-phase separation was noted in the Cl-O system, but not in the F-O system. The latter system exhibited behavior similar to the formation of solid solutions which are indicative of systems whose components are very similar in structure.

In general, it appears that carbonate diluents whose anions are much different in size compared with oxide ions strongly affect the carbonate decomposition reaction and that the largest equilibrium oxide ion concentration for a given carbonate concentration benefits the CO_2 scrubbing and general electrolytic behavior in the CO_2 reduction system. Thus, if the chloride system is to be used, the CO_3-Cl composition should be such that the deviations from ideal behavior are the largest. In most cases this deviation will be the greatest near the eutectic composition. However, Kleppa (ref. 17) has shown for alkali nitrates that there is an asymmetry in the ΔH_{mix} curve as a function of composition and that ΔH_{mix} is greater in systems more dilute in a large cation nitrate than it is in a system more dilute in the small cation nitrate. It has also been shown that ΔH_{mix} is greater in systems more concentrated in a small cation nitrate than it is in a system more concentrated in a large cation nitrate compared to the eutectic composition. The analogous situation for a common cation system, such as Li_2CO_3-LiCl mixtures, would be one where maximum in ΔH_{mix} would be at a composition more concentrated in the small anion than the eutectic composition. This composition, richer in LiCl than the eutectic, should yield a larger ΔH_{mix}. This fact points to the need for studying the decomposition reaction as a function of composition in order to determine the optimum composition for the electrolyte. It is predicted that this optimum composition will be that which exhibits the largest ΔH_{mix} for the system. In predicting the effects of ionic mixing on the properties of the system, it is also necessary to determine the volume changes on mixing. Baboian and Flengas (ref. 14) have shown that a positive ΔV_{mix} results in an overall relaxation of the structure of the ionic solution accompanied by a decrease in the various coulombic interactions. Cation-anion attractions will be decreased and there will be a positive contribution to the heat of mixing. However, a corresponding decrease in anion to anion and cation to cation repulsions will introduce a negative contribution to the heat. There are also cases where the cation to cation distance increases while the cation to anion distance decreases on mixing (similar to the situation with the CO_3-Cl system). The increased cation-anion interaction would make the heat effect more negative in this case. Thus a knowledge of changes in density, and thus volume, on mixing, would be important in determining the relative effects of the ionic interactions in the system, which in turn affects the oxide ion concentration in the melt.

6.1.4 (Continued)

It is strongly recommeded that density and decomposition measurements as a function of composition should be carried out as a part of future work on the CO_2 reduction system.

There are two areas of interest for future work have come to light during the course of the Li_2CO_3 decomposition experiments. First, all the data were taken on a time base recorder so that it may be possible to determine the kinetics of both the decomposition and recombination reactions. In the case of the pure Li_2CO_3 runs, the recombination was only followed after the lowest pressure run at each temperature. However the Li_2CO_3-LiCl and Li_2CO_3-LiF runs will provide data for both the decomposition and recombination at each pressure. Any future work should include the evaluation of these kinetic data, including the derivation of equations which would indicate the order of the reaction and possibly shed light on the mechanism of the reaction.

On the basis of overall observations the kinetics of the decomposition and recombination reaction for Li_2CO_3 in the Li_2CO_3-LiF mixture appear to be much slower than that for pure Li_2CO_3 or Li_2CO_3-LiCl. The errors incurred in early experiments on this system were due to changing pressure and temperatures before equilibrium was established. The times allowed before changing these parameters was based on earlier experience with the other systems where the rates of reactions were apparently faster than experienced with the Li_2CO_3-LiF system.

A second area for future work arises from the observation that the data for both the Li_2CO_3-LiCl and Li_2CO_3-LiF systems show a much lower equilibrium constant than predicted at the high temperature end of the temperature ranges investigated. In the case of the Li_2CO_3-LiCl, system it was thought that the value for K_{eq} at 640° C was in error due to excessive LiCl evaporation. However, the value of K_{eq} at 750° C for the Li_2CO_3-LiF system was redetermined several times and seems to be real. It is possible that a basic change in melt structure occurs between 100 and 150° C above the melting point of each eutectic (610° for Li_2CO_3-LiF, and 510° C for Li_2CO_3-LiCl). Thus, a relaxation of the structure reduces the stabilization effects on the oxide ion, and the systems behavior more nearly like the pure carbonate. If this effect is real, higher temperature data should be obtained to see whether a different value for ΔH is obtained.

In summary, it appears that a Li_2CO_3-LiCl composition that is more dilute in Li_2CO_3 than the eutectic composition might provide the optimum mixture for the CO_2 reduction system, and that the addition of anions smaller than the chloride ion or cations larger than lithium will decrease the effectiveness of the electrolyte for CO_2 scrubbing and for optimum formation of carbon.

6.1.5 Recommendations

The following items are recommended as a basis for future research on the Li_2CO_3-LiCl electrolyte which should provide information of direct benefit to the CO_2 reduction program.

6.1.5.1 The decomposition studies of Li_2CO_3 in the Li_2CO_3-LiCl system should be extended to include compositions more concentrated in LiCl than the eutectic composition. It is possible that the deviations from ideal behavior in this composition range may be greater than that of the eutectic composition and thus an equilibrium concentration of oxide ions would be realized that is higher than that experienced to date.

6.1.5.2 Predictions of oxide ion "stability" in the melt are strongly dependent upon volume changes on mixing Li_2CO_3 and LiCl. Thus, density measurements of the system as a function of composition would provide important data that may be correlated with the thermodynamic measurements to help predict optimum operating conditions for the CO_2 reduction system.

6.1.5.3 Kinetic data, available from the thermogravimetric studies, should be evaluated to see whether reaction rate constants and thus mechanisms for the decomposition and recombination reactions can be calculated. The rate constants can then be compared with those rates imposed by electrolysis in order to predict dynamic equilibrium concentrations of oxide in the electrolyte.

6.2 Thermodynamic Equilibria in Carbonate Melts

Work on the theoretical determination of the chemical constituents of molten alkali-metal-carbonate electrolytes considered for the electrolytic decomposition of carbon dioxide was initiated as a result of experimental observations which indicated differences in the quality and qauntity of carbon deposited at the cathode when the initial composition of the electrolyte was varied or the alkali metal was changed. It was postulated that the differences might be attributed to the different thermodynamic properties of the several chemical species which might exist in the melt or in the gas phase above the melt at the various operating temperatures. Therefore, theoretical calculations of the equilibrium compositions of the melt were performed in order to provide some degree of correlation with the experimental observations.

The study of the thermodynamic equilibria in the melts was divided into two parts: (1) a qualitative determination of the individual chemical species in a pure alkali metal carbonate melt; and (2) a determination of the actual equilibrium composition of four specific melts which are representative of the various melts considered for the electrolytic decomposition of carbon dioxide.

6.2 (Continued)

It should be noted here that the equilibrium compositions calculated may not be exactly representative of those existing in a fused salt electrolyte because it was assumed for the calculations that (1) condensed phases which may exist in the melt are insoluble in each other and therefore are separate and distinct; (2) changes from liquid to solid phase for the individual species will occur when the temperature falls below the melting temperature of the species; and (3) no ionic dissociation of the various molecular species occurs. These assumptions may restrict the usefullness of the results since the ingredients of the electrolyte are soluble in each other, and during the electrolyte decomposition of carbon dioxide a non-equilibrium condition exists. However, the equilibrium calculations could be useful as a first approximation in predicting and rationalizing trends in experimental observations.

6.2.1 Qualitative Determination of Melt Composition

The work described in this part of the study was an extension of the work performed during Phase I of this contract work which is reported in Ref. 1 . Some of the calculations performed during the Phase I work were repeated in this study to determine the effect of using updated thermodynamic data which was recently reported in the JANAF Thermochemical Tables (ref. 6). These calculations were also extended to include the effects on melt composition of the addition of water to the melt and of the substitution of barium for the alkali metal.

With the restrictions that a specific combination of molecular species be physically possible in accordance with the Gibbs Phase Rule and that one of the molecular species is an alkali carbonate, the total number of possible combinations of three condensed melt ingredients is 15 and may include condensed alkali metal, (M), condensed carbon (C), and condensed - M_2CO_3, M_2C_2, M_2O, M_2O_2, and MO_2. For reacting systems containing three condensed phases and one gas phase, specification of the temperature of the reacting system fixes the concentration of the gaseous constituents. Therefore the total pressure of the reacting system because the number of degrees of freedom of such a reacting system is one, as can be demonstrated by utilizing the Gibbs Phase Rule.

The gas composition for each of the 15 possible combinations of three condensed phases was calculated using a set of expressions for the partial pressure of the various gaseous species, which in turn were derived from expressions for the equilibrium constant for each species. If the partial pressure of any gaseous species exceeded the vapor pressure of that species at the particular temperature of interest, then that species should also be condensed and the particular combination of melt ingredients should include four condensed phases. This possibility is eliminated by the Phase Rule, since such a system would have no degree of freedom and it has been assumed that one degree of freedom exists because temperature has been specified.

6.2.1 (Continued)

Eliminating those combinations of three condensed phases which would give a partial pressure of a condensible gas which exceeded its vapor pressure, and also eliminating those combinations which would give a total pressure largely in excess of atmospheric pressure, the following combinations containing three condensed phases may exist.

Systems containing Li and Na only
$M_2O - C - M_2CO_3$

Systems containing Na and K only
$M_2O - M_2O_2 - M_2CO_3$
$M_2O - MO_2 - M_2CO_3$
$M_2O_2 - M - M_2CO_3$
$MO_2 - M - M_2CO_3$
$M - C - M_2CO_3$
$M_2O - M - M_2CO_3$

Systems containing K only
$M_2O_2 - MO_2 - M_2CO_3$

It can be seen from the list above, that there are only two product combinations in which solid carbon can exist with the carbonate, $M_2O - C - M_2CO_3$ and $M - C - M_2CO_3$. The system $Na_2O - C - Na_2CO_3$ can exist only at temperatures below 900°K. The total pressure for each permissible system is shown in table 6-XXVI. A comparison of these pressures with those reported in ref. 1 indicate that the changes in thermodynamic data resulted in a slight increase in total pressure for some of the systems.

It should be noted that for the above calculations the correct C/M and O/M ratios required to form a particular combination were assumed. Variations of these atom ratios could affect the existence of any of the combinations. The ranges of permissible atom ratios for each possible comination is shown in figure 6-10. Since the results shown in figure 6-10 were obtained from the simultaneous solution of atom balance equations, which included only the condensed phase and not gaseous products, the ranges of atom ratios obtained represent the maximum ranges which may be permitted. If concentrations of gaseous products become large, these ranges of atom ratios could be significantly decreased.

TABLE 6-XXVI

TOTAL PRESSURE ABOVE CARBONATE MELTS
CONTAINING THREE CONDENSED PHASES

Pressure in Atmospheres

Temperature (°K)	500	600	700	800	900	1000
System M_2O-M_2O_2-M_2CO_3						
M						
Li	*	*	*	*	*	*
Na	7.413×10^{-12}	1.337×10^{-8}	2.704×10^{-4}	1.349×10^{-4}	2.334×10^{-3}	2.198×10^{-2}
K	9.058×10^{-16}	2.806×10^{-12}	8.412×10^{-10}	5.968×10^{-8}	1.666×10^{-6}	2.489×10^{-5}
System M_2O-M-M_2CO_3						
Li	*	*	*	*	*	*
Na	8.582×10^{-7}	5.368×10^{-5}	1.014×10^{-3}	9.135×10^{-3}	5.012×10^{-2}	1.950×10^{-1}
K	3.138×10^{-5}	9.207×10^{-4}	1.007×10^{-2}	5.979×10^{-2}	2.363×10^{-1}	1.0471
System M_2O-C-M_2CO_3						
Li	1.292×10^{-12}	3.543×10^{-9}	3.745×10^{-7}	6.069×10^{-5}	1.488×10^{-3}	1.826×10^{-2}
Na	2.841×10^{-8}	6.352×10^{-6}	3.000×10^{-4}	5.227×10^{-3}	*	*
K	*	*	*	*	*	*
System M_2O_2-M-M_2CO_3						
Li	*	*	*	*	*	*
Na	8.582×10^{-7}	5.368×10^{-5}	1.015×10^{-3}	9.138×10^{-3}	5.018×10^{-2}	1.963×10^{-1}
K	3.138×10^{-5}	9.207×10^{-4}	1.007×10^{-2}	5.980×10^{-2}	2.365×10^{-1}	7.064×10^{-1}

TABLE 6-XXVI (Con'd)

TOTAL PRESSURE ABOVE CARBONATE MELTS
CONTAINING THREE CONDENSED PHASES

System $M\text{-}C\text{-}M_2C0_3$

Li	*	*	*	*	*	*
Na	8.582×10^{-7}	5.368×10^{-5}	1.014×10^{-3}	9.135×10^{-3}	5.012×10^{-2}	1.950×10^{-1}
K	3.138×10^{-5}	9.207×10^{-4}	1.007×10^{-2}	5.979×10^{-2}	2.363×10^{-1}	1.0471

System $M_20\text{-}M0_2\text{-}M_2C0_3$

Li	*	*	*	*	*	*
Na	6.329×10^{-3}	8.643×10^{-2}	5.216×10^{-1}	1.9025	4.9736	10.344
K	1.977×10^{-11}	5.066×10^{-9}	2.638×10^{-7}	5.067×10^{-6}	5.078×10^{-5}	3.241×10^{-4}

System $M_20_2\text{-}M0_2\text{-}M_2C0_3$

Li	*	*	*	*	*	*
Na	*	*	*	*	*	*
K	2.742×10^{-7}	5.688×10^{-6}	5.012×10^{-9}	2.576×10^{-4}	9.419×10^{-3}	2.704×10^{-3}

System $M0_2\text{-}M\text{-}M_2C0_3$

Li	*	*	*	*	*	*
Na	8.582×10^{-7}	5.368×10^{-5}	1.015×10^{-3}	9.135×10^{-3}	5.012×10^{-2}	1.950×10^{-1}
K	3.138×10^{-5}	9.207×10^{-4}	1.007×10^{-2}	5.98×10^{-2}	2.365×10^{-1}	7.064×10^{-1}

*Three condensed phases do not exist at these temperatures

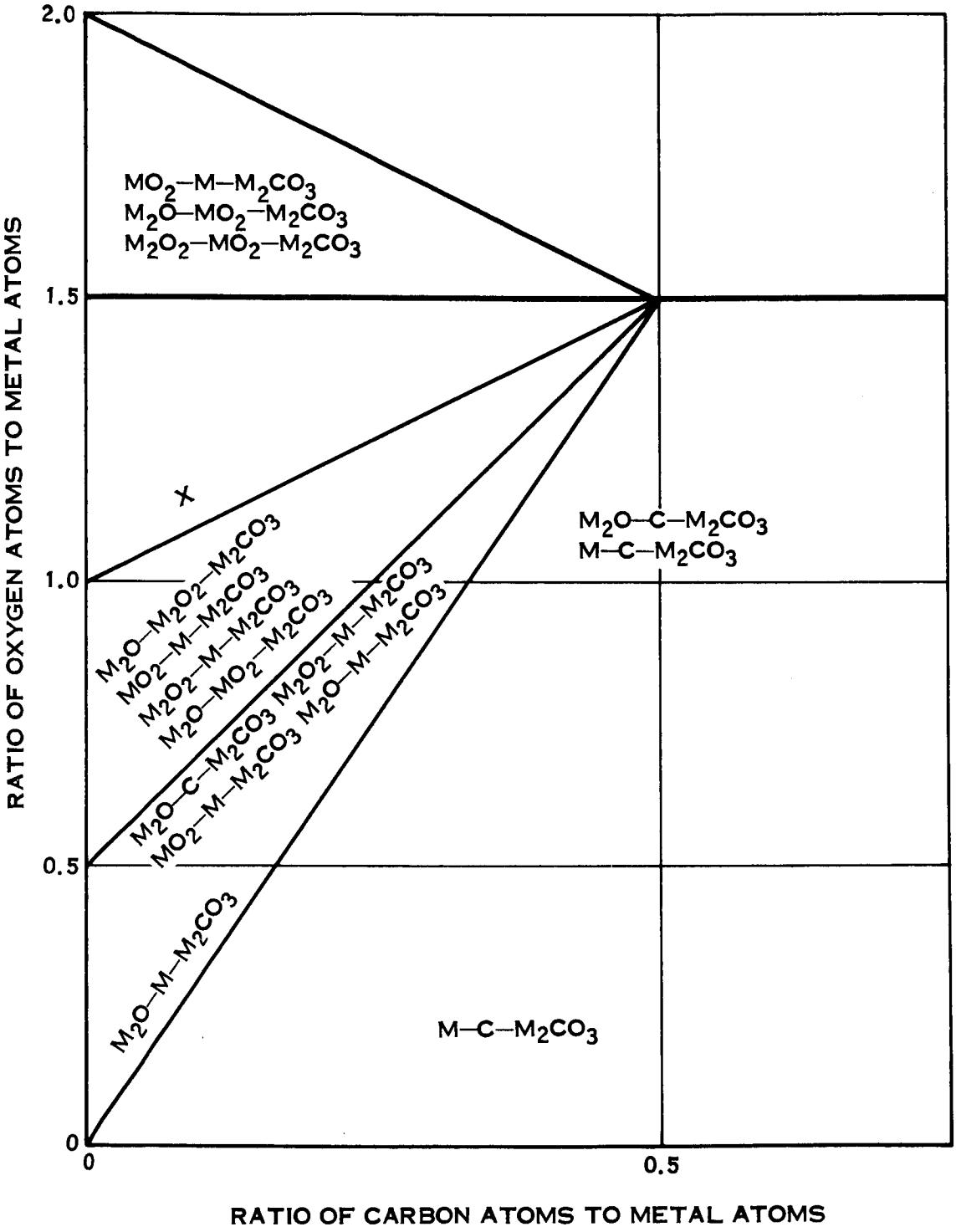


FIGURE 6–10. REGIONS OF POSSIBLE COMBINATIONS OF THREE CONDENSED PHASES IN CARBONATE MELTS

6.2.1 (Continued)

The effect of water in the melt on the composition of the melt was determined from the results of calculations made with H atom included as a melt ingredient. The addition of another atom in the system allows one more degree of freedom and therefore one more condensed phase may be present. It was assumed that any interaction between carbonate and water would result in the formation of alkali metal hydroxides. The results of the calculations indicated that the total pressure was increased because of the formation of appreciable amounts of hydrogen and methane. The introduction of H atom to the system tends to shrink the ranges of O/M and C/M, for which the various product combinations may exist because O atoms are being used to form MOH.

A limited number of calculations was performed to determine which systems may exist when barium is substituted for the alkali metal. All the product combinations that were considered for the alkali metals could not be considered in the barium calculations because thermodynamic data was lacking for many of the oxides of barium. Only one system containing carbon was found to be possible, $BaO - C - BaCO_3$.

6.2.2 Quantitative Determination of Melt Composition

The equilibrium composition of the gas above four typical molten electrolytes and the composition of the electrolytes themselves were determined for temperatures ranging from 500 to 1100° K and for a pressure of one atmosphere. For the calculations, it was assumed that 1 liter of a gas composed by volume of 99.94 percent Ar, 0.03 percent H_2O and 0.03 percent CO_2 was in equilibrium with 2000 gms of electrolyte.

The calculations of composition were performed utilizing a procedure which was developed for high speed computers and which is described in ref. 20. This procedure employs a successive approximation procedure to find the simultaneous solution of the standard equations of chemical equilibria, conservations of (atomic) mass and conservation of energy for specified values of pressure and either temperature or enthalpy. The derivation of these equations involve the following assumptions: (1) the gaseous products of reaction behave ideally and follow Dalton's law of partial pressure; (2) all condensed phases are immiscible; and (3) the gases are insoluble in the condensed phases. Further, no ionic dissociation of the products of reaction occurs.

The initial composition of each of the four melts considered was as follows: (1) 60% by weight LiCl - 40% by weight Li_2CO_3; (2) 35% by weight Li_2CO_3 - 65% by weight K_2CO_3; (3) 58 moles LiCl - 42 moles KCl to which was added 1.5 moles Li_2CO_3; and (4) 8 moles Li_2CO_3 - 6 moles K_2CO_3 - 6 moles Na_2CO_3.

6.2.2 (Continued)

The results of the calculations indicated that the compositions of the melts were not appreciably changed over the entire temperature range between 500 and 1000°K. However, dissociation of Li_2CO_3 into Li_2O and CO_2 begins to occur at a temperature of 1100°K. Also, for those melts which contain K_2CO_3, a small amount of condensed potassium appears at 1100°K.

The partial pressures of the major components of the gas phase above each melt is shown in figures 6-11 through 6-14. It can be seen from the figures that significant dissociation of the condensed ingredients does not occur until a temperature of 900°K is reached. For those melts which contain chlorides, the major dissociation products are the monomer and dimer of LiCl or KCl. For those melts which contain carbonates only, the major dissociation products appear to be the monomer and dimer of the alkali metal hydroxides.

In order to determine the effect on the composition of the melt when solid carbon is added to it, calculations of the composition of the gas above the LiCl-Li_2CO_3-C melts at 900°K were performed for several different values of added carbon. The partial pressures obtained from these calculations are shown in figure 6-15. It can be seen that the addition of carbon to the melt drives the equilibrium toward the formation of substantial amounts of H_2 and CO. When approximately 0.01 weight percent has been added to the melt, condensed Li_2O is formed in the melt and solid carbon appears when 0.02 weight percent has been added. The melt composition and the gas composition remain essentially unchanged as the carbon concentration is increased above 0.02 percent.

The significant results of this study task can be summarized as follows: (1) the possible carbonate melt compositions in which solid carbon coexists with the carbonate are Li_2O-C-Li_2CO_3, Na_2O-C-Na_2CO_3 (for temperatures below 900°K), Na-C-Na_2CO_3, K-C-K_2CO_3, and BaO-C-$BaCO_3$; (2) The melt weight losses noted in experiments may be attributed to the formation of the gaseous monomer and dimer of alkali metal halides or hydroxides; (3) The addition of carbon to a melt composed of 60 weight percent LiCl and 40 weight percent Li_2CO_3 causes the formation of Li_2O in the melt and of significant amounts of CO and H_2 in the gas phase above the melt.

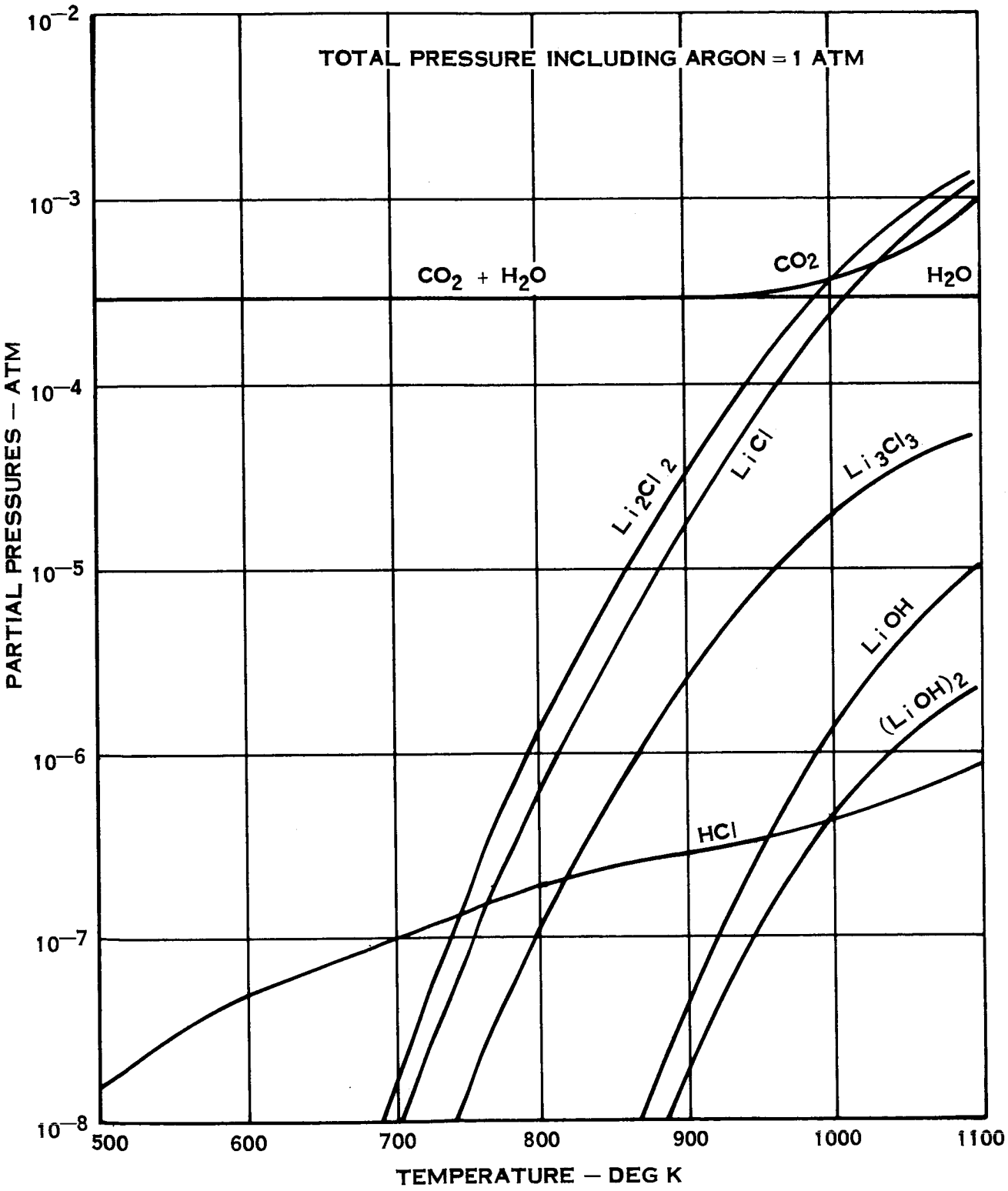


FIGURE 6–11. PARTIAL PRESSURES OF GASES ABOUT A MELT CONTAINING 60% LiCl –40% Li_2CO_3 BY WEIGHT

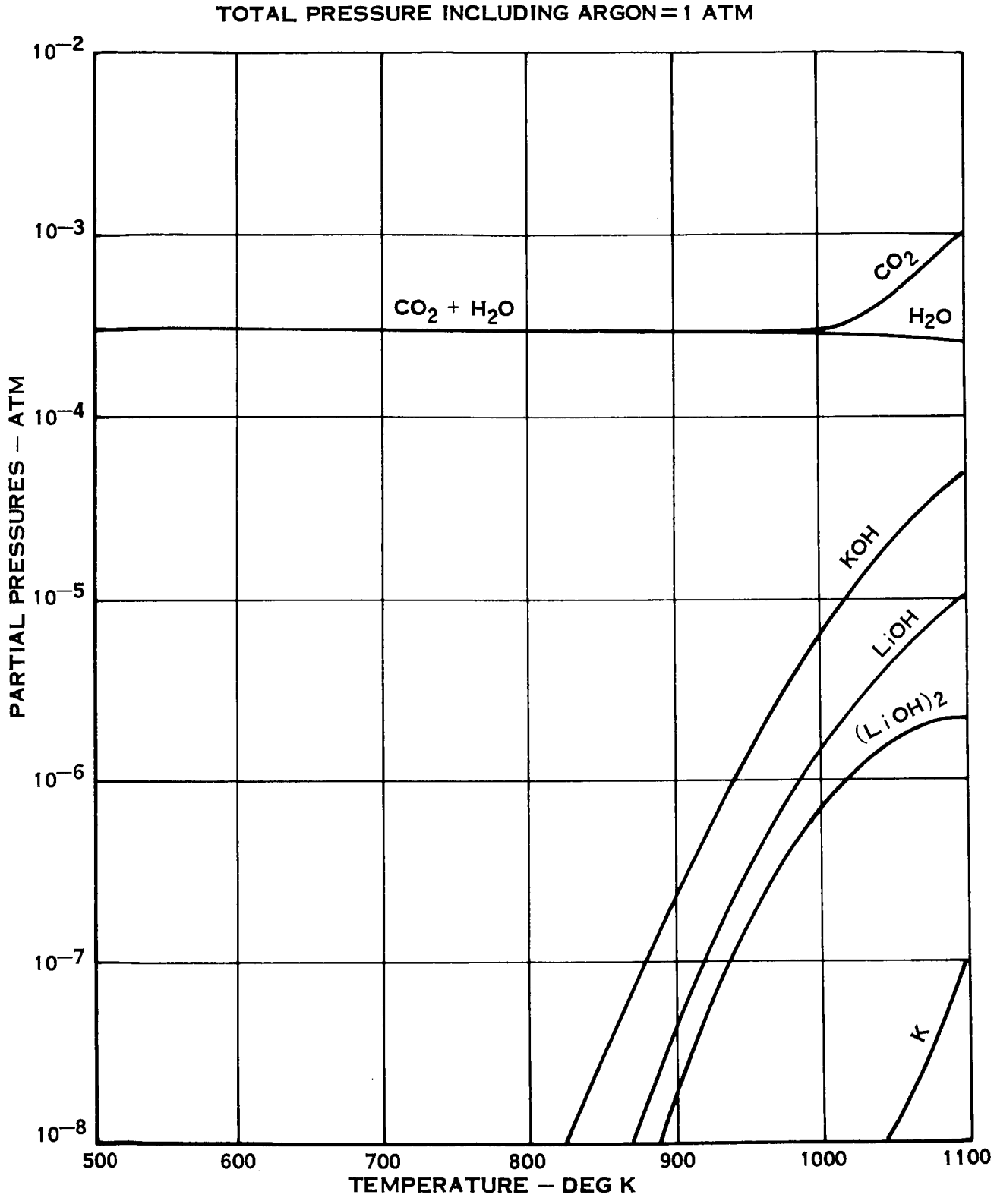


FIGURE 6–12. PARTIAL PRESSURES OF GASES ABOVE A MELT CONTAINING 35% Li_2CO_3 – 65% K_2CO_3 BY WEIGHT

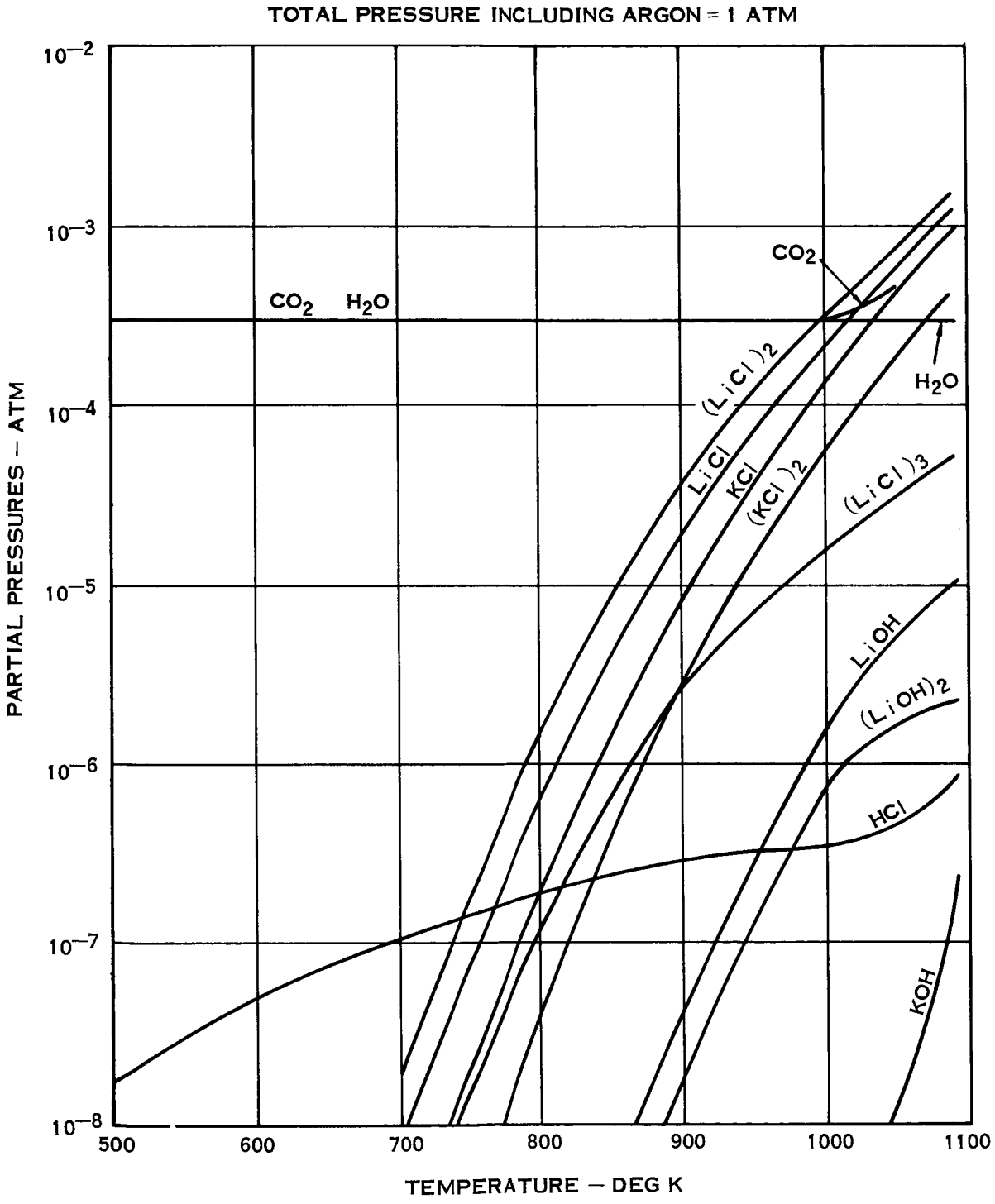


FIGURE 6–13. PARTIAL PRESSURES OF GASES ABOVE A MELT CONTAINING 58 MOLES Li C –42 MOLES KCL–1.5 MOLES Li_2CO_3

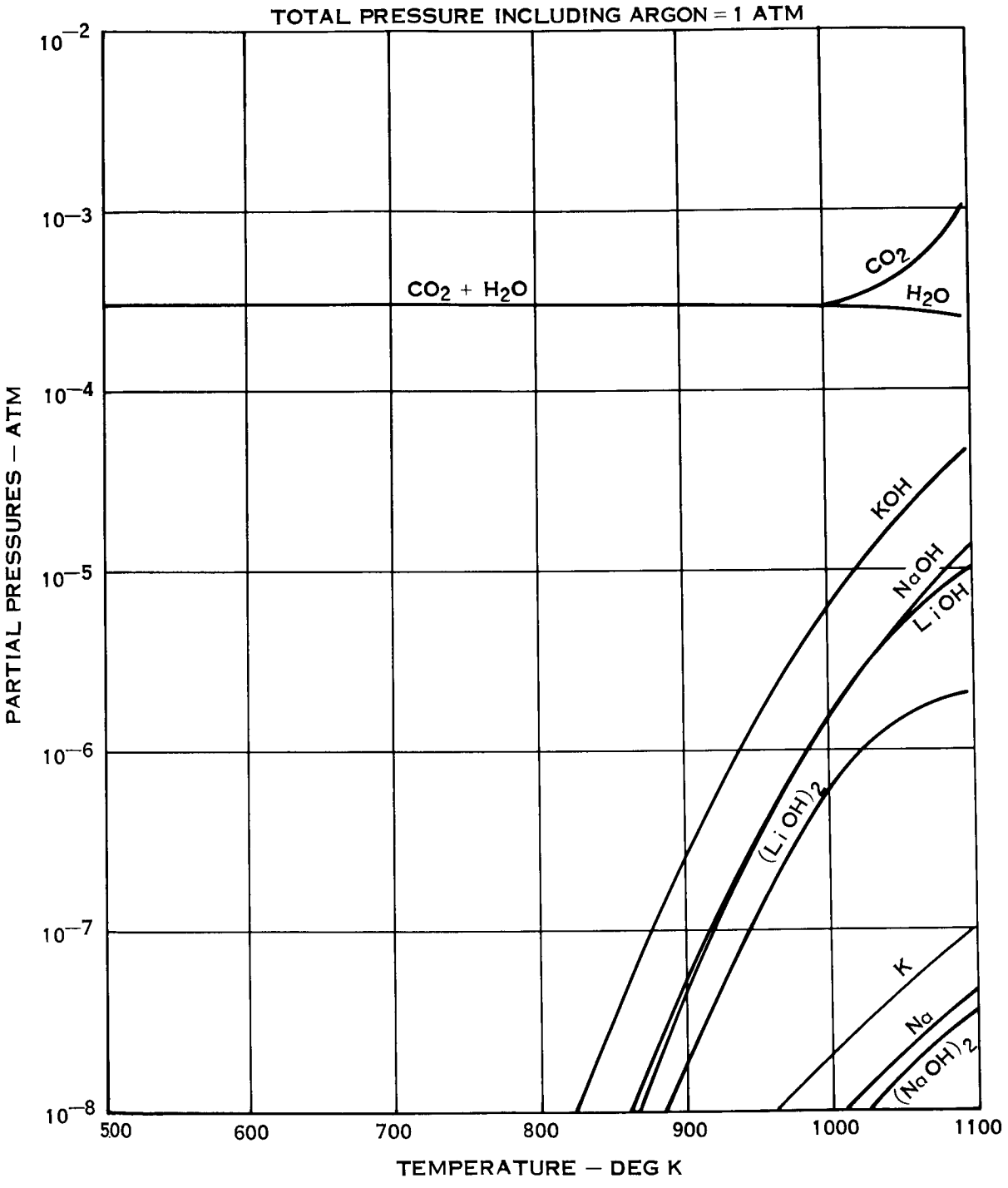


FIGURE 6–14. PARTIAL PRESSURES OF GASES ABOVE A MELT CONTAINING 8 MOLES Li_2CO_3 – 6 MOLES K_2CO_3 – 6 MOLES Na_2CO_3

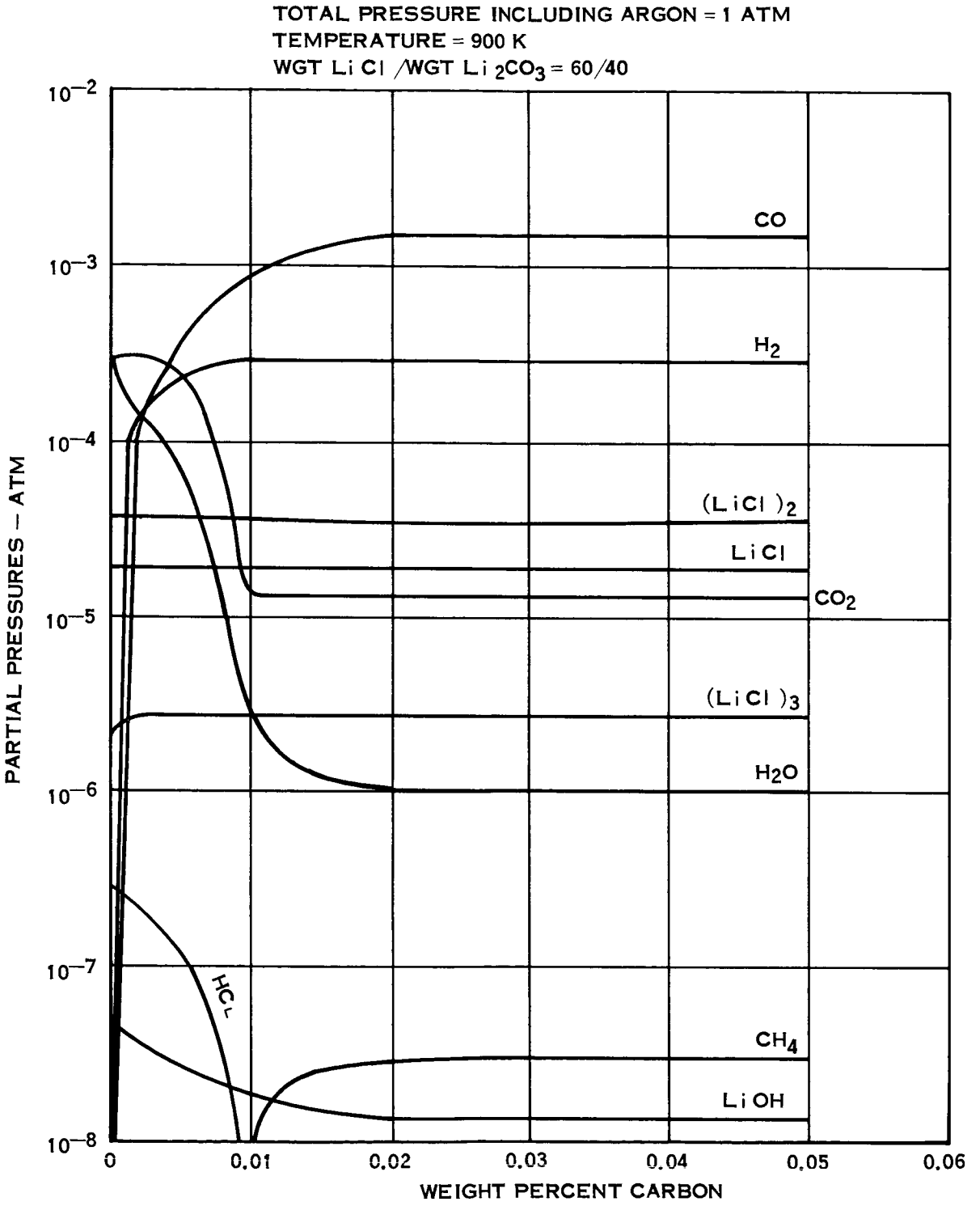


FIGURE 6–15. PARTIAL PRESSURES OF GASES ABOVE A MELT CONTAINING LiCl – Li_2CO_3 – C

6.3 Electrolyte Carry-over Investigations

6.3.1 Introduction

All components making up the candidate melt compositions for the electrolytic reduction of carbon dioxide have vapor pressures which, as a result of continuous and prolonged passage of gases over or through the melt, could lead to significant losses of the melt components. In most cases the percentage of the total melt lost in this way would be negligible but the condensation and deposition of the vaporized materials in other parts of the system could lead to serious losses in efficiency and to other operating difficulties. In addition to actually carrying material away in vapor form, the bubbling of gases through the melt could lead to the formation of a mist of minute droplets of melt which might also be carried in the gas stream and deposited in locations outside of the heated zone.

To provide some insight into the magnitude of these problems, this portion of the present research program was undertaken (1) to determine the extent and nature of melt component losses from a single melt composition at a single temperature as a function of flow rate of carrier gas and water content of the carrier gas, and (2) to determine whether passage of the gas through or over the melt affected the extent of melt component losses. The geometry of the melt container and the volume of melt in the container were held constant. The experiment was set up in such a way as to generate data which could be used in the engineering design of an electrolytic cell and related systems in which to carry out the reduction of CO_2 in a fused salt electrolyte.

The study was restricted to a melt composition and a temperature which had already been tentatively agreed upon as being likely conditions for operation of prototype cells.

6.3.2 Experimental

6.3.2.1 Apparatus and Procedure

The apparatus used in measuring melt component losses consisted of four principal parts: (1) a means for supplying a known flow rate of nitrogen containing known concentrations of water vapor; (2) a melt container permitting the molten salts to be maintained at a fixed temperature and providing for passage of gas over or through a melt and the escape of the gas into a trapping system; (3) a means for trapping and collecting in solid form all melt materials carried in the gas stream; and (4) a means for monitoring the moisture content of the effluent gas and measuring the volume of such gas. A schematic diagram of the entire assembly is shown in figure 6-16. Photographs of the assembly and of the melt container are shown in figures 6-17 and 6-18.

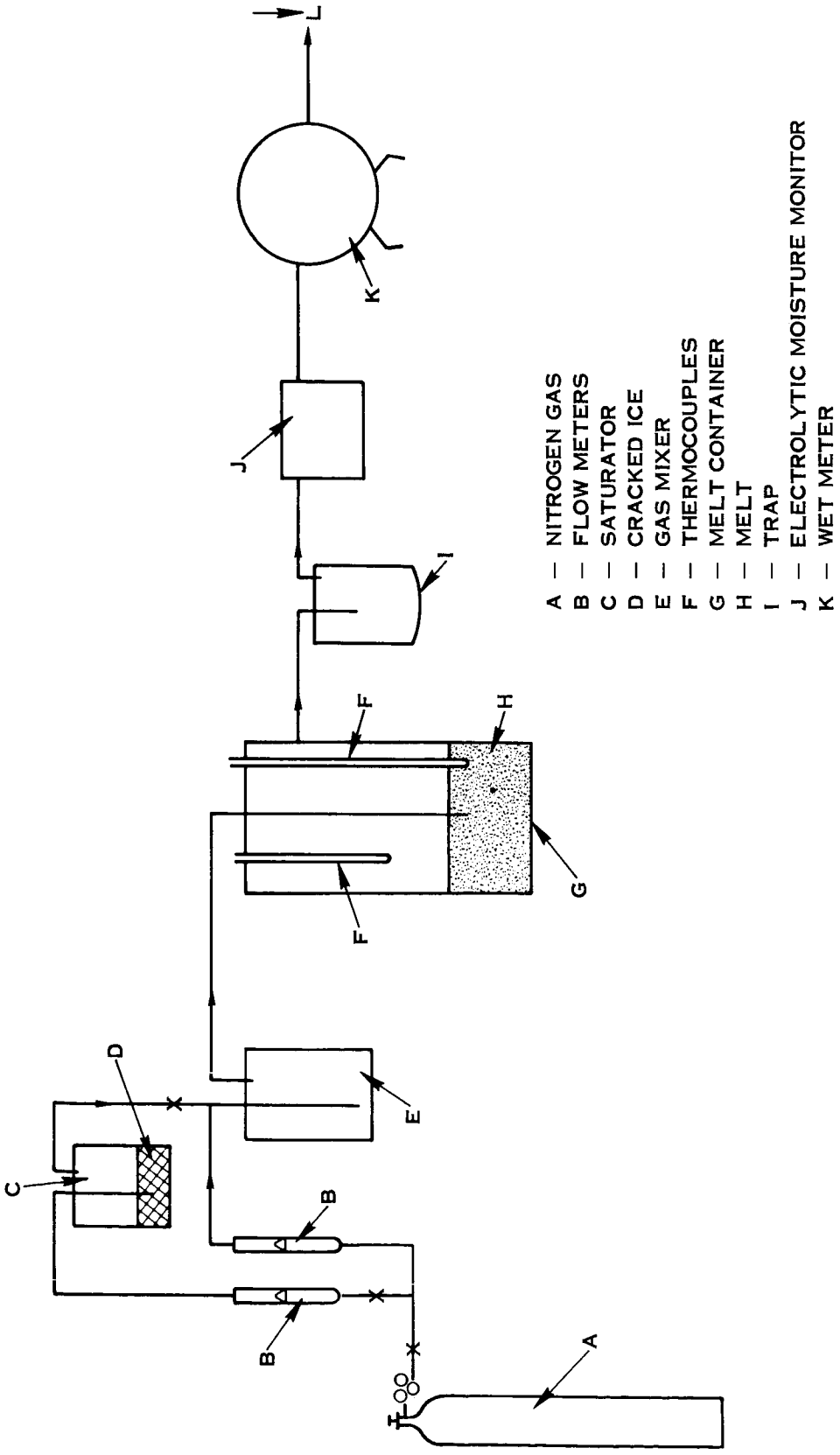


FIGURE 6—16. SCHEMATIC: MELT LOSS APPARATUS

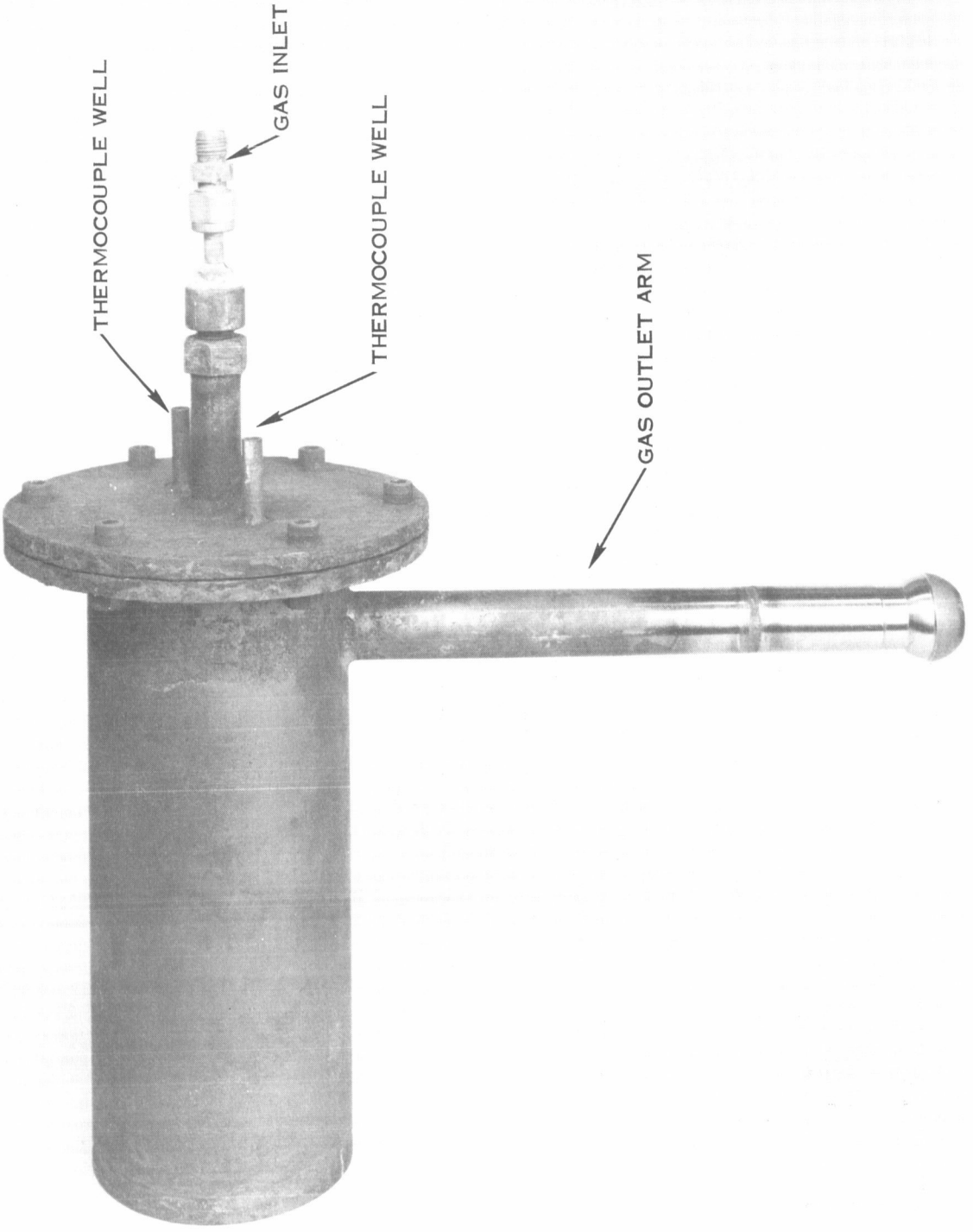


FIGURE 6–17. MELT CONTAINER

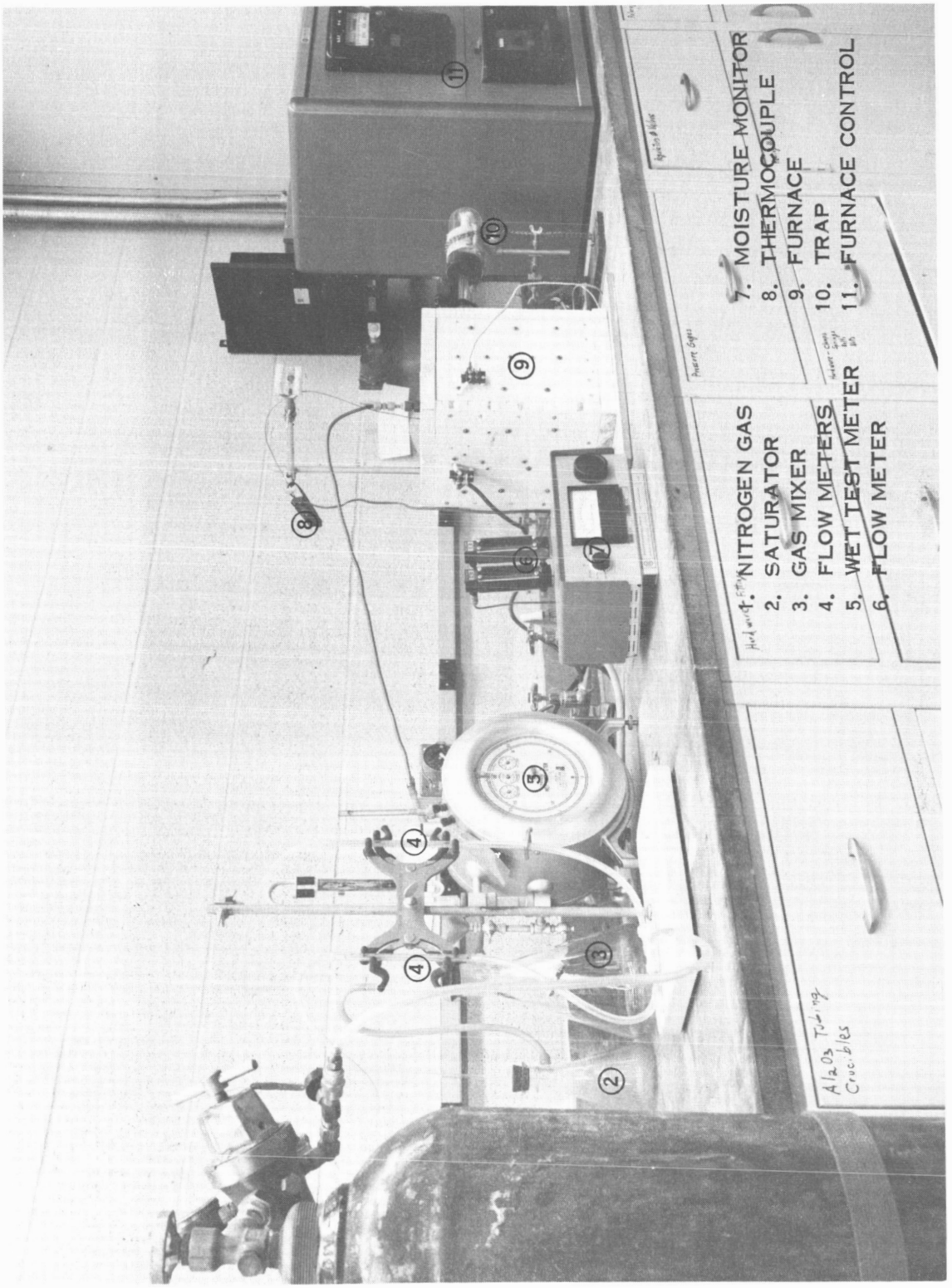


FIGURE 6–18. MELT LOSS APPARATUS

6.3.2.1 (Continued)

Nitrogen gas (Linde) containing 20-30 ppm water vapor was used as the dry gas. When the gas was used in the dry condition it was fed through a calibrated flowmeter and then directly to the melt container. When a higher water content was desired in the gas, the dry nitrogen flow was split, as shown in figure 6-16, and both parts passed through flowmeters. The smaller flow was led through a saturator consisting of a flask containing chopped ice. The gas, now saturated with water at $0^{o}C$, was then led to a mixing tank at room temperature where it was mixed with the dry gas making up the rest of the total gas flow. The mixed gas containing the desired water content was then led to the melt container. The wet gas composition desired was about 300 ppm. The actual water concentrations ranged between 200 and 280 ppm.

Two melt containers were used during this study. The same general design was followed in each; however, the first container was made entirely of impervious alumina while the second was made entirely of type 304 stainless steel. The change to stainless steel was made because of the fragility of the alumina container. Since most of the work was done with the stainless steel container, its dimensions and construction are given in some detail.

The steel melt container was fabricated from a 7 1/2" length of 3" i.d. pipe having a 1/8" wall thickness. A flat bottom plate 1/4" thick was heliarc welded to the cylinder at one end and a 1/4" thick flange plate 5 1/4" diameter with a 3" diameter central hole was welded at the other end of the pipe. This flange had a number of equally spaced holes to accommodate bolts for fastening the cover assembly to the container. The face of the flange was grooved to accommodate a 20-mil gold "O" ring to seal the top and bottom portions of the melt container. Near the top of the cylinder an 8" side arm was attached by heliarc welding. The side arm consisted of heavy wall tubing terminating in a 28/15 S.S. male standard ball joint.

The top of the container consisted of a circular steel plate 5 1/4" in diameter and 1/4" thick. A 0.530" diameter hole was drilled in the center of the plate and two small holes, 0.180" diameter, located on 1" centers from the large hole, were also drilled. On the top side of the plate a 1 5/8" length of 0.625" o.d. tubing was centered on the large hole and welded. Five-inch and seven-inch lengths of 1/4" tubing closed at the lower ends were welded to the under side of the plate in line with the small holes to serve as thermocouple wells. The bottom of the top plate was grooved to accommodate the gold "O" ring mentioned before. The top also had holes spaced to match those in the container flange to accommodate bolts.

To provide a means for passing gas either over or through the melt in the melt container, two gas inlet assemblies were fabricated from 304 stainless steel. They consisted of, respectively, 8 1/2" and 10 1/2" lengths of 1/2" O.D. x 0.095" wall tubing, each threaded for 1 1/8" at one end with 5/8 x 12 thread. On each tube a steel collar 1/2" thick and 1 3/8" diameter was welded such that the top surface of

6.3.2.1 (Continued)

the collar was 2 1/2" below the top of the threaded end of the tubes. The top surfaces of the collars were grooved to accommodate 20-mil gold "O" rings 1" in diameter. The shorter of the tubes extended into the melt container a distance of 5 1/2" and was used for studies where gas was passed over the melt surface. The longer tube extended 7 1/4" into the melt container and was used where gas was bubbled through the melt. The shorter tube was sized to discharge the gas about 1/4" above the melt level. The longer tube discharged approximately 1 3/4" below the nominal melt surface.

The gas inlet tubes were assembled into the melt container unit in such a way that the steel collar with its gold "O" ring contacted the lower side of the top plate and the threaded end of the tube extended above the large tubing welded to the top side of the plate. The tube was fixed in place by placing a steel washer over the threaded tube and running a steel nut down the threads to press against the washer and standpipe. This arrangement provided a leaktight joint.

The entire melt container assembly, after filling with the required components to make the melt, was placed in an electrically heated furnace. The heating elements were arranged so that the furnace was heated continuously to a temperature just below the control point using a variac to control the heat input. The fine control of temperature was achieved by means of an automatic control on the auxiliary heater. A thermocouple in the well extending into the melt was used for the furnace control. Another thermocouple in the well in the gas phase above the melt was connected to a Pyrotest meter.

The trapping and collecting portion of the apparatus included the stainless steel side arm and glass trap as shown in figure 6-16. This consisted of a 10" length of pyrex tubing having a 28/15 female standard ball joint at one end. The other end was stuffed with pyrex glass wool to serve as a gas permeable surface against which particulate matter could impinge and be caught. This glass tube extended into a large glass test-tube through a rubber stopper.

To ensure that any material condensing out in the cooler portion of the steel side arm was collected and analyzed, a single roll of stainless steel foil 6" long was inserted into the side arm at the start of each experiment. At the end of a run this foil was withdrawn and any melt materials on the foil were included with those collected in the glass trap.

The gas leaving the solids trap was led first through a CEC electrolytic moisture monitor where the water content of the exhaust gas was continuously monitored, and then through a wet test meter for measurement of the total gas flow exiting from the melt container.

6.3.2.1 (Continued)

The melt container was filled with 300 g of a LiCl-Li_2CO_3 eutectic mixture (60 wt % LiCl). The chemicals used were reagent quality and were used without further treatment. After the melt container was filled, it was closed, heating was started and a slow stream of CO_2 was passed over the salts. Flow of CO_2 through or over the melt was continued for several hours after the operating temperature was readied. The desired flow of nitrogen gas (dry or wet) then was passed over or through the melt. The collecting trap and the various meters were connected to the melt container and the test started. Tests with nitrogen flowing through the system were carried out over periods from 50 to 120 hours. Vaporized or particulate melt components deposited on the walls of the metal liner in the outlet tube, on the walls of the glass tube, and on the glass wool plug. No visible solids were detected beyond this plug but some fouling of flowmeters on the moisture monitor after prolonged use suggest that not all of the materials were completely trapped. During a test, the temperature of the furnace and of the gas phase of the melt container, the gas flows indicated on the flowmeters, moisture content of the exhaust gas, and the total gas flow were recorded at two- or three-hour intervals during the working day. Tests continued unattended the rest of the time.

At the termination of a test run, the nitrogen gas flow was stopped and the total flow through the apparatus was recorded. The metal liner in the outlet tube from the melt container was removed and was washed thoroughly with water to remove soluble salts. The solids in the glass tube and on the glass wool were also dissolved in water and all solutions combined and submitted for chemical analysis.

Chemical analysis of the solutions of the materials caught in the trap was carried out for lithium ion by atomic absorption, and for chloride ion and carbonate ion by standard titration procedures. The results were reported in terms of milligrams of each ion in the total sample.

The data gathered in this study were obtained from three separate melts, all having the same composition. The first melt was used in the one test using the all-alumina reactor mentioned earlier; the second melt was used for tests 2 through 4. The third melt was used for tests 5 and 6.

6.3.2.2 Test Results and Discussion

The experimental conditions and the associated chemical analysis of the materials which escaped from the melt container and which were recovered in the trapping system are tabulated in table 6-XXVII.

There appears to be no marked dependence of the amounts or nature of the materials lost from the melt on the moisture content of the gas stream. Whether the gas passes over the melt or is bubbled through the melt also appears to have no effect on the amounts or nature of materials lost.

TABLE 6-XXVII

LOSS OF MELT COMPONENTS FROM $LiCl-Li_2CO_3$ EUTECTIC AT 670°C

Run No.	Duration Test hrs	N_2 Flow Rate cc/min (at NTP)	Water Content of Gas Input ppm	Water Content of Gas Exhaust ppm	Operating Mode	Chemical Analysis of Trapped Solids Li^+ mg.	Li^+ meq.	Cl^- mg.	Cl^- meq.	$CO_3^=$ mg.	$CO_3^=$ meq.
1	100	200	20-40	20-30	Gas through melt	27.3	3.94	113	3.19	10	0.33
2	120	186	20-40	30-40	Gas over melt	29.5	4.25	158	4.43	none	none
3	84	163	250	230±30	Gas over melt	19.7	2.84	95.6	2.69	none	none
4	70	163	20-40	85-100	Gas over melt	10.8	1.56	80.5	2.27	none	none
5	77	104	20-40	180	Gas through melt	16.0	2.3	106	3.0	none	none
6	52	318	250	250±30	Gas through melt	11.2	1.6	55.6	1.57	none	none

6.3.2.2 (Continued)

One interesting observation relating to runs 4 and 5 indicates that the flow of dry gas through or over the melt for more than seventy hours is not sufficient to dry the melt since the exhaust gas still contains relatively large amounts of water vapor. The total weight of H_2O lost during this time amounted to only 0.03-0.05 g or approximately 0.01-0.02 percent of the weight of the melt.

Further discussion and interpretation of the experimental results are presented under the headings of Materials Lost from Melt, Rate of LiCl Evaporation, and Vapor Pressure of LiCl.

6.3.2.2.1 Materials Lost from Melt

The chemical analysis (table 6-XXVII) of the solids recovered in the trapping section of the apparatus demonstrates clearly that LiCl is the principal or only component of the LiCl-$LiCO_3$ eutectic melt which is removed from the melt under the conditions described. The presence of small amounts of carbonate in one case (Run #1) probably represents melt material carried over mechanically in the form of spray under conditions of violent agitation by a high gas flow bubbling through the melt. A gas surge was known to have occurred when a new gas cylinder was connected to the system about midway through the experiment.

It is probable that the extent of melt loss due to mechanical carryover depends primarily on design of the melt container and that proper baffles above the melt would reduce losses of this type to a low level.

The loss of LiCl from the melt appears to be an evaporative process and it is believed that the LiCl is carried as a vapor out of the heated melt container and condenses as a finely divided solid as the gas stream cools and either settles on the walls of the gas exit lines or on surfaces against which the gas stream impinges.

6.3.2.2.2 Rate of LiCl Evaporation

The data presented in table 6-XXVII permit calculation of the rate of evaporation of LiCl from the surface of the eutectic melt under the conditions of the experiment. This is strictly correct for those experiments where no carbonate was detected in the collected solids. Where Li_2CO_3 was detected and presumably represented melt carryover in particulate form, the total LiCl collected should be reduced by the LiCl content of the mechanically transported melt.

The rates of LiCl evaporation, expressed as grams LiCl/minute/cm^2 of melt surface, are listed in Table 6-XXVIII. The surface area of the melt under quiescent conditions was assumed to be 46 cm^2. When the surface was agitated by gas bubbling through the melt, the effective surface area from which evaporation occurred was increased to an unknown extent. For purposes of calculation the melt surface was assumed to

TABLE 6-XVIII

RATES OF EVAPORATION OF LiCl FROM LiCl-Li_2CO_3 EUTECTIC MELT AT 670°C
(Melt surface assumed to be 46 cm^2)

Run #	Condition	Rate ($g/min/cm^2$)	Gas Flow Rate (cm^3/Min)
1	Dry N_2 through melt	6.0×10^{-7}*	200
2	Dry N_2 over melt	$5.6 \pm 0.1 \times 10^{-7}$	186
3	Wet N_2 over melt	$5.1 \pm 0.1 \times 10^{-7}$	163
4	Dry N_2 over melt	$4.4 \pm 0.1 \times 10^{-7}$	163
5	Dry N_2 through melt	$5.3 \pm 0.7 \times 10^{-7}$	104
6	Wet N_2 through melt	4.7×10^{-7}	318

*Corrected for mechanical carryover of melt

6.3.2.2.2 (Continued)

be quiet in all experiments and the tabulated data should be considered in this light.

The rates of evaporation are seen to be fairly constant. Lack of dependence of rates on water content of the gas suggests that hydrolysis of melt components probably does not constitute a major source of volatile materials. Lack of dependence of evaporation rates on whether or not the gas was passed through or over the melt suggests that the same degree of loading of the gas with LiCl is achieved in both cases. It is possible that the gas flow rates were slow enough such that equilibrium conditions were approached in both cases.

6.3.2.2.3 Vapor Pressure of LiCl

The procedure used in determining the extent of loss of melt components is actually a crude form of the well-known transpiration method of measuring vapor pressures of liquids. If an inert gas is bubbled through a liquid at constant temperature and at a sufficiently slow rate, the gas will become saturated with vapor of the liquid and the partial pressure of the vapor in the resulting mixture of gases equals the vapor pressure of the liquid. That is, if Dalton's law of partial pressures holds and the vapor and inert gas behave ideally,

$$PV = \frac{W}{M} RT$$

where P = partial pressure of vapor
V = total volume of gas and vapor
W = wgt of liquid vaporized
M = molecular weight of vapor

As the measurements were carried out in this study, no attempt was made to ensure saturation of the gas with vapor by using extremely slow gas flow rates. Rather, the gas flows selected were of the order of magnitude expected to be applicable to the planned use of the melt for continually removing carbon dioxide from an air stream.

Pressures of LiCl vapor above a LiCl-Li_2CO_3 eutectic maintained at 670°C have been calculated from the data presented in table 6-XXVII and are shown in table 6-XXIX.

TABLE 6-XXIX

CALCULATED PRESSURES OF LiCl VAPOR OVER LiCl-Li_2CO_3 EUTECTIC AT 670°C

Run No.	LiCl Vapor Pressure (atm)
1	6.5×10^{-4}
2	$7.9 \pm 0.2 \times 10^{-4}$
3	$8.2 \pm 0.2 \times 10^{-4}$
4	$5.0 \pm 1.0 \times 10^{-4}$
5	$13.5 \pm 2.0 \times 10^{-4}$
6	$3.9 \pm 0.4 \times 10^{-4}$

No data are known which provide information about the vapor pressure of LiCl over molten mixtures containing LiCl as one component. If such mixtures behaved in a simple fashion, it would be expected that the LiCl vapor pressure would be less than the vapor pressure of pure LiCl at the same temperature.

The only available literature data for the vapor pressure of pure LiCl are cited in International Critical Tables and also in Foote Minerals Brochure [1] on Chemical and Physical Properties of Lithium Compounds. These data, obtained over the temperature range 1045-1325°C, are tabulated in table 6-XXX. When plotted as log vapor pressure vs 1/T °K a reasonably good straight line is obtained. When the long extrapolation of these data to much lower temperatures is made, the vapor pressure of LiCl at 670°C appears to lie between 2 and 4×10^{-4} atmospheres.

TABLE 6-XXX

LiCl VAPOR PRESSURE VS TEMPERATURE

Literature Data

Temp °C	LiCl Vapor Pressure mm Hg	T^{-1} °K	Log. Vapor Pressure
1325	760	6.26×10^{-4}	2.881
1287	567	6.41	2.754
1266	445	6.50	2.648
1235	360	6.63	2.557
1210	275	6.75	2.440
1180	205	6.89	2.312
1045	60	7.59	1.779

6.3.2.2.2 (Continued)

The vapor above pure molten LiCl is known to consist of LiCl (monomer), $(LiCl)_2$ (dimer) and $(LiCl)_3$ (trimer) and may also contain traces of the ions Li^+ and Cl^-. The liquid LiCl must also contain these same species but not necessarily in the same ratios as they appear in the vapor. It is expected that the complex equilibria relating the various species in the melt could be altered by the addition of a new component to the melt. If the change brought about is in the direction of an overall increase in the mole fraction of the more volatile species of LiCl, then it appears possible for the vapor pressure of LiCl above a molten mixture to be greater than that above "pure" LiCl.

The results of the calculations of the vapor pressure of LiCl over the LiCl-Li_2CO_3 eutectic presented in table 6-XXIX indicate that in all experimental runs the apparent LiCl vapor pressure is greater than that extrapolated from the high-temperature vapor pressure data for pure LiCl. The results suggest that the behavior postulated above may in fact occur.

If these observations can be confirmed, it seems indicated that some melt composition different from the eutectic may have a lower LiCl vapor pressure and result in decreased loss of material from the melt. Such a circumstance could reduce the extent of condensation of vaporized LiCl in heat exchangers and other parts of the system external to the electrolytic cell.

It seems imperative, therefore, that further studies be carried out which are aimed specifically towards the precise measurement of the vapor pressure of Li Cl over pure LiCl melts and over a number of compositions consiting of LiCl and Li_2CO_3 and possibly one additional component.

The independent measurements of LiCl evaporation rates as determined using the vacuum balance are in good agreement with the data presented above. The evaporation rates plotted in figure 6-11 may be compared to the above data by extrapolating to 760 mm CO_2 and converting to g/min/cm^2. Thus at 600°C the evaporation rate is about 2×10^{-7} g/min/cm^2 and at 640°C it is about 8×10^{-7} g/min/cm^2. These values are slightly higher but the experiments were performed in a static system (no gas flow) under conditions where the entire system was not at the same temperature. The vapor was easily condensed very near the surface of the melt. Taking these differences in experimental procedures into account, the results are in excellent agreement.

The calculated vapor pressures take into account all the LiCl vapor species. Figure 6-15 shows the calculated vapor pressures of each species of LiCl as a function of temperature. At 670°C (943°K) the pressure of LiCl is 6×10^{-5} atm, Li_2Cl_2 is 1×10^{-4} atm and Li_3Cl_3 is 7×10^{-6} atm for a total pressure of 1.67×10^{-4} atm. This value is somewhat lower than the data in Table 6-XXIX but still may be considered to be in good agreement with the experimental data.

6.3.3 Summary of Results and Conclusions

1. Extent of losses of melt components from a LiCl-Li_2CO_3 eutectic melt have been measured at 670°C.

2. LiCl was found to be the only or principal component lost from the melt.

3. Addition of water vapor to the LiCl-Li_2CO_3 melt did not change the nature or amounts of materials lost from the melt.

4. Over the range of gas flow rates used in this study (100-300 cc/min), passage of the gas through or over the melt caused no change in the evaporation rate of LiCl from the melt.

5. Small amounts of the melt, in the form of particulate matter, can be lost if agitation is sufficiently violent.

6. The amounts of LiCl lost from the melt were in fair agreement with that expected on the basis of published vapor pressure data.

7. The average rate of evaporation of LiCl from the eutectic melt at 670°C is about 5×10^{-7} g/min from each square centimeter of melt surface when gas velocities are between 1 and 6 cm/min.

6.3.4 Recommendations

1. For engineering design purposes, a LiCl evaporation rate of 5×10^{-7} g/min from each square centimeter of melt surface may be considered as typical for gas flow rates ranging from 100 to 300 cc^3/min through a LiCl-Li_2CO_3 eutectic melt maintained at 670°C and having a surface area approximating 50 cm^2.

2. The use of internal baffles in an electrolysis cell should be adequate to prevent loss of melt material by mechanical carryover. LiCl losses due to evaporative processes will not be affected by such baffles.

3. Precise measurements of LiCl vapor pressure at a number of temperatures and from a number of melt compositions would be desirable in order to determine LiCl activity in these melts. LiCl activity measurements in various melt compositions should also be determined from electrochemical techniques using a chloride-sensing electrode.

REFERENCES

1. Phase I Final Report: Research and Development Program for a Combined Carbon Dioxide Removal and Reduction System. Contract No. NAS 1-4154, Hamilton Standard Report HSER 3732, pp. 161-164 (October 1965).

2. "Molten Salt Chemistry." John Wiley & Sons, New York, edited by M. Blander (1964).

3. Hill, K. J. and E. R. S. Winter: Thermal Dissociation Pressures of Calcium Carbonate. J. Phys. Chem. 60, pp. 1361-1362 (1956).

4. Johnston, J.: The Thermal Dissociation of Calcium Carbonate. J. Am. Chem. Soc. 32, pp. 938-946 (1910).

5. Smyth, F.H. and L.H. Adams: The System, Calcium Oxide-Carbon Dioxide. J. Am. Chem. Soc, 45, pp. 1167-1184 (1923).

6. Thermochemical Data." Compiled for the Joint Army-Navy-Air Force-ARPA-NASA Thermochemical Working Group by the Thermal Research Laboratories of the Dow Chemical Co., Midland, Michigan; (including supplements through March 19

7. Brown, O. L. L and W. M. Latimer: The Heat Capacity of Lithium Carbonate from 16 to 300°K. The Entropy and Heat of Solution of Lithium Carbonate at 298°K. The Entropy of Lithium Ion, J. Am, Chem, Soc. 58, pp. 2228-2229 (1936).

8. Gunn, S. R. and L G. Green: The Heats of Formation at 25° of the Crystalline Hydrides and Deuterides and Aqueous Hydroxides of Li, Na, and K. J. Am. Chem. Soc. 80, pp. 4782-4786 (1958).

9. Messer, C. E., L. G. Fasolino and C. E. Thalmayer: The Heats of Formation of Li, Na, and K Hydrides. J. Am. Chem. Soc. 77, pp. 4524-4526 (1955).

10. Wagman, D. D. and W. H. Evans: (No Title Avaliable). J. Res. Natl. Bur. Std. Technical Note 270-1, (October 1, 1965).

11. Stern, M.: (National Bureau of Standards.) Private Communication.

12. Kelley, K. K.: Heats of Fusion of Inorganic Substrates. U. S. Bureau of Mines 5, Bulletin #393, p. 166 (1936).

13. Lorenz, M. R. and G. J. Janz: A Dynamic Method for Measuring Dissociation Pressures. J. Chem. Ed. 40, pp. 611-612 (1963).

14. Baboian, R. and S. N. Flengas: High-Temperature Solution Calorimetry - Part II, Thermodynamic Investigation of the Systems: AgCl-KCl, AgCl-RbCl, and AgCl-CsCl. Canadian J. Chem. 45, pp. 813-820 (1967).

15. Temkin, M.: Mixtures of Fused Salts as Ionic Solutions. Acta Physicochim. U. R. S. S. 20, pp. 411-420 (1945).

16. Zarzycki, J.: High-Temperature X-Ray Diffraction Studies of Fused Salts: Structure of Molten Alkali Carbonates and Sulphates. "The Structure and Properties of Ionic Melts." A General Discussion of the Faraday Society, pp. 38-48 (1961).

17. Kleppa, O. J.: A New Twin High-Temperature Reaction Calorimeter. The Heats of Mixing in Liquid Na-K Nitrates. J. Phys. Chem. 64, pp. 1937-1940 (1960).

18. Cantor, S.: Freezing Point Depressions in NaF. Effect of Alkaline Earth Fluorides. J. Phys. Chem. 65, pp. 2208-2210 (1961).

19. Janz, G. J., et al: High-Temperature Heat Content and Related Properties for Li_2CO_3, Na_2CO_3, K_2CO_3 and the Ternary Eutectic Mixture. Trans. Faraday Soc. 59, pp. 841-845 (1963).

20. Zeleznik, F. J. and S. Gordon: A General IBM 704 or 7090 Computer Program for Computation of Chemical Equilibrium Compositions, Rocket Performance, and Chapman-Jouguet Detonations. NASA Technical Note D-1454, (October 1962).

21. Chemical and Physical Properties of Lithium Compounds. Foote Mineral Company, Philadelphia, Pennsylvania, (January 1957).

7.0 INTRODUCTION TO ENGINEERING ACTIVITIES

As defined by the statement of work, the research activities of Phase IIA were to be accompanied by concurrent advanced development effort. The objectives of the development (engineering) effort were:

(a) "Identify problems and provide preliminary evaluation of the feasibility of design concepts resulting from the studies of phase I "... and thereby..." provide necessary information with regard to the engineering problems related to concept selection for zero gravity application of the molten salt system."

(b) The definition by detailed design of a one-sixth gravity laboratory prototype CO_2 removal and reduction cell complex, capable (as a target) of the removal and reduction of nine pounds of CO_2 per day from a nitrogen-oxygen atmosphere at 14.7 psia and containing CO_2 at an inlet partial pressure of 3.8 mm. Hg.

(c) The design, fabrication, and shipment to NASA-LRC, of a second laboratory demonstration model that might include design improvements over the Phase I model.

(d) The preparation of a Preliminary Specification of a Zero Gravity Flight Prototype Fused Salt CO_2 Removal and Reduction System.

Sections 7.0 - 13.0 of Part II of this report present the conclusions, recommendations, and results of the engineering and advanced development activities during Phase IIA with respect to objectives (a) through (d) above. The one-sixth g cell design (b above), and the Preliminary Zero-Gravity System Specification, are being forwarded under separate cover.

8.0 ENGINEERING & DEVELOPMENTAL CONCLUSIONS

8.1 General Conclusions

8.1.1 Short duration tests have shown that variations between air, nitrogen, or argon as the diluent in the influent gas do not discernibly effect the electrolytic process regarding removal and reduction of carbon dioxide. Longer duration tests with other process variables standardized will be necessary to confirm that secondary and more subtle interactions are entirely absent.

8.1.2 Deposit thickness variation at any time over the cathode surface is dependent upon the thickness of the adherent catholyte film at local points. Configurations employing continuous static submergence of a portion of the cathode within the electrolyte tend to form bulbous deposits in the electrode region so exposed. Carbon purity in such areas is significantly poorer than in thinner adherent zones.

8.1.3 Anode life can be considerably lengthened by creating rapid distribution of electrolyte-contained cations (or the electrolyte itself) to the anode surface.

8.1.4 The critical environment with respect to the compatibility and life of materials employed within the electrolytic cell appears to be the gaseous environment existing within the ullage gas itself - in contrast to materials submerged within the electrolyte.

8.1.5 Longitudinal vibration of the cathode at frequencies and applitudes extending to 25 Hz and 0.010", respectively, do not act to cause noticeable improvement in carbon deposit purity.

8.1.6 Variations in cathode shapes and geometries do not appear to significantly effect the purity of carbon deposits, but under certain conditions can be usefully employed to achieve rectangular or cylindrical deposit envelopes.

8.1.7 Near perfect ($\cong$ 100%) cathode current efficiencies can be achieved with moderately good carbon purities (80% - 85%) for at least one configuration tested (the oscillating electrolyte). The repeatability and potential improvement of these performances must still be confirmed, but postulations made are felt to warrant optimism.

8.1.8 Spectral, x-ray, and current image scanning of a bi-component (gold-nickel) anode (following use) have provided much insight into the behavior of this electrode as a result of fused salt electrolytic exposure. In general it was shown that for the particular anode material examined the noble metal constituent (gold) was not consumed by the electrolytic process but rather experienced inward migration (i.e., the nickel diffused outward in a classical parting phenomenon). A postulation has resulted in which it is felt that anode life can be considerably lengthened by employing a composite anode, using the semi-conductive characteristic of nickel-oxide as the outer ply and employing gold (or other noble metal) as the inner ply to provide both structural strengt and a favorable conductive path.

8.1.9 It was analytically determined that under a 1/6 g environment the terminal velocity of oxygen released at the anode would be 1/3.8 of that of a one-g environment. The effect of the diminished oxygen rise-time through the electrolyte is obviously dependent upon the specific configuration. For the configuration selected, the effect is felt to be inconsequential; further testing of that configuration, however, will be needed to confirm the validity of this conclusion.

8.1.10 Analytical effort was expended to quantify theoretical relationships in carbon dioxide "scrubbing" effectiveness, based upon passage of CO_2 laden influent gas through cyclically wetted plates. It was generally concluded that the CO_2 mass transfer rate is directly dependent upon the "scrubbing" area, the log-mean difference in partial pressure levels between the CO_2 levels in the electrolyte and gas phases, and in the gas-side mass transfer coefficient dependent in-turn upon specific aspects of the flow passage. In general it is felt that effective CO_2 mass transport adsorption will be achieved for the 1/6 g cell-complex as designed.

8.2 Specific Conclusions (relating to the oscillating electrolyte configuration concept)

8.2.1 Through proper use of electrolyte surface tension characteristics inherent in a particular design, this concept is adaptable to a 1/6 g environment - with potential of future adaptation to a "zero g" environment.

8.2.2 Near 100% cathode current efficiencies are generally achieved with this configuration and seem to be less dependent upon cathode current densities than with other configurations attempted.

8.2.3 Cathode carbon purities with this configuration (hypothetically would also apply to others) are dependent upon the electrolyte CO_2/H_2O partial pressure ratio, within certain limits; the text of this report makes certain postulations as to potentially "optimum" partial pressures of both constituents and qualitatively defines the optimum zone.

8.2.4 The Oscillating Electrolyte Cell (O.E.C.) concept can be shown to offer prospects for favoring anode life through the mechanism of forced convection of anode-generated oxygen away from that electrode's surface thereby reducing potential polarization problems; other considerations favoring forced electrolyte circulation (even under zero gravity) allow certain conclusions to be made which give promise of increased anode life with respect to competitive concepts.

8.2.5 Since the O.E.C. concept employs a passive system for liquid-gas phase position control, and due to the "zoned" location of the cathode electrodes, it is concluded that at a time warranted, automatic removal and replacement (or removal, carbon-stripping, and replacement of a repeatedly used cathode) can be adapted to the configuration.

8.2.6 Because of the empirical nature of the "scrubber" design, the need to solve certain material problems, the need to achieve uniformity in the cathode deposit thickness, and to demonstrate further high carbon purity and anode life, it is forseen that Phase IIB tests and analyses will probably dictate minor changes in the 1/6 g design submitted in this phase.

9.0 RECOMMENDATIONS

The following recommendations are made with respect to future engineering activities and the need to emphasize specific tasks during follow-on parts of the subject contract:

9.1 The one-sixth g cell complex design (or a major part of it) described in section 13.0 and separately detailed, should be fabricated in the next phase of this program for the following reasons:

(a) The cell complex, when fabricated, will provide a bed to allow full-scale testing of CO_2 scrubbing, anode life, cathode carbon formation and purity, and overall cell performance,

(b) The cell complex will provide a bed upon which the effectiveness of process control equipment can be evaluated,

(c) The cell complex will serve to demonstrate the workability and reliability of the various cell segments individually and as a major subsystem.

9.2 The materials investigation task should be amplified during the next part of this program to:

(a) Define suitable materials capable of withstanding the corrosive high-temperature electrolyte and ullage gas environment,

(b) Establish in detail the electrochemical mechanisms which limit anode life and, based upon this knowledge,define suitable anode materials capable of prolonged operation.

9.3 A complete fused salt zero gravity electrolytic CO_2 removal and reduction system should be designed during part IIB of this program for the following reasons:

(a) It will focus attention upon the overall system development objectives by forcing consideration of electric power, thermal insulation, system (and cell) start-up and conditioning requirements, caused by variation in influent moisture concentration, etc.

(b) The design of a flight concept prototype zero gravity system during the contract phase is necessary such that the subsequent fabrication and test efforts can be pursued within an acceptable program time base.

9.4 Development testing on approximate full-sized cells (test article configuration) should be directed at:

9.4 (Continued)

(a) Achieving consistency of high purity carbon deposits employing automatic electolytic process controls,

(b) Obtaining more detailed information on the change in chemical composition of the electrolyte with time,

(c) Obtaining quantitative information on fused salt vapor carry-over based upon full air flow through the specific scrubbers planned for use in deliverable systems,

(d) Tests to establish empirical sizing relationships and general adequacy of the CO_2 scrubber configuration.

(e) Evaluating endurance of the hardware over a 100 day period of continuous operation.

9.5 Engineering analyses should be conducted in certain areas as described below. Note: other analyses, akin to cell electrolysis performance and processes, are necessary and will be done in conjunction with the research and process investigations described in Part I of this report:

(a) Analyses to demonstrate the theoretical workability of the cell in a zero gravity environment,

(b) Design analyses to predict the failure modes possible and the inherent reliability of the zero-gravity system.

(c) Analysis to demonstrate that the electrolyte level positioning and cycling instrumentation and control technique will adequately meet the overall objectives for properly positioning the electrolyte within the cell,

(d) Analysis to calculate the rate at which the electrolyte and/or its components will be lost from the cells, together with a breakdown in this quantity to establish loss due to vapor carry-over and loss due to cathode occlusions,

(e) Analysis to establish the significance of temperature variation in the electrolyte from the standpoint of effect upon surface tension, viscosity, and other significant physical properties,

(f) Analysis to establish the warm-up time of the electrolyte within the cell subsystem,

(g) Analysis to establish the effect of flow variations between cells resulting from the manifolding and valving air distribution scheme, together with permissible variation to achieve satisfactory performance in all cells,

9.5 (Continued)

(h) Analyses to select the desiccant bed diameter and length to allow achievement of water removal requirements,

(i) Analyses to demonstrate that techniques proposed will not result in sorption of excessive moisture from the influent stream,

(j) Analysis to confirm that heat exchanger performance within the system will:

a. Be satisfactory with respect to proper control of inlet temperature at the electrolytic cell subsystem,

b. Yield the satisfactory temperature for the proposed cycle duration,

c. Adequately cool the effluent gas stream from the electrolytic cell subsystem.

(k) Analyses to establish that the interaction of the compressor/blower, desiccant, and heater process controls will be acceptable.

10.0 RESULTS OF ENGINEERING TESTS

This section describes and discusses the engineering tests conducted during phase IIA of this contract. In general, effort was expended on two classifications of tests. Paragraph 10.1 of this section pertains to tests done on establishing performance or operation of the electrolyte process itself on various cell configurations; paragraph 10.2 pertains to results of the materials investigation undertaken to determine suitable materials for melt containment or for use within the cell.

10.1 Performance Tests

10.1.1 Tabulation

Figure 10-1 tabulates the 27 performance tests conducted during phase IIA to establish and define the developmental parameters of basic concern for a four-man cell design. The figure shows:

(a) The objective of each test

(b) The conditions under which each test was performed, and

(c) The results of each test from the standpoint of anode efficiency, carbon deposit purity, cathode current efficiency (carbon recovery), etc.

The tabulation also shows the duration of each test, nominally 24-48 hours, and makes reference to figures contained in the engineering appendix of this report which describes the test article and electrode configurations used in the engineering cell performance test program.

10.1.2 General Description and Results of Tests

10.1.2.1 Description of Engineering Fused Salt Test Facility - Because the engineering department had not performed actual testing during phase I of this contract, attention was focused upon building a test facility early in phase IIA. Two separate test beds sharing common instrumentation were built to provide the potential of concurrent materials and cell performance tests. As designed, both test beds could be employed if necessary for performance tests. As with the research test facility, the engineering fused salt test stand was designed to:

- Allow the controlled flow of argon, air, or nitrogen containing a desired concentration of carbon dioxide and moisture into the fused salt test article,

- Conduct the test article effluent stream through instrumentation to provide measurement of cell outlet moisture, oxygen, and carbon dioxide,

10.1.2.1 (Continued)

- Provide for measurement of moisture, oxygen, or carbon dioxide from the cell cathode and anode ullage areas as desired,
- Control the temperature of the electrolyte during tests over a practical temperature range,
- Allow for the monitor and control of cell electrical input.

The facility was built during the months of October through December, 1966 under contract money, and was installed in the Research Laboratory to capitalize on obtaining a closer working relationship with that organization. Figures 10-2 through 10-4 show the test facility as built; figure 10-5 (flow schematic) depicts one of the two (nearly identical) test beds.

As tabulated in figure 10-1 and illustrated in the appendices of this report, the specific design of the cell test article was varied from time to time to accomplish various test objectives. In general, the test article consisted of a specially designed furnace (initially developed by the Hamilton Standard Research Laboratory for test purposes of this contract) containing a Lindberg ceramic-clad heating element, Perlite thermal insulation, a nickel furnace-liner, an alumina crucible, and a Transite crucible cover. Miscellaneous alumina tubing within the crucible were used to serve as scrubber tubes, anode and cathode electrode shields, thermocouple shields, etc. The initial test articles consisted of a valve-actuator system driven by an industrial timer to produce vertical oscillation of the cathode during a test. At other times, the test article configuration was modified to permit use of various anodes, electrolyte instead of cathode oscillation, and/or scrubber 'sparge-tube' displacement relative to the melt surface.

10.1.3 Conduct of Tests

In general, the engineering test series were run with current levels within the range of 1.8-3.0 amperes. Under these conditions, 5-9 grams of carbon would be deposited upon the cathode within 24-48 hours with 'scrubber' inlet flow rates averaging 700 scc/min and containing a 1% CO_2 concentration. The 5-9 gram deposits provided sufficient carbon for subsequent chemical analysis, and further permitted the 27 tests to be performed during phase IIA. The number of tests would have been substantially reduced had longer duration tests been performed.

During the tests, periodic instrumentation readings were taken to establish influent flow rates, voltage-current relationships, fused salt and gaseous temperatures, CO_2 partial pressures at cell inlet and outlet, inlet and outlet dew points, and anode oxygen partial pressures.

Hamilton Standard — DIVISION OF UNITED AIRCRAFT CORPORATION — UA®

TEST NO.	OBJECTIVES	TEST DURATION	ELECTROLYTE CONDITIONS						TEST PARAMETERS					
			COMPOSITION			DEW POINT	PCO_2	TEMP.	CARRIER	SCRUBBER	PCO_2 IN	CYCLE TIME ~ SEC.		
		HOURS	% WLiCl	%WLi_2CO_3	%WLi_2O	°F	mmHg*	°C	GAS	FLOW-CC/MIN	mmHg	TOTAL	UP	DOWN
1.	TEST FACILITY CHECKOUT	29.45	60.0	40.0	–	−30 TO −34	0.22–1.35	650–658	A⊛	400–500	8.0–11.5	7.8	5.0	1.0
2.	BASE LINE TEST–RECIPROCATING CATHODE	28.25	≃60.0	≃40.0	–	−45 TO −48	0.18–0.42	640–649	A	415–430	3.0–12.4	7.8	5.0	1.0
3.	PROCESS TEST – HIGH SCRUBBER FLOW	27.50	≃60.0	≃40.0	–	−40 TO −47	0.10–0.32	637–649	A	1630–1700	3.4–3.9	7.8	5.0	1.0
4.	PROCESS TEST – NITROGEN COMPATIBILITY	46.00	≃60.0	≃40.0	–	−47	0.15–0.28	626–647	N_2	1700	3.5	8.0	5.0	1.5
5A.	PROCESS TEST – NITROGEN COMPATIBILITY	5.00	≃60.0	≃40.0	–	−40	0.12–0.30	640–648	N_2	1700	3.3	13.2	8.0	1.9
5B.	PROCESS TEST – NITROGEN COMPATIBILITY	76.00	≃60.0	≃40.0	–	−23 TO −54	0.16–0.63	625–652	N_2	850–1700	3.3–6.7	13.3	8.2	1.8
6.	PROCESS TEST – AIR COMPATIBILITY	23.25	≃60.0	≃40.0	–	−31 TO −55	0.23–0.70	628–634	AIR	1700	3.5	13.1	8.2	1.7
7.	CENTRIFUGAL ANODE TEST	72.00	≃60.0	≃40.0	–	−9 TO −28	0.23–0.65	610–627	AIR	2000	3.8	13.1	8.2	1.7
8.	CO_2 SCRUBBING PERFORMANCE TEST	3.0 TO 4.0	≃60.0	≃40.0	–	−12 TO −41	0.15–3.80	618–628	AIR	500–2000	3.8	13.1	8.2	1.7
9.	CARBON DEPOSITION ON VIBRATORY CATHODE	18.0 TO 20.0	≃60.0	≃40.0	–	−10 TO −22	0.21–1.15	623–642	AIR	375–1000	7.0–16.7	–	–	–
10.	OSCILLATING ELECTROLYTE CONFIGURATION FEASIBILITY TEST	46.5	≃60.0	≃40.0	–	−11 TO −18	0.23–1.59	638–661	AIR	1450	7.2–7.6	8.0	4.0	4.0
11.	OSCILLATING ELECTROLYTE CONFIGURATION FEASIBILITY TEST	71.43	≃60.0	≃40.0	–	−6 TO −42	0.19–0.75	640–647	A	1190	6.9	8.0	4.0	4.0
12.	OSCILLATING ELECTROLYTE CONFIGURATION FUNDAMENTAL INVESTIGATION TEST	40.75	≃60.0	≃40.0	–	−16 TO −19	0.42–1.30		A	570	6.8–8.7	8.0	4.0	4.0
13.	OSCILLATING ELECTROLYTE CONFIGURATION FUNDAMENTAL INVESTIGATION TEST	24.25	≃60.0	≃40.0	–	−15 TO −18	0.26–1.10	645–647	A	700	7.6	8.0	4.0	4.0
14.	OSCILLATING ELECTROLYTE CONFIGURATION CYCLE TIME VARIATION TEST	45.25	67.0	33.0	–	−7 TO −34	0.30–1.20	640–649	A	780	7.6	4.0	2.0	2.0
15.	OSCILLATING ELECTROLYTE CONFIGURATION CYCLE TIME VARIATION TEST	47.25	≃67.0	≃33.0	–	−12 TO −18	0.20–0.45	628–651	A	570	7.6	8.0	3.0/5.0	5.0/3.0
16.	OSCILLATING ELECTROLYTE CONFIGURATION CURRENT DENSITY VARIATION TEST	48.00	≃67.0	33.0	–	−10 TO −20	0.18–0.34	632–658	A	700	7.6	8.0	4.0	4.0
17.	OSCILLATING ELECTROLYTE CONFIGURATION CATHODE SHAPE TEST	23.00	60.0	40.0	–	−6 TO −14	0.29–0.49	674–678	A	540	7.6	8.0	4.0	4.0
18.	OSCILLATING ELECTROLYTE CONFIGURATION CARBON QUALITY TEST	48.00	≃60.0	≃40.0	–	−10 TO −12	0.10–0.41	685	A	580	7.6	8.0	4.0	4.0
19.	OSCILLATING ELECTROLYTE CONFIGURATION CARBON QUALITY TEST	47.50	≃60.0	≃40.0	–	−13 TO −21	0.23–0.37	658–697	A	400	7.56	8.0	4.0	4.0
20.	OSCILLATING ELECTROLYTE CONFIGURATION CARBON QUALITY TEST	66.75	60.0	40.0	–	−8 TO −16	0.23–0.56	685	A	700	7.6	8.0	4.0	4.0
21.	OSCILLATING ELECTROLYTE CONFIGURATION CATHODE BAFFLE TEST	46.47	54.6	44.9	0.48	−18 TO −23	0.19–0.46	673–689	A	700	7.6	8.0	4.0	4.0
22.	OSCILLATING ELECTROLYTE CONFIGURATION CATHODE BAFFLE TEST	49.50	58.4	41.6	TRACE	−18 TO −21	0.28–0.66	658–679	A	700	7.6	8.0	4.0	4.0
23.	OSCILLATING ELECTROLYTE CONFIGURATION CARBON QUALITY TEST	48.00	59.6	40.3	0.10	−16 TO −25	0.19–0.44	667–669	A	700	7.6	8.0	4.0	4.0
24.	OSCILLATING ELECTROLYTE CONFIGURATION CARBON QUALITY TEST	46.08	59.56	40.2	0.24	−18 TO −26	0.12–0.26	673–681	A	700	7.6	8.0	4.0	4.0
25.	OSCILLATING ELECTROLYTE CONFIGURATION CARBON QUALITY TEST	47.00	≃59.5	≃40.2	0.30	3 TO −16	0.093–0.233	668–675	A	700	7.6	8.0	4.0	4.
26.	OSCILLATING ELECTROLYTE CONFIGURATION CARBON QUALITY TEST	23.50	59.52	39.75	0.83	−18 TO −19	0.09–0.19	667–673	A	600	7.6	8.0	4.0	4.0
27.	OSCILLATING ELECTROLYTE CONFIGURATION CARBON QUALITY TEST	49.65	59.89	39.0	1.11	−17 TO −29	0.093–0.278	668–675	A	600	7.6	7.8/4.0	3.9/4.0	3.9/4.0

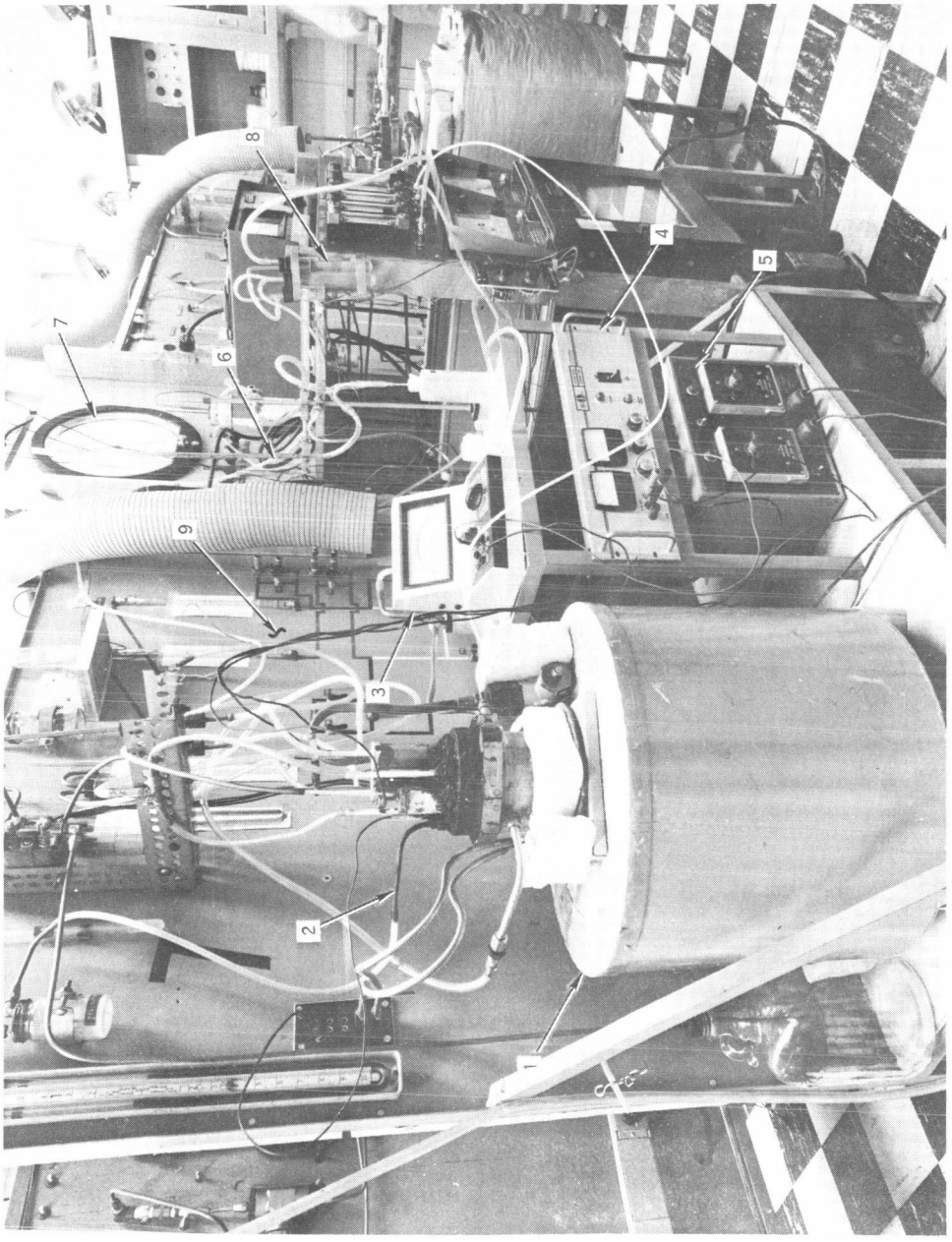
*— SEE APPENDICES A AND B OF THIS REPORT FOR DEFINITIONS AND PROCEDURES FOR DETERMINING PARAMETERS

⊛— A = ARGON

⊠— SEE DISCUSSION PARAGRAPH 10.1.5.5

LL AGE TS	CELL CURRENT AMPERES	ANODE CONFIG. NO.	ANODE CURRENT MA/CM²*	CATHODE CONFIG. NO.	CATHODE CURRENT MA/CM²*	CATHODE QUANTITY	SCRUBBER CONFIG NO.	SCRUBBER CONFIG. NO.	SCRUBBER QUANTITY	TEST RESULTS ~ ANALYSIS: ANODE EFFICIENCY % *	O_2 PURITY % *	CATHODE CAREON DEPOSIT %PURITY*	CATHODE CAREON DEPOSIT CARBON W_1 GRAMS	CATHODE CAREON DEPOSIT RECOVERY % *	CO_2 SCRUBBING EFFICIENCY % *
	2.9	1	435	1	22.5	1	1	1	1	–	30.0	–	–	–	≈97.0%
7	2.9	1	435	1	22.5	1	1	1	1	50.0	80.0	63.0	8.92 GR.	97.1	≈96.0
2.6	2.9	1	435	1	22.5	1	1	2	2	45.5	95.0	62.0	7.86	86.3	≈93.0
2.5	2.4	1	360	1	18.6	1	1	2	2	–	94.0	68.0	9.45	80.5	–
2.8	1.7–2.5	1	255–375	1	13.2–19.4	1	1	2	2	–	–	–	–	–	–
2.7	1.8–2.7	2	270–398	1	13.9–20.6	1	1	2	2	–	87.0	59.0	15.93	80.0	–
3.2	2.0–2.6	3	300–390	2	15.5–20.1	1	1	3	2	56.4	94.0	52.0	5.53	94.5	≈88.0
3.8	3.0	4	91.1	2	23.2	1	1	3	2	–	81.0	–	–	–	–
3.4	1.4–3.4	3	204–510	3	43.6–105.0	1	1	1	1 OR 2	–	–	–	–	–	12.0–100.0
4.3	0.5–2.5	5	–	4	19.4–97.0	1	1	2	2	100.0	–	13.4–59.0	0.3–4.0	–	≈95.0
10	3.15	6	16.3	5	200	2	2	2	2	85.5	100.0	–	–	–	
60	2.90	6	15.0	6	91.9	2	2	2	2	–	100.0	65.0/–	8.06/6.57	70.1/57.1	
40	1.50	6	7.8	7	237.0	2	2	2	2	–	100.0	53.1/57.0	2.59/2.05		
-2.45	1.90	6	9.9	9/8A	103.0	2	2	2	2	82.6	100.0–	69.8/75.0	2.09/2.22	88.3/82.7	
-2.50	2.15–2.30	7	10.4–11.1	8B/10	105.0	2	3	2	2	85.9	100.0	45.9/55.5	5.16/6.31	110.0/90.0 [*]	
-2.30	1.65–1.70	7	8.8	7	230.0	2	3	2	2	96.5	100.0	56.5/61.2	5.73/3.56	98.0/103.0 [*]	
-2.23	1.95–2.05	7	9.9–10.8	9/8A	108.0	2	3	2	2	85.1	100.0–	67.0/74.8	5.28/5.45	99.1/102.2 [*]	
-1.93	1.60	7	7.75	12/11	112.0	2	3	2	2	67.3	100.0	67.7/60.6	2.79/2.64	95.9/90.8	
-2.05	1.70	7	8.8	8B/9	83.1/92.4	2	3	2	2	77.0	100.0	78.5/81.5	4.89/5.15	100.0/104.0 [*]	
-1.77	1.10	7	5.3	8A/9	59.8	2	4	2	2	56.0	98.0	63.6/78.5	2.84/2.97	97.1/101.5	
-2.55	1.83	7	8.9	13	89.5	2	5	2	2	100.0	99.6	67.8/68.1	6.88/6.72	100.6/98.4	
-2.17	1.83	7	8.9	13	89.5	2	5	2	2	85.0	99.2	35.0/36.0	4.92/ –	99.0/ [*]	
-2.41	1.83	8	8.9	13	89.5	2	5	2	2	85.0	99.2	31.6/32.3	5.43/5.66	107.0/111.8 [*]	
-2.20	1.83	8	8.9	13	89.5	2	4	2	2	85.0	99.0	68.8/68.8	5.45/5.85	110.5/119.0 [*]	
-2.23	1.83	8	8.9	13	89.5	2	4	2	2	75.0	100.0	69.9/60.5	5.01/4.67	106.0/99.0 [*]	
-2.37	1.83	8	8.9	13/14	89.5/95.3	2	4	2	2	78.0	100.0	23.4/25.5	3.62/4.14	77.9/83.2	
-2.3	1.75	8	8.5	14	91.1/91.1	2	4	2	2	79.0	100.0	84.6/	2.40/	103.0/ [*]	
-2.46	1.75	8	8.5	14	91.1	2	4	2	2	80.0	100.0	57.4/57.0/62.5	2.62/2.49/3.94	86.6	

FIGURE 10–1. TEST TABULATION
PHASE IIA



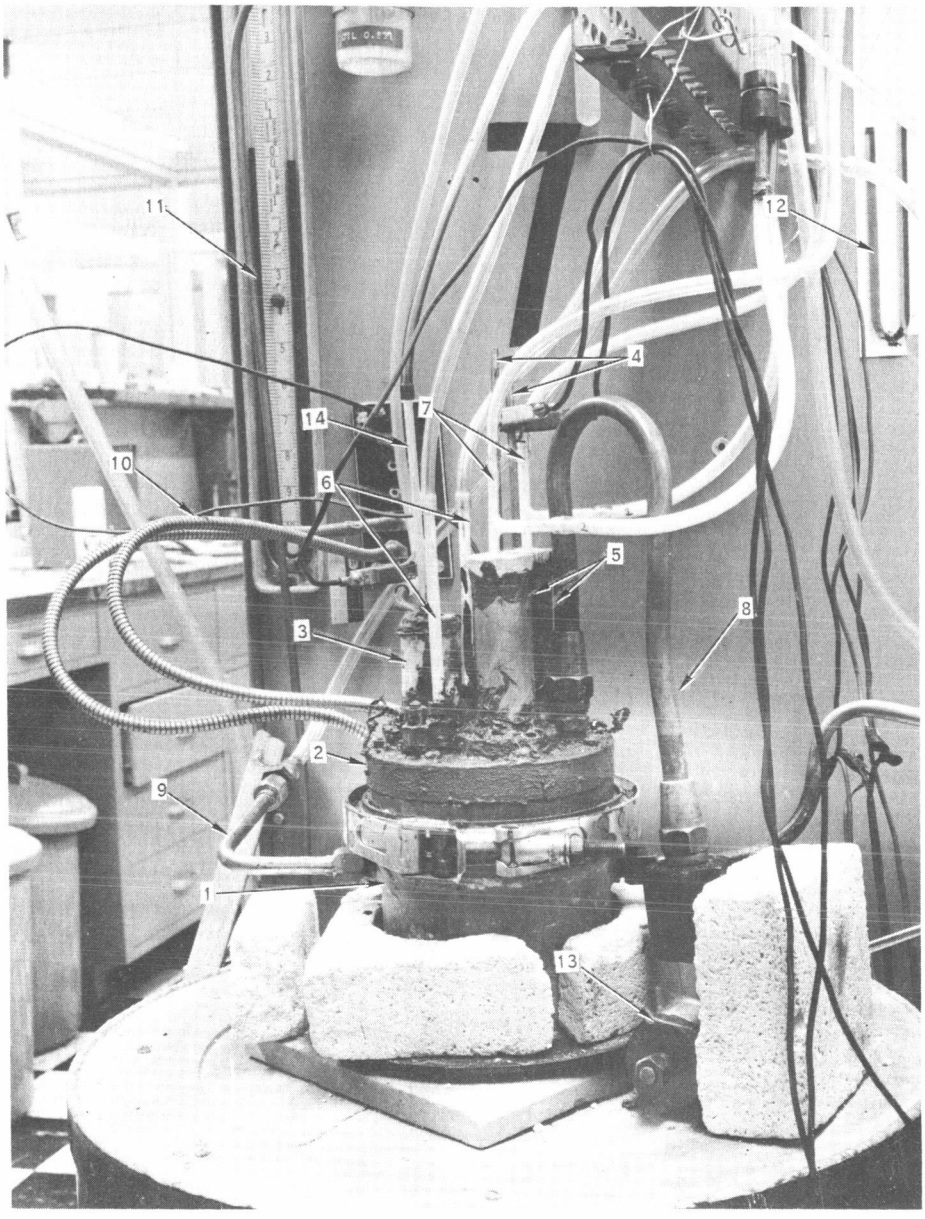
1. TEST ARTICLE OVEN
2. ULLAGE PRESSURE LINE
3. VOLT OHM AMMETER
4. POWER SUPPLY
5. TIMER (WIRED TO SOLENOID VALVE)
6. ANODE PIPETTE FLOWMETER
7. PRESSURE GAUGE
8. ANODE PRESSURE REGULATING SYSTEM
9. CONTROL PANEL (SUPPLY GAS CONTROLS)

FIGURE 10—2. MOLTEN CARBONATE CELL, CONTROL PANEL AND POWER CONTROL SYSTEM



1. DEW POINTER
2. OXYGEN ANALYZER
3. OUTLET GAS CO_2 ANALYZER
4. INLET GAS CO_2 ANALYZER
5. CALIBRATION GASES
6. FLOWMETERS FOR REGULATING FLOW TO INSTRUMENTS
7. TEMPERATURE RECORDER
8. THERMOCOUPLE SELECTION SWITCH
9. THERMOS (32°F REFERENCE FOR TEMPERATURE RECORDER)

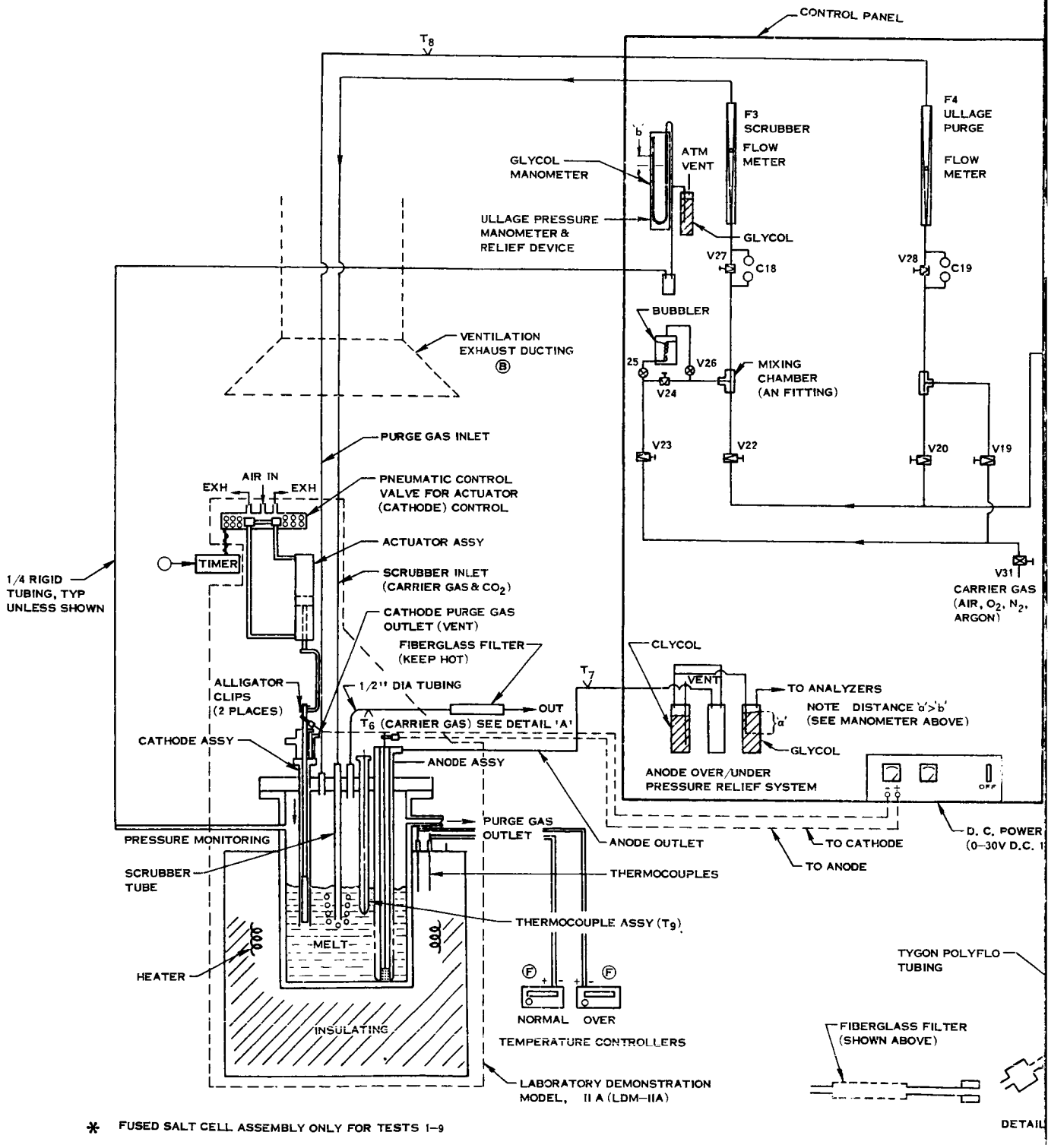
FIGURE 10–3. INSTRUMENTATION AND CALIBRATION GASES



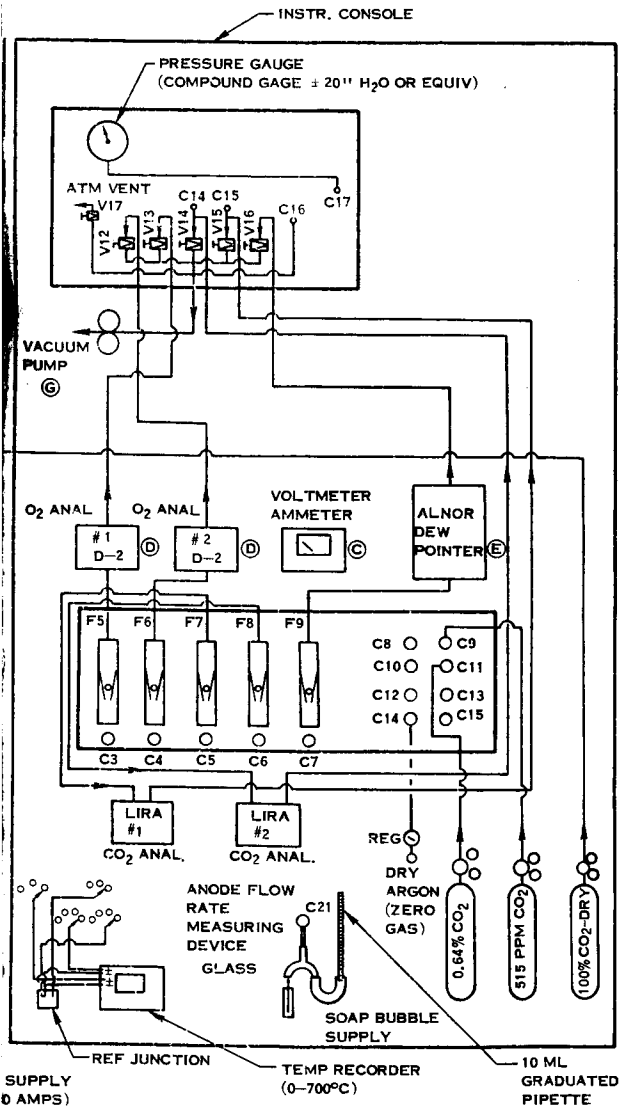
1. NICKEL FURNACE LINER
2. TRANSITE COVER
3. ANODE
4. CATHODES
5. CATHODE NICKEL WELLS
6. SCRUBBERS
7. CATHODE PRESSURIZATION LOOP
8. OUTLET SAMPLE LINE
9. PURGE INLET
10. TEMPERATURE CONTROL THERMOCOUPLES
11. ULLAGE SENSING MANOMETER
12. CATHODE PRESSURE MANOMETER
13. OUTLET FILTER
14. ANODE OXYGEN OUTLET SAMPLE LINE

FIGURE 10–4. OSCILLATING ELECTROLYTE TEST ARTICLE

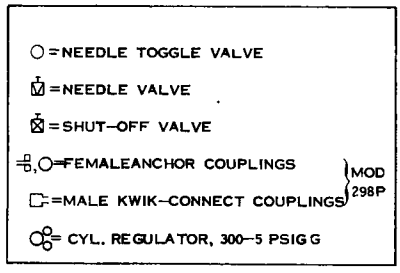
THIS PAGE IS BLANK



* FUSED SALT CELL ASSEMBLY ONLY FOR TESTS 1-9



ITEM	NOMENCLATURE	DESCRIPTION	QUAN
V30 – V31	SHUT–OFF VALVE	WHITEY, MOD, RB 271	2
V25 – V26	TOGGLE VALVE	HOKE, 541, 1/8" NPT (FEMALE CONNECTIONS)	2
V19 – V24	NEEDLE VALVE	HOKE, 1315 M4B, 1/4" NPT (MALE CONNECTIONS)	6
V17,V27,V28, V12 – V17	NEEDLE VALVE	WHITEY, MOD ORM 2–A, ANGLE, PANEL MOUNT, MICRO–REGULATING	10
F5 – F9	FLOW METERS	F & P, SERIES 10A 3137M, 0–900 ML/MIN	5
F3,F4,F11	FLOW METERS	MANOSTAT CORP., 36–541–12, RANGE 7.5 – 2100 ML/MIN	3
C3 – C21	DISCONNECT	IMPERIAL EASTMAN CORP., KWIK–CONNECT COUPLER POLY–FLO TO MALE PIPE ¼" 298P, 129B BULKH ADP	19
Ⓖ	VACUUM PUMP	AIR–SHIELDS, INC. DIA PUMP, MOD EF	1
Ⓕ	TEMP CONTROLLER	HONEYWELL, R7161B1377 (VERSITRONIC, 0–2000°F CHROMEL – ALUMEL)	2
Ⓔ	DEW POINTER	ALNOR INSTR. CO., MOD 7000 U (ROOM TEMP TO –80°F)	1
Ⓓ	OXYGEN ANAL.	BECKMAN, MOD, RANGE 0–100 ACCUR ±2% (CORROSION RES MOD)	1 (2 OPT)
Ⓒ	VOLT–OHM–MILLI–AMMETER	MANCIB CO., MOD 80, OR EQUIV	1
Ⓑ	VENTILATION EXH. DUCTING		1
Ⓐ	TIMER	INDUSTRIAL TIMER CORP., DUPLEX 15 SECOND CU–A	1



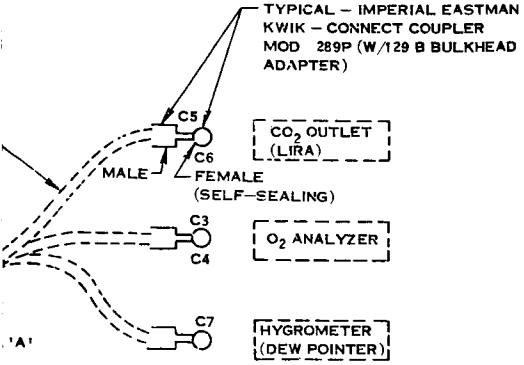


FIGURE 10–5. ENGINEERING TEST FACILITY – FLOW SCHEMATIC*

10.1.3 (Continued)

The techniques and procedures employed for starting a test, for performing instrument calibration, for calculating cathode current efficiency, cathode carbon purity, anode efficiency, etc., were defined and standardized early in the test program. Some are documented generally in the appendix of this report.

Significant events applicable to the test program with reference to test article hardware changes, replacement of fused salt electrolyte, etc., are shown in figure 10-6.

10.1.4 Test Descriptions

The twenty-seven development tests are described on the following pages.

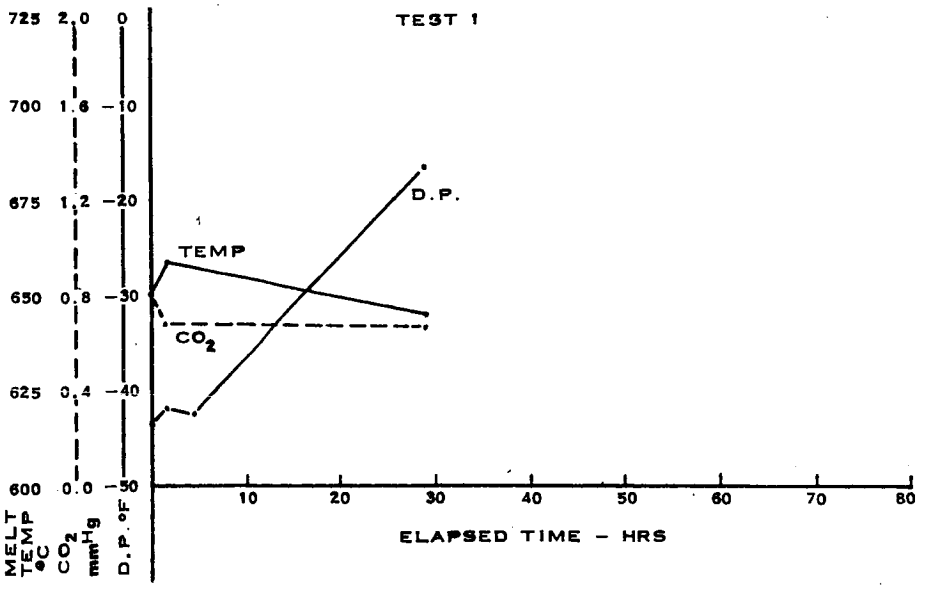
Each test description includes a graphical presentation of electrolyte, pH_2O, pCO_2 and melt temperature as a function of time. No attempt was made to eliminate descriptions of tests where it appeared that basic test objectives were not achieved or where tests were prematurely stopped as a result of difficulty.

10.1.4.1 Test Number 1

Description of Test

Objective: Test Facility Checkout

Date of Test: 1-20-67 to 1-21-67 (29 + hours)



NEW ANODE INSTALLED			X								X						
TEST HARDWARE CHANGE (REF LEGEND)			A						B	C		D					
ADDITION OF Li_2O (IN GRAMS) TO ELECTROLYTE PRIOR TO TEST	4	0		4	4	4	6	4	7	5	8	4	4	5	5	10	11
CHANGE OF ELECTROLYTE IN TEST ARTICLE			X			X					X						
TEST NUMBER	11	12	13	14	15	16	17	18	19	20	21	22	23	24	25	26	27

LEGEND: (TEST ARTICLE HARDWARE CHANGE)

A. ALUMINA CATHODE CONTAINMENT TUBE REPLACED WITH NICKEL TUBE (ON CATHODE NO. 2)

B. ALUMINA CATHODE CONTAINMENT TUBE REPLACED WITH NICKEL TUBE (ON CATHODE NO. 1)

C. ADDED BAFFLE PLATE BETWEEN CATHODE CONTAINMENT TUBES

D. REMOVED BAFFLE PLATE

FIGURE 10–6. TABULATION OF SIGNIFICANT EVENTS ASSOCIATED WITH OSCILLATING ELECTROLYTE CONFIGURATION

10.1.4.1 (Continued)

Composition: Melt 60% LiCl, 40% Li_2CO_3

Cathode Deposit: Not analyzed

Significant Events: During the heating of the electrolyte prior to the start of this test, trouble was encountered with both the temperature controllers and the protective circuit breakers installed to guard against electrical overload of the test article oven. A successful test was conducted once the trouble had been corrected, and run for one day before being discontinued because of excessive CO_2 concentrations in the effluent gas stream. Anode O_2 partial pressure was low (225 mm H_g) during this test.

Discussion of Results

This test was run to verify the ability of the test facility to provide a suitable test bed for the fused salt engineering test program. In general, the test equipment functioned satisfactorily by introducing a desirable influent gas mixture, maintaining melt temperature, and providing workable instrumentation to measure the process parameters.

The test article appeared to function properly, with the exception of the rapid dissolution of the gold anode. When examined, following the test, gold sponge was found to have migrated to the alumina fence surrounding the electrode. It was acting to obstruct free circulation of melt through the fence. It is suspected that the low partial pressure of oxygen observed during the test resulted directly from this obstruction and was caused by either:

(1) Insufficient oxide ions reaching the anode nugget and the subsequent generation of chlorine at the anode, or

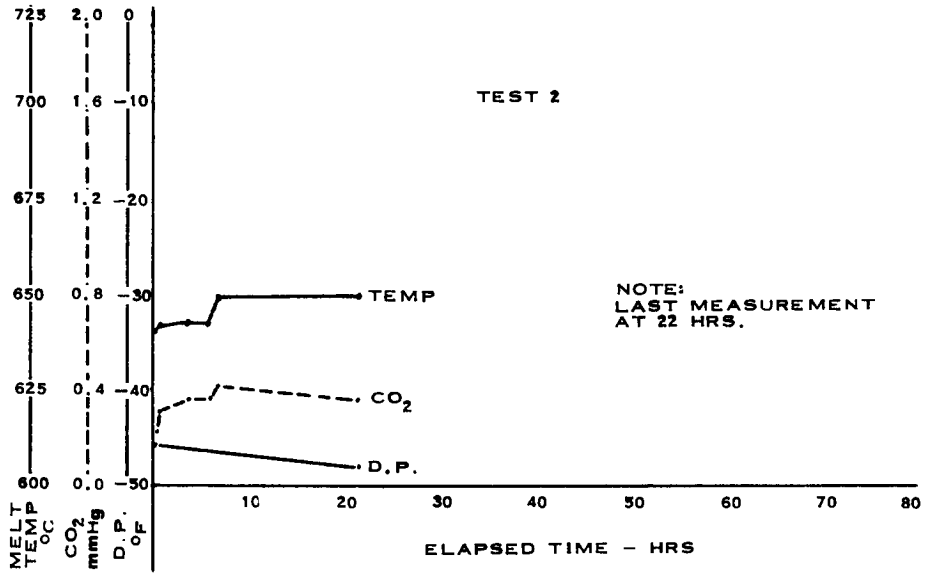
(2) Dilution of the small O_2 flow within the anode shield with air, i.e., leakage became a significant factor.

10.1.4.2 Test Number 2

Description of Test

Objective: Base Line Test - Reciprocating Cathode

Date of Test: 1-26-67 to 1-27-67 (28 + hours)



Composition: Melt: 60% LiCl, 40% Li_2CO_3

Cathode Deposit: 48% purity on sides of cathode; 66.5% on lump at bottom of cathode; average carbon deposit purity, 63%.

Significant Events: The partial pressure of oxygen within the anode containment tube increased to 610 mm Hg over the first 21 hours of test. Both the effluent dew point and CO_2 concentrations were maintained at relatively constant levels throughout the test. A 7.61 cm cathode stroke was used. Cathode cycle time was 7.8 seconds of which 5 seconds was with cathode "up", 1 second was with cathode submerged, and the balance was in transition between these two positions. In the "up" position, electrical contact between the cathode and electrolyte was still made to permit the electrolyte deposition of carbon upon the electrode.

Discussion of Results

The 63% carbon deposit purity was noted to be consistent with the results achieved to date by Hamilton Standard Research Laboratory tests of a reciprocating cathode. The

10.1.4.2 (Continued)

50% anode current efficiency (reference figure 10-1) is believed to be explainable by leakage into-and-from the anode shield and instrumentation tubing. Historically, testing experience has demonstrated anode current efficiencies of 100%. In view of this, only minimum effort was spent in an attempt to correct the slight leakage in the anode circuit.

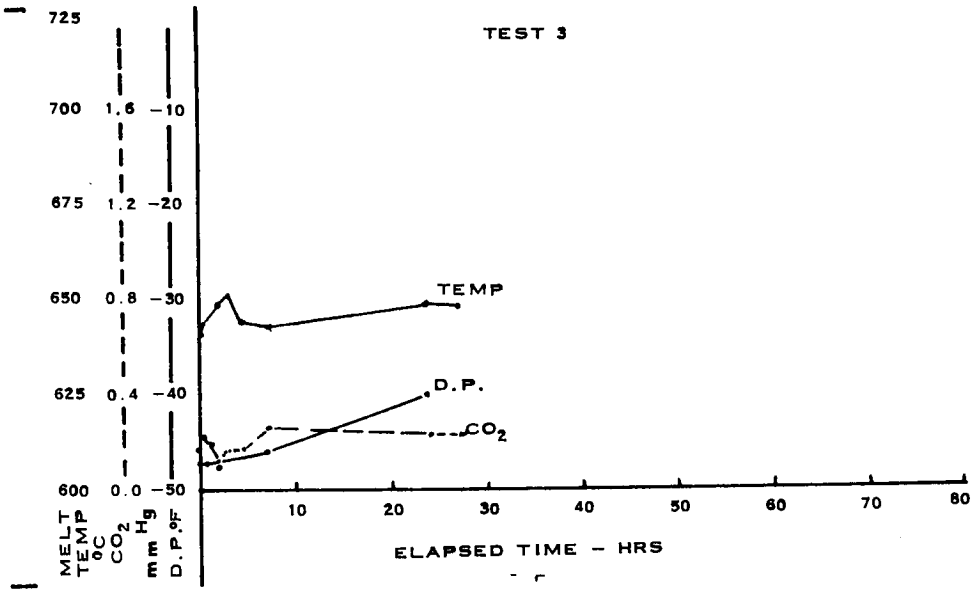
It was concluded that this test paralleled the results obtained in recent applied research and attention should next be focused on performing tests specifically directed toward engineering aspects of the process.

10.1.4.3 Test Number 3

Description of Test

Objective: Process Test - High Scrubber Flow

Date of Test: 1-31-67 to 2-1-67 (27 + hours)



Composition: Melt: 60% LiCl, 40% Li_2CO_3

Cathode Deposit: 62% purity carbon

Significant Events: This test was performed with a higher inlet flow rate (1700 scc/min) to establish whether significant splashing of the electrolyte would prohibit the use of such flow rates in the engineering test program. Larger flow rates were used so that the CO_2 partial pressure could be reduced to a desirable range of 3-3.5 mm Hg to more meaningfully simulate end-usage CO_2 concentrations.

A failure of the oscillation cathode mechanism 1-1/2 hours after the start of the test due to binding within the cathode rod seal caused a temporary delay. The problem was corrected and the test continued a short time later; no adverse effects upon the validity of the test were foreseen as a result of this difficulty.

10.1.4.3 (Continued)

Discussion of Results

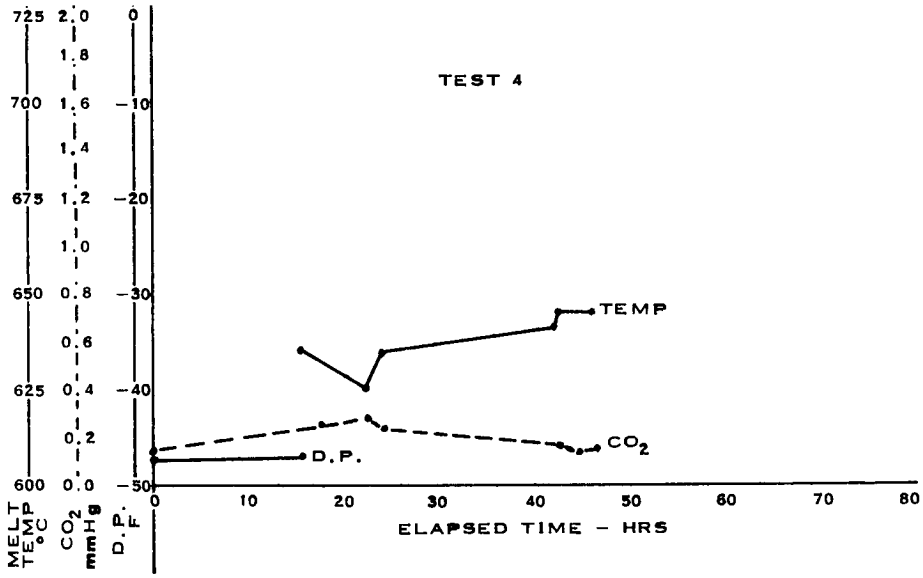
The 62% cathode purity, together with the 93% CO_2 scrubbing efficiency achieved, lent testimony to the fact that the 1700 scc/min flow rates can be satisfactorily employed within the engineering test article. The similarity in performance with respect to test number 2, reflects the independence of cell performance upon CO_2 partial pressure over the range examined. As a result of the higher "scrubber" flow, the cell ullage outlet fittings tended to become obstructed more frequently, evidencing a higher melt vapor carry-over rate. Since some form of surface CO_2 scrubbing will be ultimately dictated, the obstruction problem is not believed significant - except as it effects the test program.

10.1.4.4 Test Number 4

Description of Test

Objective: Process Test - Nitrogen Compatibility

Date of Test: 2-1-67 to 2-3-67 (46 + hours)



Composition: Melt: 60% LiCl, 40% Li_2CO_3

Cathode Deposit: 68% carbon purity

Significant Events: This test, run at CO_2 concentration of 3.5 mm Hg, used nitrogen as the influent carrier gas. Argon had been employed in the earlier three tests as well as being generally used in Hamilton Standard Division's applied research tests. It was believed desirable to confirm the fact that nitride or nitrate compounds possibly forming in the electrolyte would not compromise the process--at least to an obvious extent observable within a 48 hour test period.

Melt temperature was observed to drop after twenty-two hours of the test. The drop was attributed to an electric fan blowing on the test article. The fan had been set up to accelerate the hardening of RTV on the Transite anode cap.

Discussion of Results

The 68% carbon deposit purity and the 80% cathode current efficiency achieved in this test indicate the non-criticality of a nitrogen influent atmosphere to the process. It is felt that the crack discovered within the alumina anode containment tube on 2-6-67 during the post test inspection may have been caused by the inadvertent decay in electrolyte temperature (to approximately 560°C).

.1.4.5 Test Number 5-A

Description of Test

Objective: Process Test - Nitrogen Compatibility

Date of Test: 2-9-67 (5 hours)

Composition: Melt: 60% LiCl, 40% Li_2CO_3

Cathode Deposit: Not analyzed

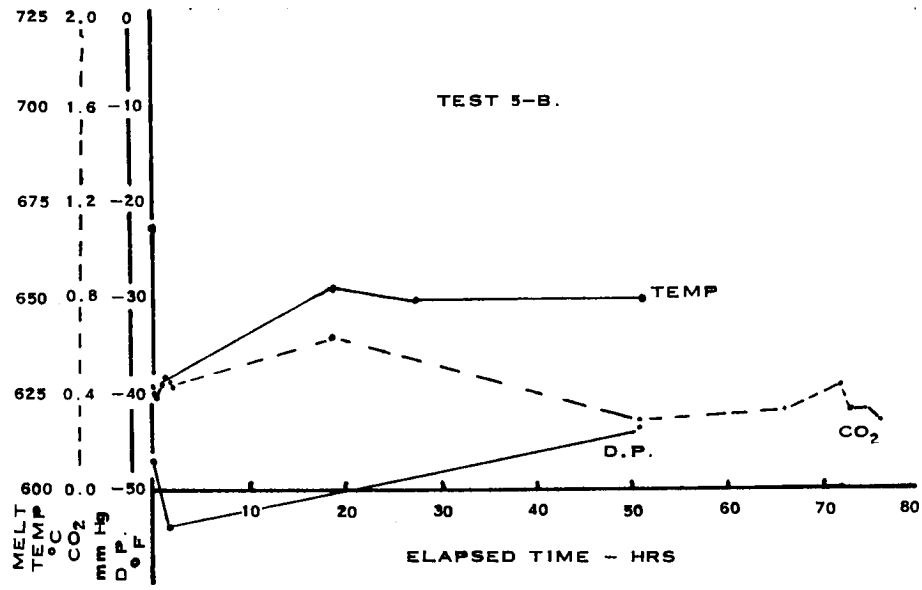
Significant Events: This test was aborted five hours after start. Documentation is included in this report to explain this difficulty, which concerned CO_2 being evolved at the anode. In phase I of this program, it has been theoretically and experimentally established that a depletion of $CO_3^{=}$ at the anode would result in the generation of CO_2 at that electrode. Such depletion of $CO_3^{=}$ could foreseeably arise from an insufficient Li_2CO_3 content within the melt or by other means acting to prevent $CO_3^{=}$ from reaching the anode. In the case of test number 5-A, subsequent anode examination established that gold sponge generated by anode dissolution had largely blocked the passeges between the alumina tubes of the anode containment assembly.

10.p.4.5 Test Number 5-B

Description of Test

Objective: Process Test-Nitrogen Compatability

Date of Test: 2-10-67 to 2-13-67 (76 + hours)



Composition: Melt: Approximately 60% LiCl, 40% Li_2CO_3

Cathode Deposit: 59% carbon purity

Significant Events: Prior to this test, the anode fence was opened up by removing some of the fencing. The new configuration (configuration number 2, reference figure 10-1) is documented in Appendix C, figure C-10. The solid gold anode nugget was also replaced.

A cathode stroke of 2.95 inches and a cathode cycle time of 13.1 seconds was employed in this test (1.70 seconds bottom dwell, 8.2 seconds upper dwell). During the last hour of this test, the influent CO_2 flow rate was decreased from 1700 to 855 scc/min, while CO_2 partial pressure was increased from 3.3 to 6.7 mm Hq. to ascertain whether the effluent CO_2 would change following the variation in CO_2 inlet pressure. Anode O_2 pressure was low (87% purity) during this test. An inspection of the alumina crucible following this test showed it had cracked and allowed some leakage of fused salt in the surrounding nickel canister. The test results were not believed to be compromised by this failure.

Discussion of Results: Anode oxygen pressure showed some improvements in this test over test Number 5-A. Carbon dioxide partial pressure at the anode was found to be equal to the partial pressure of CO_2 in the effluent gas stream. It is hypothesized that opening up the anode fence to enable better transfer of $CO_3^{=}$ ions had the effect of reducing CO_2 generation at that electrode.

No change in effluent CO_2 pressure followed the step-change in the influent CO_2 level in the last hour of the test.

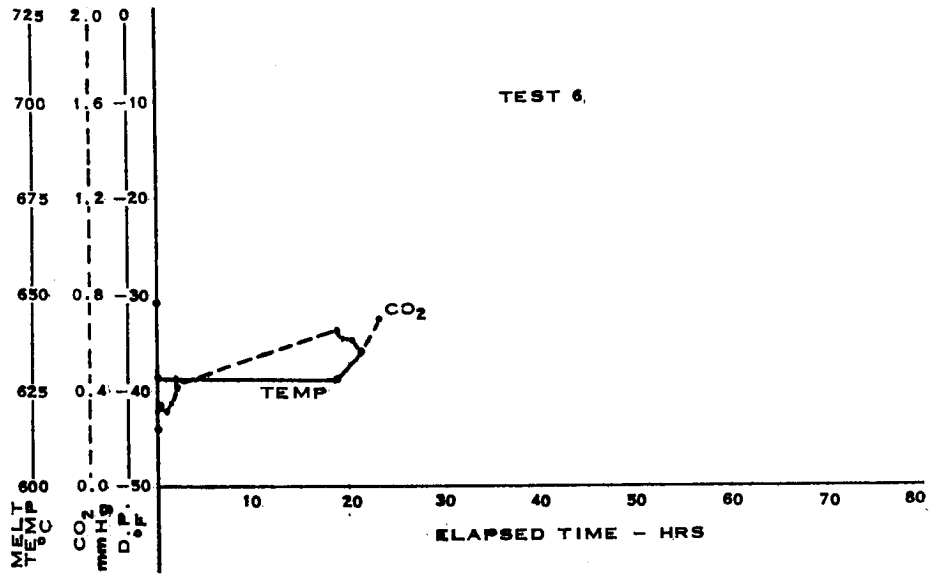
In general the results of this test in which nitrogen was used as the diluent gas showed no apparent variation from those tests employing argon. The results, again, suggest that no obvious limitations surround the use of nitrogen.

10.1.4.6 Test Number 6

Description of Test

Objective: Process Test - Air Compatibility

Date of Test: 2-21-67 to 2-22-67 (23+ hours)



Composition: Melt: 60% LiCl, 40% Li_2CO_3

Cathode Deposit: 52% carbon purity

Significant Events: The electrolyte was changed prior to the start of this test. The anode was changed to a new configuration (see figure 10-1 and Appendix B) prior to this test to further improve $CO_3^{=}$ transport. The air employed for the CO_2 diluent in this test had to be passed through a silica-gel desiccant bed designed and fabricated for this test to maintain a low dew point. Current was increased from 2.0 to 2.6 amps in an attempt to maintain a suitable effluent pCO_2 pressure. The test was halted when the electrolyte was inadvertently forced up the anode and solidified. Subsequent examination of the test article showed that gold sponge had clogged some of the holes in both scrubber tubes (see Appendix B and figure 10-1 for configuration).

10.1.4.6 (Continued)

Discussion of Results: The 52% carbon purity, together with the other performance characteristics of this test, appeared to be consistent with previous tests employing argon and nitrogen as the diluent gas. As with test Number 5, anode pCO_2 appeared to be the same as the partial pressure of CO_2 in the cell effluent gas stream.

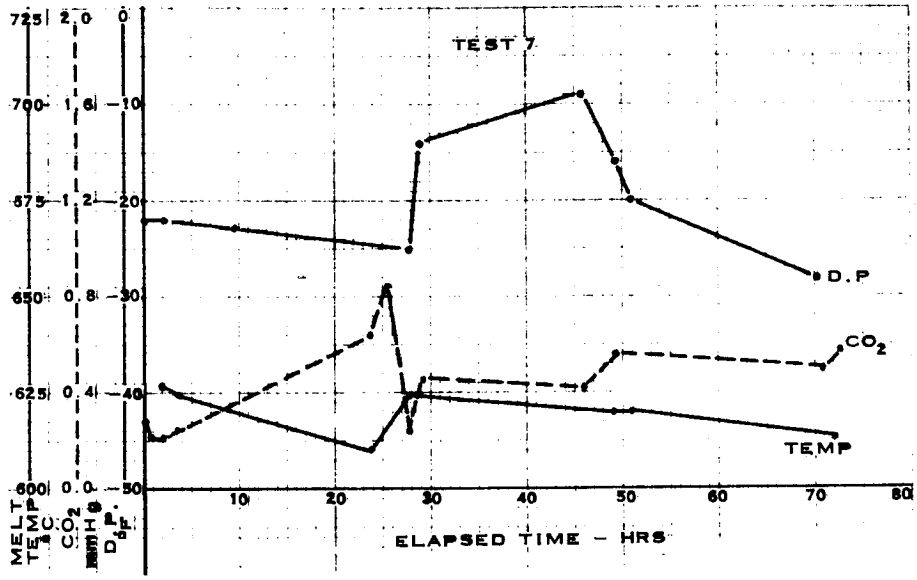
The difficulty experienced with anode clogging with gold sponge has been an annoying one, and it was planned to minimize the detrimental consequences of sponge formation through the attempted use of a centrifugal anode.

10.1.4.7 Test Number 7

Description of Test

Objective: Centrifugal Anode Test

Date of Test: 3-26-67 to 3-29-67 (72 hours)

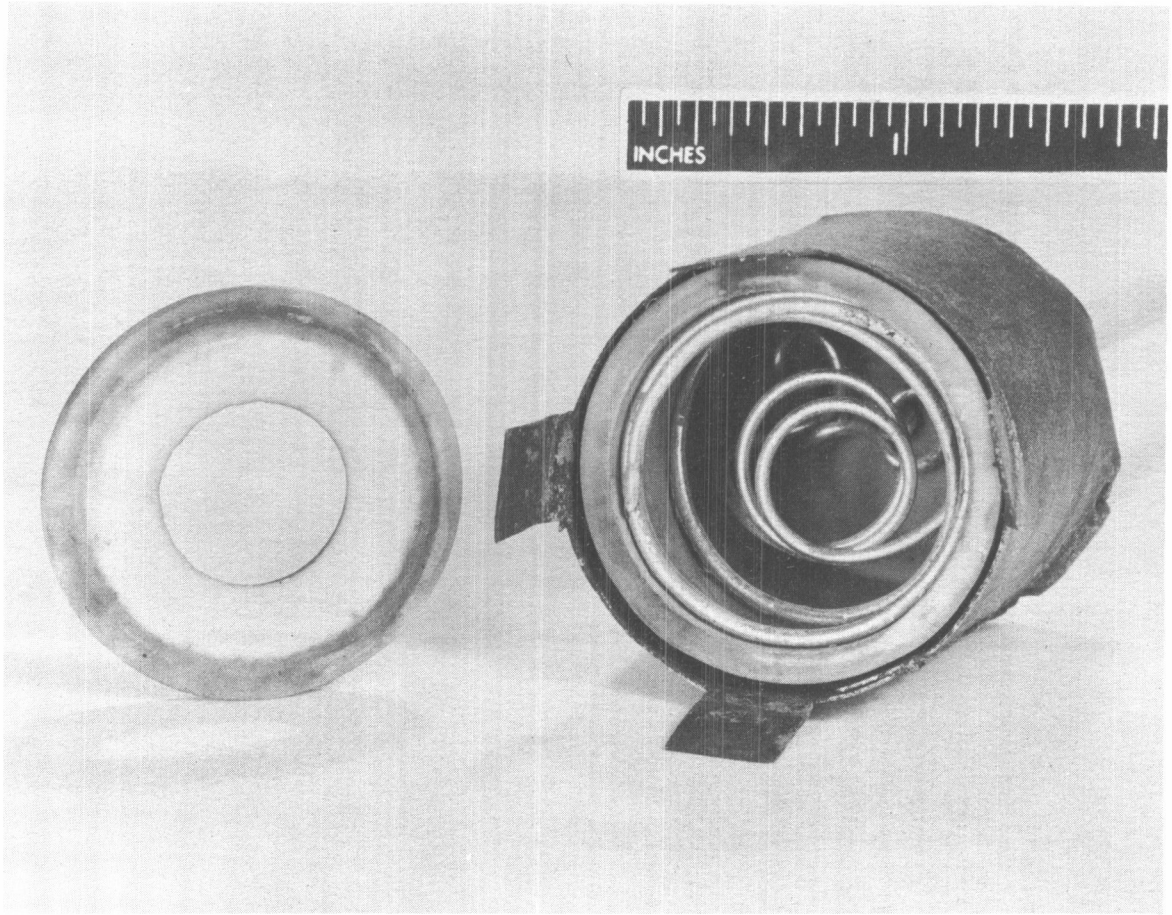


Composition: Melt: 60% LiCl, 40% Li_2CO_3

Cathode Deposit: Not analyzed

Significant Events: **The Appendix C of this report defines (figure C-11) the configura**tion of the anode experimentally tried on this test. As may be noted, the anode consisted of gold wire coiled against the inside surface of a surrounding nickel tube that used alumina as an electrical insulator. The entire subassembly was rotated at 525 RPM during the test, with electrical contact with the anode gold wire being accomplished through the use of a carbon brush. A 1/8 inch diameter hole was provided in the disc lid to allow for the evolution of O_2 at that electrode. The gold wire anode had a weight of 39.00 grams prior to the start of the test, of which 22.2 grams was active (immersed in electrolyte).

The test was run under constant current conditions (3.0 amps). Figure 10-7 shows the anode subassembly as removed following the test. When removed it was discovered that gold sponge had built up on the outer surface of the gold wire but in general the anode appeared to have experienced a minimum of dissolution. Subsequent weighings showed that the anode had experienced a dissolution rate of 0.029 gms/ampere-hour.



PHOTOGRAPH SHOWS ANODE FOLLOWING TEST. CERAMIC DISC ON LEFT OF PHOTO HAS BEEN REMOVED FROM ASSEMBLY 'BOTTOM' WHERE IT WAS HELD BY THE FOUR 'TABS': GOLD WIRE APPEARED BRIGHT WITH ONLY SIGN OF DISSOLUTION BEING SMALL QUANTITY OF 'SPONGE' AGAINST INNER BORE OF CERAMIC LINER.

FIGURE 10–7. ROTATING ANODE USED IN TEST # 7

10.1.4.7 (Continued)

Discussion of Results: Per Faraday's equation, $W_t = \frac{ItM}{nF}$ (where W_t = gold anode weight loss-gain, I is current-amperes, t = time-seconds, M = atomic weight of gold, n = valance of gold, F is Faraday's number, 96,500). Accordingly, the theoretical weight loss in gold from the anode during the test would have been 294 grams, if subsequent to the reformation of atomic gold at that electrode the sponge were non-adherent to the gold nugget.

The loss of 2.10 grams of the electrode represented 0.715% of the theoretical maximum loss. An anode current density of 102 ma/cm^2 was used in the test. With reference to table 5-1, it is observed that the anode dissolution efficiency (0.715%) compares well with the best results achieved to this date. The low dissolution is felt to be explainable by improvement in oxide transport to the anode surface caused by the local agitation, and was probably further benefited by the forced displacement of O_2 bubbles from the active anode surface.

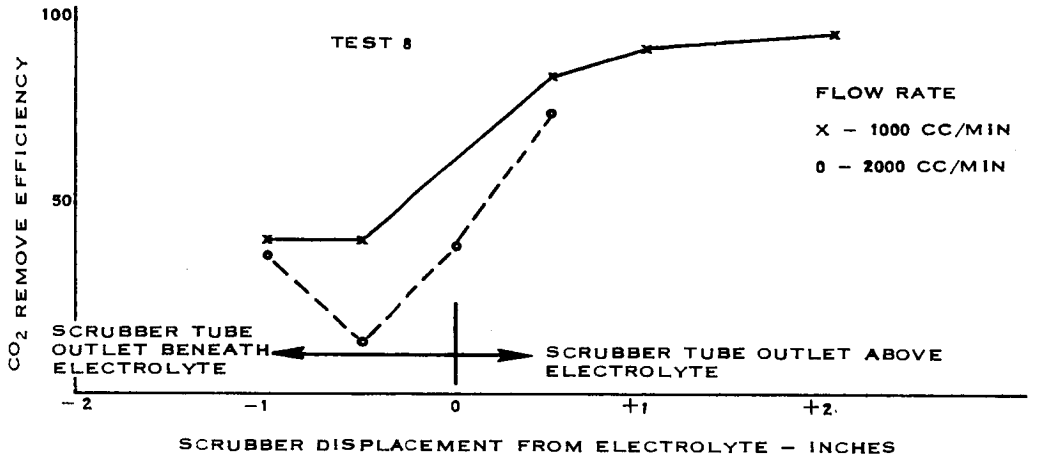
The results suggest that if dissolution continues to cause test article problems, a rotating anode should be considered to minimize these problems. It was subsequently found that with the configuration adapted (beginning with test 10) that the dissolution problem no longer significantly compromised testing.

10.1.4.8 Test Number 8

Description of Test

Objective: CO_2 Scrubbing Performance Test

Date of Test: 4-4-67 to 4-20-67 (intermittently run)



Composition: Electrolyte: 60% LiCl, 40% Li_2CO_3

Cathode Deposit: Not analyzed

Background & Discription of Test: Until this test in the engineering program, the flow path of the influent CO_2-diluent gas was through a sparge tube (or tubes) submerged at depths varying from 1 to 2 inches below the surface of the electrolyte. Two questions had arisen concerning the efficiency of which CO_2 was absorbed by the electrolyte --was the efficiency dependent upon the depth the sparge tube was immersed?...and would it be possible to elevate the sparge tubes above the surface of the electrolyte so that higher influent flow rate could be obtained? (Note: it had been established that severe bubbling and clogging of test hardware accompanied the increase in flow rate above 1700-2000 ml/min with submerged tubes).

This test varied the displacement of the end of the sparge tube relative to the surface of the electrolyte. The variation was from one inch above to two inches below the surface. Inlet flow rates were varied from 1000 to 2000 ml/min. Air was used as the diluent gas. Each test was continued until an apparent equilibrium in CO_2 outlet partial pressure was reached.

10.1.4.8 (Continued)

Discussion of Results: This test reflects.

1. CO_2 scrubbing efficiency improves with diminishing flow rate.

2. CO_2 scrubbing efficiency improves with sparge tube penetration depth in the electrolyte, but suggests that the rate of improvement diminishes after a given depth (approximately 3/4 - 1 inch for the data shown),

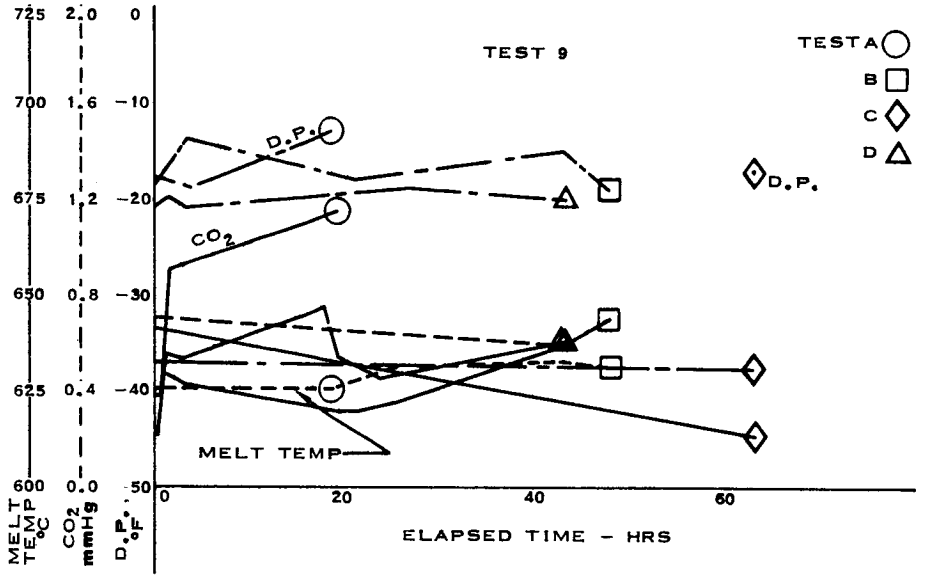
3. A less significant CO_2 removal efficiency results from surface scrubbing - i.e., with the influent air being directed at the melt from above.

Observation Number 3, above, is believed to be the most interesting. The data suggests that if surface scrubbing could be accomplished through the use of cylically wetted plates, for example, an even higher scrubbing efficiency (due to more intimate contact) might result. Some surface scrubbing tubes were used later in the program to further investigate this.

10.1.4.9 Test Number 9

Objective: Carbon Deposition on Vibrating Cathode

Date of Test: 5-2-67 to 5-15-67 (18+ hours)



Composition: Melt: Approximately 60% LiCl and 40% Li_2CO_3

Cathode Deposit:

Test	Purity	Cathode Current Efficiency %	Vibration Frequency Hz,	Vibration Displacement inches	Cathode Current Density ma/cm^2
A	36.0%	73.3	30	0.07"	190
B	59.0%	67.8	30	0.07"	39
C	27.6%	8.7	100	negligible	15.5
D	13.4%	49.4	100	--	62

Significant Test Events: The cathode was subjected to vibration of varying frequencies and amplitudes (tests A, B, C). **The amplitude of the vertical displacement varied inversely with the frequency; at 30 Hz, the displacement was 0.07 inches; at 100 Hz,** it was not measurable. In test D, the cathode was immobile and the electrolyte was agitated by vibrating a 1.0 inch square paddle immersed 2.8 inches in the electrolyte.

10.1.4.9 (Continued)

Discussion of Results: Vibration of the melt and the cathode during this test were done in the interest of improving carbon purity, current efficiency, and cathode deposit shape. Both carbon purity and cathode current efficiency were lower than in tests using an oscillating cathode. The purity and efficiency were lowest for test C and D.

Conclusions:

1. Stationary cathodes yield the worst carbon purity and deposit efficiency. Based on this test, it appears that vibrating the cathode at 30 cps over small displacements of approximately 0.07 inches acts to improve the overall cell performance. An increase in cathode vibratory displacement may yield further benefits, and should be investigated when such a configuration would appear to offer other advantages.

2. The deposit formed on the vibrating cathodes appeared to have uniform thickness over the entire electrode surface, figure 10-8.



PHOTOGRAPH SHOWS RELATIVE UNIFORM CARBON DEPOSIT RESULTING IN THIS TEST, PRESUMABLY AS A RESULT OF THE VIBRATION OF THE CATHODE.

FIGURE 10–8. CATHODE DEPOSIT FROM TEST #9

10.1.4.10 Test Number 10

Description of Test

Objective: Oscillating Electrolyte Configuration - Feasibility Test

Date of Test: 5-22-67 to 5-24-67 (46.5 hours)

Note 1. No performance curves are presented for this test. When withdrawing the cathodes at the end of the test, it was found that all cathode welded areas had failed and the cathode itself had fallen to the bottom of the crucible, apparently soon after test initiation. The resulting current density on the cathode support rod was excessive, and due to the poor deposit no chemical analysis was made to establish carbon purity.

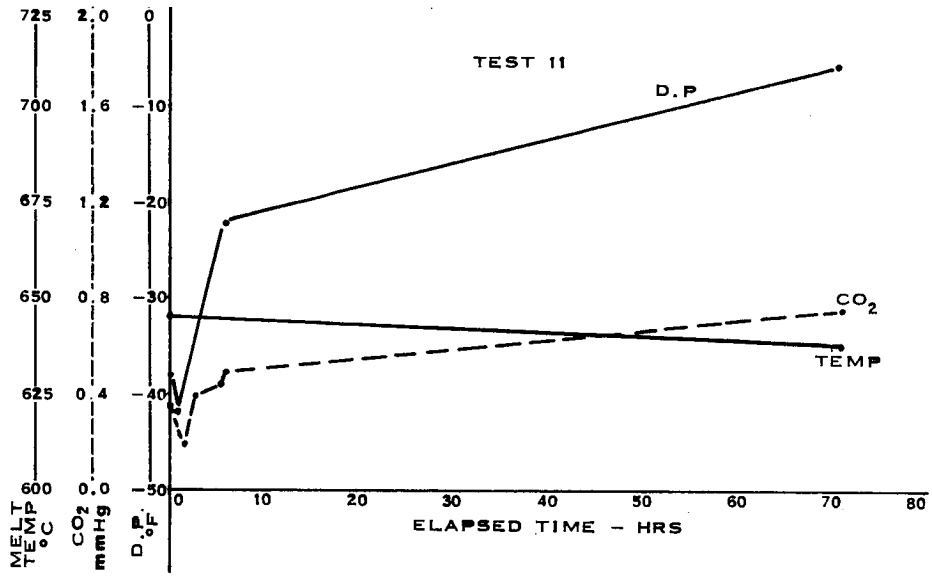
Note 2. Figures C-2 and C-3 in Appendix C of this report describe the test article configuration employed for tests Number 10 - Number 27. Figure C-2 describes the basic cell; figure C-3 defines the pneumatic mechanism used to oscillate the electrolyte.

10.1.4.11 Test Number 11

Description of Test

Objective: Oscillating Electrolyte Configuration - Feasibility Test

Date of Test: 5-26-67 to 5-29-67 (71+ hours)



Melt Composition: 60% LiCl, 40% Li_2CO_3

Cathode Deposit: 65% carbon purity

Significant Events: This test was run over a weekend. Although electrolyte displacement was adjusted at the start of the test to permit an electrical continuity break beneath cathodes, it was observed following the weekend that neither cathode Number 1 or Number 2 current flow was interrupting cyclically. Subsequent examination of the cathode deposit showed that carbon on both electrodes had bridged over to their respective alumina containment tubes. Otherwise, the test proceeded smoothly. Anode O_2 pressure reached 760 mm Hg abs. after approximately 8 hours of test. Both cell CO_2 and H_2O outlet partial pressures increased during the test. It is of interest to note that one of the two scrubber tubes completly clogged over the weekend deflecting all CO_2 influent flow through the single remaining tube. This was not thought to significantly affect the test data.

10.1.4.11 (Continued)

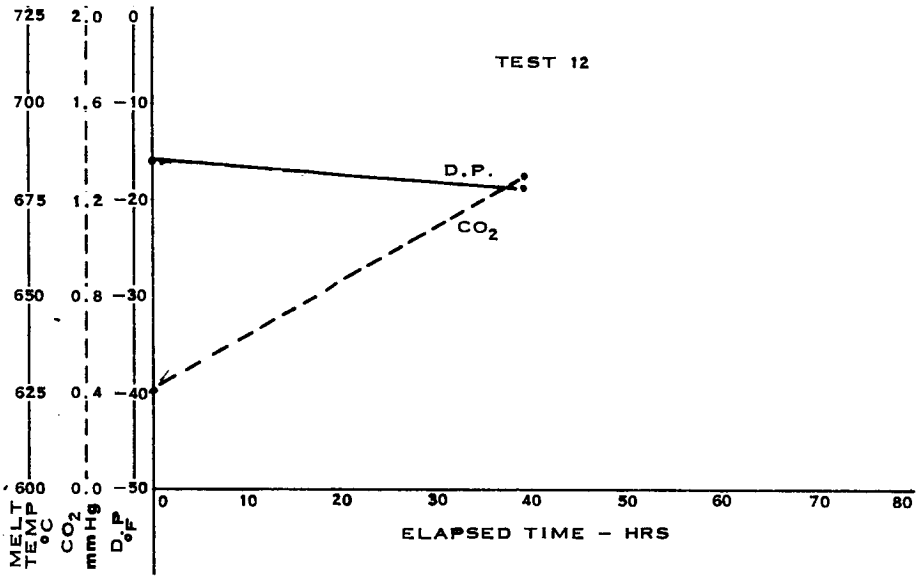
Discussion of Results: The relatively good carbon quality (65%) achieved on this first successful dual-cathode (electrolyte-displacement) test was believed to be significant. As discussed elsewhere in this report, the configuration (if it is proven to yield favorable carbon quality and cathode efficiency) is believed to offer potential for zero g considerations aside from certain other aspects (an aid in preventing anode polarization, etc.). The 4 sec/4 sec cathode submerged/uncovered cycle was arbitrarily selected, and, with additional testing may prove to be a significant variable. A fairly rapid electrolyte displacement velocity (estimated 0.2 - 0.4 seconds up-down time) gives clear indication that at least in the early portion of the test, when the cathode current flow was interrupted half of each cycle, the carbon deposit which totally accrued under the melt instead of above it, was favorable. The relatively poor cathode current efficiency was believed to be attributed to the "bridge-over" problem and the loss of some of the carbon during the removal of the cathodes from their containment tube

10.1.4.12 Test Number 12

Description of Test

Objective: Oscillating Electrolyte Configuration - Fundamental Investigation Test

Date of Test: 5-29-67 to 5-31-67 (40 hours)



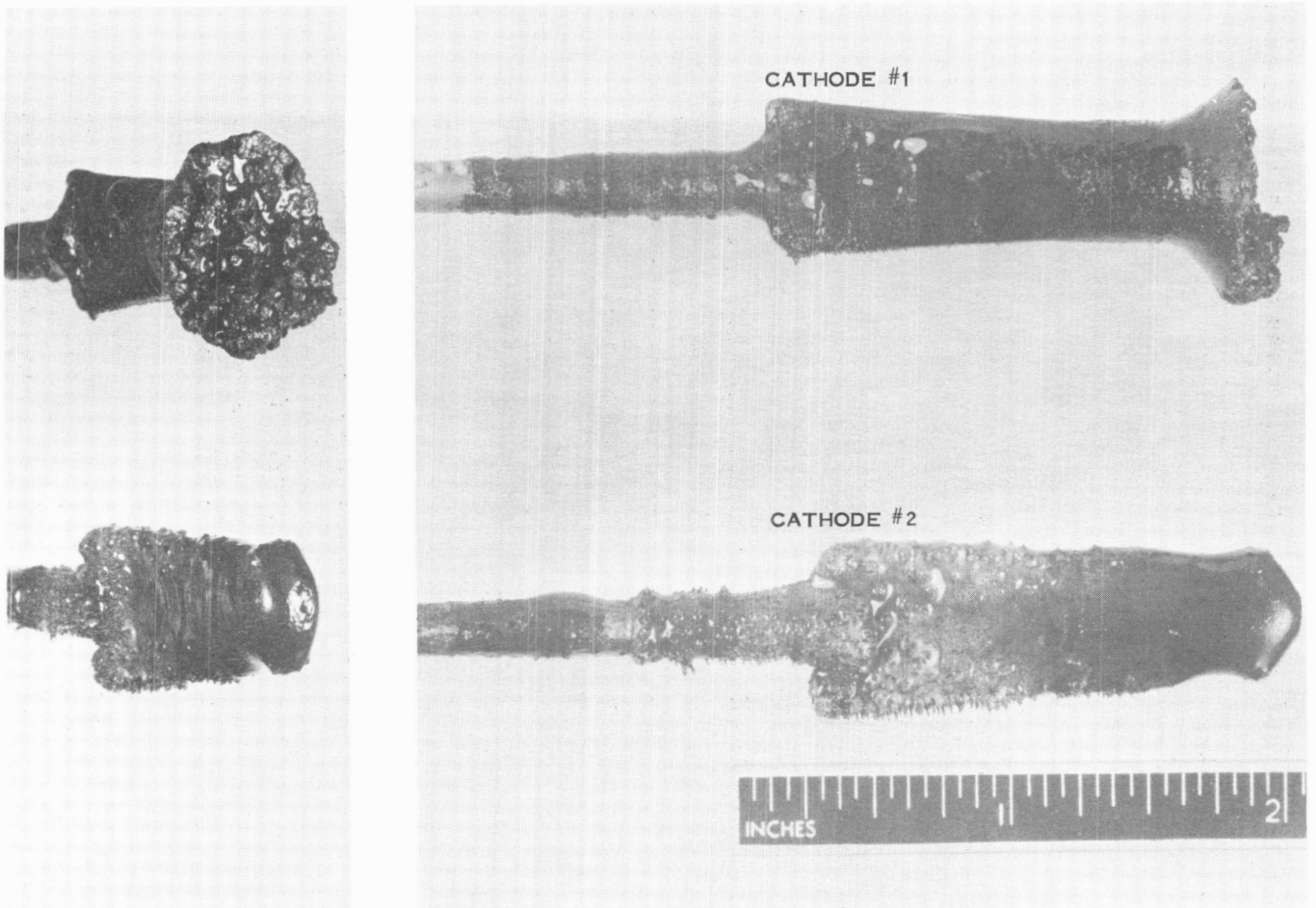
Melt Composition: 60% LiCl, 40% Li_2CO_3

Cathode Deposit: 53-57% carbon purity

Significant Events: During the test the CO_2 partial outlet pressure rose from an initial value of 0.4 to 1.3 mm Hg abs. As with test number 11, the electrolyte displacement oscillation was insufficient to cyclically interrupt the current throughout the entire test. Consequently, for some indeterminate time during the test, cathode number 1 was in continuous contact with the melt. The cathode current density employed for this test was 200 ma/cm^2 which was believed excessive when it was selected, but was imposed to yield additional information on the configuration being examined. In addition, the cathode electrode shape was varied from rectangular to tapered in an attempt to achieve a rectangular carbon deposit. (Note: typically, the carbon deposit has been thicker at the bottom of the electrode.)

10.1.4.12 (Continued)

Discussion of Results: Figure 10-9 shows cathodes number 1 and number 2. The picture clearly indicates the effect of continuously submerging cathode number 1 during what is presumed to be a significant portion of the test. Also visible in the photograph is the nature of the carbon growth showing stalagtite formations on both deposits but more obvious on cathode number 2. Cathode number 2, which was exposed cyclically to the melt and ullage gas phases during the entire test, did develop into a nearly rectangular envelope giving promise that tapered electrodes might be usefully employed to achieve satisfactory cathode envelope shapes. The steady rise in the effluent CO_2 level during the test is felt to reflect non-ideal conditions, probably accounting for the 53-57% carbon deposit purity, but cannot be quantitatively explained at this time.



CATHODE #2 (REMOVED FROM MELT EVERY 4 SEC FOR 4 SEC) DEVELOPED A NEAR RECTANGULAR DEPOSIT. CATHODE #1 REMAINED IN CONTACT WITH THE ELECTROLYTE THRU MOST OF TEST & DEVELOPED CHARACTERISTIC BULBOUS GROWTH ON LOWER END.

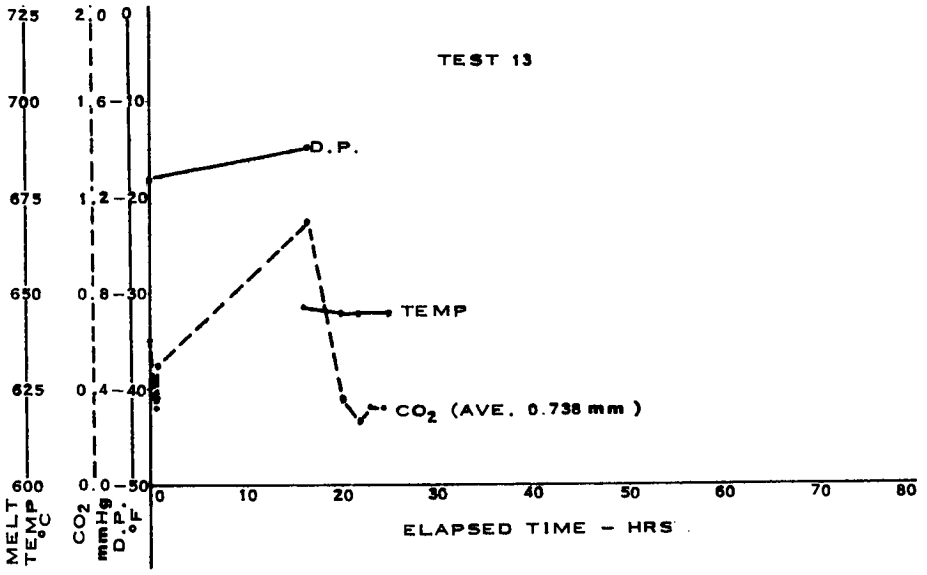
FIGURE 10—9. DEPOSIT FROM CATHODES IN TEST #12

10.1.4.13 Test Number 13

Description of Test

Objective: Oscillating Electrolyte Configuration - Fundamental Investigation Test

Date of Test: 6-1-67 to 6-2-67 (24+ hours)



Melt Composition: 60% LiCl, 40% Li_2CO_3

Cathode Deposit: 70-75% carbon purity

Significant Events: The CO_2 and dew point rose gradually during this test. After approximately 16 hours and in an attempt to reduce pCO_2, influent flow was interrupted for seven hours, during which time the melt CO_2 level decreased to 0.3 mm Hg. In spite of the precautions taken, the average melt pCO_2 value during the test was significantly high (approximately 0.74 mm Hg). Cathode current density for this test was 100 ma/cm^2.

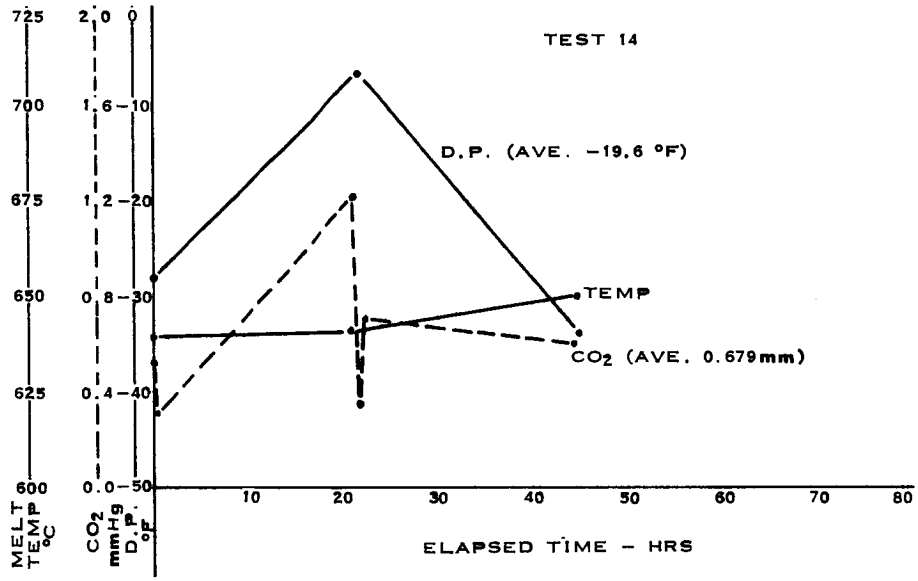
Discussion of Results: The achievement of 70% and 75% carbon purity values on cathodes number 1 and number 2, respectively, was significant. It is also significant that the cathode current efficiency (84.5%) represented the best achieved in tests to date with this condiguration. Additional tests are needed over a wider (and lower CO_2 partial pressure) before quantitative relationships can be established. All previous tests of this configuration employed: (1) an old melt (unchanged since test number 5) and, (2) a non-varying eletrolyte displacement cycle time of 8 seconds (4 seconds up/4 seconds down). Alterations of these criterion were pursued in test 14.

10.1.4.14 Test Number 14

Description of Test

Objective: Oscillating Electrolyte Configuration - Cycle Time Variation Test

Date of Test: 6-10-67 to 6-12-67 (45+ hours)



Melt Composition: New melt; 67% LiCl, 33% Li_2CO_3; contamination unknown, but believed small.

Cathode Deposit: 46-55% carbon purity

Significant Events: Both pCO_2 and dew point increased during the initial 21 hours of test. Influent CO_2 flow was terminated for a period of 20 minutes at 21 hours and the following decay of effluent pCO_2 was rapid.

A carbon rod (1/8-inch diameter) was accidently dropped into the melt at 0900 hours on 6-11-67 and could not be recovered. It is not believed that this incident influenced the test data. The cycle time of the electrolyte oscillation was decreased in this test to 4 seconds (2 seconds up, 2 seconds down) in an attempt to ascertain the effect on the process. The alumina tube surrounding cathode number 2 was replaced with a nickel tube prior to test number 14 to establish whether this material would noticeably affect the quality of the deposit.

10.1.4.14 (Continued)

Discussion of Results: Carbon purities of 46% and 56% were achieved at cathodes number 1 and number 2, respectively. Based upon this one test, it does appear that the substitution of nickel in place of an alumina shield around the cathode acts to favor the formation of higher quality carbon. Additional testing is necessary to confirm this. The poorer carbon obtained during this test maybe a function of, at least partially, the shorter cycle time employed. Again, further testing on shorter and longer cycle times is required to demonstrate the effect of cycle time variations. The achievement of a 100% cathode current efficiency during this test is felt to be significant. It remains to be determined whether the high efficiency can be maintained as carbon purity improvements are made with this configuration.

It appears that the increase in the chloride composition of the melt (i.e., 67 weight percent instead of 60%) did not significantly affect the process.

Figure 10-10 shows x-ray photographs of the carbon deposit on both cathodes. The primary regions of carbon growth appear to be (1) on horizontal areas of the electrode, and (2) in the lower region of the electrode.

It was also observed (Figure 10-10) that a small void occurred between and at the top of the "prongs".

Figures 10-11 and 10-12 are photographs of the cathode deposits. The carbon void referred to above may be observed on figure 10-12, which further shows the near-cylindrical shape of that electrode carbon deposit.

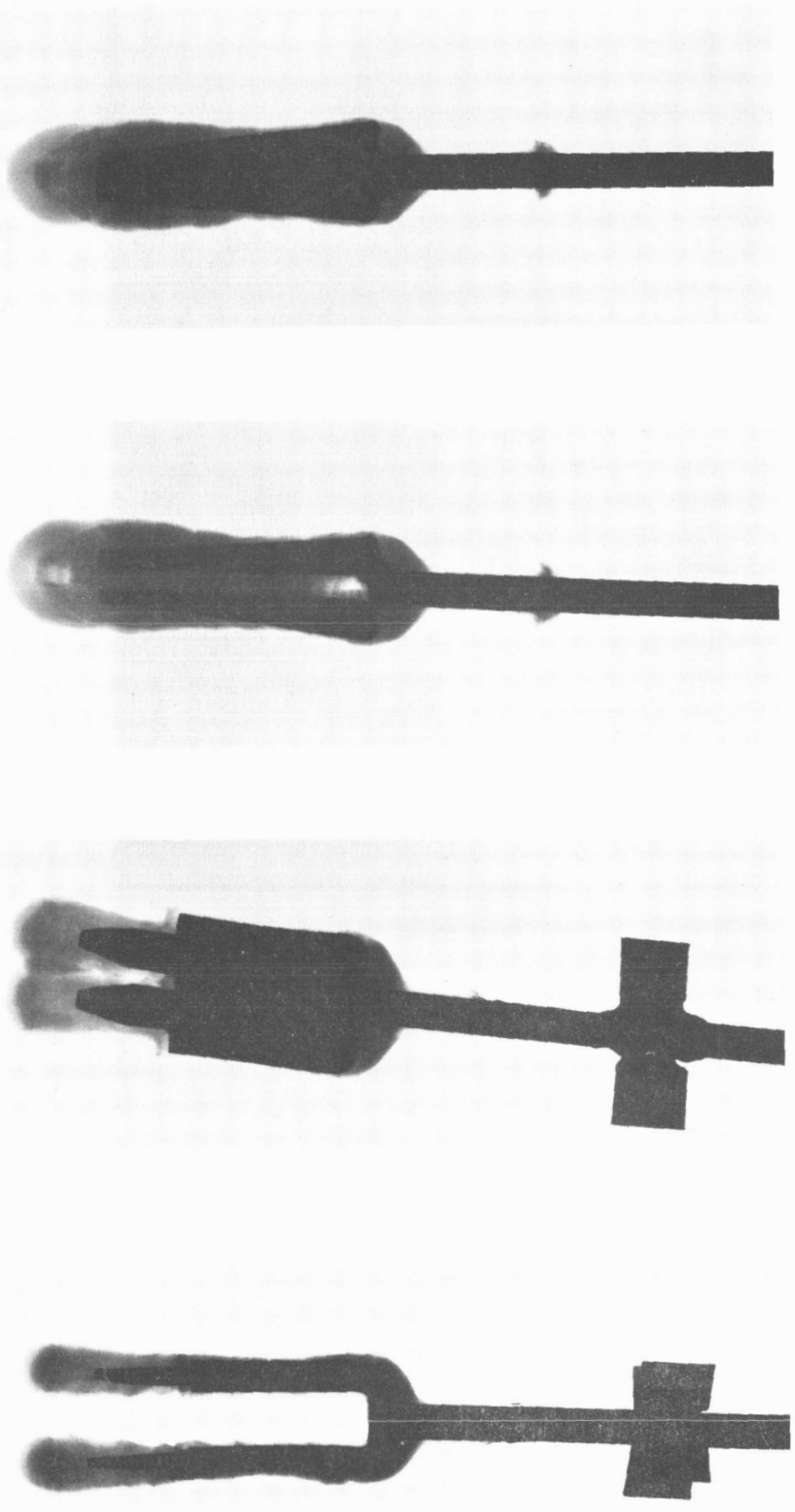


FIGURE 10—10. X—RAY PHOTOGRAPH OF CATHODES FROM TEST #14. NOTE THAT CYLINDRICAL ENVELOPE OF CATHODE #2 RESULTED BECAUSE OF TAPER IN ELECTRODE ITSELF

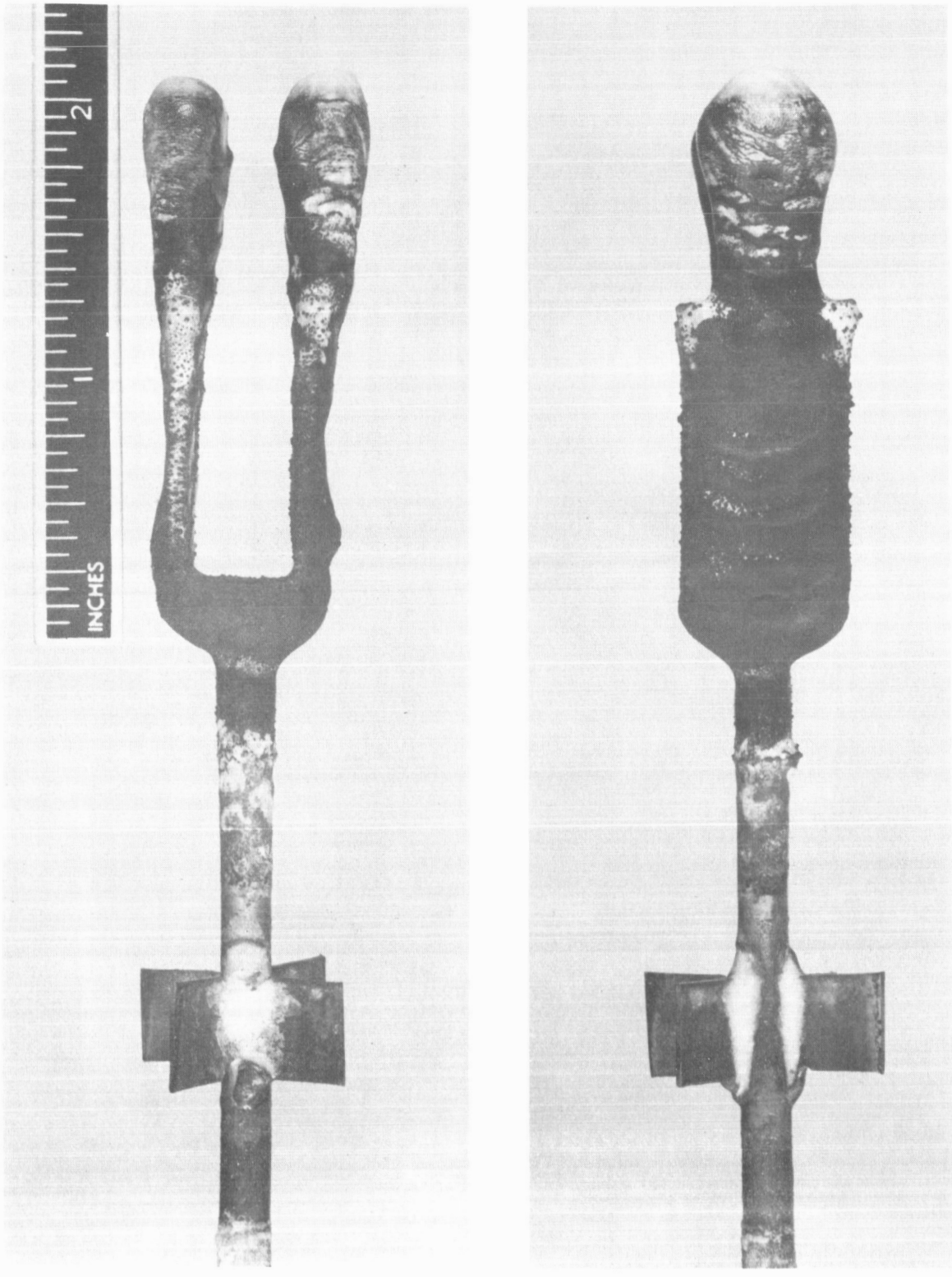
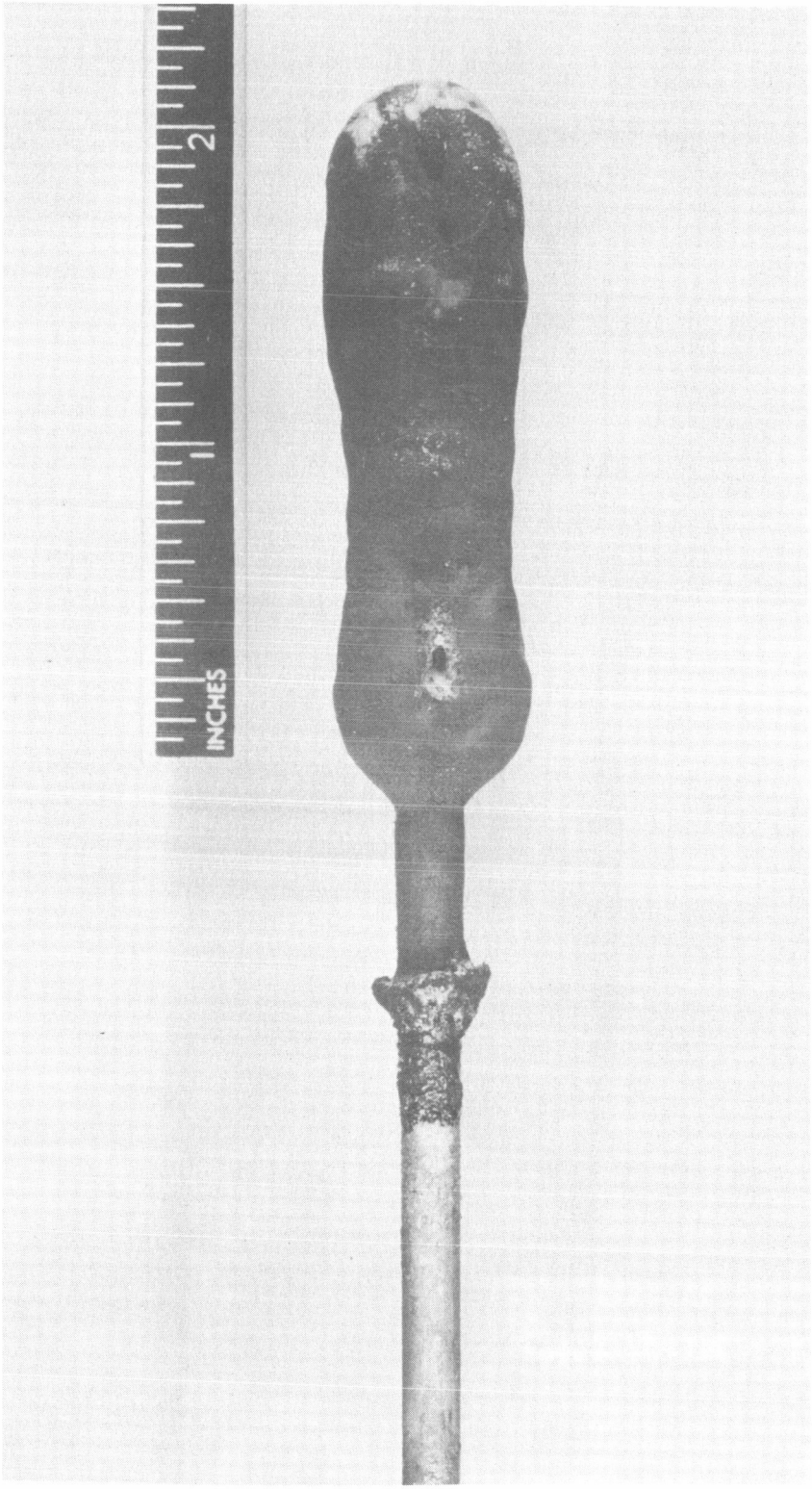


FIGURE 10—11. CATHODE #1 (CONFIGURATION #8B) FOLLOWING TEST #14



NEAR CYLINDRICAL DEPOSIT. FIGURE 10—10 SHOWS X—RAY OF THIS DEPOSIT (CATHODE #2) AND CONFIRMS SMALL VOID WITHIN CYLINDER EVIDENCED BY 'BLOW HOLE' IN THIS PHOTOGRAPH

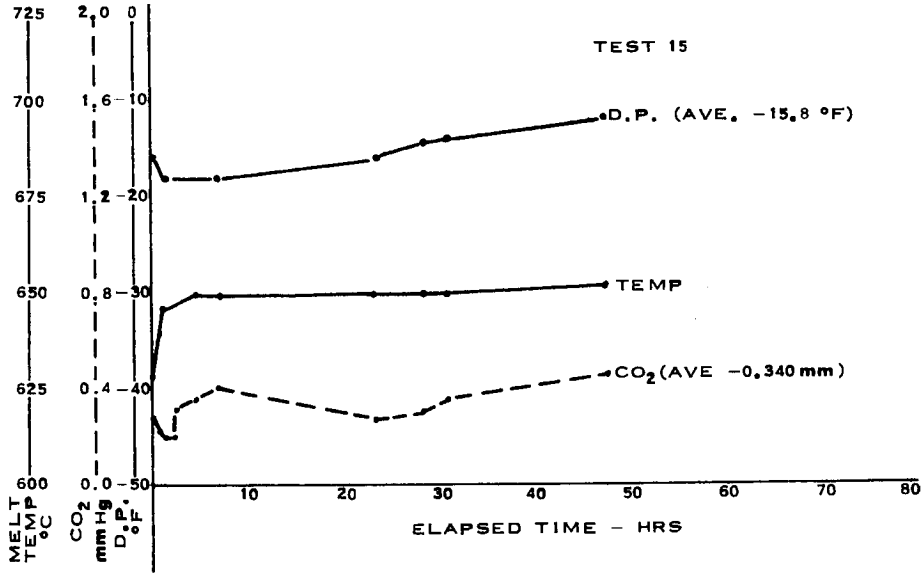
FIGURE 10—12. CATHODE #2 (CONFIGURATION #10) FOLLOWING TEST #14.

10.1.4.15 Test Number 15

Description of Test

Objective: Oscillating Electrolyte Configuration - Cycle Time Variation Test

Date of Test: 6-13-67 to 6-15-67 (47+ hours)



Melt Contamination: 67% LiCl/33% Li_2CO_3 approximately; contamination level unknown

Cathode Deposit: 56%-61% carbon purity.

Significant Events: A cathode current density of 230 ma/cm^2 was employed for this test. Cycle time was further varied to expose cathode number 1 to the ullage gas for 3 seconds and to the melt for 5 seconds. Cathode number 2 was exposed to the ullage gas for 5 seconds and to the melt for 3 seconds. Unlike test numbers 13 and 14, inlet CO_2 flow did not require interruption during the test to maintain CO_2 level within the effluent gas stream. The CO_2 effluent concentration was maintained at an average level of 0.34 mm Hg throughout the test; effluent dew point averaged -16°F.

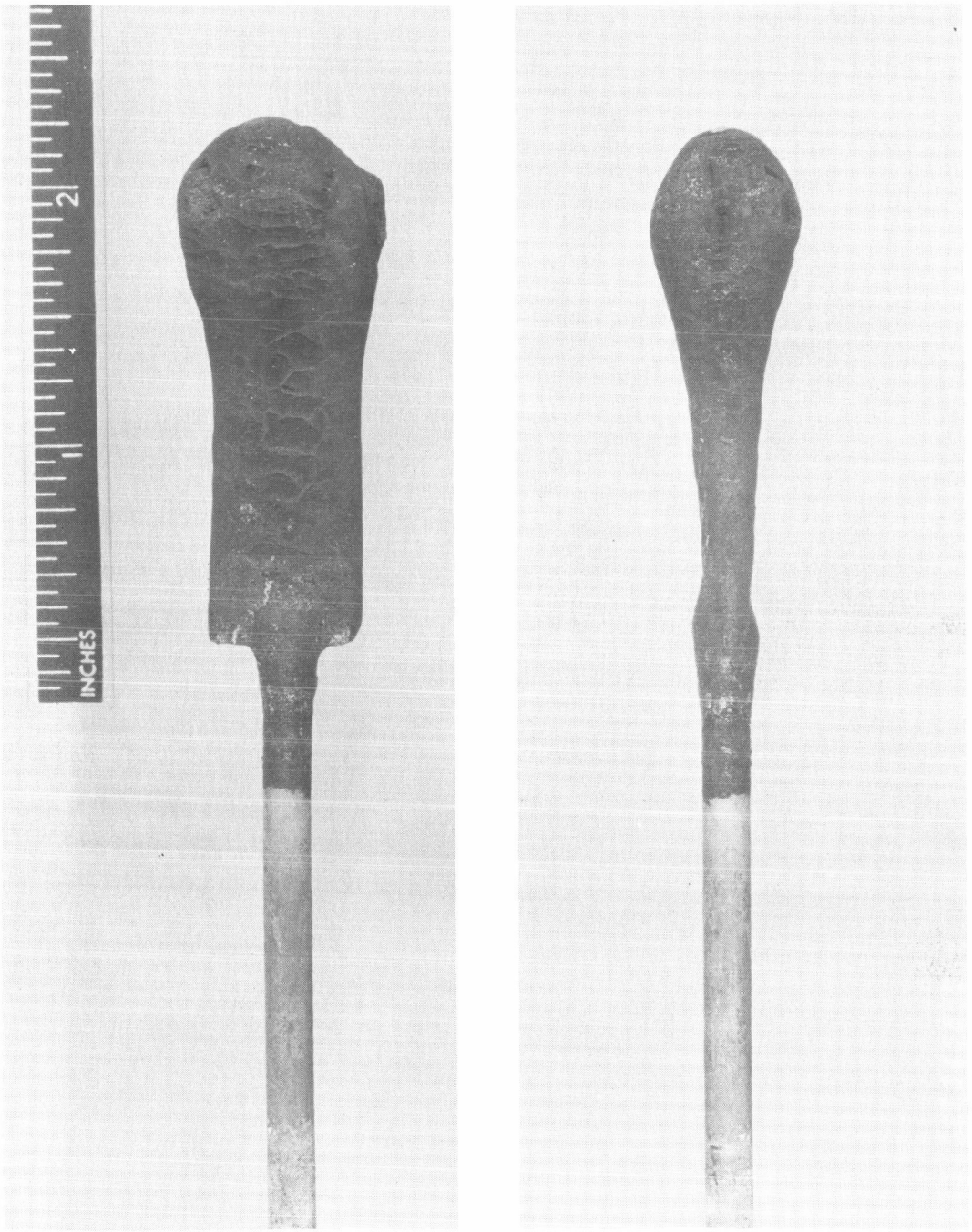
Discussion of Results: Carbon purities of 56% and 61% were obtained on cathodes number 1 and 2, respectively. The average CO_2 level maintained in the effluent gas stream during this test was the lowest of all previous tests of this configuration. The absence of significant variation between the carbon purities on cathodes number 1 and 2, together with the low CO_2 level (presumed to be closely related to the CO_2 level

10.1.4.15 (Continued)

within the electrolyte), indicates that the CO_2 level in itself does not control carbon purity. Over the 3-5 second boundaries tested, it does not appear that cycle time is a critical variable. The achievement of 100% cathode current efficiency is again felt to be significant. It is believed that cathode current density should be reduced to less severe levels on subsequent tests and that in the immediate future, electrolyte cycle times should be standardized at 8 seconds (4 seconds up, 4 seconds down). Again, it was observed that the nickel tubing surrounding cathode number 2 may in some manner be responsible for the 5% higher carbon purity obtained on that electrode. This was investigated in test number 13 and will be pursued in a later test.

Figure 10-13 shows x-ray photograph of carbon growth on both electrodes. As expected, cathode 1 has the larger carbon deposit mass (5.73 grams) vs 3.56 grams for cathode 2 as a result of experiencing a larger current flow. Figures 10-14 and 10-15 picture photographs of the carbon deposit on both electrodes.

FIGURE 10—13. X—RAY PHOTOGRAPH OF CATHODES #1 & #2 FROM TEST #15. THE GROWTH OF CARBON BELOW THE ELECTRODE MAY BE OBSERVED TO BE NEARLY EQUAL FOR BOTH THE 3 AND 5 SECOND CYCLES



COMPARISON WITH FIGURE 10—15 SHOWS THAT CATHODE #1 HAD MORE CARBON DEPOSITED — OWING TO ITS 5 SECOND CYCLIC SUBMERGENCE TIME IN ELECTRO—LYTE

FIGURE 10—14. CATHODE #1 FOLLOWING TEST #15

THIS CATHODE OPERATED UNDER CYCLIC CONDITIONS OF 3 SECONDS SUBMERGED – 5 SECONDS RAISED ABOVE ELECTROLYTE

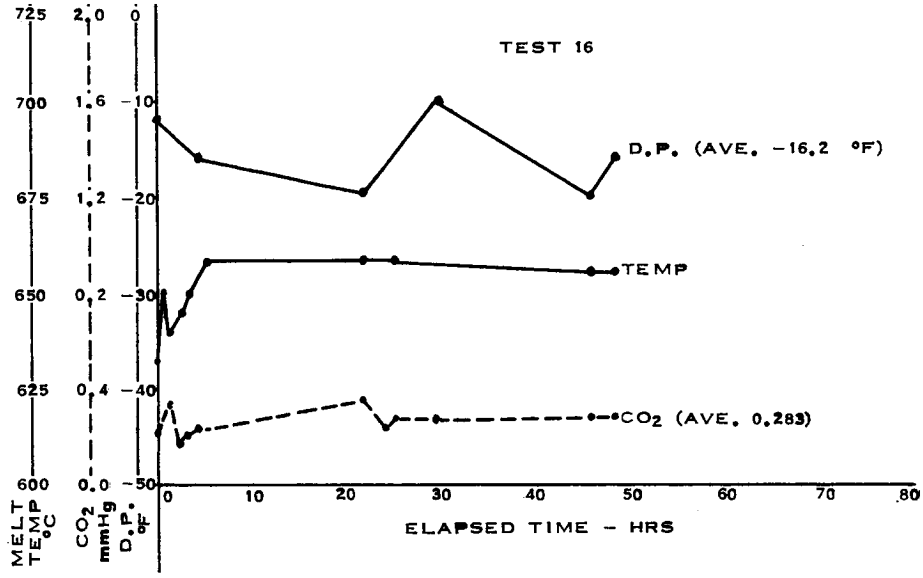
FIGURE 10–15. CATHODE #2 FOLLOWING TEST #15

10.1.4.16 Test Number 16

Description of Test

Objective: Oscillating Electrolyte Configuration - Current Density Variation Test

Date of Test: 6-20-67 to 6-22-67 (48 hours)



Melt Composition: 67% LiCl, 33% Li_2CO_3 contaminant levels unknown

Cathode Deposit: 67%-75% carbon purity

Significant Events: Effluent CO_2 and moisture levels maintained during this test were similar to those achieved in the preceding test. Cathode current density and cycle time, however, were varied to values believed to be more nominal and/or desirable as discussed in test number 15.

Discussion of Results: The results of this test are similar to those of test number 13 in that carbon purity achieved was 67% and 75% for cathodes 1 and 2, respectively. Cathode current efficiency, however, was 100% in contrast to the 85% level achieved in test number 13. The average pCO_2 within the effluent gas stream (0.28 mm Hg) was significantly lower than test number 13 (0.738 mm Hg), further confirming that melt pCO_2 level, in itself, does not establish cathode carbon purity.

10.1.4.16 (Continued)

Figures 10-16 and 10-17 show the carbon deposit on cathodes 1 and 2, respectively. The "spider" assembly on the stem of cathode 2 was included to assure stand-off of the electrode from the nickel cathode containment tube.



FIGURE 10–16. CATHODE #1 FOLLOWING TEST #16

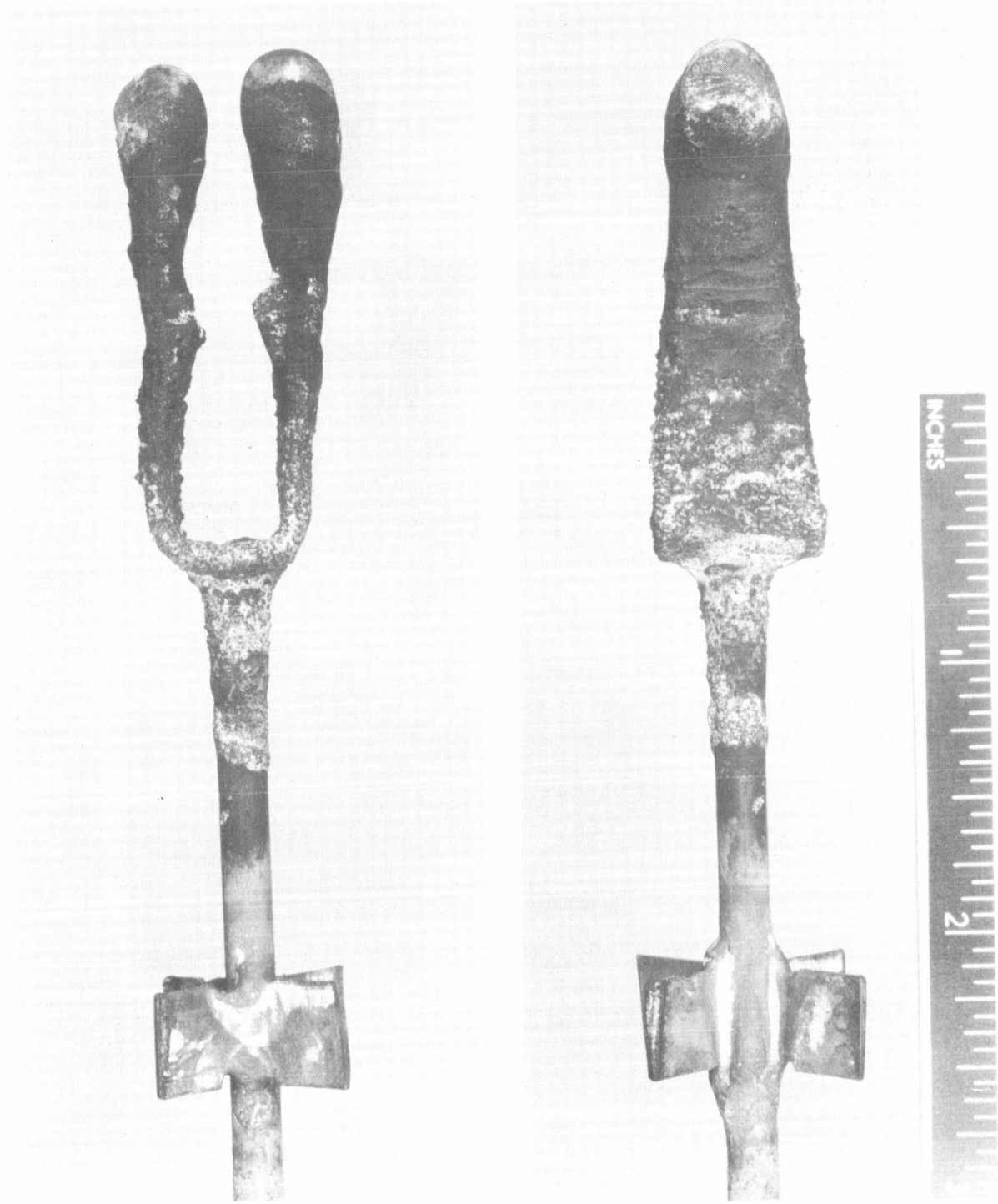


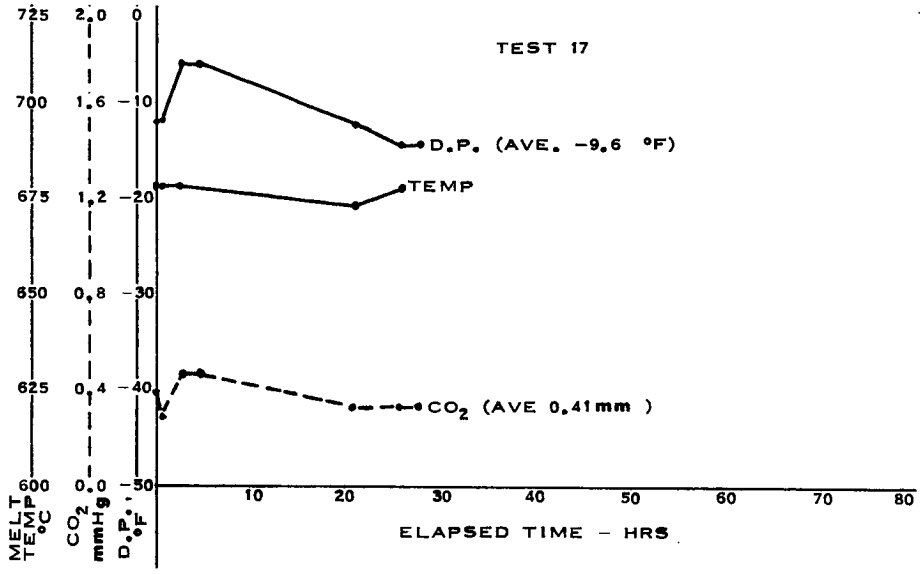
FIGURE 10–17. CATHODE #2 FOLLOWING TEST #16

10.1.4.17 Test Number 17

Description of Test

Objective: Oscillating Electrolyte Configuration - Cathode Shape Test

Date of Test: 6-29-67 to 6-30-67 (28 hours)

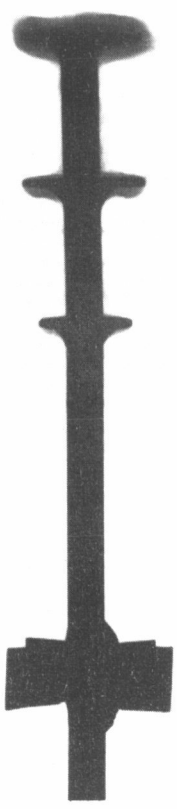


Melt Composition: 60% LiCl, 40% Li_2CO_3. New melt used in this test. Foreign contamination unknown - suspected low

Cathode Deposit: 67%-60% carbon purity

Significant Events: As indicated in the above figure, CO_2, and moisture levels in the effluent gas stream generally decreased during this single-day test. At 0900 hours (22 hours after initiation of test), it was observed that cathode number 1 was not electrically breaking during cycling, and this electrode was raised to achieve cyclic current interruption. Average CO_2 and H_2O levels in the effluent gas stream were 0.41 mm Hg. and -9.6°F, respectively. Cathode current densities averaged 112 ma/cm^2. The cathode configuration (number 11 and 12) used for this test differed from those employed in earlier tests in that they primarily utilized horizontal surfaces to evaluate techniques of controlling carbon growth.

Discussion of Results: It is believed significant that the carbon purity achieved on cathode number 1 (67%) is identical to that obtained on the preceding test (number 16), while cathode number 2 had a 60% carbon purity deposit (in contrast to 75% for the same position in test number 16). One hypothesis (figure 10-18 is) that melt was



CONFIGURATION #11



CONFIGURATION #12

FIGURE 10–18. X–RAY OF CATHODE #1 (CONFIG. #12) FOLLOWING TEST #17. PICTURE CLEARLY SHOWS CONCENTRATION OF CARBON DEPOSIT ABOVE & BENEATH HORIZONTAL AREAS OF ELECTRODE

10.1.4.17 (Continued)

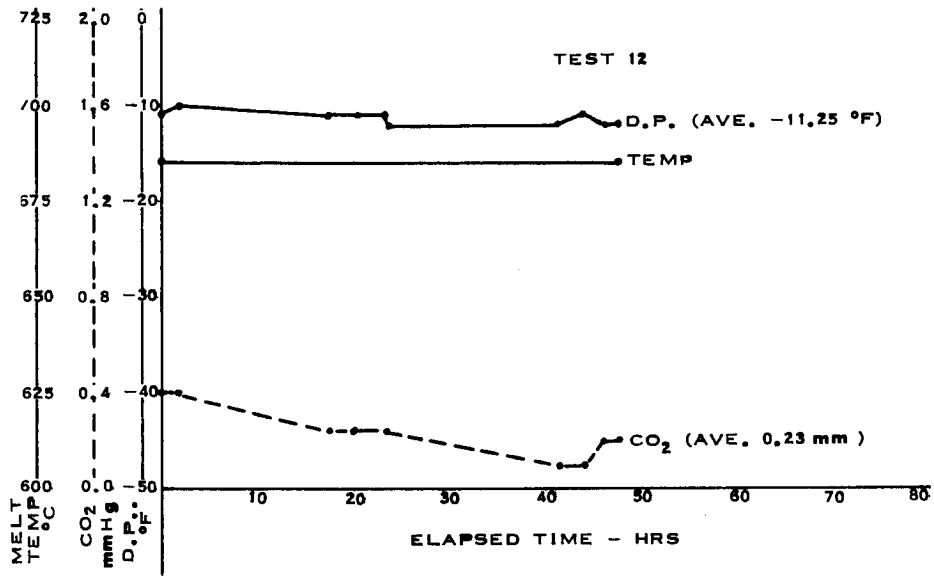
more easily entrapped on the cathode shape due both to a slightly larger diameter (0.624 inch instead of 0.574 inch) and to closer spacing of the lower two discs. It is concluded that cathode shape may be significant in determining carbon quality, but that tests to establish this should be delayed until the relationship of the basic melt process variables (i.e. pCO_2, pH_2O, contaminants) are more fully understood. This was later done and is explained in paragraph 10.1.5. Cathode geometrics employing primarily vertically orientated deposit surfaces shall generally be employed on subsequent tests.

10.1.4.18 Test Number 18

Description of Test

Objective: Oscillating Electrolyte Configuration - Carbon Quality Test

Date of Test: 7-5-67 to 7-7-67 (48 hours)



Melt Composition: 60% LiCl, 40% Li_2CO_3. Contamination level unknown

Cathode Deposit: 78-81% carbon purity

Significant Test Events: As observed on the above curve, the CO_2 and moisture concentrations within the effluent gas stream were at favorable levels and had a general downward trend during this test. It is also noted that electrolyte temperature was maintained at a slightly higher level than had been employed in other tests to date.

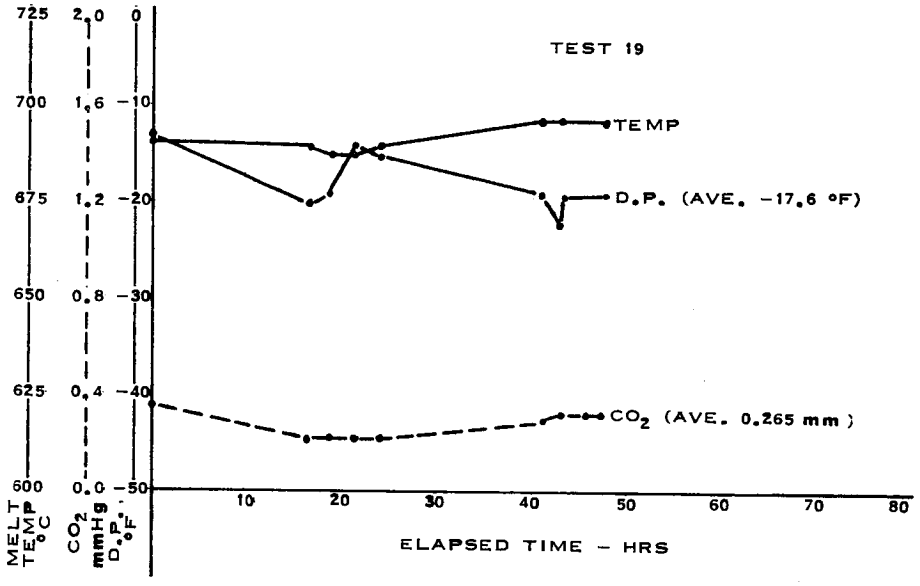
Discussion of Results: The carbon purities (78.5% and 81.5%) for cathodes number 1 and 2, respectively, together with the 100% cathode current efficiency yielded the best results achieved to date for this configuration. It may be postulated that although no obvious parameter can be identified as being singularly unique during this test, as compared to preceding tests, quite possibly as a consequence of having all of the obvious parameters controlled at a desirable level, favorable carbon quality and cathode efficiency resulted. It may be further postulated that the electrolyte temperature, being somewhat higher than normal, favored the process.

10.1.4.19 Test Number 19

Description of Test

Objective: Oscillating Electrolyte Configuration - Carbon Quality Test

Date of Test: 7-12-67 to 7-14-67 (47+ hours)



Melt Composition: 60% LiCl, 40% $LiCO_3$; foreign contaminants unknown.

Cathode Deposit: 63-76% carbon purity

Significant Events: As indicated on the above curves, CO_2 and H_2O effluent concentrations, were maintained throughout the test at values believed to be consistent with yielding good carbon (0.26 mm. Hg and -17°F. dew point, respectively). During the test, periodic gas samples of the cathode ullage gas were taken and on each occasion pCO was found to be between 60 and 70 ppm. This is presently believed to be an acceptable level. Anode O_2 flow rate was observed to be low. Following the test, it was observed that the anode had slipped out of position and had fallen below the anode shield tubing. Cathode current density for the test was set at a low level (60 ma/cm^2). The electrolyte was operated at the highest temperature of any test to date (682°C.).

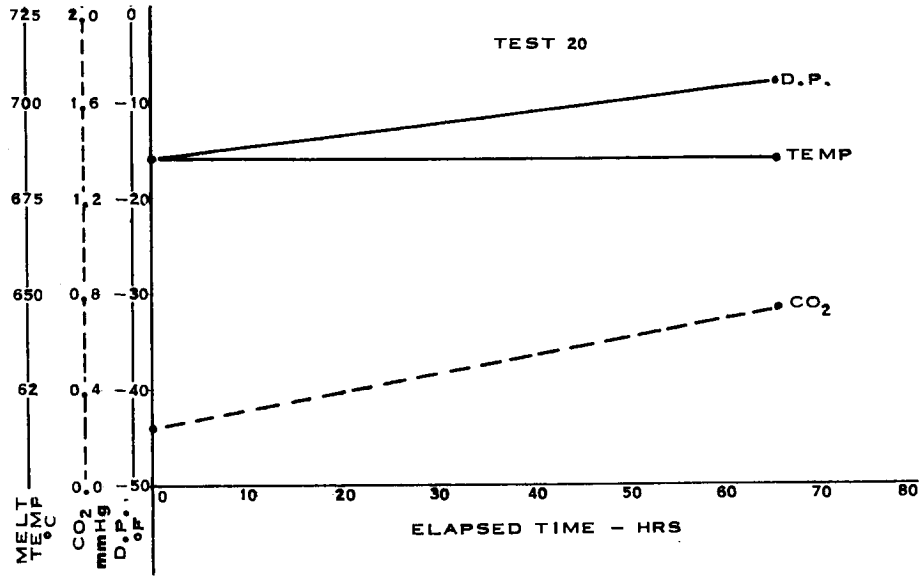
Discussion of Results: Carbon deposits having purities of 64% and 78% on cathodes 1 and 2, respectively, were achieved in this test. Low anode O_2 flow was probably associated with the slippage of the anode from normal position; it is believed that some of the liberated oxygen escaped the surrounding anode tube and consequently reduced the O_2 flow from that area. Detrimental effects upon carbon quality arising out of either the low current density or the above normal electrolyte operating temperature were not apparent.

10.1.4.20 Test Number 20

Description of Test

Objective: Oscillating Electrolyte Configuration - Cathode Carbon Quality Test

Date of Test: 7-21-67 to 7-24-67 (66+ hours)



Melt Composition: 60% LiCl, 40% Li_2CO_3; foreign contaminants prior to test unknown: foreign contaminants following test as follows (a) Melt, 0% nickel, 0.02% silicon, 0.0001% Fe; (b) Carbon deposit, 0.25% Ni, 0.06% Silicon, 0.006% Fe.

Cathode Deposit: 67% and 68% carbon purity.

Significant Events: This test was initiated on a Friday and no data was obtained after initial reading until Monday, when it was observed that cathode 2 was not electrically breaking contact each cycle. The test was stopped at this point. Although the limited data does not provide desirable assurance as to the pCO_2 and H_2O melt conditions during the entire test period, the fact that pCO_2 in the effluent gas had not increased more than it did (also the dew point) gives some credibility to the path functions being represented by the graph as drawn above. Prior to the start of this test, the alumina shield surrounding cathode 1 was replaced with a nickel shield, as had been earlier done (test number 14) on cathode 2. It had been suspected that carbon quality was favored by a nickel containment tube; one of the objectives of this test was to establish whether the historical difference in quality between the two cathodes would vanish if the two cathodes were similarly installed. A chemical analysis of the carbon deposit and the eutectic was made following this test to establish whether significant quantities

10.1.4.20 (Continued)

of nickel, silicon, or iron existed at either of the two locations. Contamination of the melt by iron or silicon had been believed by the Research Dept. to be detrimental to the formation of high quality carbon and it was questioned whether nickel contamination might similiarly affect the process.

Discussion of Results: The close agreement between the carbon purities as deposited on cathodes 1 and 2 gives additional support to the hypothesis that nickel shields surrounding the cathodes contribute to a favorable cathode process. As an additional check upon the validity of the chemical analysis, cathode 1 was analyzed by the Research Laboratory, while the deposit on cathode 2 was analyzed by the Space Systems Engineering personnel normally responsible for such analyses on these engineering tests.

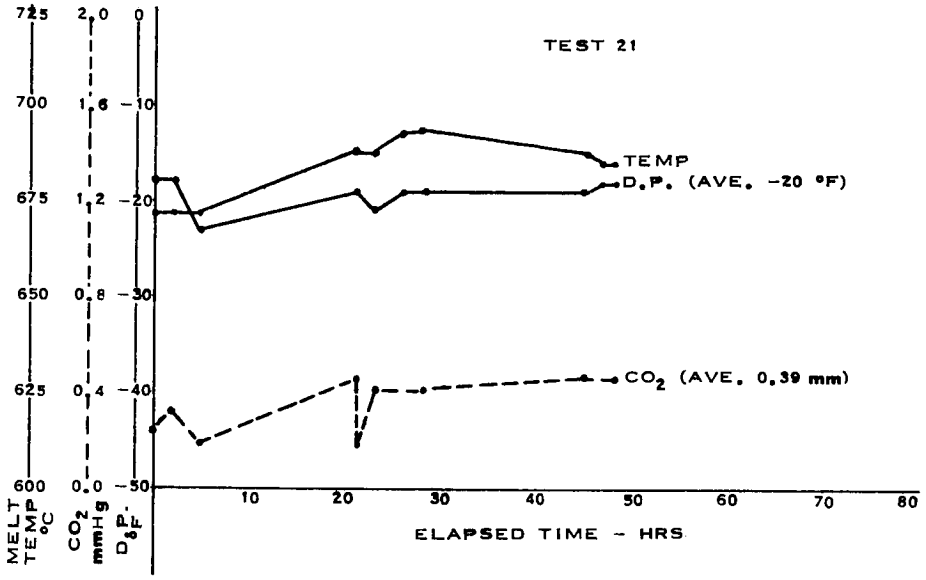
The level of the carbon purity achieved in this test appears consistent with that obtained in tests 11 and 17 which had CO_2 histories similar to test number 20. There is no evidence to support the fact that the measured nickel, silicon, and iron contaminants had a significant affect upon the carbon purity level or, for that matter, are not grossly representative of concentrations of these elements, which had not been the subject of analysis in previous deposits.

10.1.4.21 Test Number 21

Description of Test

Objective: Oscillating Electrolyte Configuration - Cathode Baffle Test

Date of Test: 8-2-67 to 8-4-67 (48+ hours)



Melt Composition: 60% LiCl, 40% Li_2CO_3; foreign contaminations: prior to test estimated to be similar to post analysis of test Number 20. Following test Number 21, unknown, but estimated to contain, 0.25% nickel.

Cathode Deposit: 35%-36% carbon purity

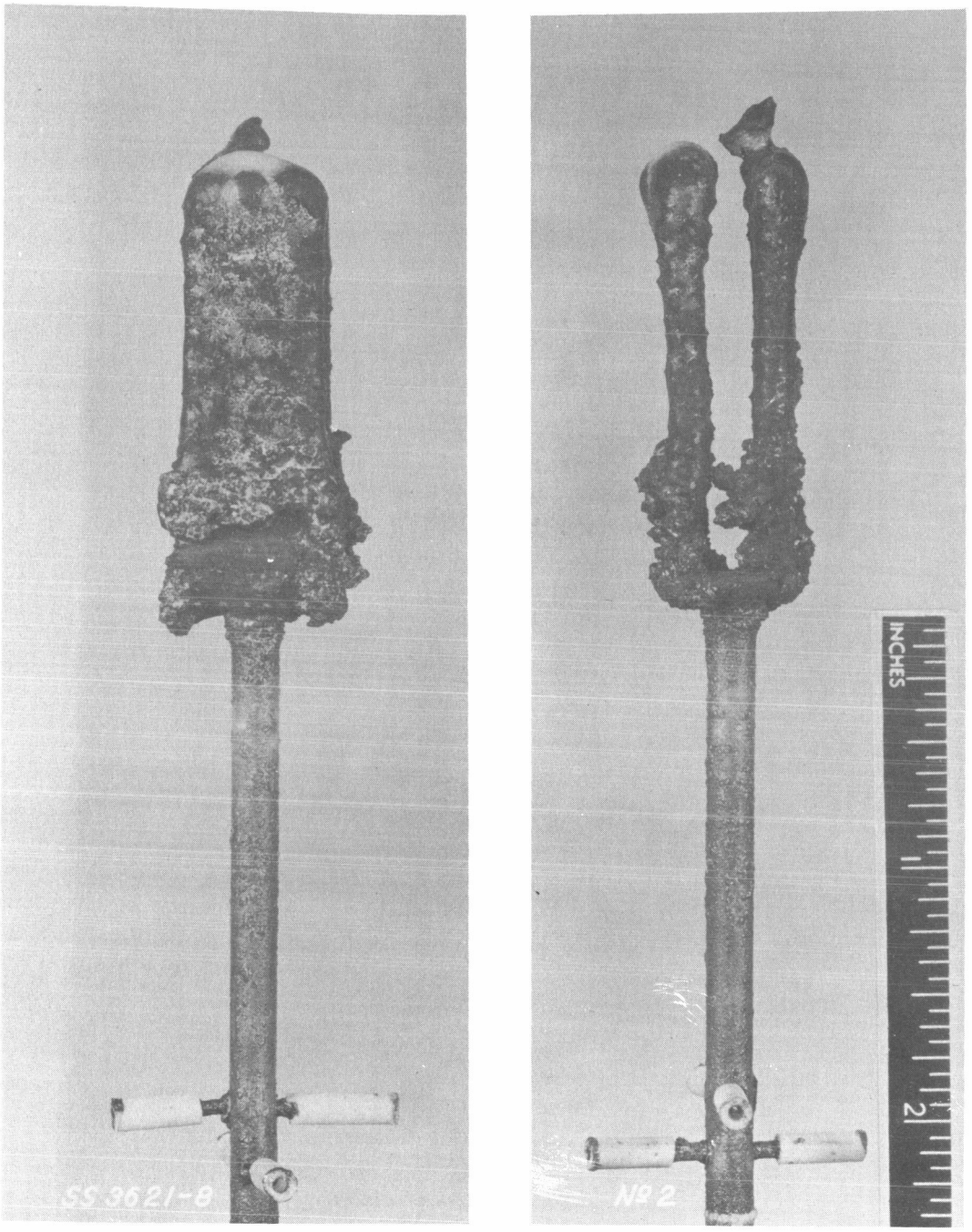
Significant Events: Prior to the start of this test, a baffle plate was installed between the two nickel cathode containment tubes at their extreme lower ends to impede the circulation of the melt contained within these tubes from cross-flowing during electrolyte cycling. It was postulated that if a considerable amount of electrolyte cross-talk between the two cathode containment tubes did occur, oxide concentrations unfavorable to the cathode process might build-up in the catholite, rather than being dispersed into the bulk melt. The baffle plate was fabricated of nickel and was attached to the alumina shield surrounding the anode. The actual attachment was accomplished by a nickel clamp with stainless steel 304 screws. All portions of the assembly, with the exception of the upper portion of the clamp and one of the screws, were contained within the electrolyte. Care was taken to ensure that no electrical contact existed which would render the baffle anodic or cathodic.

10.1.4.21 (Continued)

Discussion of Results: The 35 to 36% carbon purity deposited on cathodes 1 and 2 respectively, is not explained by examination of the observed test conditions. In general, pCO_2, pH_2O, cycle time, melt temperature, current density, and pCO at the cathode appear to be typical of the values in other tests, except in this test the pCO_2/pH_2O ratio was abnormally high. It is difficult to postulate how any of these variables individually would have given rise to the low carbon purity achieved. It is believed possible that directly or indirectly the installation of the baffle plate prior to this test may have been responsible for the poor performance and it is concluded that the electrolyte should be replaced and the installation of the baffle examined prior to the next test. See figures 10-19 and 10-20.

TOTAL OPERATING TIME APPROXIMATELY
388 HOURS (664 AMPERE–HOURS)
THIS ANODE WAS SUBSEQUENTLY ANALYZED
BY MICRO–PROBE

FIGURE 10–19. ANODE (CONFIG. #7) AS REMOVED FROM TEST ARTICLE FOLLOWING TEST #21



SHOWING 35% PURITY CARBON.
TEST #21 WAS FIRST OF TWO TESTS
EMPLOYING BAFFLE PLATE (SEE
TEST – SECTION 12.1.4.21)

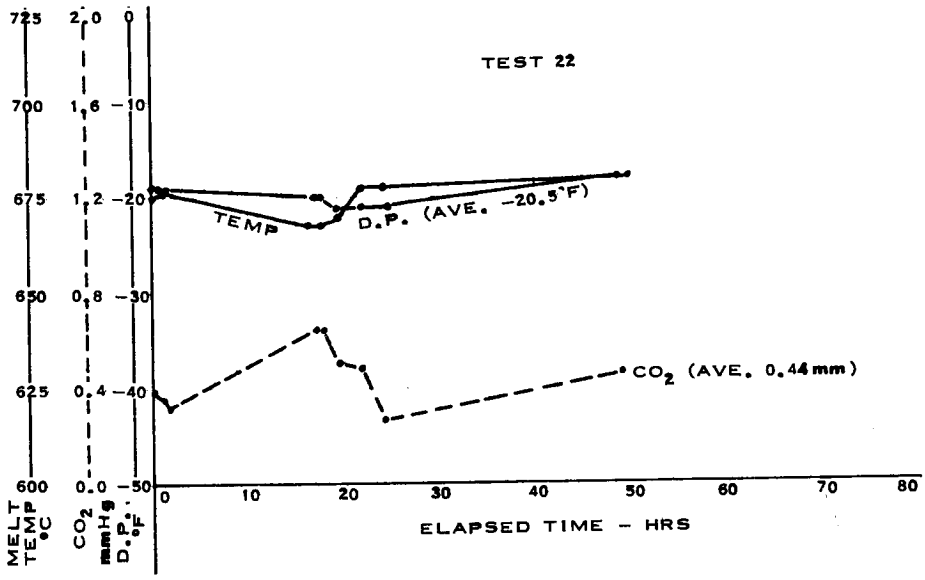
FIGURE 10–20. CATHODE #2 (CONFIGURATION #13)
FOLLOWING TEST #21

10.1.4.22 Test Number 22

Description of Test

Objective: Oscillating Electrolyte Configuration - Cathode Baffle Test

Date of Test: 8-10-67 to 8-12-67 (49+ hours)



Melt Composition: 60% LiCl, 40% Li_2CO_3

Cathode Deposit: 31%-32% carbon purity

Cathode Deposit Inpurities: 1.28% Ni, 0% Si, 0.005% Fe

Significant Events: The electrolyte was replaced and the baffle plate installation inspected prior to the test. The inspection showed that the baffle plate was not in electrical contact with any part of the anode or with either of the cathode shields. The test was initiated and, as reflected in the above data plot, had average pCO_2 and pH_2O values of 0.44 mm Hg and -20°F, respectively, during the 49 hours of operation. The enclosed ullage volume above the cathode contained concentrations of CO which varied between 400-750 ppm during the 18-24th hour of testing. During the same time, influent CO_2 flow was stopped to reduce the CO_2 level within the melt.

10.1.4.22 (Continued)

Discussion of Results

This test again yielded low carbon purities of 31.6 and 32.3% for cathodes 1 and 2, respectively. Cathode current efficiency was calculated to be 109.5%*. The above values represent the lowest carbon purity and the highest recovery efficiency recorded in the test series to date. As with test 21, the baffle plate was believed to be one of two possible causes of the low carbon purity. As a result, the cell was disassembled following this test and it was discovered that the baffle plate, although not in apparent contact with either electrode, appeared to be generally brighter than when inserted. Indications were that the plate had experienced electrolyte attack, with the result that nickel had gone into the solution within the electrolyte and had been subsequently codeposited with carbon on the cathode.

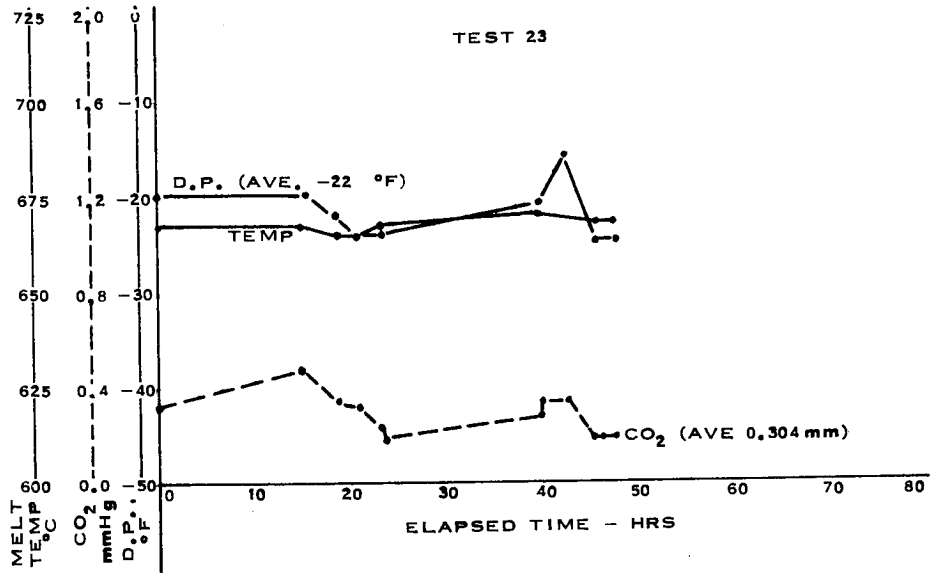
* An efficiency in excess of 100% is obviously impossible. Paragraph 10.1.5.5 discusses the probable reasons for the high values and concludes that inaccuracies in the carbon purity chemical analyses probably account for the overvalue.

10.1.4.23 Test Number 23

Description of Test

Objective: Oscillating Electrolyte Configuration - Carbon Quality Test

Date of Test: 8-16-67 to 8-18-67 (48 hours)



Melt Composition: 60% LiCl, 40% Li_2CO_3

Carbon Deposit: 68.8% carbon purity; 0.25% Ni; 0.07% Fe; trace of Si

Significant Events: The data graph shown above reflects an average pCO_2 and pH_2O in the effluent gas stream of 0.304 mm Hg and -22°F dew point, respectively. Carbon dioxide influent flow was discontinued between the 16-24th hour and between the 40-46th hour to reduce cell outlet pCO_2. At 0820 hours on 8-18-67 cathode 2 was raised 3/8 of an inch to reinstate the programed cyclic operation. Carbon monoxide pressure in the ullage of the enclosed cathode tube had a typical value of 75-100 ppm when measured at the 19th, 40th and 43rd hour of test, but had a value of 500 ppm earlier during the 16th hour of the test. Chemical analyses of the cathode deposit following the test established that the deposit contained 0.25% nickel.

NOTE: As stated in the discussion of test number 22, the cathode baffle plate had been removed from the test article prior to the start of this test; the electrolyte, however, was not changed.

10.1.4.23 (Continued)

Discussion of Results

This test yielded a carbon purity of 68.8% on both cathodes. The indicated cathode current efficiency (based upon the Faraday relationship) was 115%.* The steady and at times rapid increase in effluent CO_2 partial pressure cannot be explained by influent CO_2 concentrations, flow rate, cell voltage, or current level variation during this test. This fact is felt to be generally true of other tests in which a general rise in the CO_2 effluent concentration has been observed. One possibility, and a fundamental one, is that the increase in effluent CO_2 partial pressure could most easily be explained by an insufficient supply of oxide ions to the region of the scrubber, due in turn either to a lack of necessary cell current or to a failure to transmit oxide ions from the cathode to the scrubber region, or a combination of these factors. Following test number 13, in which a sharp increase in CO_2 effluent concentration was observed, a chemical analysis of the carbon reflected a 4.87% weight of LiOH + Li_2O within the deposit. For test number 13, it had been established that not all the oxide ions were transmitted from the cathode to the scrubber region. In the case of this test, since a chemical analysis of the carbon was not performed to establish LiOH + Li_2O presence, it can only be hypothesized the the CO_2 increase during this test might be similiarly explained.

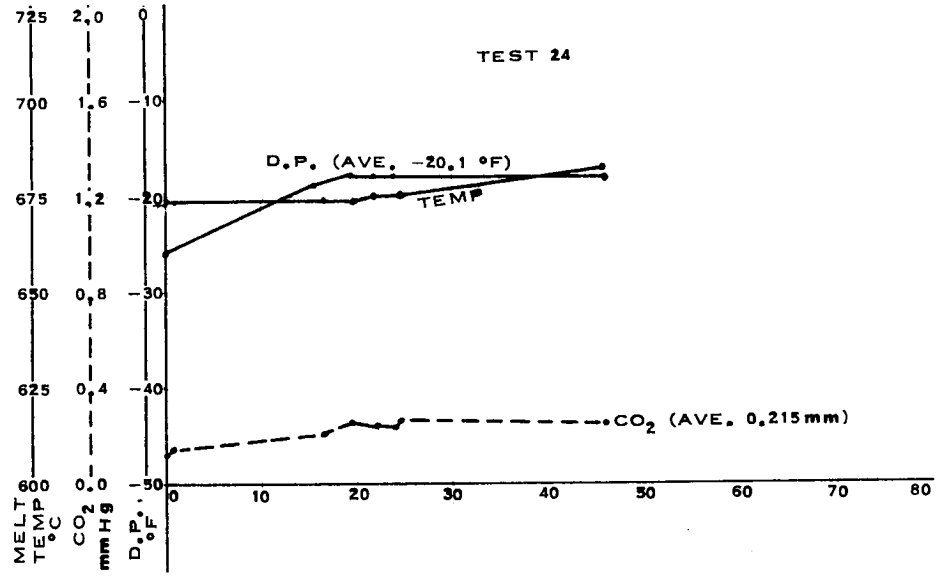
*See footnote following discussion in paragraph 10.1.4.22.

10.1.4.24 Test Number 24

Description of Test

Objective: Oscillating Electrolyte Configuration - Carbon Quality Test

Date of Test: 8-24-67 to 8-26-67 (46^{+} hours)



Melt Composition: 60% LiCl, 40% Li_2CO_3 - estimated
Foreign Contamination: melt and carbon - unknown

Cathode: 60 - 69% carbon purity

Significant Events: CO_2 and moisture partial pressures within the melt (as established from their concentrations in the effluent stream) were maintained over apparently acceptable limits during this test, averaging 0.215 mm Hg and -20°F, respectively. Carbon dioxide influent flow was interrupted between the 17th and 22nd hour of the test to maintain melt CO_2 level. Carbon monoxide partial pressure within the cathode containment tube averaged 50 ppm during the test (not monitored continuously).

Discussion of Results

Carbon quality achieved for this test was 69% and 60% for cathodes number 1 and number 2, respectively. It may be observed that the average values of dew point and CO_2 partial pressure for this test were lower (therefore presumably better) than in test number 18 which yielded 80% carbon purity. Again it appears that

10.1.4.24 (Continued)

the determining criteria of the quality of the deposit involves more than the absolute value of these two variables* individually considered.

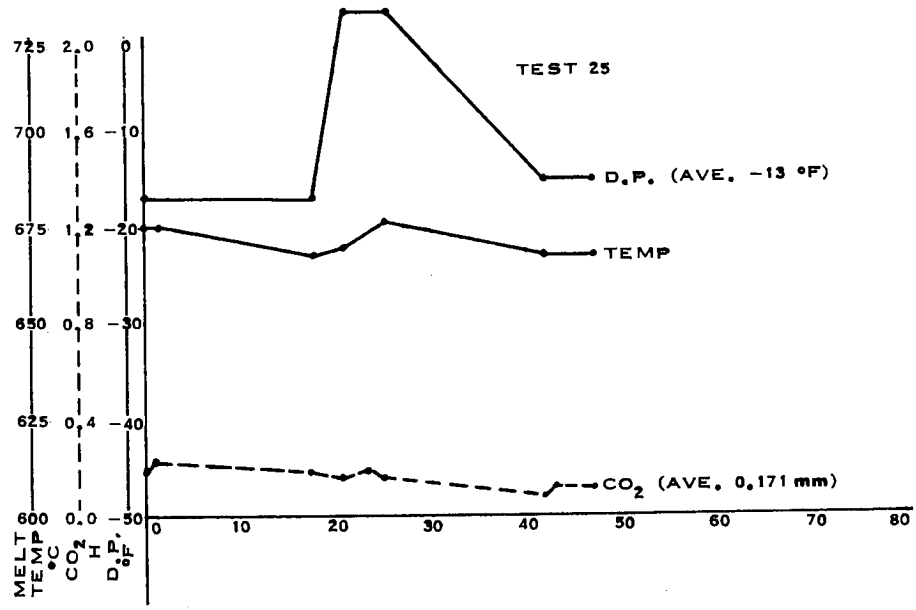
* See paragraph 10.1.5.1 for a detailed discussion of carbon purity versus process variations. Paragraph 10.1.5.1 considers carbon purity based on the total test findings.

10.1.4.25 Test Number 25

Description of Test

Objective: Oscillating Electrolyte Configuration - Carbon Quality Test

Date of Test: 9-5-67 to 9-7-67 (47 hours)



Melt Composition: 60% LiCl, 40% Li_2CO_3 - estimated

Cathode Deposit: 23-25% Carbon purity

Significant Events: The pH_2O in the effluent gas during this test, as indicated by the Alnor dewpointer, rose to +3°F between the 21st and 25th hour. No explanation could be found for the sudden increase. An unsuccessful attempt was made to verify the high dewpoint with a second Alnor dewpointer, but it did not fuction properly when inserted into the system. It was concluded that some question of validity should be assigned to all the dewpoint data recorded during this test. On separate occasions during the test it was determined that cathodes 1 and 2 were not breaking electrically with the oscillation of the electrolyte. In each instance, the situation was remedied by raising the cathode a fraction of an inch. One reading, made 24 hours after test start, showed a CO pressure of 50 ppm in the cathode.

Discussion of Results

The 23.4% and 25.5% carbon purities achieved represent the poorest quality recorded on any of the tests. While the CO_2 partial pressure of the effluent gas was unusually low, indications were that the dewpoint concentration within the same stream may have been uniquely high. As previously discussed and in the light of the questionable

10.1.4.25 (Continued)

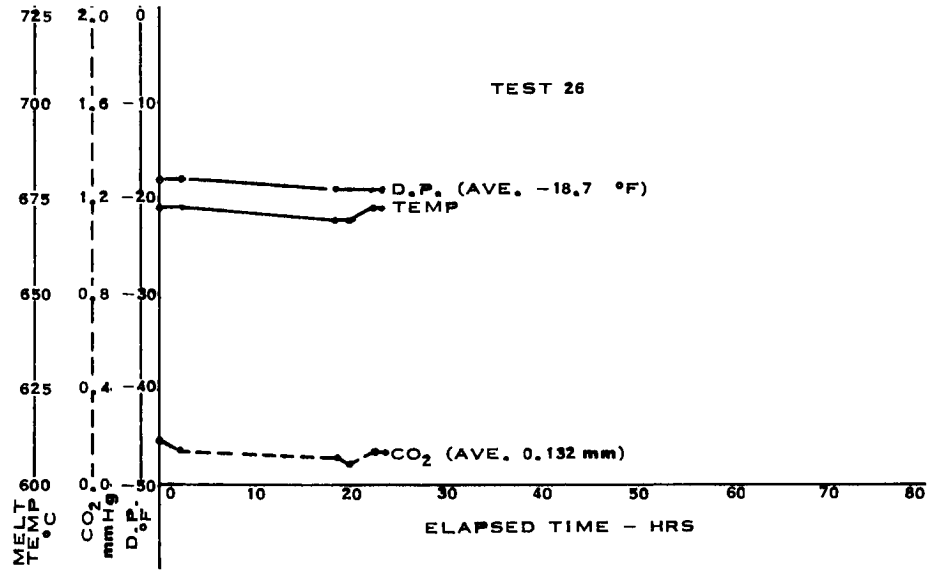
validity of the moisture data, the difficulty could be explained by assuming the +3°F data valid and that the entire test was performed under this wet condition. Unfortunately there is no way of substantiating this assumption. It is concluded that this test should be discounted due to the questionable nature of the water vapor concentration within the electrolyte.

10.1.4.26 Test Number 26

Description of Test

Objective: Oscillating Electrolyte Configuration - Carbon Quality Test

Date of Test: 9-12-67 to 9-13-67 (23+ hours)



Melt Composition: 60% LiCl, 40% Li_2CO_3 - estimated

Cathode Deposit: 85% carbon purity; 1% Ni, 1.5% Li; 0.6% Au; 0.25% Fe; 0.02% Si, 0.01 Cu; 0.001% Mg; 0.003% Mn; 0.003% B; 0.01 Md; 2.8% Cl.

Significant Events: A coulometer was connected into the cell electrical circuit prior to this test, in an attempt to cross-check the cathode current efficiency as normally obtained from the current vs time profile. During the 19th hour of test, 50 ppm of CO was measured in the cathode shield.

Discussion of Results

This test yielded a cathode deposit of 85% purity and a cathode current efficiency of 103%.* It represents the best test to date-- fully demonstrating the applicability of the fused salt electrolytic process for effectively removing and reducing CO_2 from simulated spacecraft atmospheres. Ironically, it follows the low 25% carbon purity achieved in test number 25. Paragraph 10.1.5.1 postulates the reason for the extremely favorable carbon purity results in terms of both pCO_2 and pH_2O levels within the electrolyte

* See footnote following paragraph 10.1.4.22.

10.1.4.26 (Continued)

during this test. It is interesting to note that the coulometer reflected 41.4 ampere-hours of electrolysis, whereas the ammeter vs time reading (as done on previous tests) reflected 41.2 ampere-hours. In both cases then, the indicated cathode current efficiency was 103%.* This efficiency does not consider the metallic impurities which were subsequently found in the deposit and which would reduce the apparent current efficiency to a level between 95 and 100%, depending whether lithium is combined as Li_2CO_3 or was contained as pure lithium metal.

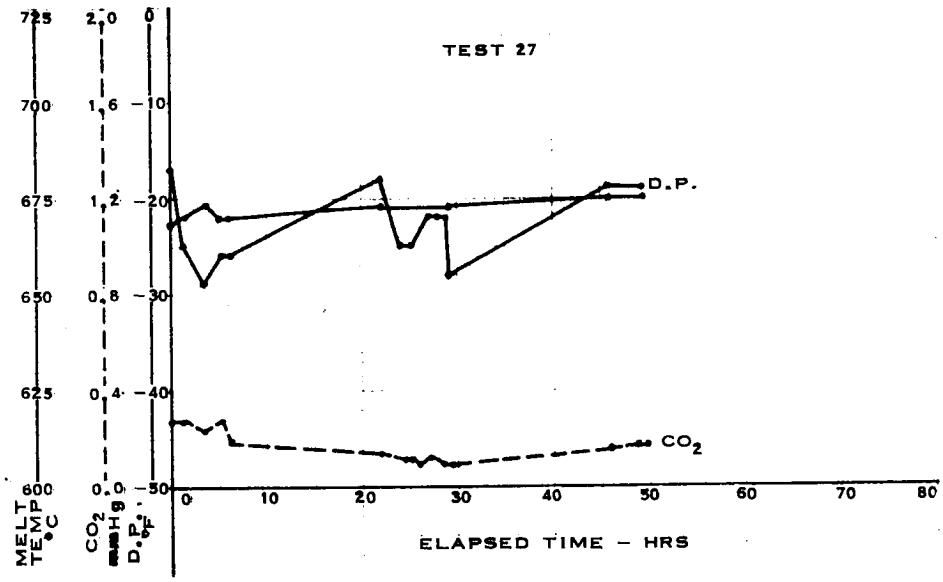
* See footnote following paragraph 10.1.4.22.

10.1.4.27 Test Number 27

Description of Test

Objective: Oscillating Electrolyte Configuration - Carbon Quality Test

Date of Test: 9-26-67 to 9-28-67 (49+ hours)



Melt Composition: 60% LiCl, 40% Li_2CO_3

Cathode Deposit: 57% - 62.5% carbon purity.

Significant Events: During this test, three cathodes were used in an attempt to get repeatable results under similar conditions. The cathode in 'well' 1 was used during the entire test while the cathode in 'well' 2 was replaced with a new cathode after 28.9 hours of operation. Although the electrolyte displacement was adjusted at the start of the test, it was observed that the cathode in 'well' 1 and the first cathode in 'well' 2 did not have cyclic current interruption following the first overnight run. Test conditions were observed closely - in an attempt to maintain low pCO_2 and pH_2O within the eutectic.

Discussion of Results

The carbon quality of the cathode used in 'well' 2 for the first 24 hours had a carbon purity of 57%. The cathode employed in 'well' 1, which ran for the entire 49+ hour period of the test, had a carbon purity of 57.4%. The second cathode in 'well' 2, which ran for the last 20 hours of the test, had a 62.5% carbon purity.

10.1.4.27 (Continued)

The CO measured at the cathode reached 500 ppm at 28.5 hours and thereafter decreased to 50 ppm by the end of the test. These high CO concentrations seem to indicate high local CO_2 concentrations and most likely may be responsible for the low current efficiency (81 - 87%) and partially for the low carbon quality. All indications, however, as shown in the graph above, imply relatively low CO_2 concentrations in the electrolyte at all times.

10.1.5 General Results and Interpretation of Engineering Test Program

10.1.5.1 Carbon Purity

Twenty-three of the twenty-seven tests performed in the engineering development program yielded cathode carbon purities varying over the range of 25-85%. The distribution of purities resulting from the test program in terms of the numbers of times they occurred is as follows:

Carbon Purity, %	# of Tests
20-30	1
30-40	3
40-50	0
50-60	7
60-70	8
70-80	4
80-85	2

In reviewing the carbon quality frequency distribution, tabulated above, it should be recognized that a considerable amount of experimentation was given to purposeful variations between test parameters such as cycle time, changes in basic melt composition, cathode geometry, melt temperature, pCO_2 and pH_2O, cathode current density, and cell configuration changes (e.g. baffle plate installation employed on two of the tests).

It is perhaps more significant to examine those tests in which major variables were controlled. For this purpose it may be observed from figure 10-1, as well as from the individual test descriptions, that tests #18-20, #23, #24, #26, #27 constitute a more meaningful and representative population of carbon purities after standardization was made of prime process variables. The average carbon purities for these seven representative tests (each employing the oscillating electrolyte, using essentially the same melt, the same general cathode current density, the same melt temperature, and the same cyclic period) amounted to 71% and had an average cathode current efficiency of 100%.

It had been theoretically deduced in the NAS 1-4154 Phase I Final Report (ref. section 4.6, pp. 17 ff) that the ratio of the partial pressures of CO_2 and water vapor, which existed locally within the electrolyte near the cathode, bore significantly upon the process. Figure 10-21 shows a plot of pCO_2/pH_2O within the general melt vs carbon purity for all tests employing the oscillating electrolyte. Three of the seventeen tests employing the oscillating electrolyte configuration have been excluded from figure 10-21. It is believed that these three tests were singularly different (two employed different cycle times; one had a questionable water vapor pressure measurement).

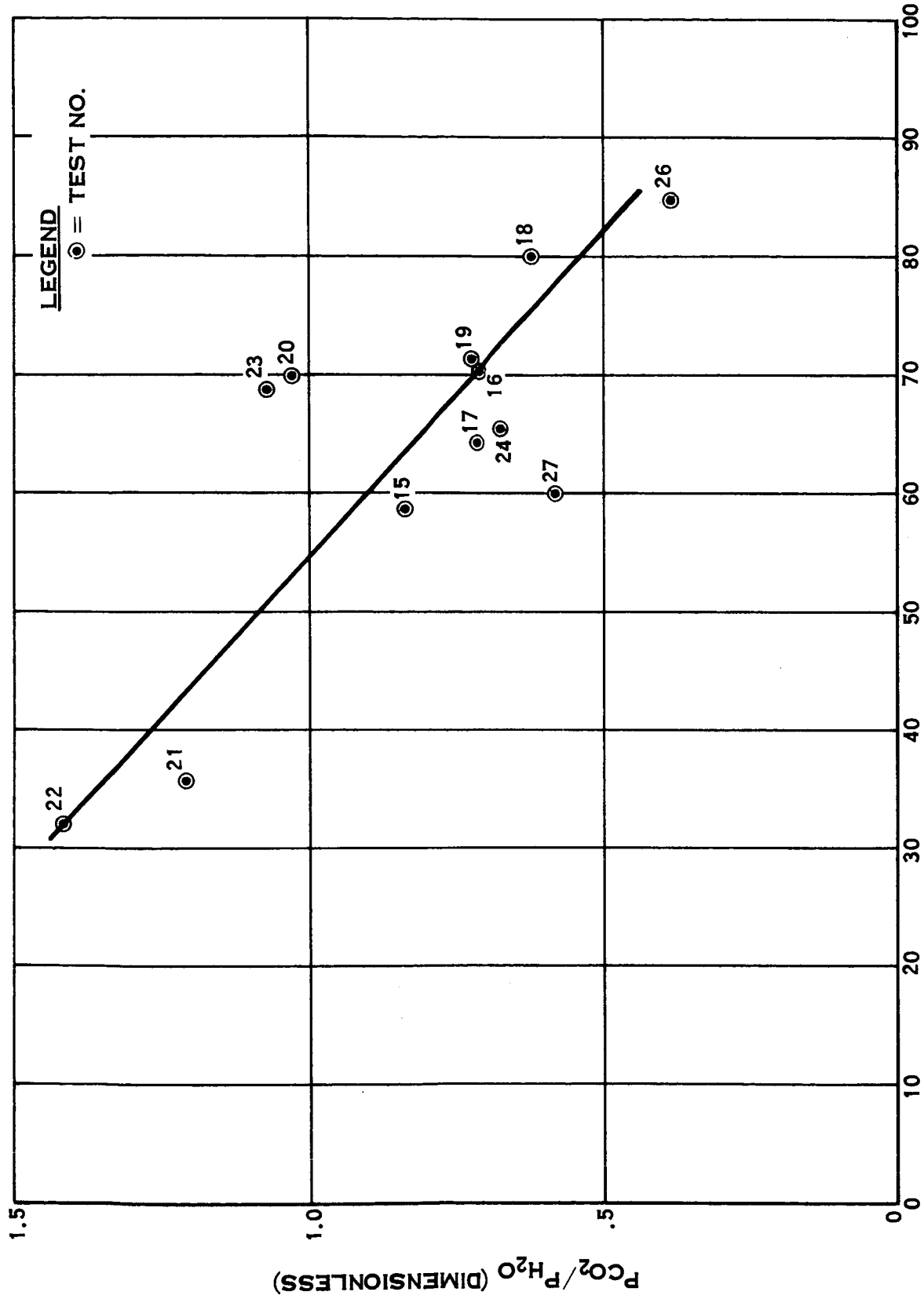


FIGURE 10–21. AVERAGE RATIO CO_2/H_2O VS CARBON PURITY

10.1.5.1 (Continued)

Figure 10-21 does suggest a relationship between pCO_2/pH_2O and cathode carbon purity. Correlation is made difficult because of the following:

a. The nature of the acid insoluble carbon purity analysis (see procedure number 1, Appendix B) which in spite of being a practical procedure, does allow some error in the purity determination.

b. The pCO_2/pH_2O ratios for each of the tests indicated on figure 10-21 were based upon the average values of these individual parameters over the test period. Due to the limited number of test points in some tests (i.e. test 20 had only two points), the average values of pCO_2 & pH_2O so calculated may not be representative. The ratio of these parameters consequently would not be precise.

c. Variation in parameters believed to be less critical, from test to test, e.g. temperature, flow rate variation in cathode ullage, etc.

It is believed that the water vapor and carbon dioxide partial pressure as plotted in figure 10-21 are representative of the bulk electrolyte, but do not directly represent the values of these gases in the region of the cathode itself while electrolyzing.

A basic limitation to figure 10-21 rests with the fact that it does not imply any dependency of carbon quality upon the absolute values of the water vapor or carbon dioxide pressure levels, but only upon the ratio of these two values.

Past testing experience has demonstrated that excessive pCO_2 and pH_2O levels within the melt act to increase the concentrations of CO, H_2, CO_2, et al, ref. equations (1) and (2) in the vicinity of the cathode to the extent that above some critical level, CO gas bubble formation occurs at that electrode. When this occurs, such evolution causes formation of carbon with gas pockets resulting in poor carbon purity because of inclusion of the electrolyte or its components within these pockets.

(1) $CO_2 + C \xrightarrow{K_1} 2CO$, and

(2) $H_2O + C \xrightarrow{K_2} CO$ ($+H_2$ in indeterminate quantities $+CO_2 + CH_4$ etc.)

The foregoing treatment, then, discusses why there would exist some theoretical maximum pCO_2 and pH_2O level within the melt near the cathode to achieve a favorable deposit, and why figure 10-21, since it cites only the ratio of these variables, cannot be theoretically valid over an unlimited and high partial pressure level.

1.5.1 (Continued)

Regarding low pCO_2 and pH_2O levels, it will be recalled that earlier efforts to achieve a favorable cathode deposit (in the years 1963-1964) met with little success in obtaining purities much in excess of 1 to 10%. The difficulty was related to the buildup in oxide ion concentration in the cathode surrounding the electrode, leading to its precipitation and occlusion with the carbon. Associated with measures taken to agitate or otherwise disperse the high oxide concentration, a very noticeable improvement in carbon purity resulted. The oscillating electrolyte technique was conceived as one method of minimizing difficulties associated with oxide ions concentrating at the cathode. The technique assumes that oxide ions generated at, and encompassing the cathode, will combine with pCO_2 in the cathode ullage gas to form $CO_3^{=}$ and resupply the catholyte. Excess $CO_3^{=}$, in turn, would be dissipated into the bulk melt when the electrolyte subsequently wetted the cathode.

It is therefore evident that some lower partial pressure limit of CO_2 in the cathode ullage gas is needed to bring about the desired $O^{=}/CO_3^{=}$ transformation. Figure 10-21, with its sole reference to the ratio of pCO_2/pH_2O, does not reflect this. In summary, it is cited that however important the ratio of pCO_2/pH_2O, both an upper and lower limit must be attached to the absolute concentration of CO_2 and H_2O comprising this ratio to achieve optimum carbon purity.

Figure 10-22 graphically displays the results of the oscillating electrolyte test series by examination of the magnitude of melt pCO_2 and pH_2O levels in terms of how these levels affect carbon purity. Figure 10-22 shows pCO_2 versus pH_2O and identifies test number and carbon purity for each data point. As in figure 10-21, the data appear to have some associated scatter, but in general is believed to suggest that carbon quality improves with increase in ratio of partial pressure levels of H_2O to CO_2 over the range of concentrations studied. It would be interesting to conduct experiments within that area defined in figure 10-22 within the "dashed - envelope" to establish the validity of the suggestions offered by that figure.

10.1.5.2 Cathode Deposit Inclusions

At various times throughout the engineering test procedure, cathode deposits were subjected to chemical analysis to establish the presence of metallic and non-metallic contaminants. Such contaminants are basically undesirable because:

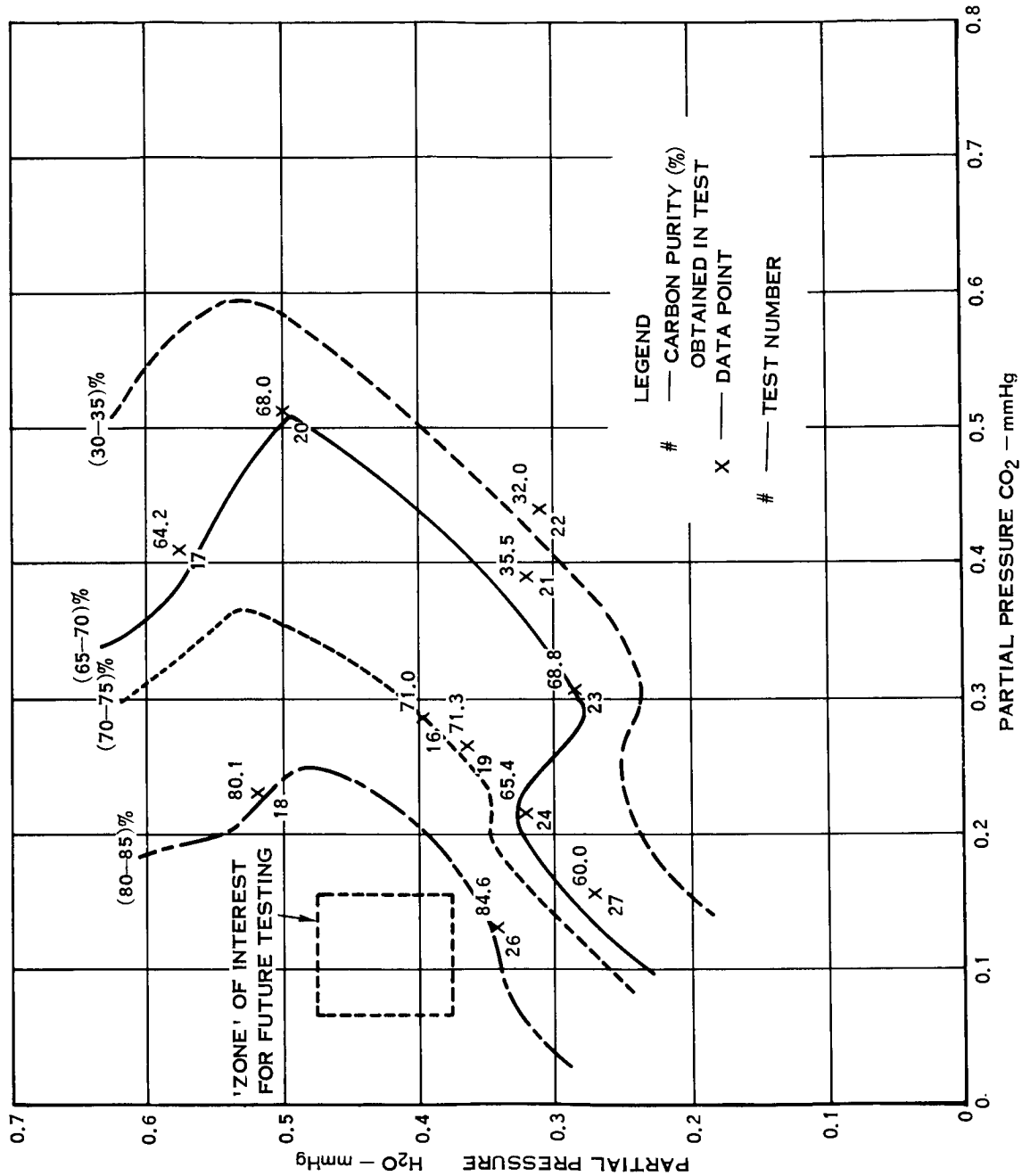


FIGURE 10–22. CO_2 & H_2O PARTIAL PRESSURES IN ELECTROLYTE VS CARBON PURITY

10.1.5.2 (Continued)

a. They constitute a weight penalty to the process if they comprise a significant weight percentage of the cathode deposit, and

b. They could adversely influence the electrolytic process itself, (i.e., cathode current efficiency, etc.).

The following tabulation presents the findings of the cathode deposit chemical analyses as done four times during the test program. More frequent analyses were not made because of the cost factor.

TABLE 10-1
RESULTS OF CATHODE DEPOSIT CHEMICAL ANALYSIS IN TESTS 20 TO 26

	Weight Percent of Contamination in Cathode Deposit			
Contaminant	Following Test #20	Following Test #22	Following Test #23	Following Test #26
Silicon	0.6	0	trace	0.02
Iron	0.006	< 0.005	0.07	0.25
Nickel	0.25	1.28	0.25	1.00
Aluminum	----	----	----	0.002
Boron	----	----	----	0.003
Copper	----	----	----	0.010
Magnesium	----	----	----	< 0.001
Manganese	----	----	----	0.003
Molybdenum	----	----	----	0.010
Lithium	----	----	----	1.50
Gold	----	----	----	0.60
*Chloride	----	----	----	2.80
*Carbonate	----	----	----	0.28
*Oxide (Hydroxide)	----	----	----	-0-

NOTE: "--" Indicates that no attempt was made to establish concentration.

*Occluded Electrolyte

An attempt has been made to establish the source of the contaminants. The following list provides some explanation of these sources:

10.1.5.2 (Continued)

1. Ceramic Materials Employed in the Test Article

NOTE: McDanel Type AP-35 Alumina

Composition	Weight Percent (Spec. Value)
Al_2O_3	99%
SiO_2	0.7%
MgO	0.07%
Na_2O	0.05%
Fe_2O_3	0.07%
CaO	0.03%

2. Nickel Employed within Test Article

NOTE: INCO, Nickel-200

Composition	Weight Percent Max. Spec. Value	Typical Anal.
C	0.15	0.03
Mn	0.35	0.28
Fe	0.40	0.04
S	.010	0.005
Si	0.35	0.08
Cu	0.25	0.01
Ni	99.0 (min)	99.53

3. Gold-Nickel Anode

NOTE: Premabraze 130 (Handy-Harmon)

Au	82 ± 0.5%
Ni	Balance
Cu, Ag	0.15% Max.

.0.1.5.2 (Continued)

4. Lithium Carbonate (Li_2CO_3)

NOTE: A.C.S. Reagent Grade (low sulphate content)
Lithium Corporation of America -
Bessemer City, N. Carolina

Composition	Weight Percent
Li_2CO_3	99.43%
H_2O	0.05%
Cl	0.007%
SO_4	0.004%
Na	0.0013%
Fe_2O_3	0.0002%

5. Lithium Chloride (LiCl)

NOTE: A.C.S. Reagent Grade (low sulphate content)
Lithium Corporation of America

Composition	Weight Percent
LiCl	99.60
Li_2CO_3	0.003
H_2O	0.20
NaCl	0.005
$CuCl_2$	0.014
$BaCl_2$	0.002
SO_4	0.002
Fe_2O_3	0.001
Insolubles	0.002

Figure 10-23 reflects the weight penalty associated with various carbon deposit purities. The figure assumes removal of 9 lb of CO_2 per day (4 men) over a mission length of 1 year.

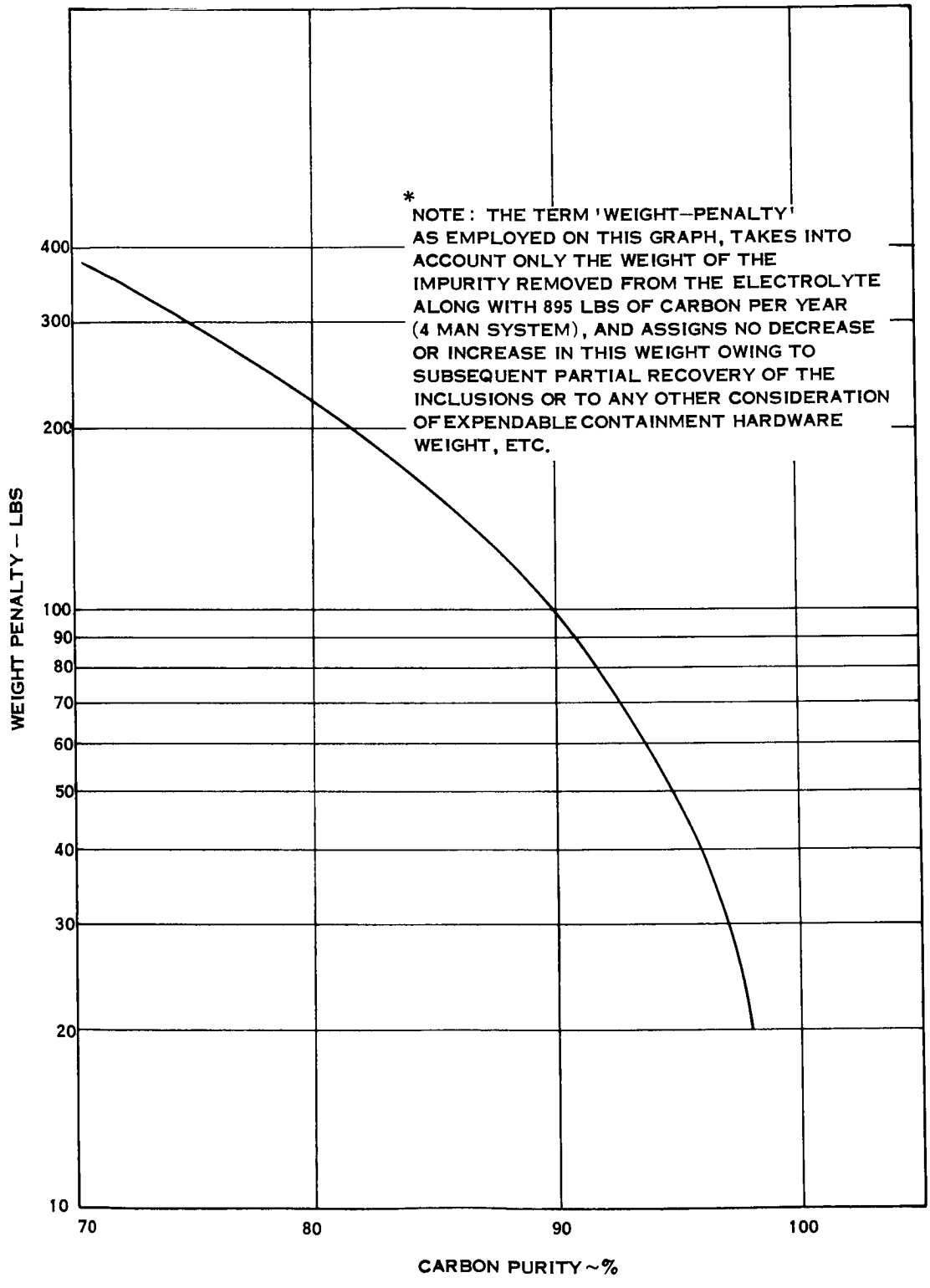


FIGURE 10–23. WEIGHT PENALTY* AS FUNCTION OF CARBON PURITY

10.1.5.3 Cathode Geometry

As tabulated in figure 10-1, fourteen different cathode electrode shapes were evaluated during the engineering test program. Dimensions for the various cathodes are given in Appendix C.

Various shapes for the cathode were investigated throughout the test program to establish:

a. The effect (if any) of cathode shape upon carbon purity, and

b. The effect of cathode shape upon the geometry of the cathode carbon deposit.

No evidence is seen to support a significant relationship between cathode shape and carbon purity ("a" above). The presence of certain similarities between the tests and cathode configurations, however, does not permit a general conclusion to be reached with respect to the complete non-interrelationship of these two parameters, (e.g., the active cathode length was generally 1.5" - 2" instead of experimenting with lengths over an extended range such as 1 inch - 5 inches).

Of primary concern is the shape of the cathode deposit itself ("b" above). From the standpoint of a workable design, it was recognized early in this phase that a need would exist:

1. To reliably predict the shape of the cathode deposit growth for a given Faraday exposure, and

2. The necessity to achieve deposit shape consistent with the specific requirements of a given design.

During Phase I, it had been generally experienced that the shape of the cathode deposit typically increased in thickness along its length (thickest at bottom) until reaching a point at which the cathode maintained continuous contact with the electrolyte. Below this point, the deposit was typically bulbous. Figure 5-16, contained in an earlier section of this report, typifies this type of deposit. In general, depending upon the details of the test, the bulbous growth amounted, weightwise, to 50-60% of the entire deposit. However, it generally contained a higher inclusion of salt so that its assay would be 20-50% pure carbon in contrast to 60-80% for the non-bulbous growth. The bulbous growth was felt to be somewhat analogous to the very earliest program experiences in which the use of completely non-moving cathodes beneath the surface would result in considerable melt inclusions, porous deposits, and low carbon purity (1-10%). It may be observed from test number 2 of the engineering test series, that the bulbous portion of the cathode deposit had a somewhat higher purity than did the deposit adherent to the side of the electrode; it should be noted that this test was one of the first to be performed by the Engineering Department and for this or other reasons, the results of this test are dissimilar to previous or subsequent findings.

10.1.5.3 (Continued)

Experimentation by the Engineering Department during Phase IIA was first directed at attempting to minimize the bulbous growth on the lower end of the cathode in the configuration tests beginning with test number 10. Unlike any of the preceding tests, the oscillating electrolyte test series completely separated the lower end of the cathode from the electrolyte (through depressing the electrolyte within the cathode containment tube) so that no portion of the cathode remained in continuous contact with the melt. NOTE: Since current flow between the electrodes was interrupted as a result of electrical contact loss, a second cathode, working out-of-phase with the first, was added such that cell current flow would be continuous.

As a result of the complete physical separation between the cathode and electrolyte during each cycle of electrolyte oscillation, the extent of the bulbous growth on the cathode was largely reduced, but was still present to an undesirable degree.

In an attempt to establish whether the tapered deposit was acceptable (assuming that a rectangular or cylindrical deposit shape having a significant thickness would be consistent with the design configuration to be selected), tapered electrodes were employed beginning with test number 14. The appendix of this report documents the shapes of the cathodes, and figures 10-11 and 10-12 (cathode number 2) show that electrode tapering could be employed successfully to obtain near cylindrical or rectangular deposits for the cathodes tested. As previously discussed in test number 14, the X-ray photographs of the deposit evidence that although the carbon growth was still tapered, the overall envelope of the deposit was favorable.

Attention has been devoted to an understanding of the mechanism by which the inherent shape of the cathode deposit thickens along the length of the electrode. Possible explanations which have been considered are as follows:

a. When the melt is depressed, the thickness of the electrolyte adherent to the cathode would be expected to increase along its length toward the bottom as a result of gravity drainage or run-off of the electrolyte.

b. The closely surrounding cathode shield would reduce the annular cross-section of the electrolyte adjacent to the cathode and inhibit overall ionic transport to the upper portion.

c. The fact that the lower end of the cathode experiences a larger current/electron flow than the upper end of that electrode as a consequence of some finite melt oscillation velocity (i.e., given a 4 sec up- 4 sec down - 0.2 sec transition time up and down, the lower end of the cathode will be in contact with the melt for a period of approximately 0.4 seconds longer, i.e., 10%).

10.1.5.3 (Continued)

Certain conclusions and specific postulations can be made concerning the possible significance, validity, and effect of the three possibilities discussed in (a)-(c) above. In general, it is concluded that (a) the increasing thickness of the electrolyte film along the cathode length is the primary reason for the tapered deposit, (b) that restriction of ion flow within the shielded cathode region does not significantly (or at all) contribute to the tapered deposit, as evidenced by certain tests done in this phase which will be cited in this section, and (c) the longer exposure time of the lower end of the electrode does partially explain the taper problem but at least for the cycle time and melt oscillation velocities normally employed is of secondary importance relative to (a).

A brief description of each of these considerations is given in the following paragraphs. The effect of the deposit tapering, unless it can be controlled, may be expected to seriously compromise the required cathode replacement frequency for the one-sixth g design configuration defined in this phase of the program. This is true because the cathode is separated from its containment wall by only 3/8 inch. It is believed necessary, then, to understand the phenomenon causing the problem and, once understood, to postulate means for correcting or minimizing the deposit taper.

0.1.5.3.1 Effect of Thickening 'Film' Along Cathode-Length on 'Tapered' Deposit

As separately discussed, it is a necessary step in the deposition of high quality carbon to convert oxide ions into carbonate ions within the catholyte surrounding that electrode at an appropriate rate. With the oscillating electrolyte configuration, this conversion is brought about when the electrolyte within the cathode cavity is depressed so that the oxide ions can be acted upon by the CO_2 in the cathode ullage gas. For a given concentration of CO_2 within all zones of the ullage gas and for a uniform (constant) thickness of catholyte, some finite time will be required for this conversion to be completely realized. With increases in catholyte (oxide-enriched) film layers, some longer period of time will be required. The nature of the catholyte thickness varying along the length of the cathode (thickening at the bottom) would therefore give rise to the supposition that more complete conversion to $CO_3^{=}$ ions would take place in the upper region of the electrode and less complete conversion would exist at the lower end of the electrode.

The result would be a varying carbon purity from the upper regions of the electrode to the lower end of the electrode.

The following should be investigated to reduce the thickening adherent electrolyte layer along the length of the cathode:

10.1.5.3.1 (Continued)

1. Decreasing the viscosity of the bulk electrolyte by increasing the temperature.

2. Decreasing the viscosity of the cathode adherent melt by local heating of the cathode itself.

3. Varying the rate at which the melt washes the cathode in its downward excursion.

   NOTE: It has been observed in paint dip coating processes that a more even coating results when the withdrawing velocity of the article being coated is reduced; this action is contrary to consideration (c) presented earlier but it is felt that steps could be taken to optimize the melt oscillation velocity.

4. Making certain minor shape or aspect ratio (cathode height/length) changes of the cathode itself.

5. Employing a small anodic charge to the cathode for a brief period following re-immersion of the cathode which might serve to create a non-wetting phenomenon (observed in past tests) and which in turn might tend to make the subsequent film layer uniform along the cathode height.

10.1.5.3.2 Contribution of Electrolyte/Cathode Voltage-Drop Considerations to Tapered Cathode Deposit

The current flow in the electrolyte is ion flow rather than electron flow. There are a surplus of Li^+ ions surrounding the cathode (Li^+ are the most numerous ions) and there is an equal probability of Li^+ capturing an electron from any point on the cathode surface. It would follow that the cathode deposit should be uniform rather than tapered.

It was initially believed that the differences between electrical resistance of the melt, the metal electrodes and the carbon deposit on the electrode, may contribute to the overall shape of the cathode deposit. The current flow between anode and cathode was looked at as current running through different conductors in parallel, one conductor being the electrolyte, one the cathode, and a third the deposit on the cathode.

It was thought that the current would flow preferentially through the path of least electrical resistance. Resistivities for the materials of concern, and at 625°C, are:

10.1.5.3.2 (Continued)

a) Cathode (Inconel X assumed): 0.000135 ohm-cm

b) Carbon: 0.00136 ohm-cm

c) Electrolyte mixture: 0.22 ohm-cm (assuming a eutectic mixture)

The formula for the resistance of a given material is (1) $R=\sigma L/A$ where σ is the resistivity, L is the length of the material in the direction of current flow, and A is the cross-sectional area presented to the current. Based on these resistivities, and from a purely electrical viewpoint, the path of least electrical resistance for an electron (with no deposit on the cathode) from the upper tip of the cathode to the lower tip of the anode would be: through the cathode length to its lower tip, then through the electrolyte. With increasing carbon deposition, the cross-sectional area is larger than that of the cathode, and the resistance of the carbon deposit becomes equal to and eventually less than that of the cathode. The current flow would be split between the cathode and the carbon deposit with only a very small fraction entering the melt above the tip of the cathode deposit. With a greater proportion of current entering the melt at or near the lower tip of the cathode, it is reasonable to conclude that most of the carbon deposition would occur in this area, thereby substantiating test findings regarding tapered cathode deposits.

The reasoning expressed in (a) and (b) above have been overridden by the ion flow concept as mentioned in the beginning of the paragraph.

10.1.5.3.3 Effect of Melt-Oscillation Velocity on Tapered Deposit

It can be shown that the total time available for electrolyte drainage from the "uppermost" portion of the cathode is equal to:

(1) $2\left(\frac{L+\Delta_2}{\bar{V}}\right) + t_1$, where

$\bar{V}$ = electrolyte oscillating velocity (assumed to move at equal up-and-down rates and to be constant)

Δ = excursion of electrolyte (Δ_1 above cathode top; Δ_2 below cathode bottom)

L = vertical height of cathode

t_1 = dwell time at top and bottom (assumed equal)

10.1.5.3.3 (Continued)

By similar calculation, the total time available for electrolyte drainage from the lowest region of the cathode is:

$$(2)\quad 2\frac{\Delta_2}{\overline{V}} + t_1$$

The difference between equations 1 and 2 then equals:

$$(3)\quad \Delta T = \frac{2L}{\overline{V}}$$

where ΔT = difference in time of exposure of top and bottom of cathode to ullage gas

Coupled with the discussion in (a) (thickening of electrolyte film along cathode length), it can be seen that a compound effect is present to explain the thickening deposit, with melt oscillation velocity yielding minimum ullage gas exposure time at that cathode location having the thickest film.

The most direct and positive method for minimizing the ullage exposure time variation will probably result from reduction in cathode vertical height, or increases in the melt oscillation velocity, or a combination of these two. It appears quite likely that reducing the cathode height will be of most benefit, because such reduction will further minimize film thickness. In contrast, increasing melt oscillation velocity although reducing ullage gas (and melt) exposure time differences, would be expected to adversely affect constant cathode adherent film thicknesses.

10.1.5.4 Anode Life

Introduction: In tests to date, dissolution of the anode electrode has constituted a problem discussed frequently in part II of this report. This paragraph attempts to summarize observations concerning the anode during the engineering portion of the NAS1-4154 phase IIA program; describes the results of both a Light Photomicrograph and an Electron Beam Scan Analysis (EBS) of a used anode; and postulates means for extending anode life such that it does not compromise cell longevity.

Background: Figure 10-1 shows that eight anodes of various configurations were employed in the twenty-seven engineering tests. Descriptions of each of the anodes is given in the appendix of this report. The descriptions show that pure gold anodes were employed early in the phase IIA program, but that as a result of gold sponge formation impeding development tests, other configurations including the rotating gold anode (ref. test 7) and later gold-nickel alloy sheet anodes were used.

Part I of this report treats the dissolution of anode materials as a function of current density, electrolyte composition, and other variables, and shows that anode life is dependent upon these variables. As reported in engineering test 7 (rotating anode), the dissolution efficiency achieved (0.715%), lends additional testimony to the fact that favorable oxide transport to the parent anode surface would act to extend anode life.

In a separate qualitative test (not documented in this report) a gold-nickel anode was operated over a current density of 5-25 ma/cm^2 immersed within a room temperature lithium chloride/water electrolyte. It was observed that oxygen bubbles, generated at anode, acted to nearly completely encompass the anode surface, giving rise to the proposition that only a small portion of the anode surface might be typically available for electron exchange, the major portion being 'masked' with small O_2 bubbles. It was further observed that with slight anode movement during this test, the O_2 bubbles previously adherent to the anode surface experienced continuous release from that electrode, and that such motion (typified by the electrolyte concept) might act to increase anode life by effectively implementing a more favorable $O^{=}$ exchange at that electrode surface.

It should also be noted that visual examination of anodes throughout the test program have evidenced no oxide formation in those cases employing 100% gold anodes, but a black oxide-appearing surface covered all nickel-gold anodes. Subsequent portions of this section provide further information as to the composition of this deposit.

Photomicrograph & Electron Beam Scan Analysis of Au-Ni Anode

The Premabraze #130 anode removed from the engineering test article following test 21 was forwarded to the United Aircraft Research Laboratory (UARL) for detailed examination by the engineering materials group.

10.1.5.4 (Continued)

The anode, as it was removed from the test artical prior to its examination by UARL, is shown in figure 10-19. As observed, it had been severely corroded as a result of the tests to which it had been subjected.

The anode was submitted to electron microprobe analysis at UARL for nickel, gold, aluminum, oxygen, and chlorine, in an attempt to better understand the chemical and electrochemical deterioration.

INSTRUMENTAL TECHNIQUES:*

An analysis of these samples used the following techniques:

Spectral scanning
X-ray image scanning
Specimen current image scanning
X-ray distribution scanning

In general, an electron probe microanalyzer contains an electron optical column which generates a very small diameter beam (~one micron) of high energy electrons (~ 30 KV). The electron beam is focused on the surface of the specimen, which is viewed by an optical microscope. Exact registration of the electron beam on the point of interest is assured by aligning the microscope reticle and electron beam on the spot to be analyzed. As a result of the electron bombardment, the specimen gives off characteristic X-rays corresponding to the elements present. The X-rays are analyzed by diffracting them with a crystal and measuring them with an appropriate detector. The output of the detector is channeled through electronic signal processing equipment and then to a strip chart recorder. In this manner spectral scans are generated.

X-ray image distribution photomicrographs are qualitative or semi-qualitative measurements which may be made over small areas of the specimen by scanning the area with the electron beam. Since the output of the spectrometer, tuned for a specific spectral line, is an indication of the relative concentration of the corresponding element, displays of the location and concentration of that element may be obtained. This is accomplished by displaying the raster scan of the specimen on an oscilloscope so that the X and Y coordinates of the specimen correspond to the same axes of the oscilloscope. Then by having the X-ray intensity modulate the oscilloscope, a picture of the elemental distribution may be shown. Permanent photographic records may then be made from the oscilloscope.

* Note: This and other paragraphs in this section identified by an asterisk are reprints from the UARL report submitted to Hamilton Standard following completion of their investigation.

10.1.5.4 (Continued)

Similarly, specimen current images may be obtained and photographed from the oscilloscope. Since only a portion of the incident electrons, which make up the analyzing electron beam, penetrate into the sample to induce X-ray emission, the remaining portions are backscattered and are normally referred to as backscattered electrons. This backscattered fraction or backscattered current has a positive correlation with the atomic number of the element being analyzed, i.e., the greater the atomic number of the material, the greater the backscatter fraction. That portion of electrons that does penetrate into the specimen gives rise to a current flow in the sample, this current being referred to as the sample current. This current varies as the inverse of the backscatter fraction. Therefore, there is a different measurable current for each atomic number in the periodic table. If the sample is rastered, as in X-ray image scanning, a picture of atomic number variations across the specimen may be obtained. This presentation is useful because the sample current mode is sensitive to chemistry changes on the surface of the sample and a sample current image appears quite similar to a light optical photomicrograph.

Finally, by aligning the two analyzing spectrometers to particular characteristic X-ray wavelengths, and slowly translating the sample under the electron beam, the elemental distributions of two elements may be simultaneously obtained.

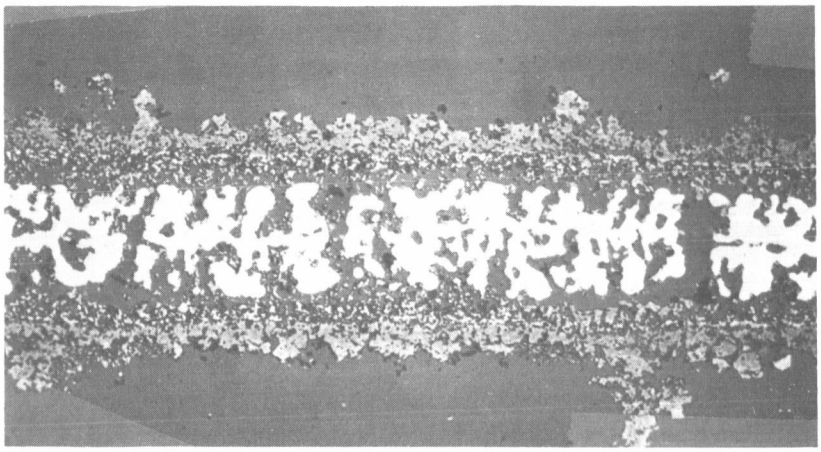
ANALYSIS:*

The anode assembly was impregnated and mounted, then metallographically prepared and examined under a light microscope. In general, the anode was found to be approximately 6.5 mils wide; the porous gold center was approximately 2.8 mils wide. Along one surface of the sample, large oxide particles (~0.5 to 2.0 mils in diameter) were observed to be randomly distributed. Also, two areas of the sample examined were found to be ruptured through the gold core. Representative photomicrographs are presented in figure 10-24.

Electron beam scan (EBS) analysis for nickel, aluminum, and gold was then performed upon an area of the sample containing an oxide particle on the surface (figure 10-25). The X-ray images are easily correlated with each other since they were obtained from the same precise location. Similarly, they may also be compared to the light photomicrographs. Chlorine and oxygen images were also obtained but were not reproduced because:

1. Although oxygen was generally found to be associated with the nickel, and always with the oxide particles, even more oxygen was found in the mounting compound to overshadow these findings. The resultant photographs revealed nothing.

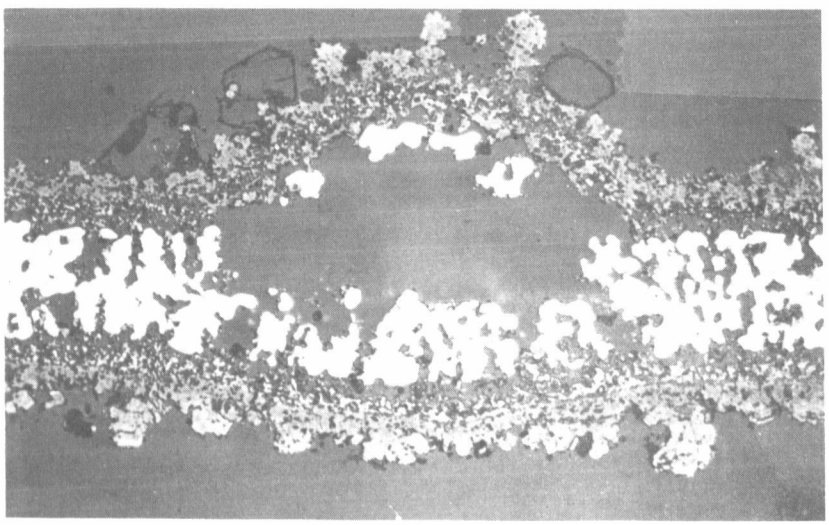
MAG: 200X



A. NORMAL AREA



B. CONTAMINATED AREA



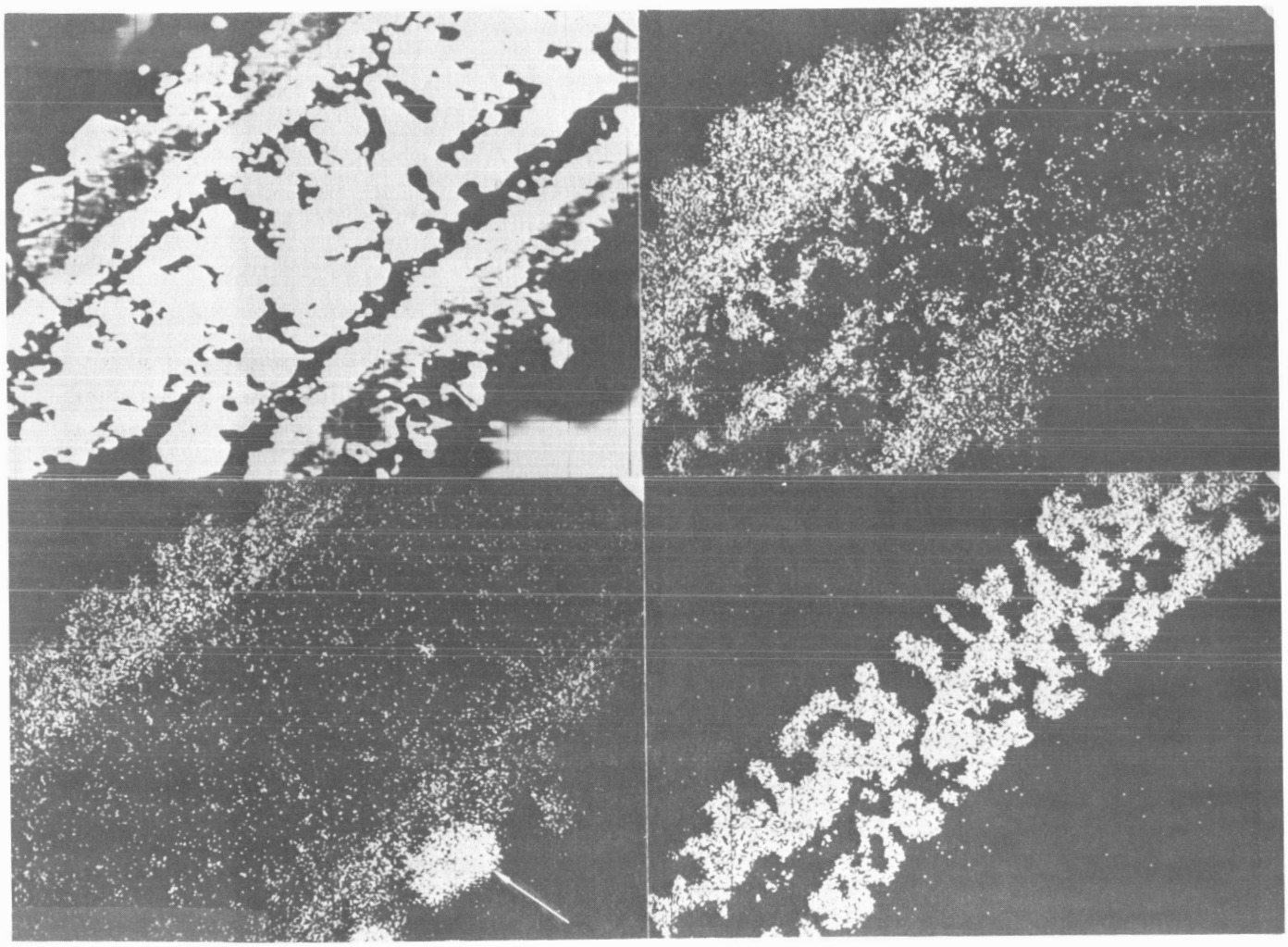
C. BROKEN AREA

FIGURE 10–24. LIGHT PHOTOMICROGRAPH OF THE THREE TYPES OF REGIONS OBSERVED. LARGE OXIDE PARTICLES (ARROW) WERE FOUND IN SOME AREAS OF THE ANODE OTHER REGIONS APPEARED TO HAVE BEEN SPLIT OR RUPTURED AS SHOWN IN C.

MAG: 340X

SPECIMEN CURRENT

NICKEL X–RAYS



ALUMINUM X–RAYS

GOLD X–RAYS

FIGURE 10–25. ELECTRON BEAM SCAN ANALYSIS OF AN AREA OF THE SAMPLE. THE ARROW INDICATES A LARGE ALUMINUM OXIDE PARTICLE. THE RANDOM DOTS IN THE GOLD X–RAY IMAGE E.G. ARE BACKGROUND NOISE PULSES AND ARE NOT ASSOCIATED WITH ELEMENTAL CON–CENTRATION.

10.1.5.4 (Continued)

2. Little or no chlorine was detected. At best, only trace quantities were found in the nickel-rich areas of the sample. The X-ray images reveal only background noise.

Next, a spectral pattern was obtained from an oxide particle (figure 10-26). An analysis revealed that in addition to oxygen, only aluminum was present. The phase was therefore aluminum oxide.

Finally, X-ray distribution scans for nickel, gold and aluminum were obtained (figures 10-27 and 10-28). Since it was possible to monitor two elements simultaneously, nickel was arbitrarily chosen as an internal standard.

OBSERVATIONS*

The gold core within the 'used' electrode was no longer found to be alloyed with the nickel. The gold was also found to be free from oxygen or chlorine contamination. Nickel (also oxygen and to a lesser extent aluminum) was found within the pores of gold.

Close examination of the light photomicrographs reveals a bright region in the casing adjacent to the gold core (~0.6 mils). This zone is essentially nickel; however lesser amounts of oxygen and aluminum were also detected in this layer. This is substantiated by the X-ray images and distribution scans. The roles of nickel and aluminum are reversed in the outer portion of the case. In this region, the major element is aluminum with less nickel being detected. Oxygen was also found in this zone.

Finally, aluminum oxide particles were found on one surface of the anode, which substantiates findings reported in section 5 of this report that in operation the anode may become coated with aluminum oxide if alumina structural elements are present in the cell system and have gone into solution in the electrolyte.

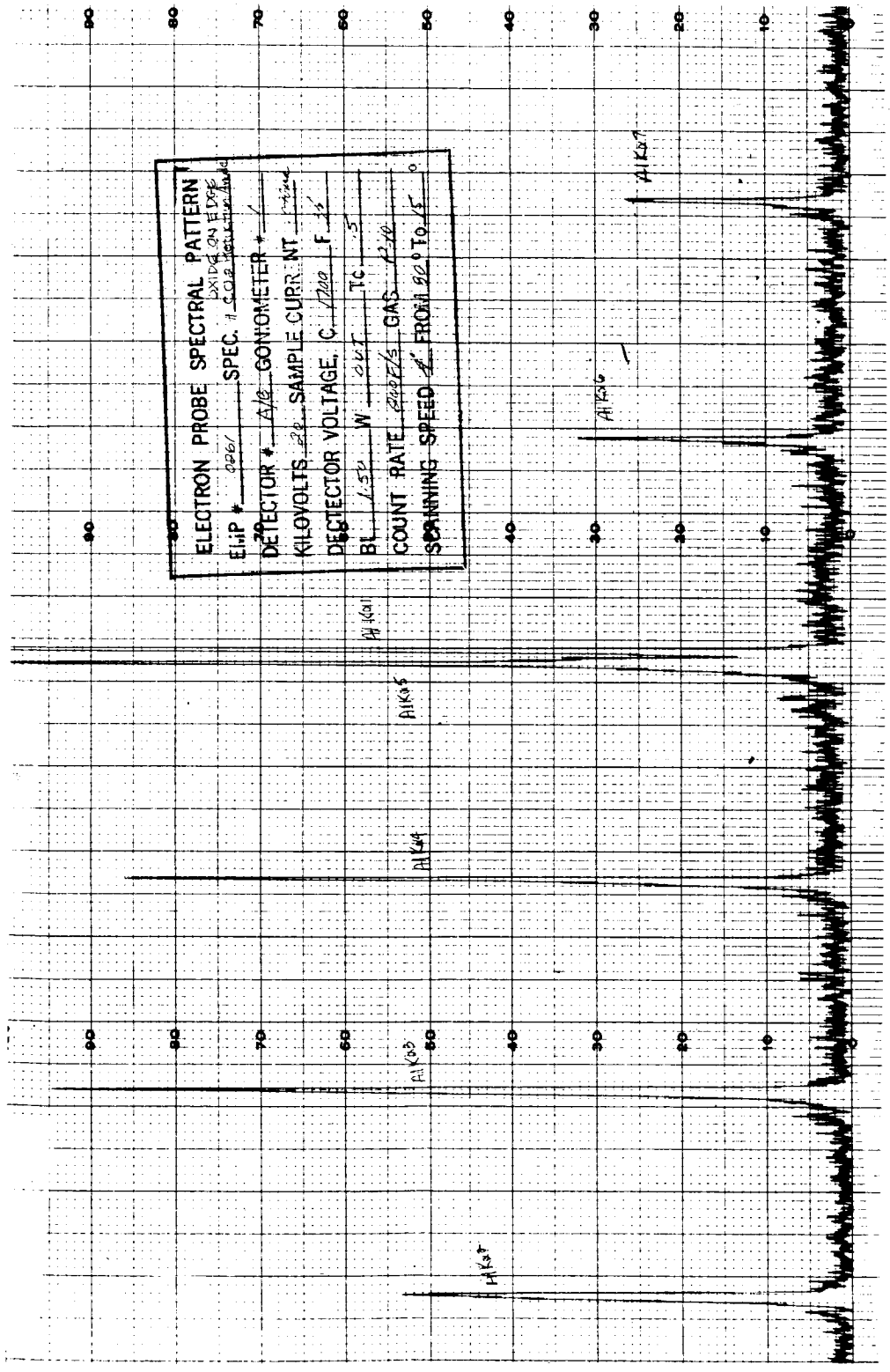


FIGURE 10–26. SPECTRAL PATTERN OBTAINED FROM AN OXIDE PARTICLE SIMILAR TO THOSE INDICATED IN FIGURE 10–25

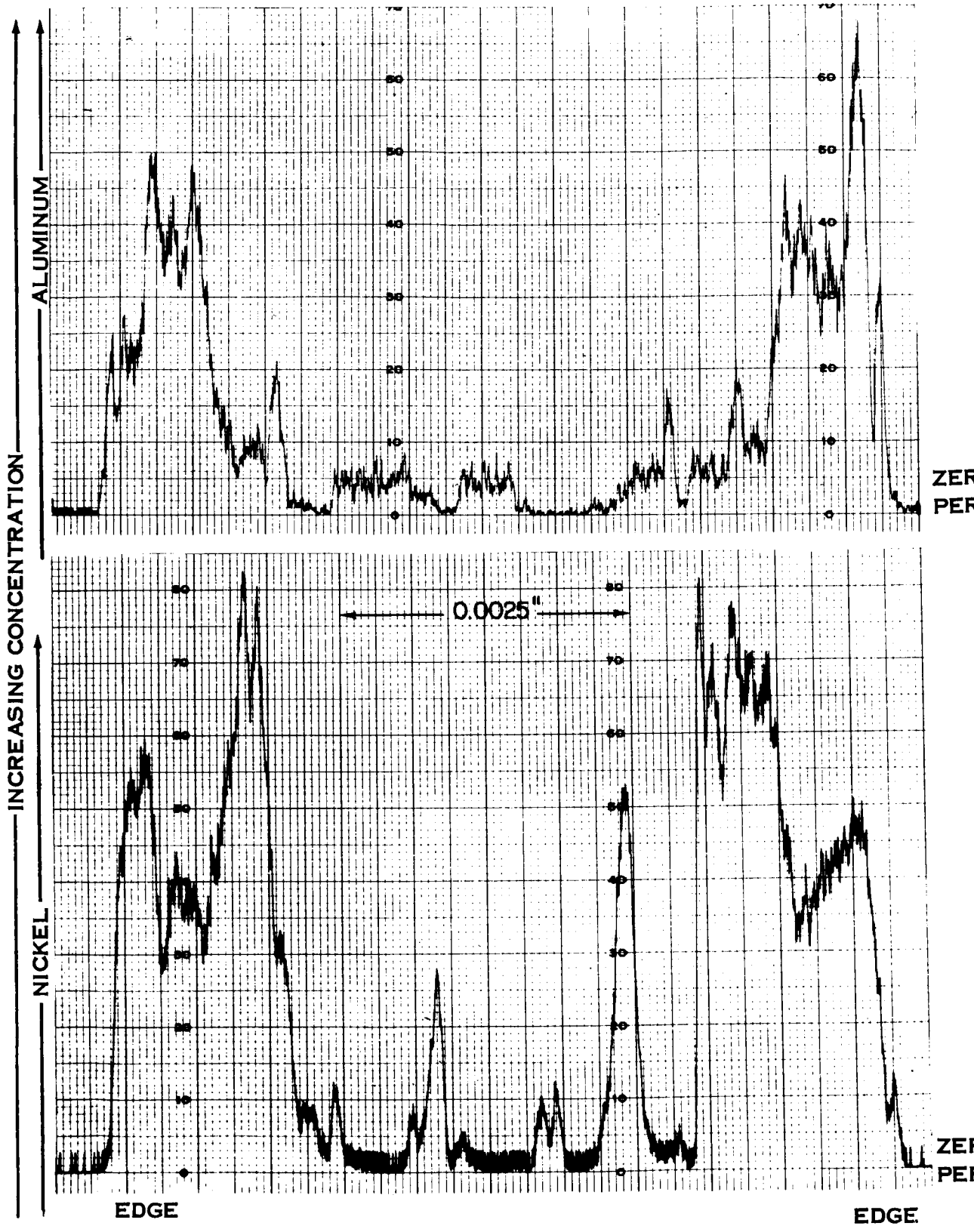


FIGURE 10—27. ALUMINIUM AND NICKEL DISTRIBUTIONS ACROSS A NORMAL AREA OF THE ANODE

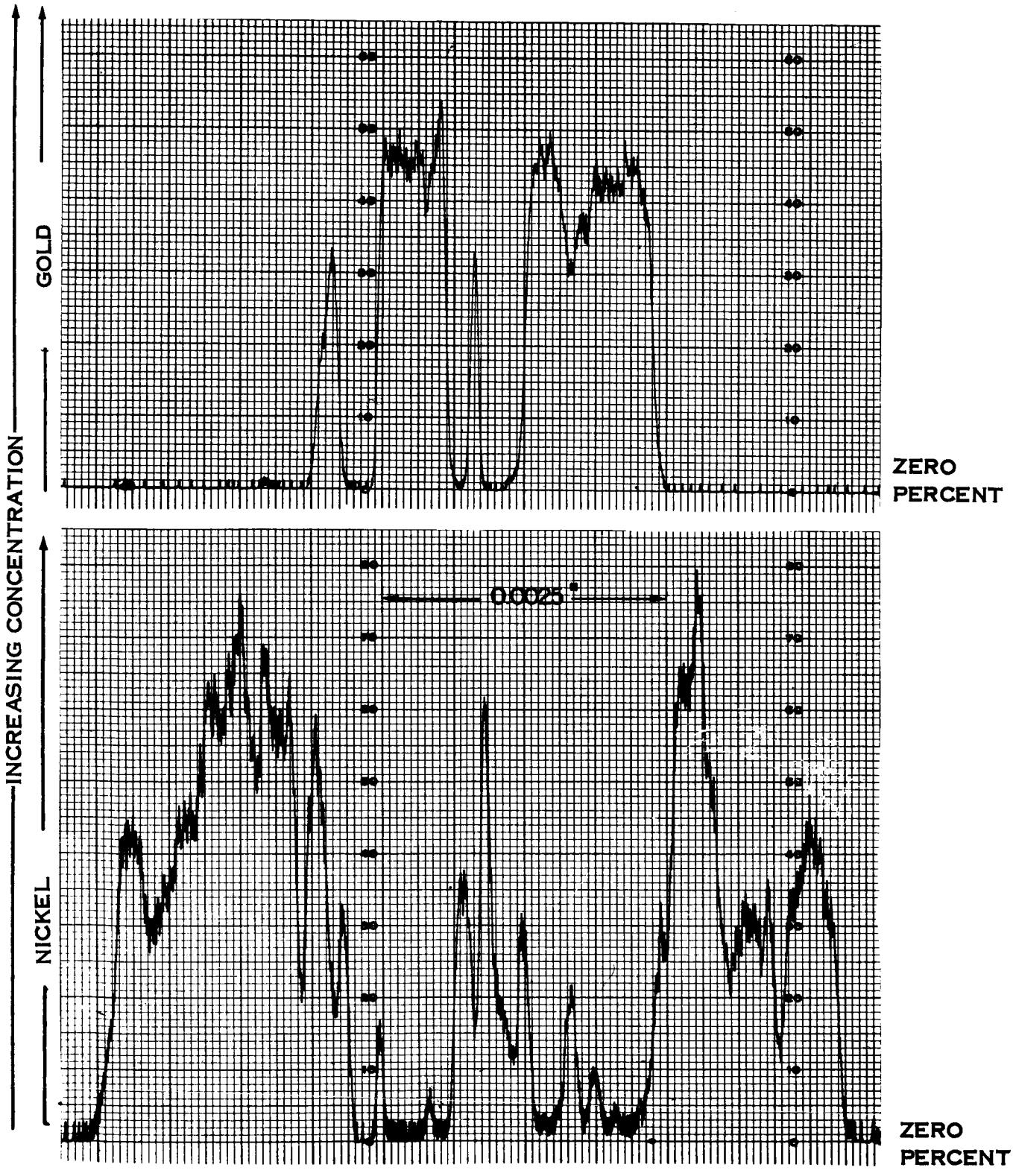


FIGURE 10–28. GOLD AND NICKEL DISTRIBUTIONS ACROSS A NORMAL AREA OF THE ANODE

CONCLUSION & INTERPRETATION OF RESULTS

In general, the analysis shows that the gold constituent of the anode material was not significantly consumed during the electrolyte operation of the cell. An examination of the anode stratification layers (figure 10-24), shows that essentially all of the gold initially present in the anode material has diffused into the center of the anode. The following calculation, with one assumption,** confirms this.

If it is assumed that the gold has not been consumed, then

[1] $\left[M_{Au}\right]_f = \left[M_{Au}\right]_i$, where: M = Mass. Subscripts "i" and "f" represent initial and final (after test) anode material compositions, resp

The initial mass of gold in the Premabraze alloy was

[2] $\left[M_{Au}\right]_i = \left[0.82\right]_i \left[D_{Au\text{-}Ni}\right]_i \left[V_o\right]_i$

where: 0.82 = weight present composition of gold in premabraze, initially

$D_{Au\text{-}Ni}$ = density of the alloy

V_o = arbitrary volume

The mass of gold in the center of the 'used' anode (from figure 10-24) is:

[3] $\left[M_{Au}\right]_f = \left[D_{Au}\right]_f \left[V_o\right]_f$, where D_{Au} = gold density

Assuming a constant area in the anode, equations (1), (2), & (3) can be combined.

** That the extent of gold porosity or void volume within the anode 'core' is insignifican

$$[4]\ \left[0.82\right]\left[D_{Au\text{-}Ni}\right]\left[W_{Au\text{-}Ni}\right] = \left[D_{Au}\right]\left[W_{Au}\right]$$

Where: $W_{Au\text{-}Ni}$ & W_{Au} is the thickness of the original premabraze stock and the gold center 'core', respectively.

The known values for eq. [4] are:

D_{Au} = 19.32 g/cc

D_{Ni} = 12.97 g/cc

$W_{Au\text{-}Ni}$ = 0.004 - 0.0042 inches

The width of the gold 'core' then can be calculated from eq. [4] and is found to be 0.0027 inches to 0.0028 inches. Figure 10-24 reflects a value of 0.0028 inches for the gold 'core' thickness.

It is thereby observed that the gold did not react with the electrolyte, but that accompanied by nickel diffusing outward, the gold migrated toward the center of the anode sheet. Such separations are not uncommon and are called 'parting' - occuring when the chemical potential of one element in an alloy is greater than the other element for a specific regent.

The alumina/aluminum deposited on the anode surface would have been expected since with the presence of aluminum oxide within the system, the typical reaction -

$Al_2O_3 \cdot O^{=}$ would have occurred, as does similarly

$CO_2 \cdot O^{=}$; $H_2O \cdot O^{=}$; and $SO_2 \cdot O^{=}$

It might be postulated, that anode life could be extended by fabricating a composite anode having a gold foil center and nickel oxide powder surfaces. In such a configuration, the gold 'core' would provide both structural strength and a favorable electrode conductive path. Gold (or other noble metal) must be employed as the 'core' material to prevent loss through diffusion through the oxide surface film - and to further promote structural strength of the 'core' which would result if porosity within the core developed. The semi-conductive properties of nickel-oxide at this temperature (or of a lithiated nickel oxide) would provide a conductive surface - as evidenced by the ability of the anode examined to still accomplish electron exchange, prior to its removal. It might be further suggested that nickel oxide could be attached to the gold anode core by sintering.

Although not cited earlier, a post examination was made by UARL of the 'virgin' Premabraze stock from the same 'lot' that the subject anode had been initially fabricated from.

The results of the examination showed:

(a) Complete homogeneous structure of the Ni-Au across the 0.004 Premabraze sheeting (under 500 x magnification), and

(b) An electron beam scan showing uniform distribution of gold and nickel across the same thickness. The results also suggested that the nickel content of the Premabraze was approximately 20% (by weight), agreeing with the chemical analysis of the material.

10.1.5.5 Cathode Current Efficiency

Experimental Details

The engineering performance test program (tests number 1 - 27) can be considered as being of two parts. In the first nine tests, the cathode was cyclically raised and lowered without 'breaking' electrical contact with the electrolyte. During these tests, the cathode was held in the 'up' position for the greater part of the cycle so that carbon deposition occurred predominantly when an adherent 'thin-film' of electrolyte covered the bulk of the electrode. This technique has provided higher quality carbon deposits in prior research studies.

The second group of tests (test number 10, ff.) employed a stationary cathode but cyclically oscillated the electrolyte to cover and uncover the cathode. As explained earlier in this report, at the low end of the electrolyte excursion, electrical contact with the cathode was interrupted - primarily intending to avoid the build-up of a bulbous deposit at the tip which was typically identified with continuous cathode submergence into the melt. In order to prevent intermittent electrical operations, a double-cathode adaptation was employed with the electrolyte cycled out-of-phase in the two cathodes to provide continuous cell current flow.

Results

Shortly after initiation of tests involving the oscillating electrolyte configuration, the cathode current efficiencies (η_c) obtained with that concept were noticeably improved over the earlier oscillating cathode tests. As further testing with the oscillating electrolyte configuration continued, it became all the more evident that typical efficiencies of 100 ± 5% resulted on all except a few of these tests.

In general, η_c values, achieved for various tests (throughout the Research and Engineering program) were found to be typified by the following ranges.

(1) Oscillating cathode: 40% - 90% (directly dependent upon cathode current density).

(2) Oscillating electrolyte: 95 to 105%: η_c did not appear to be dependent upon the current density, over the 100 - 200, ma/cm^2 ranges tested.

(3) Rotating cathode (completely submerged at all times): 60%. NOTE: 75% when 'spalled-off' carbon from the rotating cathode was collected by envelope screening. As with the oscillating cathode configuration, carbon purity was dependent upon cathode current density.

NOTE: These η_c values may represent slight inflation over actually achieved values, owing to failure of the 'acid-insoluble' carbon analysis technique to 'leach' all non-carbon components from cathode deposit.

10.1.5.5 (Continued)

Discussion of Results - General

The significance of achieving a favorable cathode current efficiency is believed to be self-evident. With efficiencies less than 100%, some of the carbon contained within the absorbed CO_2 is not 'captured' by the cathode - and with time acts to contaminate the electrolyte (or be given off as carbon monoxide, methane, etc.). As such, the true significance of achieving a η_c value approaching 100% does not concern the 'heat' loss due to the electrical inefficiency of the process, but concerns rather the adverse electrolyte contamination and/or gaseous discharge considerations.

This section considers the factors which promote a favorable cathode current efficiency - with the intent of postulating an explanation/s conducive to an ideal process (e.g. $\eta_c \approx 100\%$), and to examine in further detail the relative advantages or disadvantages inherent in the oscillating electrolyte concept selected for the 1/6 g design.

To postulate primary factors favoring high η_c values, it is interesting to examine the similarities and differences among the three techniques employed (ref. 1 - 3 above).

Discussion of Results - Detailed (ref. Table 10-II)

Variable A, B and G will be eliminated from consideration in this section as variables not pertinent to the achievement of high process η_c values.

Relative Motion Between Cathode and Electrolyte During Deposition (C).

As stated in the results of this section, cathode current efficiency typically increased from 60% to 75% when a 'screen' was encased about the rotating cathode to collect any carbon-containing deposit material hypothetically 'spalled-off' the spinning cathode. This observation allows some deduction to be made regarding the mechanics of the cathode deposition itself - implying that the 'adherence' of the deposit to the cathode surface is affected by inertial forces - and allows a conclusion to be reached that such inertial forces act to compromise adherence of the deposit to the cathode. It may be concluded that centrifugal or other environments should be avoided if η_c is to be optimized. It may be postulated that enclosure of the rotating cathode by a finer-mesh screen would probably have yielded higher 'recovered' carbon, although not satisfying the basic requirement for an adherent cathode deposit.

Interruption of Cathode Current Flow ('D')

There is insufficient information from tests to date to establish positive relationships of current interruption versus high η_c values. Ninety percent cathode current efficiency values have been achieved in the oscillating cathode configuration not favored

TABLE 10-II. DIFFERENCES IN ENVIRONMENTS FOR THREE CONFIGURATIONS TESTED

	Evaluated by:	Research & Engineering	Engineering	Research
	Configuration:	Oscillating cathode	Oscillating electrolyte	Rotating (Submerged) Cathode
Variable	Environment			
A	Cathode location during deposition	in cathode ullage	in melt	in melt
B	Catholyte temp. during deposition	melt temp.	melt temp.	melt temp.
C	Motion of electrolyte with respect to cathode during deposition	no relative motion	no relative motion	Considerable motion (depends upon cathode configuration and rotating speed)
D	Interruption of cathode current flow, cyclically	no	yes	no
E	Exposure of catholyte to ullage gas	yes (B)	yes (A)	no
F	Complete exposure of catholyte to ullage gas	no (partial)	yes (completely)	none
G	Enshroudment of cathode by containment tube	no (Except test #6-#10)	yes	no
Resulting	Typical Results (Cathode Current Efficiency)	40 - 90% (directly dependent upon cathode current density)	95 - 105% (appeared to be independent of cathode current density over 80 - 200 ma/cm^2 tested.	60 - 75%

(A) Catholyte exposed to specific ullage gas within cathode containment tube - which probably differs somewhat from 'cell' ullage gas.

(B) Same as (A) for tests numbered 6-10; other tests exposed cathode to cell ullage gas.

TABLE 10-III. LIKELY EFFECT OF VARIABLES UPON FAVORABLE CATHODE CURRENT EFFICIENCY.

Variable	Significance	Comments/Conclusion
A	No	Not important as a variable: Good η_c results were obtained under both conditions
B	No	Not important as a variable over ranges tested (625 - 690°C)
C	Probable	Highest η_c values obtained with no relative motion
D	Possibly	Highest η_c values were obtained in oscillating electrolyte configuration and having cyclic current interruption.
E	Possibly	Highest η_c values obtained when cathode was cyclically exposed to cell ullage/cathode ullage, gas
F	Possibly	Highest η_c values achieved when entire cathode area is exposed to ullage gas
G	No	High η_c values were obtained both in configurations employing and not employing cathode containment.

10.1.5.5 by current interruption, but it is further noted that under these circumstances high cathode current densities were required to achieve favorable η_c values, with subsequent compromises in the purity of the carbon deposit. More testing is needed to further examine the effects of current interruption on cathode current efficiencies.

Exposure of Cathode to Ullage Gas ('E')

As a consequence of exposure of the catholyte to the ullage gas, it is postulated that carbon is more likely to be retained on the cathode than without such ullage gas exposure. One possible explanation is that a more adherent carbon deposit results from a more complete conversion of CO_2 to $CO_3^{=}$ at the cathode surface when this conversion is accomplished in the ullage gas.

Complete Exposure of Cathode to Ullage Gas ('F')

As discussed in ('E') above, if a higher conversion of CO_2 to $CO_3^{=}$ is associated with the ullage gas and in turn favors adherent deposits, then any configuration which exposes a greater fraction of the total catholyte to this ullage gas would tend to achieve more effective carbon recovery. As discussed earlier, the carbon quality in the bulbous region of the oscillating cathode configuration was not as good as that deposit benefited by ullage gas exposure. The bulbous region showed a greater percentage of oxide and as a result would be expected to contribute to catholyte 'freezeout' adhesions. It is suggested that the poorer deposition within the non-ullage exposed cathode region led to spalling and accounted for the poorer overall η_c values achieved for the oscillating cathode (OC) configurations. If this supposition is correct, it might be hypothesized that a reduction in the cathode areas maintained in continuous contact with the electrolyte on OC configurations would result in higher η_c values.

Summary of Discussion

The preceding paragraphs within this section have contrasted differences between three configurations with respect to achieving favorable cathode current efficiencies. The results of these discussions are summarized on table 10-III.

Various postulations have been made which may be subsequently proven or replaced with more valid ones. Additional experimental and analytical attempts should be made to allow a further understanding of controlling factors of a 100% efficient cathode. Such understanding ultimately is necessary to capitalize on design ingenuity and more readily allow performance predictability.

From a practical standpoint there does not appear to be an immediate need to give priority to achieve a full understanding of the process variables as they affect η_c. The selection of the oscillating electrolyte concept for the 1/6 g design does appear to offer near 100% η_c performance based upon configuration tests to date. It is not anticipated that the 'scale-up' of prototype hardware during subsequent parts of this program will differ from the results achieved to date with the oscillating electrolyte configuration; i.e., $\eta_c \cong 100\%$.

10.1.5.5 (Continued)

Technical Details - Cathode Efficiences > 100%

As documented in figure 10-1, several of the oscillating electrolyte tests had cathode current efficiences in excess of 100%. Several theories/explanations have been set forth in an attempt to understand this. They are:

(a) Inaccuracy in carbon purity chemical analysis, which, if indicating an erroneously high carbon purity reflect cathode removal efficiencies larger than 100%.

(b) Error in measuring or recording the total number of ampere-hours of electrolysis - during a given test (e.g. if more ampere-hours were perhaps 'input' than actually measured, the cathode current efficiency would reflect an unrealistic and high value).

(c) Thermal breakdown of CO_2 to CO and/or C within the melt requiring a lesser passage of current to deposit a specific quantity of carbon on the cathode.

It is believed that explanation (a) represents the most probable reason for the 'excessive' cathode current efficiencies experienced in certain of the tests. As an example, the carbon deposit from test number 26 which reflected a η_c of 103% was subjected to a thorough chemical analysis embodying:

(a) Examination if lithium in the deposit by the use of an atomic absorption spectrometer,

(b) Examination of chloride, through colorimeter methods,

(c) Examination of oxide, hydroxide, and carbonate, by means of titration, and,

(d) Examination of all other metals and foreign contaminants by means of emission spectrography.

Table 10-I documents the results of this cathode deposit chemical analysis. The detailed chemical analysis was performed subsequent to the preparation of figure 10-1. Although the later figure shows carbon purity and cathode current efficiency values of 84.6 and 103% respectively, proper adjustment for the findings of the detailed chemical analysis results in these values being actually reduced to 81 and 96.6%, respectively. It is assumed that other tests (e.g., tests 22 and 23) would have similar explanations accounting for their relative high cathode current efficiency levels.

The likelihood of human or calibration errors in the ampere hours of electrolysis over which specific tests were conducted was scrutinized during test numbers 26 and 27 with a coulometer. The Faraday values in these two tests cross-checked within a fraction of 1% through the two techniques. It was concluded that errors or calibration considerations do not explain the excessive current efficiencies on these tests - and in similar manner are not likely to explain other cases.

10.1.5.5 (Continued)

A brief analysis of the thermal break-down of CO_2 at 650°C showed that the decomposition is of small magnitude and is not likely to explain the η_c values > 100%.

10.2 Material Tests

10.2.1 Introduction

Until Phase IIA, test articles employed on the NAS 1-4154 fused salt CO_2 removal and reduction program have relied heavily on the use of ceramic or graphite materials for melt containment, and where necessary metals for use in thermocouple glands, etc. were included. The use of metal was generally restricted because of the highly corrosive action of the melt. It is generally regarded by the aerospace engineering industry that wherever possible the use of ceramics as the prime structural material should be avoided in preference to metal structures because:

(a) Less susceptibility of metals to thermal shock,

(b) Better adaptability of metals to withstand typical aerospace environments of impact, vibration, higher strength-weight ratios, etc.

(c) The overall economy, range of selectivity, and other miscellaneous attributes of metals contrasted to ceramics (including ease of fabrication and joining metal parts, the variety of fabrication techniques available with metals, the consideration of cost of complex parts fabricated of metal in contrast to ceramics, etc.)

However, it was believed from the start of Phase IIA that specific component and installation problems could profitably employ composite (metal and ceramic) laminates or parts. It was recognized, for example, that electrical separation of the anode (and perhaps the cathode itself) from an essentially metal melt container might prove to be essential in the detailed design of any cell system - and in this application the unique properties of ceramics would dictate their usage.

Because of a general limitation in funding, the primary objective assigned to the Space Systems Materials Engineering group was to investigate and make selection (to the extent possible) of metal melt containment materials which offered immediate and/or long term promise of being effective for the prime cell structural material. As a partial back-up to this effort, and to provide a quantitative 'yardstick' of success, some effort was to be expended in establishing quantitative corrosion rates of the more frequently used ceramic materials (primarily alumina and magnesium oxide).

10.2.2 The Phase I report of this contract stated certain basic corrosion considerations for materials exposed to the LiCl and Li_2CO_3 eutectic. (Refer to pages 166-169 of Phase I report.)

10.2.2 A restatement from the Phase I report is presented below to emphasize certain factors and to indicate possible solutions.

The reaction of the LiCl component with any metal (M) can be expressed as

$$[1] \quad M^\circ + LiCl \rightarrow Li^\circ + MCl$$

Fortunately, LiCl has a higher free-energy than any structural metal, as can be seen in table 10-IV, and therefore will not react with metal by such a mechanism. The $LiCO_3$ will react with any metal (M) in accordance with the following relationship:

$$[2] \quad 2M^\circ + Li_2CO_3 \rightarrow 2Li^\circ + M_2O + CO_2$$

Generally, the metallic carbonate does not form as the temperature readily decomposes the carbonate into the metallic oxide and carbon dioxide. The formation of the gaseous carbon dioxide means a non-equilibrium condition in this open system; thus the reaction would go until all the metal would have been consumed if the metal did not form a protective metal film. The protective quality of the metallic film depends on the film's being insoluble and adherent, crack-free and non-porous, if the film is to control the diffusion of oxygen through it. It is the diffusion of oxygen that will control this reaction with the base metal. The diffusion of oxygen is relatively low due to the low operating temperature.

The formation of the oxide by reaction [2] can proceed further, depending on the relative free energies as shown in Table 10-IV.

TABLE 10-IV

FREE ENERGY OF FORMATION OF CERTAIN

METAL OXIDES AND CHLORIDES AT 637°C

ELEMENT	CHLORIDE (K CAL/GM ATOM OF 2 Cl)	OXIDE (K CAL/GM ATOM OF O)
Aluminum	- 93.1	-110.9
Beryllium	- 84.6	-122.0
Chromium	- 55.2	- 71.8
Cobalt	- 48.5	- 41.1
Columbium	- 61.2	- 72.1
Iron	- 55.4	- 49.3
Lithium	-163.2	-108.8

TABLE 10-IV (Con'd)

FREE ENERGY OF FORMATION OF CERTAIN

METAL OXIDES AND CHLORIDES AT 637°C

ELEMENT	CHLORIDE (K CAL/GM ATOM OF 2 Cl)	OXIDE (K CAL/GM ATOM OF O)
Magnesium	- 118.9	- 120.7
Manganese	- 84.5	- 83.9
Molybdenum	-	- 48.7
Nickel	- 40.6	- 37.7
Titanium	- 91.5	- 103.3
Tungsten	- 9.0	- 49.9

Reaction [3] should occur if the metal chloride has a higher free energy of formation i.e., more thermodynamically stable than the oxide.

$$[3] \quad MO + 2Cl^- \rightarrow MCl_2 + O^=$$

The extent of this reaction would depend on the chloride ion concentration,which would be low in a fused salt. The effect of reaction [3] is to strip the protective oxide from the metal as the chloride is being readily dissolved into the eutectic. As can be seen from the data in table 10-IV, nickel, iron, cobalt and manganese would corrode by this mechanism. The reaction is also helpful in predicting the action of a ceramic with the electrolyte. Ceramics such as alumina, magnesia and chromia, having higher free energy than their chlorides, should withstand the electrolyte while cobalt oxide, magnetite (iron oxide) and nickel oxide, having lower free energy than their chlorides, should dissolve.

An equilibrium could be achieved in a reaction such as reaction [3], and an immunity of the metal would be established. This immunity would be possible if the essential electrolysis resulting in the continuous deposition of metal upon the cathode did not occur. (Reference Phase I Report, page 51). The electrolysis presents a challenge to the selection of the proper metal. Restricting this deposition is the low solubility of the metal salts in the electrolyte mixture. The measurement of the metallic salt solubility should be a prime function for testing, although it is complicated due to various minor reactions of the melt with the air and the water. The following section discusses those screening tests which were used to measure the rate of corrosion and the removal or gain of the sample weights.

10.2.3 Investigation

The basic procedure was to subject all candidate materials to a "screening" test and choose the most promising for a long duration (six month) test. The screening test

10.2.3 (Continued)

consisted of partially and completely submerging the samples in the electrolyte at 1200° F for five and ten days. A "spot" test of five days was employed for samples of limited quantity.

The spot and screening tests were performed in an externally heated alumina crucible. The mixture of 60% lithium chloride and 40% lithium carbonate was conditioned and maintained at a dew point of -9°C by forcing air through the mixture which was heated to and maintained at 625° ± 10° C. The mixture temperature was regulated by a Honeywell R7161B Versatronik indicator and controller having a chromel-alumel thermocouple placed on the exterior of the crucible which compensated for the mixture's temperature.

The samples were suspended on a nickel or Nichrome wire. An alumina bushing separated the metallic samples from the wire to reduced electrochemical effects.

10.2.3.1 Test Results

The test results as reported in Table 10-V were computed by the following formular for corrosion rate R in mils (0.001") per year:

$$R = \frac{534\ W}{\rho A T}$$

where W is the weight lost (or gained) in milligrams, ρ, density in grams per cubic centimeter A, area in square inches and T, time in hours. The area was the entire area of the sample in both media, the eutectic mixture, and the ullage (the space above the eutectic mixture).

However, the rates alone are not sufficient to allow a full evaluation of the material.

The adhesion, or the lack of adhesion of the corrosion product is, therefore, reported in table 10-V. A non-adherent (flaking) scale, as seen in figure 10-32 for titanium and in figure 10-33 for nickel, could interfere with the functioning of the cell by forming particles that cause electrical shorting of the anode or cathode or restriction to the flow of electrolyte between the anode and cathode. An adherent scale as seen in figure 10-31 for Hastelloy N would not act as such an interference. The dissolving or eroding type of corrosion illustrated by alumina in figure 10-29 and 10-30 and tantalum cladded copper in figure 10-32 would be similar in action to the adherent scale, except a higher metal dissolution would be expected.

The above visual examinations do not always reveal the underlying mechanism of corrosion. Microexamination of the metal's cross-section, as seen in figure 10-34 and 10-35 clarifies the mechanism. Figure 10-34 illustrates the erosion type corrosion of tantalum cladded copper, while figure 10-35 depicts the scale formation of Hastelloy N.

TABLE 10-V

TEST RESULTS FOR CO_2 REDUCTION CONTAINER MATERIAL

Material	Vendor's Designation	Density (gms/cc)	Immersion	Time (Hrs.)	Corrosion Rate (A) (in MPY)*	Surface Condition
Ceramics						
Alumina	Mc Danel's 997	3.9	Total	120	1.15	Tarnish
			Partial	120	1.29	
			Total	240	0.34	
			Partial	240	0.23	
	De Gussa AL23	3.9	Total	137	1.50	Tarnish
			Partial	137	0.40	
			Total	240	0.56	
			Partial	240	1.39	
Titanium Oxide		3.84	Partial	120	493.	White Scale
			Partial	120	242.	
Magnesium Oxide		3.58	Total	120	(4.01)	Tarnish
			Partial	120	(7.67)	
Metals						
Pure Nickel	Nickel 201	8.90	Total	120	(300.)	Blistering and
			Partial	120	(107.)	Flaking Scale
			Total	240	9.48	
			Partial	240	(26.2)	
15% Chromium -7% Iron Nickel Alloy	Inconel 600	8.43	Total	120	(5.38)	Blistering and
			Partial	120	20.8	Flaking Scale
			Total	240	(2.98)	
			Partial	240	22.3	

*Mils per year

TABLE 10-V (Continued)

TEST RESULTS FOR CO_2 REDUCTION CONTAINER MATERIAL

Material	Vendor's Designation	Density (gms/cc)	Immersion	Time (Hrs.)	Corrosion Rate (A) (in MPY)*	Surface Condition
17% Molybdenum -7% Chromium -5% Iron Nickel Alloy	Hastelloy N	8.93	Partial Partial Total Partial	120 120 240 240	(14.0) (14.7) (7.22) (7.44)	Adherent Scale
22% Chromium -18% Iron -9% Molybdenum Nickel Alloy	Hastelloy X	8.23	Total Partial	96 96	(14.6) 45.5	Blistering and Flaking Scale
Titanium	A70	4.51	Total	120	221.0	Flaking Scale
Tantalum Electroclad Copper		16.6	Total	120	60.0	Tarnish

NOTE: Bracketed terms are weight gain valves; unbracketed terms are for weight loss.

* Mils per year

FIGURE 10–29. DEGUSSA AL 23 ALUMINA SAMPLES EXPOSED TO THE EUTECTIC FOR THE TIMES SHOWN. NOTE THE THERMAL SHOCK CRACK IN THE PARTIAL IMMERSION 240 HOURS SAMPLE

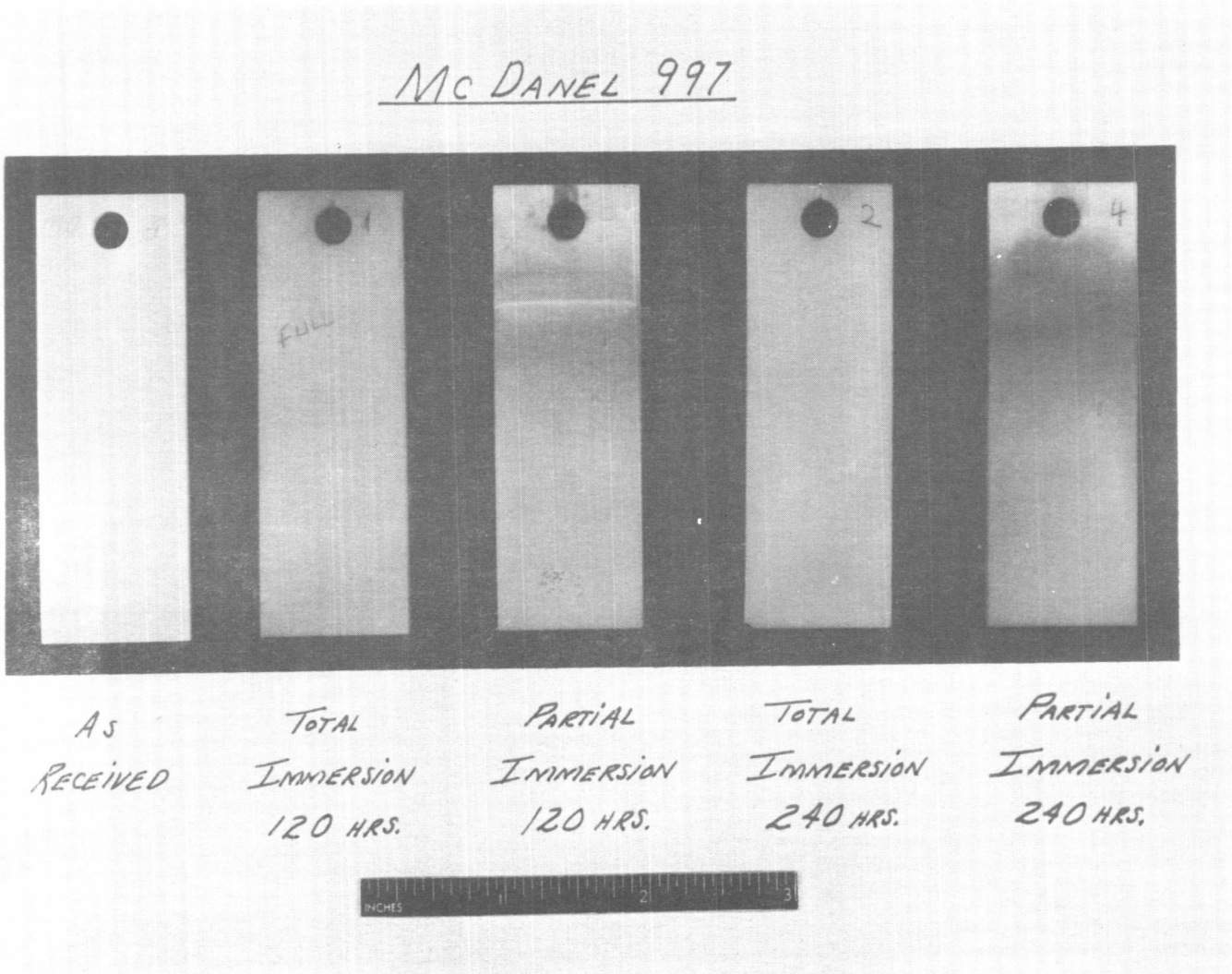


FIGURE 10—30. MC DANEL 997 ALUMINA SAMPLES EXPOSED TO THE EUTECTIC FOR THE TIMES SHOWN

FIGURE 10–31. HASTELLOY N NICKEL ALLOY SAMPLES EXPOSED TO THE EUTECTIC FOR THE TIMES SHOWN

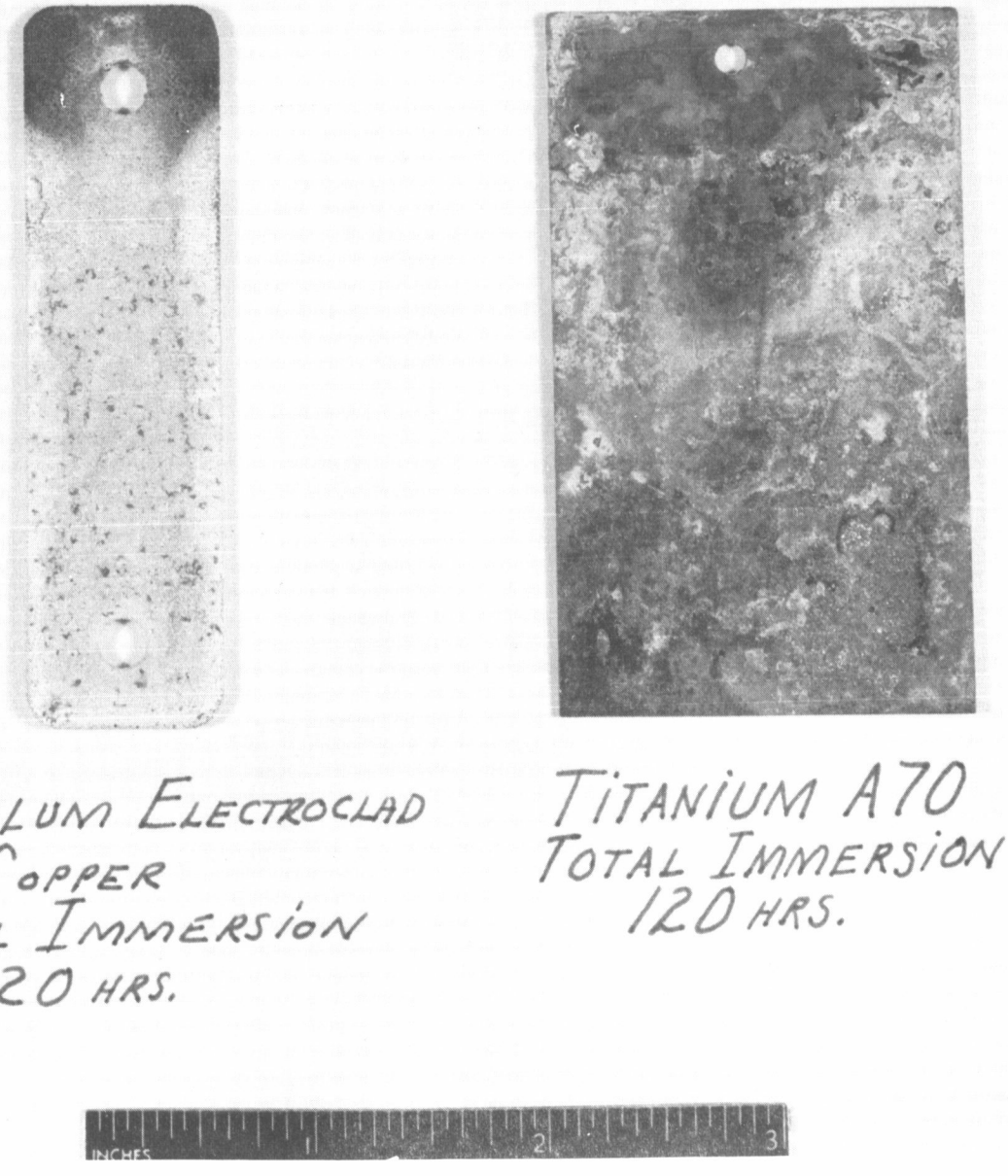


FIGURE 10—32. TANTALUM ELECTROCLADDED COPPER SAMPLE (LEFT) AND TITANIUM A70 SAMPLE EXPOSED TO THE EUTECTIC FOR THE TIMES SHOWN

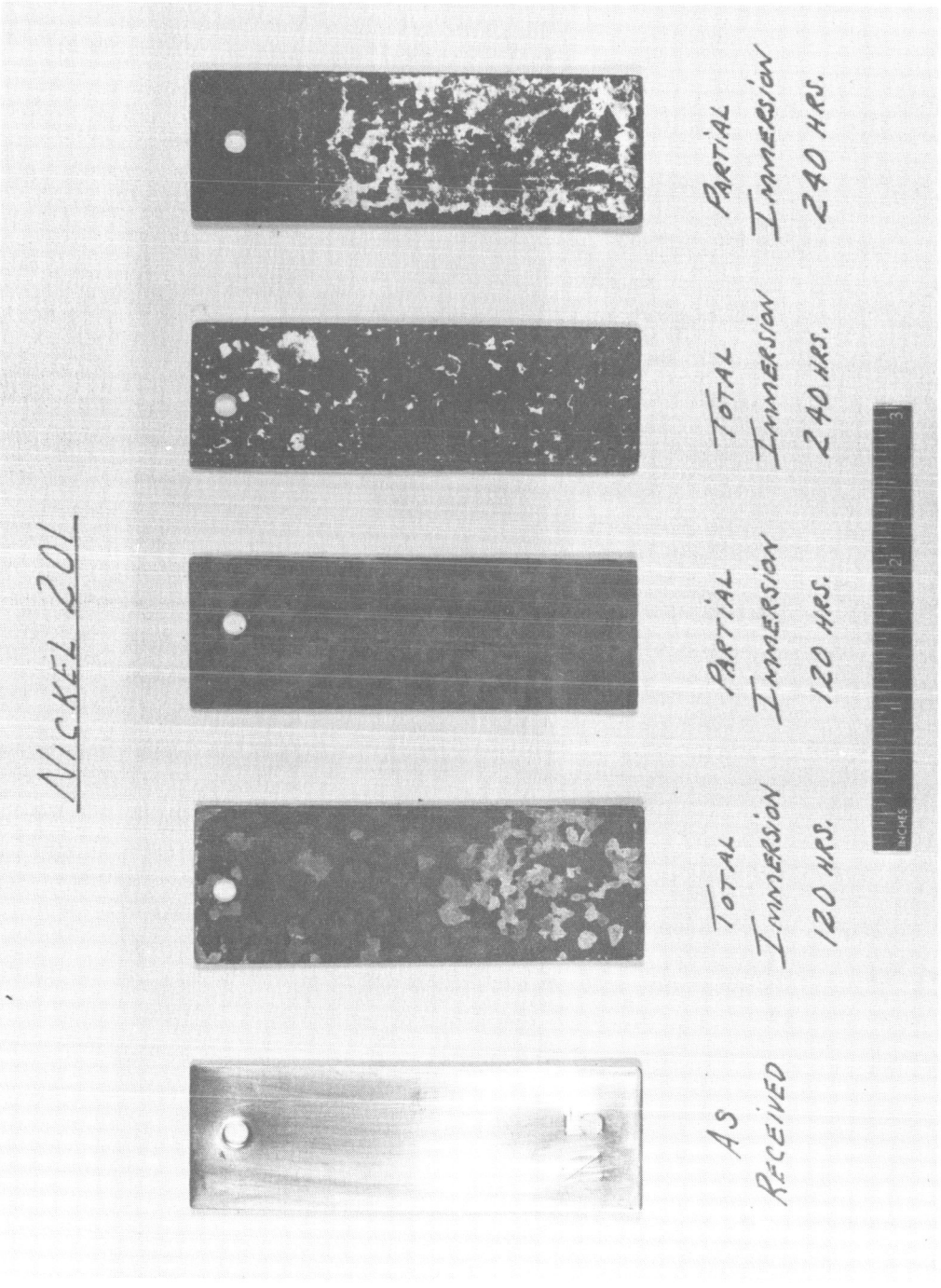


FIGURE 10—33. NICKEL 201 SAMPLES EXPOSED TO THE EUTECTIC FOR THE TIMES SHOWN

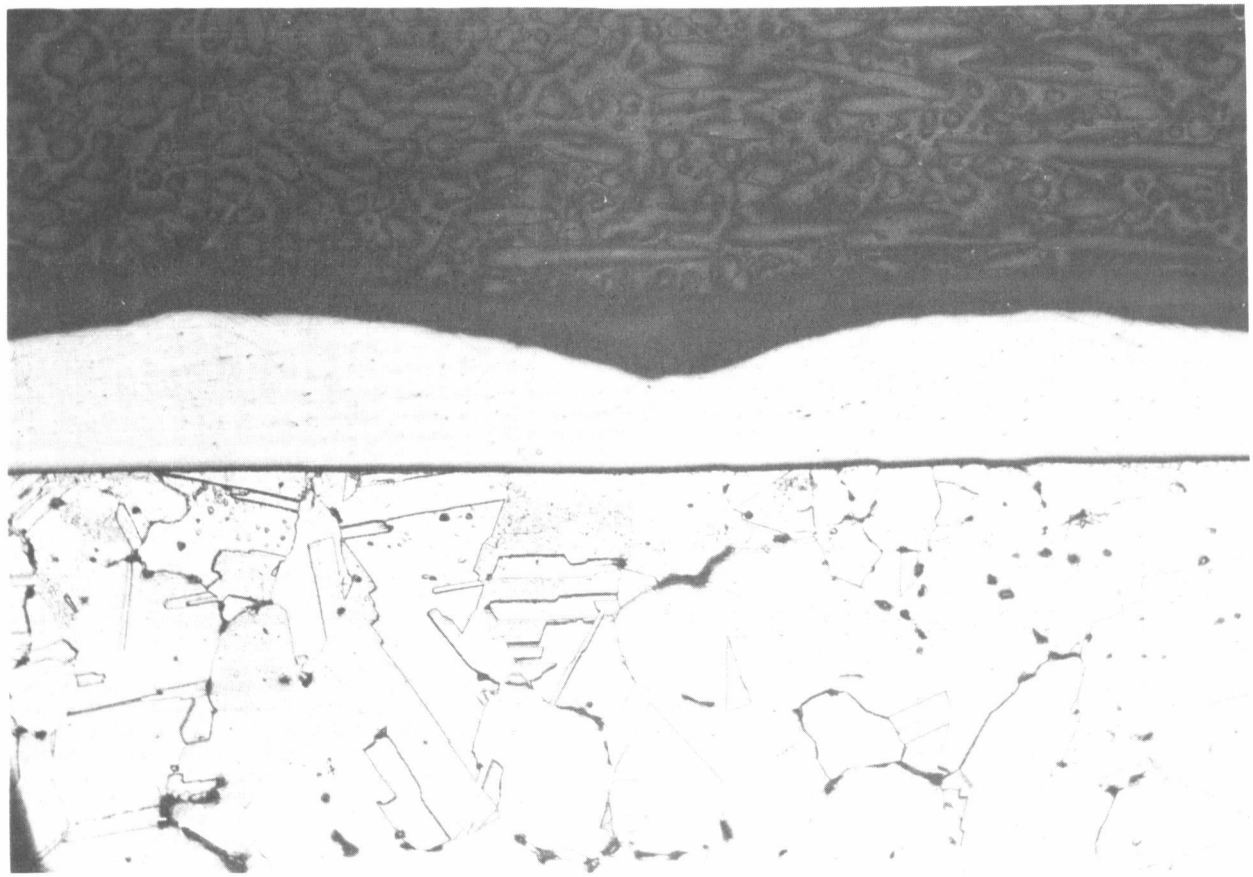


FIGURE 10—34. CROSS—SECTION OF TANTALUM ELECTRO CLADDED COPPER SAMPLE AFTER 120 HOURS EXPOSURE TO THE EUTECTIC ETCH: NH_4OH SOLUTION; 200X

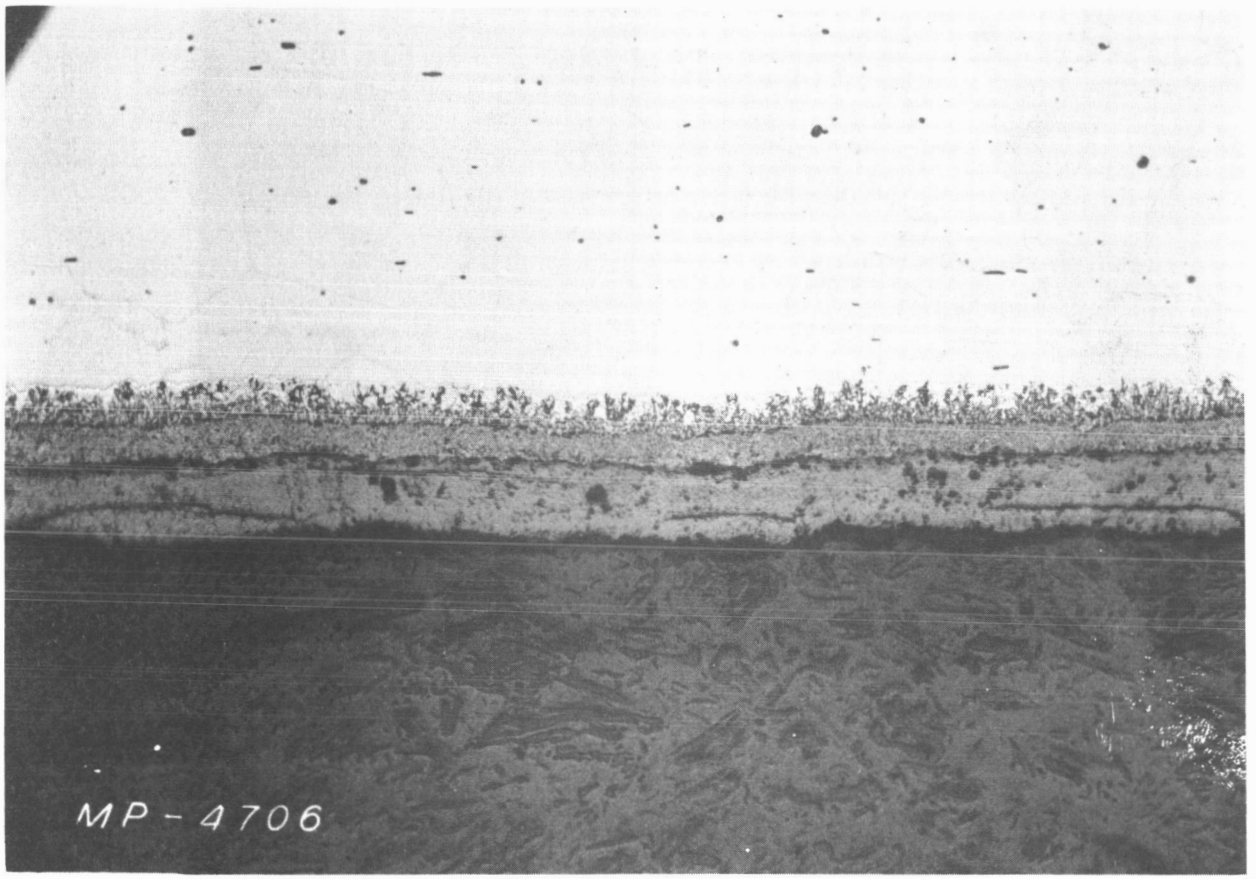


FIGURE 10—35. CROSS—SECTION OF HASTELLOY N SAMPLE AFTER 240 HOURS EXPOSURE TO THE EUTECTIC. NOTE THE THREE DISTINCT LAYERS OF THE SCALE. ETCH: ELECTROLYTIC 10 OXALIC ACID; 200X

10.2.3.2 Metallic Container

The limited volume available in a ceramic test container prevented the evaluation of certain variables and limited the number of container material samples that could be tested at one time. It was therefore decided to fabricate a metal container and to thereby obtain the needed volume. Based upon a series of corrosion tests reported in the above investigation, the nickel alloy, Hastelloy N, was chosen because its protective film showed the desired characteristics and the corrosion rates were satisfactory.

The first attempt to fabricate a container was to deep draw a 0.050-inch thick sheet using a one-die hydroforming process. The container blank was drawn until considerable work hardening had occurred and then solution-annealed at 2150° F in an accessible vacuum furnace. Unfortunately, the part was gradually cooled over a 45 minute period to room temperature instead of being forced-air cooled. Cracks developed in two of the four corners of the Hastelloy N container during subsequent hydroforming operations and the 'deep-draw' fabrication attempts on the container were abandoned at this time in favor of developing a 'welded' and rectangular container.

The new container was fabricated by welding 0.050-inch thick sheet. Following fabrication, and to relieve welding stresses, the container was solution annealed in an atmosphere furnace at 2150°F and then rapidly air cooled. A black oxide film covered the entire container and was not thought to be detrimental since it was believed it would act as a protective coating. The container was partially filled with the eutectic mixture and raised to the operating temperature. Within a twenty-four hour period, a flaking scale had occurred on the container. The test was aborted, and the molten eutectic removed. An adherent oxide film was noted to exist below the melt level with gross flaking above this level. The container was cleaned by sand blasting and liquid honing, refilled with the eutectic and again heated. The same corrosion and flaking conditions recurred within a twenty-four hour period. Figure 10-36 shows the appearance of the crucible after the melt was removed. To contribute information as to the unexpected and high corrosion rate experienced in the test attempts, a spectrographic analysis of the salt contained within the crucible was taken and showed the following decreasing order of metallic concentration:

Li, Mo, Cu, Ni, Al, Mg, Mn.

This order should be compared to the composition limits of Hastelloy N which is

Ni	Balance	Mn	0.80 max
Mo	15.00-18.00%	W	0.50 max
Cr	6.00-8.00%	Al+Ti	0.50 max
Fe	5.00 max	Cu	0.35 max
Si	1.00 max	Co	0.20 max

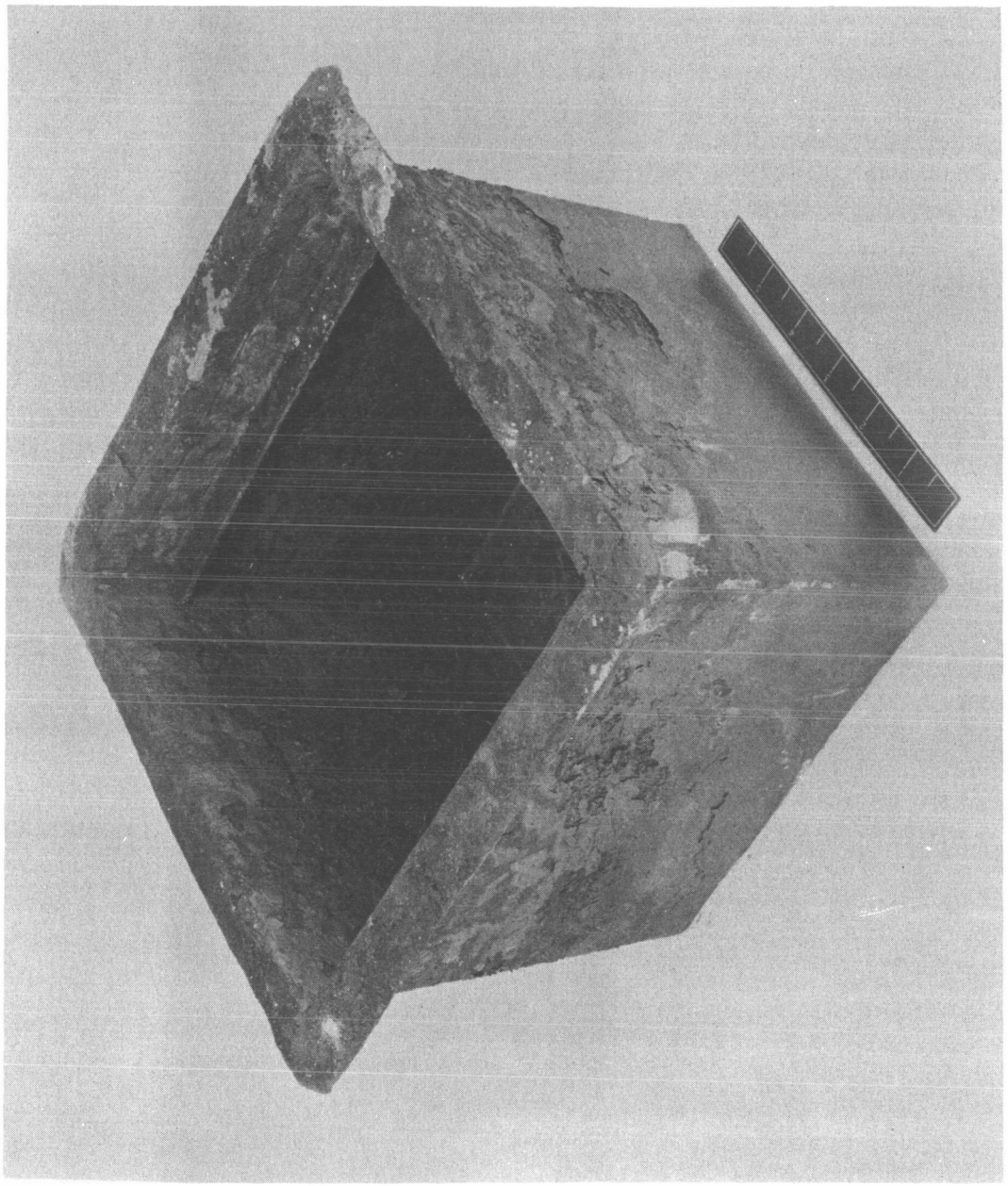


FIGURE 10–36. CONTAINER MADE OF WELDED HASTELLOY N SHEETS AFTER HAVING BEEN HEATED TO 1300 F WITH MOLTEN SALT FOR THE SECOND TIME

10.2.3.2 (Continued)

A new eutectic mixture's composition has only spectographically undetectable metallic concentrations.

It is significant that there was no trace of iron or chromium in the eutectic mixture, even though they constitute a high percentage of the alloy. The presence of molybdenum as a primary constituent of the eutectic means a high dissolution rate and is an indication to avoid the use of this element in future candidate materials. The presence of copper and magnesium in the eutectic analysis cannot be explained.

Although the Hastelloy N container failed when exposed to the melt under the surrounding 1300°F temperatures, it does serve to illustrate one major problem. The conditions in the ullage had been considered to be mild as compared to the melt, due to reduced concentrations of the eutectic's corrosive components. The promoted flaking of the Hastelloy N, however, contradicts this opinion. Nor can the severe container corrosion noted above the eutectic level be assumed to be caused by the presence of the surrounding air environment only. It had been shown that the Hastelloy N sample, heated to 1200°F in an air environment, forms an adherent black oxide scale. This fact only reinforces the statement: the ullages's chemistry is not fully understood at this time and requires additional investigation.

10.2.4 Conclusions

(1) Of the three ceramics and the six metals corrosively tested to date, the alumin has the best resistance to both the eutectic mixture and the container's ullage. Hastelloy N adequately resisted immersion in the eutectic mixture but was blistered by the ullage vapors.

(2) The cursory tests, the "screening" and "spot" tests, have yet to be completed and the long duration tests have not begun.

Recommendations

(1) A detailed study should be made of the ullage's chemistry from the standpoint of (2) above.

(2) The container material study should be enlarged to develop ceramic coated structural metals and noble metal plated common metals with diffusion barrier

11.0 RESULTS OF ANALYSIS AND STUDY

11.1 Reduced Gravity Considerations Applicable to 1/6 g Design

11.1.1 Introduction (refer to section 13.0)

An analysis of the proposed fused-salt 1/6 g cell design was performed to establish the likelihood of two potential problems:

1. Liquid-gas phase separation, and
2. Oxygen bubble release from the anode surface

This analysis discusses the examination made and presents preliminary results of findings .

11.1.2 Phase Separation - General

It is commonplace to consider the effects of gravity (body forces) as invariant in many engineering problems. When thinking is extended to "low" gravity, there is a tendency to extrapolate on an all-or-nothing basis and assume, incorrectly, that low and zero gravity are the same.

The potential for the basic phase separation problems concerns the extent to which reduced gravity forces exist in comparison with surface tension forces.

When gravitational forces are greatly reduced, other normally insignificant forces assume an increasingly important role. If a system involves only acceleration forces and surface forces, low gravity simply means that surface forces must be considered carefully.

When gravity is reduced to one-sixth its earth value, surface forces do become increasingly important, but do not overshadow gravity forces. Thus, integrity of a typical liquid-gas interface can be expected to continue. Containment of the electrolyte in the bottom of the cell can also be expected; however, a higher capillary rise will occur in small passages such as tubes, channels,and plates. In general and with regard to phase separation, if a specific cell functions in a 1 g earth gravity it will also function in one-sixth earth's gravity. There will be differences of course. Melt level position in the cell (and its control which depends on body forces) will be different. Oxygen bubble rise will be slower and more affected by drag forces.

11.1.2.1 Phase Separation - Electrolyte Properties - It is necessary to consider electrolyte surface tension and contact angles, since they must be employed in quantitative computations.

11.1.2.1 (Continued)

The surface tension of the Li_2CO_3/LiCl eutectic was calculated from experimental values of its components. Based on data of Janz (1), lithium carbonate surface tension is:

$$\gamma_{Li_2CO_3} = 247 \text{ dynes/cm. @ } 600C.$$

Smithells (2) shows the surface tensions of lithium chloride to be:

$$\gamma_{LiCl} = 138 \text{ dynes/cm. @ } 600C.$$

Combining these by means of a mixture relationship results in the approximation:

$$\gamma_m = \frac{\gamma_1 \gamma_2}{\gamma_1 X_2 + \gamma_2 X_1}$$

where:

γ_m is the mixture surface tension
γ_1 is component 1 surface tension
γ_2 is component 2 surface tension
X_2 is mol fractions of component 1
X_2 is mol fractions of component 2

For the Li_2CO_3/LiCl eutectic, therefore,

$$\gamma_m \approx 157 \text{ dynes/cm. @ } 600F.$$

Contact angle was measured experimentally by the engineering department during phase IIA employing the capillary rise method. Resulting from the measurement of the eutectic contact angle on nickel (INCO 200), it was found that $\theta \approx 25^o$.

11.1.2.2 Phase Separation - Eutectic Level - One of the preditable operating differences for the cell as designed, and between 1 and 1/6 g conditions, concerns the equilibrium levels of the liquid in various parts of the cell. Surface tension forces show that eutectic height within the 1/6 g cell will not be constant across the top surface of the eutectic.

For purposes of analysis, the cell can be divided into three regions:

1. anode chamber
2. cathode chamber
3. ullage volume

(See figure 11-1)

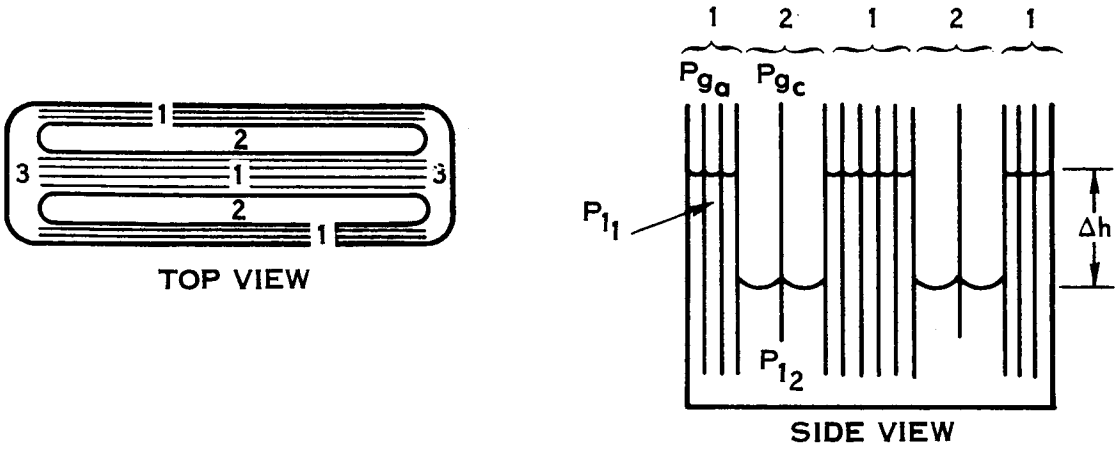


FIGURE 11–1. SCHEMATIC REPRESENTATIVE 1/6 g CELL (NOTE THAT ANODE PLATE CONFIGURATION AS DEPICTED IN THIS SCHEMATIC DIFFERS SLIGHTLY FROM THE 1/6 g CELL DESIGN AS SEPARATELY SUBMITTED.)

11.1.2.2 (Continued)

For purposes of determining eutectic rise levels, regions 2 and 3 may be combined since they are dimensionally similar.

Writing a force balance across the capillary surfaces.

$$P_{g_a} A_a - P_{l_1} A_a = S_a \gamma \cos\theta \quad (1)$$
$$P_{g_c} A_c - P_{l_2} A_c = S_c \gamma \cos\theta \quad (2)$$

By combining these equations and noting that,

$$P_{l_2} - P_{l_1} = \frac{\Delta h \, \rho a}{g_c} \quad (3)$$

we obtain,

$$\Delta h = \frac{g_c}{\rho a} \left[\left(\frac{S_a}{A_a} - \frac{S_c}{A_c} \right) \gamma \cos\theta + \left(P_{g_c} - P_{g_a} \right) \right] \quad (4)$$

where

Δh is the level difference, ft.
g_c is Newton's constant $\left(32.17 \frac{\text{lbm - ft}}{\text{lbf - sec}^2}\right)$
ρ is the liquid density, lbm/ft^3
a is the local acceleration, ft/sec^2
S_a is the anode perimeter, ft
S_c is the cathode perimeter, ft
A_a is the anode free area, ft^2
A_c is the cathode free area, ft^2
γ is the liquid surface tension, lbf/ft
θ is the contact angle (assumed as 25° for both carbon and nickel)
P_{g_c} is the gas pressure in the cathode, , lbf/ft^2
P_{g_a} is the gas pressure in the anode, lbf/ft^2

With a $= 5.36$ ft/sec^2 (1/6 earth gravity) and $P_{g_c} = P_{g_a}$)

and $\Delta h = 1.94$ inches (no carbon deposit on cathode)
$\Delta h = 1.64$ inches (with 1/4 inch carbon deposit on both sides of cathode)

11.1.2.2 (Continued)

It should be noted that the anode region includes that region which only contains an extended anode surface. The ullage region, if devoid of plates or baffles, will have the same level as the cathode region because of dimensional similarity. This was taken into account in determining the area and perimeter values used in equation (4).

11.1.3 Anode Oxygen Release

In the 1/6 g cell, oxygen is produced and released on a verticle anode surface which is swept upward and downward by the eutectic in a cyclic manner. As oxygen is produced at the anode, it nucleates at arbitrary points on the surface and, following an increase above a minimum partial pressure, forms bubbles. These bubbles are held on the surface by adhesion (surface) forces until they become large enough such that buoyancy (gravitational) forces cause their release. Once released from the anode surface they move upward to the eutectic-gas ullage interface. Since the eutectic is also in motion when a bubble forms and grows during the upward movement of the fused salt bath, it will break away at a smaller size (because of the added assist of the eutectic drag forces) than it will during the downward movement of the melt when drag forces oppose its upward motion.

In analyzing this situation, a simplified model has been assumed. Figure 11-2 shows the geometry involved.

It is assumed that the bubble is spherical and intersects the wall at the contact angle, θ.

A force balance yields:

$$-2K_1 \frac{d_w}{g_c} \gamma_1 \cos\theta \int_0^{\Pi/2} \cos\beta \; d\beta \pm K_2 V_\delta \frac{(\rho_1 - \rho_v)}{g_c} a \sin\alpha \pm K_3 A_\delta \frac{\rho_1 \bar{V}_1^2}{2 g_c} C_d = 0 \qquad (5)$$

where

K_1, K_2, K_3 are shape factors ($K_1 = K_3 = 1$; $K_2 = 0.95$)
g_c is Newton's constant (32.17 lbm-ft/lbf-sec^2)
a is local acceleration of gravity, ft/sec^2
C_d is drag coefficient on bubble
α is angle between surface and horizontal
d_w is diameter of circle of intersection, ft.
γ_1 is liquid-vapor surface tension, lbf/ft.
θ is contact angle.
β is an angular variable

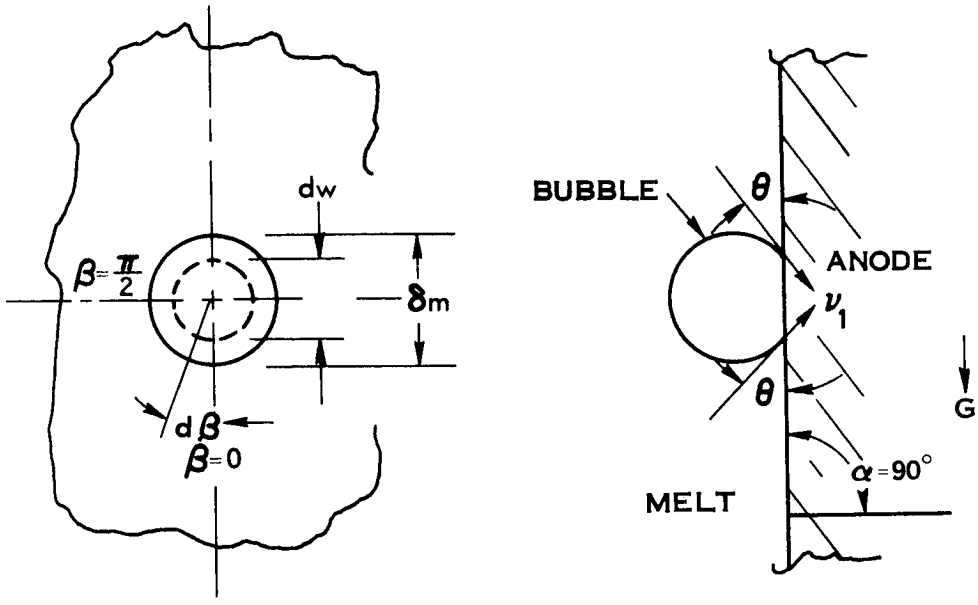


FIGURE 11—2. HYPOTHETICAL GEOMETRY OF BUBBLE ON VERTICAL ANODE

11.1.3 (Continued)

V_δ is volume of bubble, ft^3
ρ_l is liquid density, lbm/ft^3
A_δ is surface area of bubble, ft^2
$\bar{V}_l$ is liquid velocity, ft/sec.

When equation (5) was evaluated, the curves shown in figure 11-3 were produced. Figures 11-4 and 11-6 show the critical bubble diameter at break-away as a function of liquid velocity when the flow of liquid is downward for 1 g and 1/6 g, respectively. Figure 11-5 and 11-7 show the case when the liquid flow is upward.

Assuming a eutectic oscillation velocity of 0.66 ft/sec., it appears possible that oxygen bubbles could grow to approximately 1.25 inches diameter before break-away, with a downward flow at 1/6 g (about 0.375 inches at 1 g); and about 0.055 inches diameter with an upward liquid flow at 1/6 g (about 0.056 at 1 g). In the case of large bubbles, the effect of the gravity level is much more marked than in the case of small bubbles. This is believed reasonable.

Since the actual anode spacing varies from 0.08 inches to 0.232 inches, it is obvious that during the downward flow of the eutectic, bubbles may grow large enough to bridge the anode gap if sufficient time exists between subsequent oscillations of the eutectic across the plates to allow the formation of relatively large bubble diameters. In the event that the electrolyte "sweep" occurs too infrequently, or if it proves ineffective in removing bubbles before they increase significantly in size, the adhesion force will add to the difficulty of displacing anode adherent bubbles. Some tendency to plug the anode gap with froth will then reduce the effective anode surface and cause increased melt carry-over aside from possible decreasing scrubber performance.

11.2 Oxygen Bubble Terminal Velocity as a Function of "g" Level

Assuming a spherical bubble, the well known force balance gives:

$$\frac{\Pi D_b^{\,3} (\rho_l - \rho_v)\, a}{6\, g_c} = C_d \left(\frac{\rho_v}{g_c}\right)\left(\frac{\Pi D_b^{\,2}}{4}\right)\left(\frac{\bar{V}_b^{\,2}}{2}\right) \qquad (1)$$

where:

D_b is the bubble diameter, ft
ρ_l is the liquid density, lbm/ft^3
ρ_v is the vapor density, lbm/ft^3
a is the local acceleration of gravity, ft/sec^2
C_d is the drag coefficient
$\bar{V}_b$ is the bubble velocity relative to the fluid, ft/sec.
g_c is Newton's constant, $\left(32.17 \frac{lbm\text{-}ft}{lbf\text{-}sec^2}\right)$

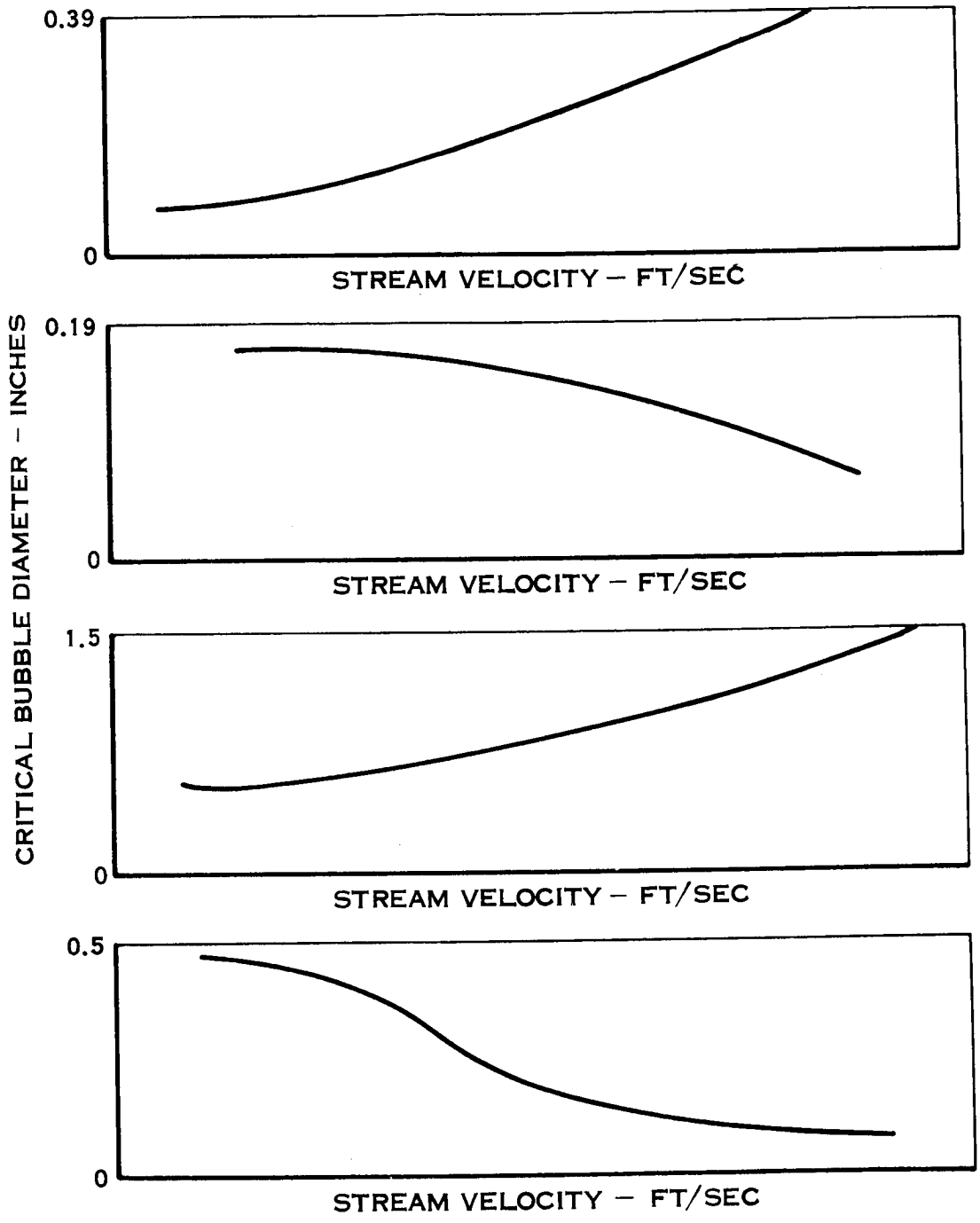


FIGURE 11–3. BREAK–AWAY O_2 BUBBLE DIAMETER AT ANODE VS GRAVITY LEVEL & DIRECTION OF ELECTROLYTE MOVEMENT

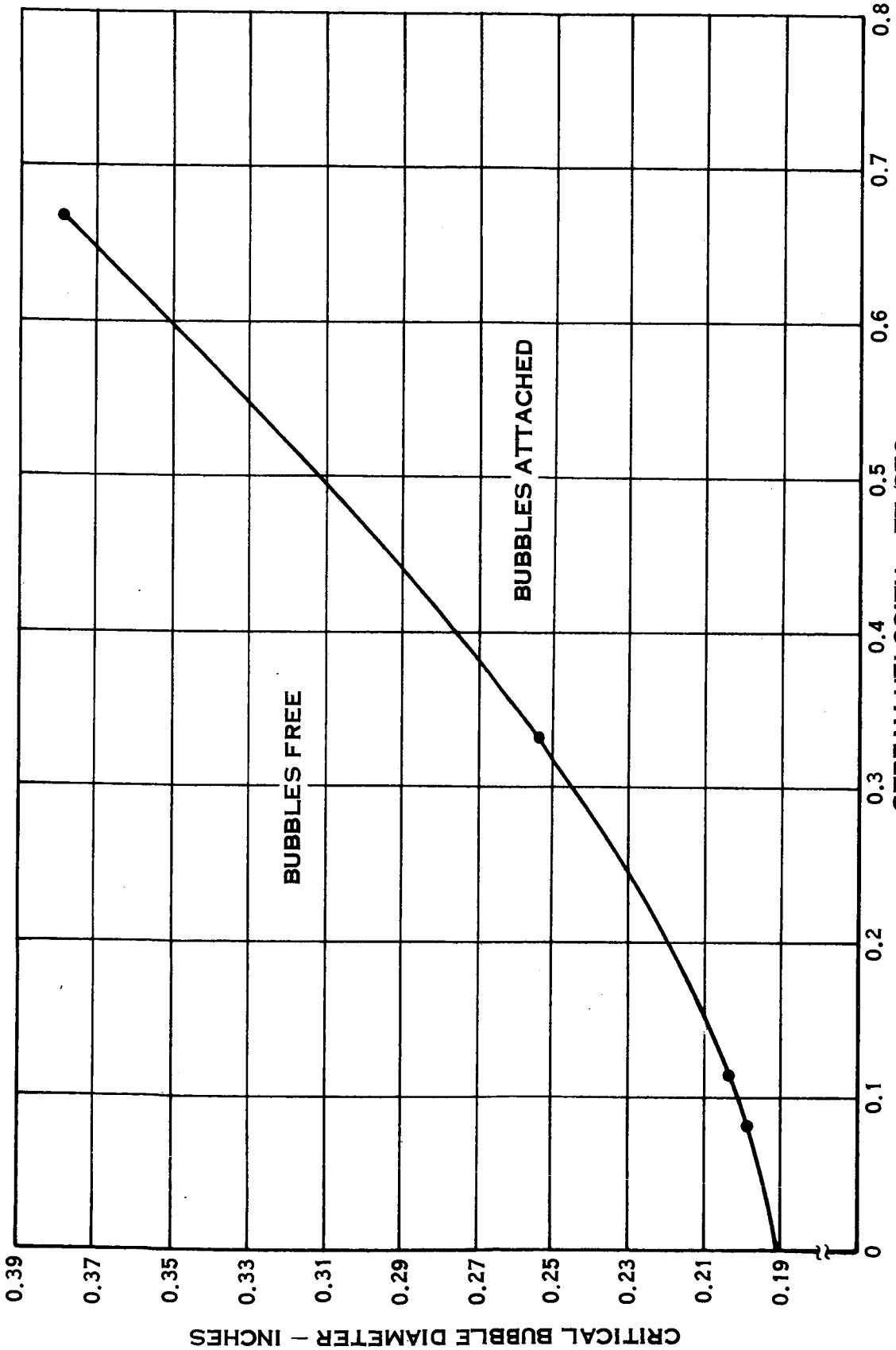


FIGURE 11–4. CRITICAL BUBBLE DIAMETER VS STREAM VELOCITY IN
a 1G FIELD WHERE DRAG AND ADHESION FORCES ARE
(–) WHILE THE BUOYANCY FORCE IS (+)

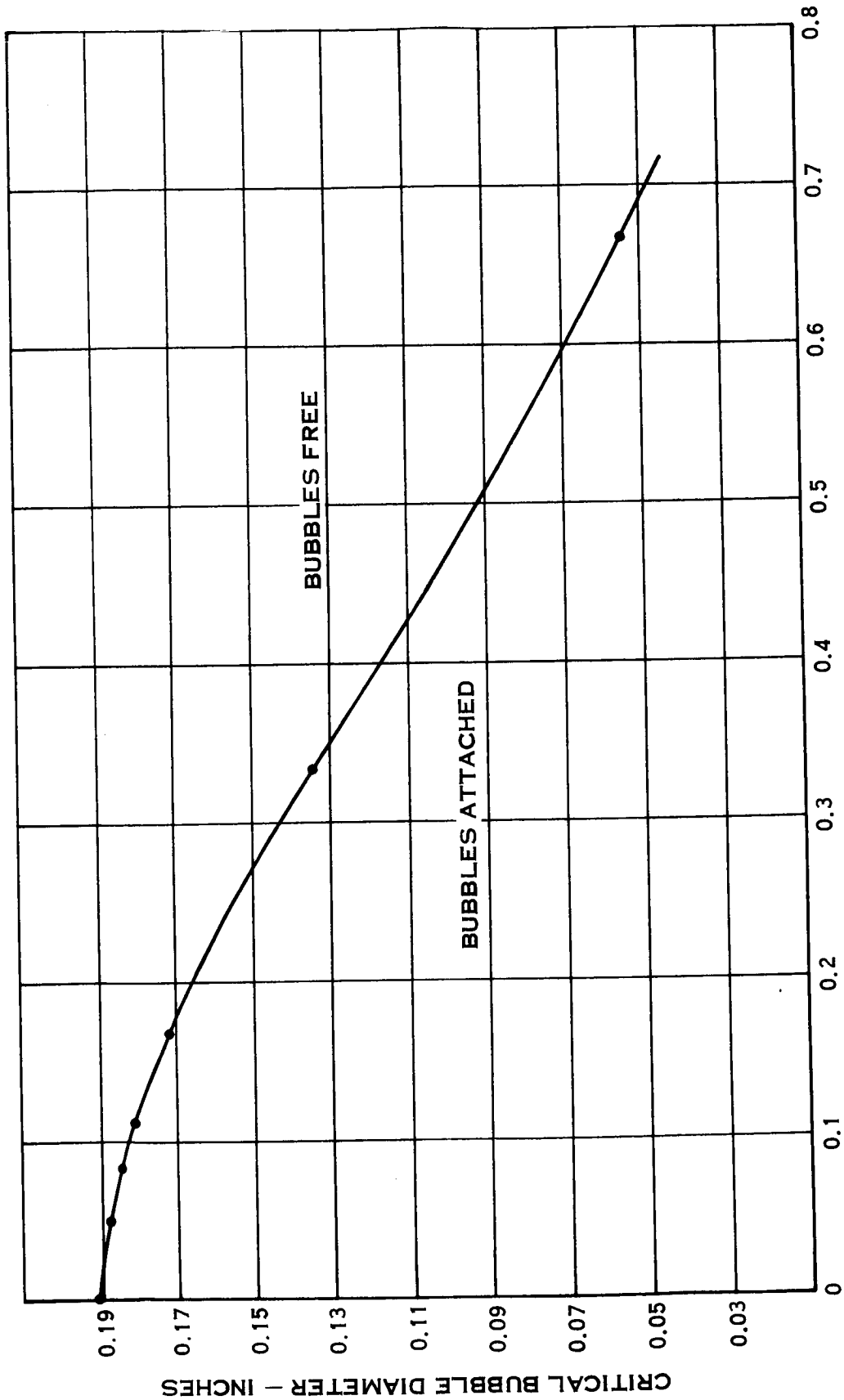


FIGURE 11–5. CRITICAL BUBBLE DIAMETER VS STREAM VELOCITY IN A 1G FIELD WHERE DRAG AND BUOYANCY FORCES ARE (+) WHILE THE ADHESION FORCE IS (–)

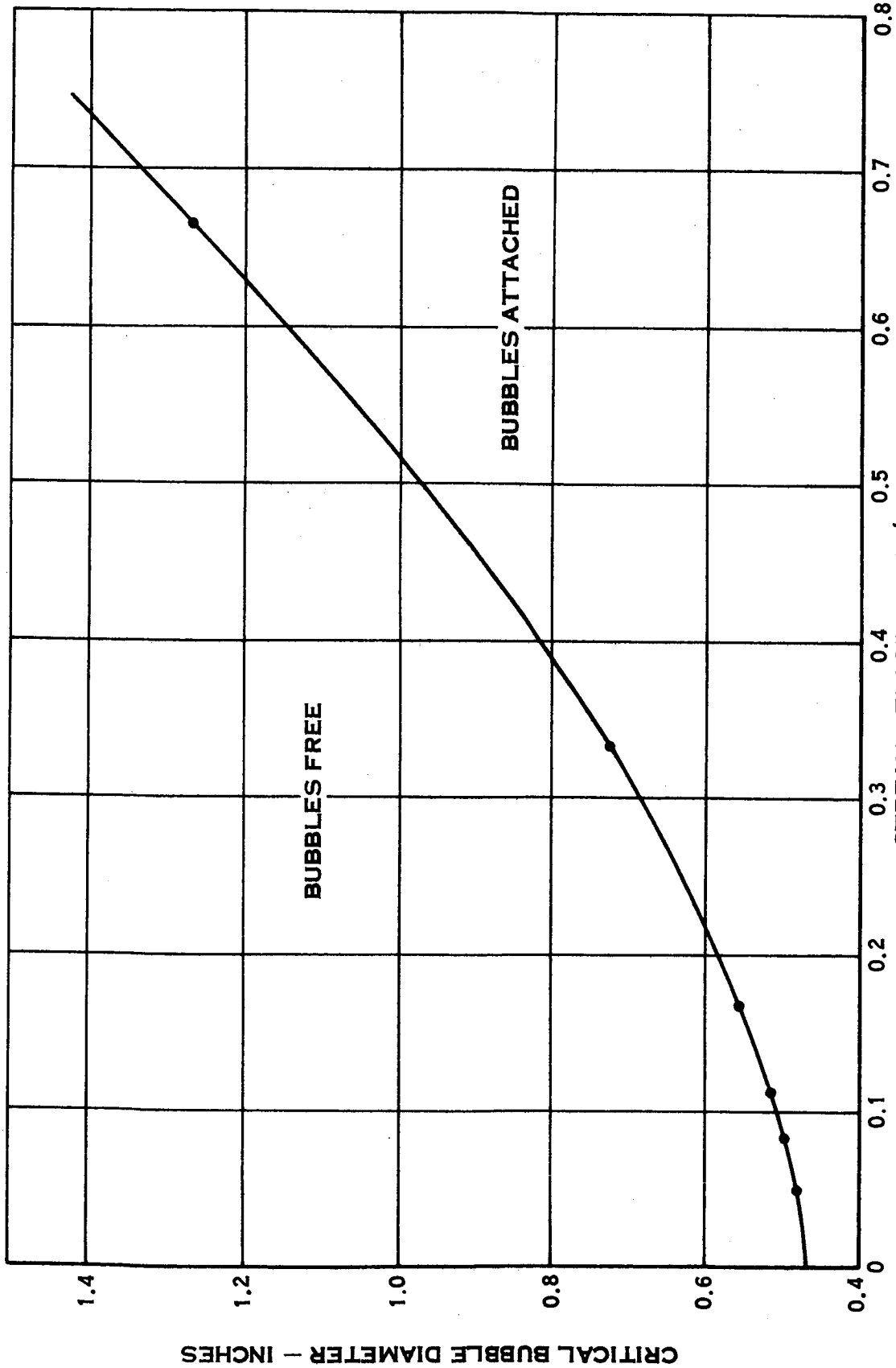


FIGURE 11–6. CRITICAL BUBBLE DIAMETER VS STREAM VELOCITY IN A 1/6 G FIELD. DRAG AND ADHESION FORCES ARE (–) WHILE THE BUOYANCY FORCE IS (+)

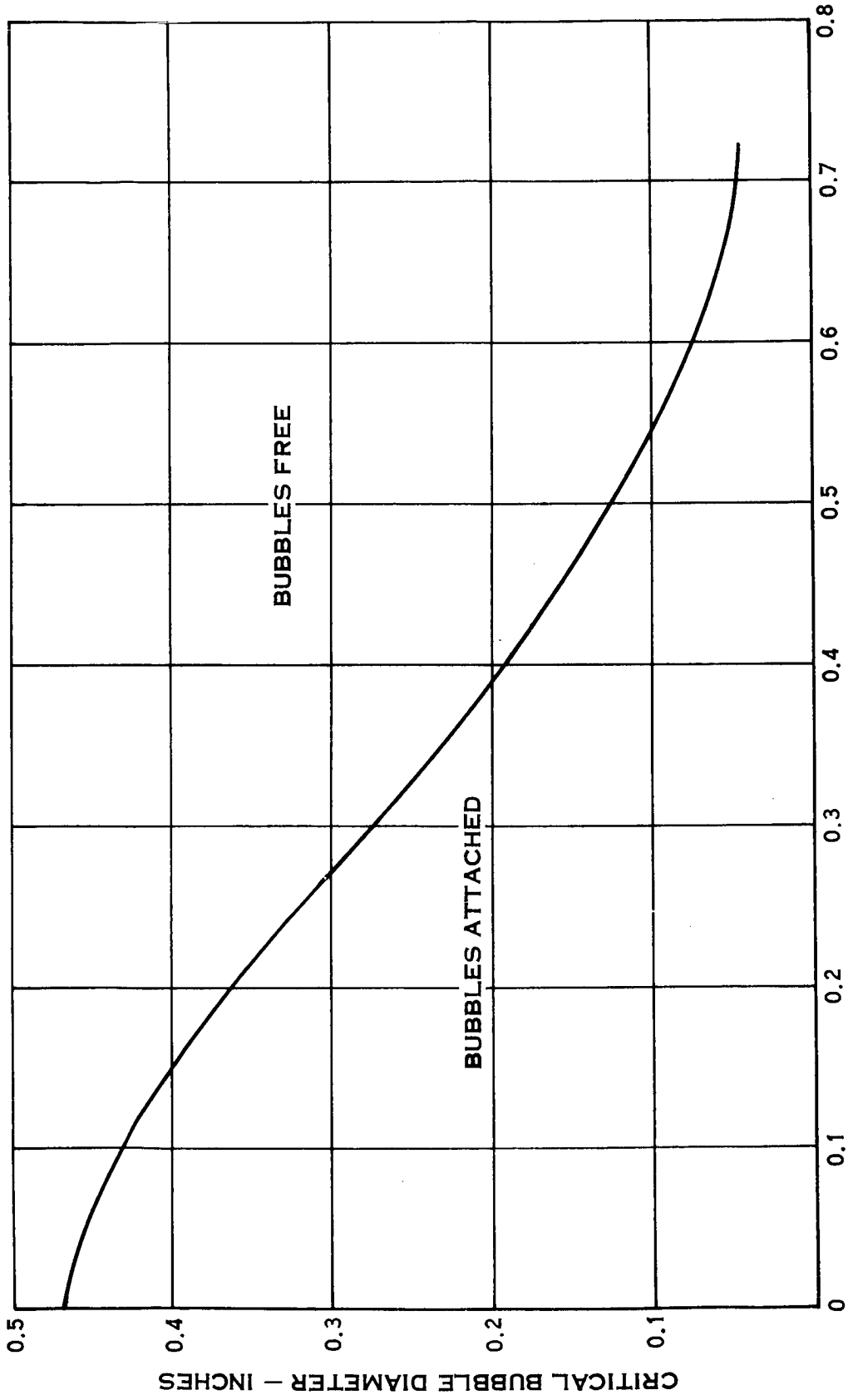


FIGURE 11–7. CRITICAL BUBBLE DIAMETER VS STREAM VELOCITY IN A 1/6 G FIELD WHERE DRAG AND BUOYANCY FORCES ARE (+) WHILE THE ADHESION FORCE IS (–)

11.2 (Continued)

If the Reynolds number is between 1 and 80,

$$C_d = \frac{24}{(N_r)^{2/3}} \qquad (2)$$

Making this substitution and solving for $\bar{V}_b$ yields

$$\bar{V}_b = \frac{(D_b)^{1.25}(\rho_1 - \rho_b)^{0.75}(a)^{0.75}}{(8.73)(\mu)^{0.5}(\rho)^{0.25}} \qquad (3)$$

The terminal velocity for the maximum bubble size which will break-away at 0.666 ft/sec. can now be calculated. From a previous analysis, this bubble size is $D_b = 0.555$ inches. Equation (3) then gives,

$$\bar{V}_b = 0.081 \text{ ft/sec.} \quad (N_r = 10.4)$$

With a fluid velocity of 0.66 ft/sec., the absolute bubble velocity is

$$\bar{V} = \bar{V}_f + \bar{V}_b = 0.66 + 0.081$$

$$= 0.74 \text{ ft/sec.}$$

Calculation of the terminal velocity of a bubble that breaks away during the downward flow of the eutectic is meaningless since these will more than likely bridge across the free space and the analysis would no longer hold.

From equation (3) it is evident that $\bar{V}_b = f(a)^{0.75}$. Thus, to calculate its value at earth gravity all that is necessary is a simple ratio, i.e.,

$$\frac{\bar{V}_{bg}}{\bar{V}_{b_{1/6g}}} = \left(\frac{a_g}{a_{1/6g}}\right)^{0.75} = 6^{0.75} = 3.83$$

$$\bar{V}_{bg} = (0.081)(3.83)$$

$$= 0.31 \text{ ft/sec.}$$

and $\bar{V}$ $= 0.66 + 0.31$

$$= 0.97 \text{ ft/sec.}$$

11.3 Analytical Model of CO_2 Scrubber Applicable to the Fused Salt Program

11.3.1 Introduction

Formulating an analytical model to describe the removal of carbon dioxide from a dilute gas mixture by absorption in a fuzed eutectic of LiCl - Li_2CO_3 undergoing

11.3.1 (Continued)

electrolysis is basically a straightforward problem in mass transfer. Similar absorption problems are discussed widely in the literature. Such discussions, however, do not consider a concurrent electrolytic process activity to control the concentration of the absorbate in the liquid absorbent.

11.3.2 Analysis Objective

The purpose of this analysis is to:

1. Present the fundamental relationships applicable to this problem,
2. Discuss the effect of electrolysis on the absorption process, and
3. Define parameters and variables of importance in testing and correlation.

11.3.3 Fundamentals - Two-Film Theory

Referring to figure 11-8, consider a gas mixture with a bulk CO_2 partial pressure $(pCO_2)_b$. The CO_2 is being scrubbed from the gas mixture by a liquid having a bulk CO_2 concentration, $(C_{CO_2})_b$.

The major resistance to mass transfer will be offered by the two boundry layers: the gas-side layer having thickness Z_g and the liquid side layer having thickness Z_l. Writing Wick's law for these laminar boundry layers gives:

Gas Side

$$N_{CO_2} = \frac{-Dg}{RT} \frac{(pCO_2)_b - (pCO_2)_i}{Z_g} \quad (1)$$

or

$$N_{CO_2} = k_g \left[(pCO_2)_b - (pCO_2)_i\right] \quad (2)$$

where:

N_{CO_2} - mass transfer rate, lb. mols/hr-ft^2
D_g - mass diffusivity of CO_2 in carrier gas, ft^2/hr.
R - gas constant, ft^{3}atm./lbmol-F
T - absolute temperature, degrees Rankine
Z_g - gas side boundry layer thickness, ft.
$(pCO_2)_b$ - bulk CO_2 partial pressure, atm.
$(pCO_2)_i$ - interface CO_2 partial pressure, atm.
k_g - gas film mass transfer coefficient, lbmol/hr.ft-atm.

Liquid Side

$$N_{CO_2} = -D_l \frac{\left[(C_{CO_2})_i - (C_{CO_2})_b\right]}{Z_l} \quad (3)$$

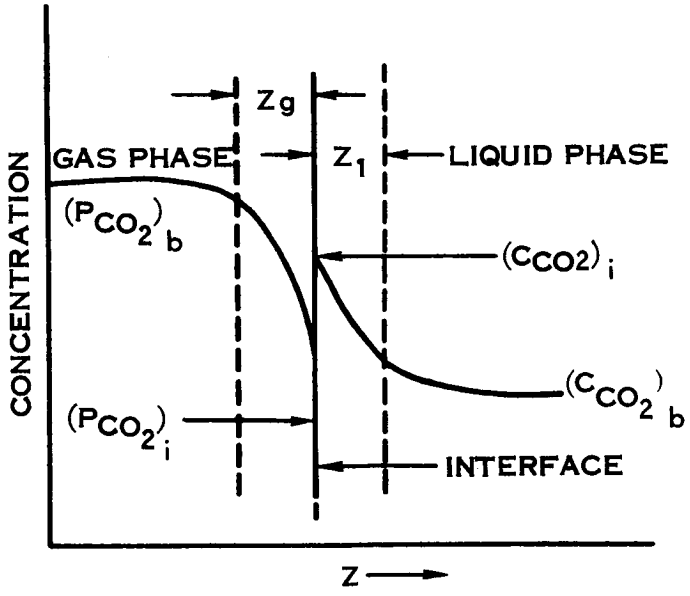


FIGURE 11—8. CONCENTRATION AS A FUNCTION OF DISTANCE THROUGH GAS—LIQUID INTERFACIAL FILM

11.3.3 (Continued)

or $$N_{CO_2} = k_l \left[(C_{CO_2})_i - (C_{CO_2})_b\right] \quad (4)$$

where all terms are as above except:

$(C_{CO_2})_i$ - interface CO_2 concentration, lb. mols/ft^3
$(C_{CO_2})_b$ - bulk CO_2 concentration, lb. mols/ft^3
k_l - liquid film mass transfer coefficient, ft/hr.

The interface discontinuity of the concentration profile shown in figure 11-8 is caused by the different expressions of concentrations used: partial pressure in atmospheres on the gas side and concentration in lb. mols per cubic foot on the liquid side. While another choice of units, specifically in chemical activity, would have resulted in a smooth profile, the units used are more conventional and convenient. Suffice it to point out that regardless of the units used, an actual continuity of mass does exist.

11.3.4 Equilibrium Mass Transfer Coefficients - Practical Considerations

Equations (1) through (4) are seldom useful for numerical computations because of the difficulty in determining either $(p_{CO_2})_i$ or $(C_{CO_2})_i$. Thus it is more useful to introduce fictitious concentrations which, nonetheless, can be evaluated.

As can be seen from the preceding equations, the mass transfer coefficients, k_g and k_l, are dependent on the diffusivity and boundary layer thickness of the gas and liquid respectively. The diffusivity, being a property of the diffusing system defined by designating the diffusing and non-diffusing materials, can be measured, for gases, as a function of absolute temperature and pressure. In general,

$$D_g = f\left(\frac{T^{3/2}}{P}\right) \quad (5)$$

In the case specifically at hand for CO_2 in air,

$D_g = 0.64$ ft^2/hr. @ 77F and 14.7 psia.

Correcting this for temperature gives:

$$D_g = (0.64)\left(\frac{1660}{537}\right)^{3/2} = 3.56 \text{ ft}^2/\text{hr}.$$

For the diffusion of gases in liquids, the relationships are less well developed. The following correlation is presented in the literature for electrolytes at infinite dilution:

$$D_l = 3.46 \times 10^{-9}\, T \left[\frac{(\lambda+^\circ)\,(\lambda-^\circ)}{(\lambda+^\circ)+(\lambda-^\circ)}\right] \left[\frac{(Z+) + (Z-)}{(Z+)\quad(Z-)}\right] \quad (6)$$

11.3.4 (Continued)

where:

D_l - diffusivity in ft^2/hr.
T - absolute temperature in degrees Kelvin
λ_{+}° - cationic conductance of infinite dilution in mhos/equivalent
λ_{-}° - anionic conductance of infinite dilution in mhos/equivalent
Z_+ - absolute valance of cation
Z_- - absolute valance of anion

Unfortunately, there is insufficient data available to allow the use of this equation to predict D_l. However, when data does become available later in the program, comparison with this equation will perhaps lend considerable insight into the diffusion process.

In order to analyze the effect of the boundary layer on diffusion, it's possible to use the analogy that exists between heat and mass transfer to predict a gas-side mass transfer coefficient.

It can be shown by dimensional analysis that for heat transfer,

$$Nu = \phi (Re)\ \psi (Pr)$$

where:

Nu - Nussult number
Re - Reynolds number
Pr - Prandtl number

and for mass transfer,

$$Sh = \phi (Re)\ \psi\ (Sc)$$

where:

Sh - Sherwood number
Re - Reynolds number
Sc - Schmidt number

Since k_g is part of the Sherwood number such a correlation is useful in determining its value.

For turbulent flow inside tubes, the heat transfer correlation is

$$Nu = 0.023\ Re^{0.8}\ P_r^{0.33} \qquad (7)$$

11.3.4 (Continued)

and the mass transfer correlation is

$$Sh = 0.023\ Re^{0.8}\ Sc^{0.33} \tag{8}$$

In the case of laminar flow, the most appropriate correlation seems to be that due to Langhaar (5) and presented graphically in (1) and (2). This shows:

$$Nu = f\left(\frac{Re \times Pr \times D}{L}\right) \tag{9}$$

where:

D is the tube diameter
L is the length of flow path

A similar correlation could presumably be used to determine k_l (assuming D_l were known). However, since correlations do not exsist which are applicable to liquids undergoing a "slosh" type agitation or internal electrolysis of the diffusing material, the relationships will ultimately have to be determined as part of the future program. Indeed, it is imperative that such testing be done if adequate sizing extrapolations are to be made or if off-design performance is to be examined.

There are numerous correlations in the literature, (5), (6), (7), (8), but because most of them were developed for large scale processing in the chemical industry, their usefulness is dubious. For the most part, scrubber design will have to be done by empirical methods

11.3.5 Emperical Postulations

For the purpose of empirical examination, consider figure 11-9. The solid black line represents the equilibrium line for the two phases, i.e.,

$$(p_{CO_2})_i = f(C_{CO_2})_i \tag{10}$$

which may be determined experimentally.

The coordinates of point I, $(p_{CO_2})_i$ and $(C_{CO_2})_i$, represent the interface condition at the location of interest in the scrubber. Point B defines the bulk concentrations.

Now consider point O on the equilibrium curve. Its abscissa is the bulk CO_2 concentration on the liquid side, $(C_{CO_2})_b$. Its ordinate represents a gas partial pressure, $p_{CO_2}^*$, equivalent to that liquid side concentration. If the equilibrium curve and $(C_{CO_2})_b$ are known, $p_{CO_2}^*$ can be easily determined.

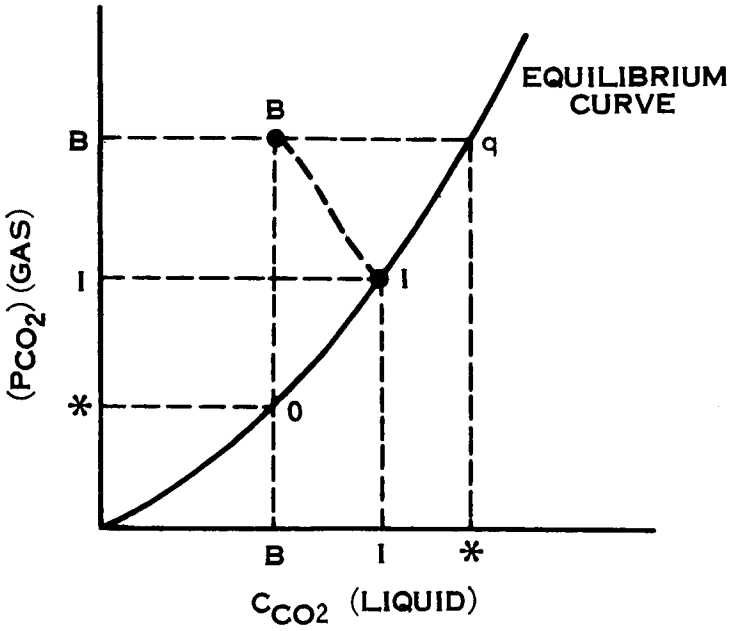


FIGURE 11–9. HYPOTHETICAL EQUILIBRIUM CURVES FOR CO_2

11.3.5 (Continued)

Further, it can be used to write an equation similar to (2) and (4) which is based only on bulk conditions.

$$N_{CO_2} = K_g \left[(p_{CO_2})_b - p_{CO_2}^*\right] \quad (11)$$

where K_g is the gas side overall mass transfer coefficient in lb/mols/hr-ft^2 atm.

In a similar fashion, by considering point q on the equilibrium curve, an expression can be written in terms of $C_{CO_2}^*$ the fictitious liquid side concentration equivalent to the bulk gas partial pressure. The equation in these terms is:

$$N_{CO_2} = K_l \left[C_{CO_2}^* - (C_{CO_2})_b\right] \quad (12)$$

where K_l is the liquid side overall mass transfer coefficient in ft/hr.

If the portion of the equilibrium curve of interest is a straight line, or nearly so, equation (10) can be written as:

$$(p_{CO_2})_i = m\,(C_{CO_2})_i + b \quad (13)$$

It follows then that

$$p_{CO_2}^* = m\,(C_{CO_2})_b + b \quad (14)$$

and

$$(p_{CO_2})_b = m\,C_{CO_2}^* + b \quad (15)$$

Furthermore, it can be shown by equating (11) and (12) that

$$\frac{1}{K_g} = \frac{1}{k_g} + \frac{m}{k_l} \quad (16)$$

and

$$\frac{1}{K_l} = \frac{1}{mk_g} + \frac{1}{k_l} \quad (17)$$

Equating (16) and (17) yields:

$$K_l = m\,K_g \quad (18)$$

11.3.6 Process Mass Transfer

The discussion up to now has centered on local mass transfer, i.e., at one point in the process equipment. If an entire process is considered, from inlet to outlet

11.3.6 (Continued)

as shown in figure 11-10 equation (11) can be written in terms of the log-mean partial pressure difference rather than the local difference.

The log-mean partial pressure difference is defined by

$$LMPD = \frac{[(pCO_2)_{b,i} - (pCO_2*)_i] - [(pCO_2)_{b,o} - (pCO_2*)_o]}{\ln \frac{[(p_{CO_2})_{b,i} - (p_{CO_2}*)_i]}{[(p_{CO_2})_{b,o} - (p_{CO_2}*)_o]}} \quad (19)$$

Using this to replace the bracketed term in equation (11) gives for the entire scrubber

$$N_{CO_2} = K_g (LMPD) \quad (20)$$

While a similar expression involving K_l and a liquid side log-mean concentration difference could be written, the above approach is favored because of the greater ease and convenience in working with the gas side where values are more easily measured.

The total transfer rate, R_{CO_2} is then given by

$$R_{CO_2} = K_g A M_{CO_2} (LMPD) \quad (21)$$

where:

R_{CO_2} - total mass transfer rate in lbm/hr.
A - mass transfer area in ft^2
M_{CO_2} - molecular weight of material transfered

In terms of the electrolytic current, assuming 100% current efficiency,

$$I = 4.05 \times 10^3 K_g A M_{CO_2} (LMPD) \quad (22)$$

where:

I - current in amperes

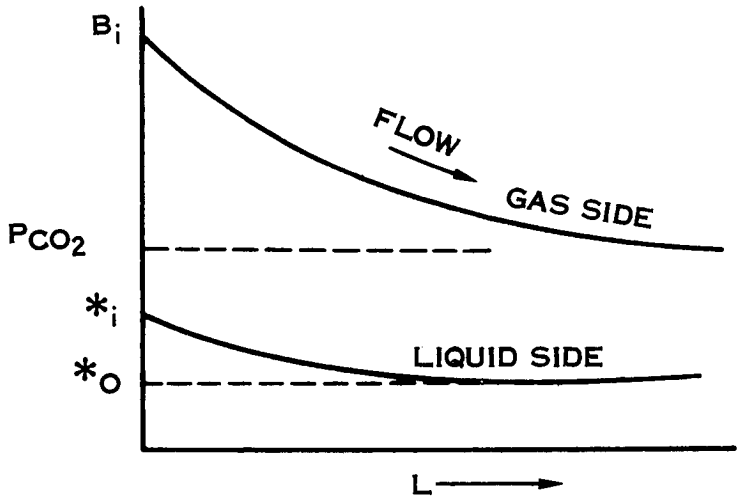


FIGURE 11–10. CONCENTRATION VARIATION IN SCRUBBER OF LENGTH L

References

1. Janz, G. J., and M. R. Lorenz, "Molten Carbonate Electrolytes: Physical Properties, Structure, and Mechanisms of Electrical Conductance," J. Electrochemical Soc., Vol. 108, No. 11, Nov. 1961, pp. 1052-1058.

2. Smithells, Colin J., (ed.), Metals Reference Handbook, Vol. 2, Butterworth and Co., 1962.

3. Kreith, F., Principles of Heat Transfer, International Textbook Co., Scranton, Pa., 1958. pp. 358, 489-506.

4. Kays, W.M., "Numerical Solutions for Laminar Flow Heat Transfer in Circular Tubes," Trans. ASME, Vol. 77, 1955, pp. 1265-1272.

5. Langhaar, H. L., "Steady Flow in the Transition Length of a Straight Tube," Journal of Applied Mechanics, Trans. ASME, Vol. 64, 1942, pp. A-55.

6. Rohsenow, W. M., and H. Y. Choi, Heat, Mass. and Momentum Transfer, Prentice-Hall, Inc., Englewood Cliffs, New Jersey, 1961.

7. Sherwood, T. K., and R. L. Pigford, Absorption and Extraction, McGraw-Hill Book Company, Inc., New York, 1952.

8. Treybal, R. E., Mass Transfer Operation, McGraw-Hill Book Company, New York, 1955, pp. 1-257.

9. Chemical Engineers' Handbook, Perry, J. H., ed., McGraw-Hill Book Company, New York, 4th ed., 1963, pp. 14-3 to 14-24.

10. Kirk-Othmer Encyclopedia of Chemical Technology, 2nd ed., Vol. 1, John Wiley & Sons, Inc., New York, 1963, pp. 44-75.

12.0 ONE-SIXTH GRAVITY CONCEPT SELECTION CRITERIA

12.1 Introduction

Beginning in February 1967, initial consideration was given to practical cell concepts available as potential condidates for the 1/6 g configuration to be designed later in Phase IIA. In approaching each of the candidate cell configuration possibilities, certain guide-lines, basic design objectives, and assumptions were defined with the intent of subjecting this trade-off evaluation to full discipline when warranted. This section summarizes and gives documentation to the review that subsequently resulted in the selection of the oscillating electrolyte concept. This is believed to be the most meaningful concept which could be pursued in this phase, in light of both immediate and long-term program objectives.

12.2 Basic Objectives of the 1/6 g Cell Complex to be Designed in Phase IIA

1. The concept selected must recognize and accept certain limitations in the-state-of-art to maximize assurance that it would be operable when subsequently fabricated.

2. 'Zero-gravity', as well as the 1/6 g environments, should be considered so that subsequent application of knowledge gained through design, fabrication, and subsequent testing would be applicable to the greatest extent possible toward the 'zero-gravity' ultimate objective of the direct CO_2 removal/reduction program.

3. Weight, volume, ability to withstand hypothetical launch loading, etc., would not be a direct objective of the concept selection, but would be considered in respect to ultimate limitations of specific configurations.

4. Simplicity (inherent reliability) would constitute a major objective.

5. The number of cells (perhaps inherent in one concept contrasted to the next) would be a major factor; the belief tends to be that a single cell involving a current flow of 450 amperes was disadvantageous; 6-9 cells each flowing 50 to 80 amps might be most satisfactory; but 30-50 cells would constitute an excessive array of manifolding, instrumentation, etc.

6. Automated cathode carbon removal would not be a major consideration of the 1/6 g laboratory prototype cell complex, as long as the configuration displayed a geometry consistent in potentially offering removal of the cathode deposit automatically in a subsequent phase.

7. The cell concept selected should avoid specific component configurations which might involve subsequent major development or experimentation.

12.2 (Continued)

8. Cost consideration, consistent with the foreseen need to minimize fabrication expense in subsequent phases, would be emphasized.

12.3 Specific Guide-Lines Pertinent to the Selection of a 1/6 g Configuration

1. Rotating cell (to achieve 1/6 g operability) should be avoided, if possible, to eliminate complications of bearings, multi-cell common drive linkages, and general complexity. Passive-phase separation devices should be used, if demonstrable to avoid cell compromises listed above.

2. A 'throw-away' cathode could be employed to minimize cell mechanisms required for carbon 'striping', if such mechanisms appeared impractical in view of funding or time restraints.

3. Air/CO_2 'scrubber-flow' would presume the inadequacy of 'sparge-tube' concepts for influent flow - arising out of foreseen difficulties with excessive electrolyte agitation and 'lift'; it was assumed that 'surface-scrubbing' must be employed.

4. The concept selected should allow sufficient space to provide cathode and anode surface areas yielding 70-110 and 9-20 ma/cm^2 current densities, respectively, unless breakthrough in these areas occurs early in Phase IIA.

5. A warm-up time of twenty-four hours preparatory to cell electrolysis would be acceptable.

6. The LiCl/Li_2 CO_3 eutectic would be assumed as the working electrolyte (due to lower associated operating temperature), unless it could be demonstrated that off-eutectic mixtures offered particular advantages.

7. In-so-far as possible, metals or metal composites would be employed as the basic cell complex structure, in contrast to all-ceramic construction to reduce thermal shock considerations, cost, ease of fabrication, joints, etc.

8. Consideration would be given to the frequency at which cathode deposits would be removed: 5-20 days being acceptable if done manually; no limitation should be imposed (except reliability considerations) if the replacement were to be accomplished automatically.

9. Melt, or it's constituents, could be replenished periodically as a result of vapor carryover or cathode inclusions by direct insertion or by pre-coating the cathode electrode.

12.3 (Continued)

10. Provisions would have to be made for:

    (a) Replacement of an individual cathode in the event that the deposit 'bridged' over to another cell component.

    (b) Controlling the temperature within the cathode (and all other) ullage areas, to prevent localized 'freezing' of the eutectic within this cell zone.

Assumptions To Be Made With Respect to the 1/6 g Cell Complex

1. Some form of relative motion between the cathode electrode and the cell electrolyte would be required by Phase IIA state-of-the-art to ensure achievement of an acceptable carbon deposit quality.

2. The use of metal or metal-ceramic composites would be assumed for the 1/6 g Phase IIA cell complex. Complete or major use of ceramics would be avoided.

3. CO_2 scrubbing, at a level of 3.8mm.Hg. within the influent air stream, would be supported by demonstrating the ability to surface-scrub during Phase IIA or during early Phase IIB.

4. A solution to the 'anode-life' problem would be solved so that anode life would not become a problem area and to necessitate provisions in the cell for periodic replacement of this electrode.

5. The early fabrication (during Phase IIB) of one or more 'cells' would allow the definition and solution of detail problems which would probably exist, so that the four-man rated cell complex, as ultimately fabricated in that phase, will satisfy the basic 'operability' objective listed previously in this section.

13.0 DESCRIPTION OF 1/6 G CONCEPT SELECTED FOR DESIGN/FABRICATION

13.1 Description

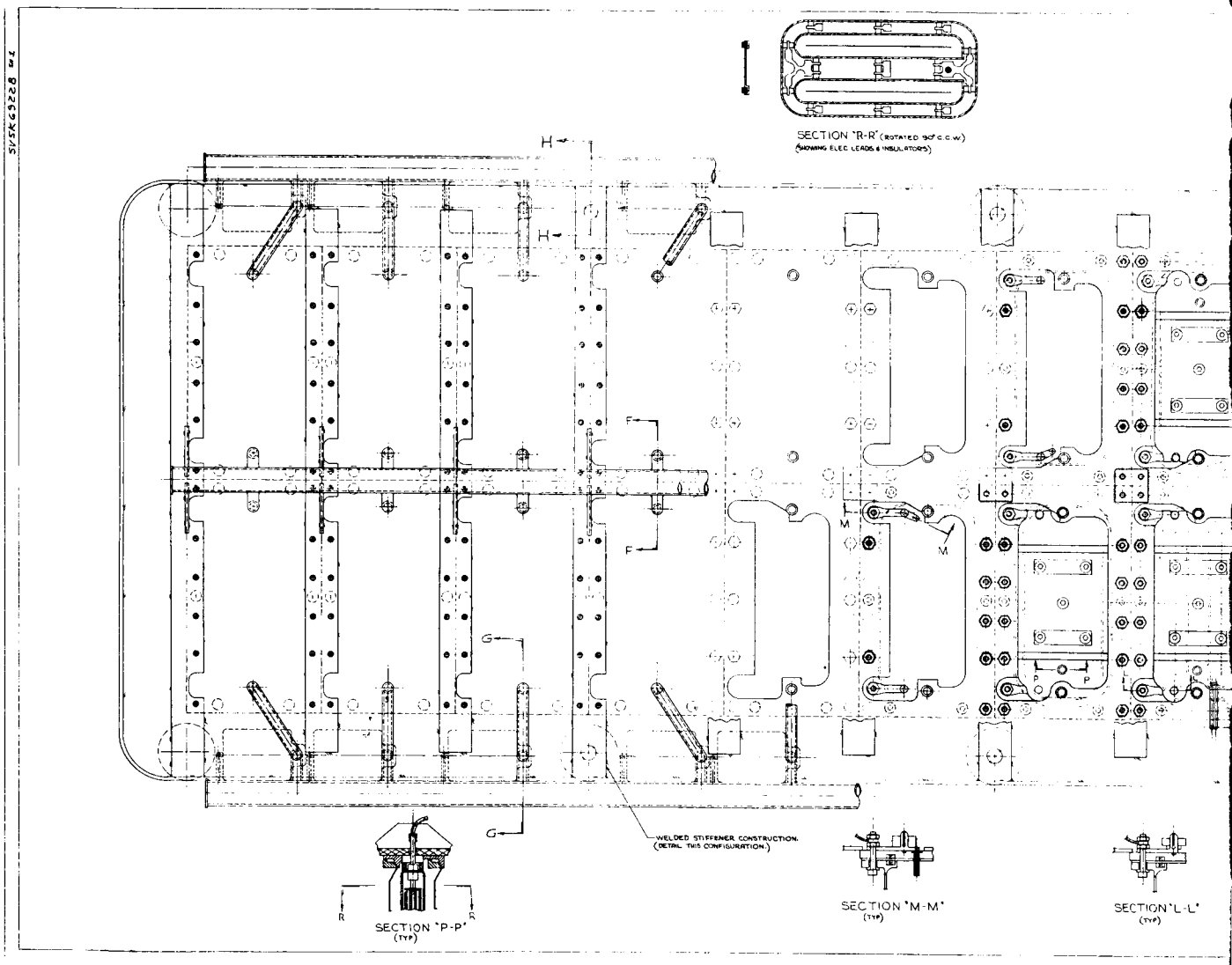
Figure 13-1 is a top view of the cell complex, which includes 18 half cells that work in conjunction to give the total carbon dioxide removal action required for a four-man mission. The complex is supported on a main support housing which provides for the mounting of each individual half cell. It has an ullage space over the top of the cell cathode covers. It also houses manifolds and wiring connections.

In figure 13-1, the cathode cover is a ceramic item that supports a pair of cathodes for each half cell. The cathode cover is placed in position over both the cathode terminal guide pin and the guide pin at the other end which locates this cover. In addition to the cathode terminal guide pin, there is an auxiliary cathode probe at the opposite end of the cell. The terminal for the auxiliary cathode probe is opposite to the cathode terminal. The auxiliary cathode probes are toward the center of the complex and the cathode terminals are on the outside edges of the complex. Beyond the structure shown in Figure 13-1, there is a heavy layer of insulation completely surrounding the ullage cover and the cell complex. The outside dimensions of the completed cell complex in the top view are approximately 26 inches wide by 52 inches long. The height of the total enclosed complex is approximately 15 inches. The insulation is approximately 3 inches thick.

Figure 13-2 shows a vertical section of a typical half cell. The basic structure of the half cell is approximately 3 inches wide by 7 inches high by 7 inches long. The elements referred to in Figure 13-2 show essentially all the working components; the parts are also referred to in Figure 13-1, in addition to the auxiliary cathode probe which is a control element. The cathode cover contains the cathode bus bar, which is the structural and electrical transmission component for each half cell. A pair of cathodes is clamped using the cathode clamps. The cathode itself is a plate approximately 5 inches wide by 5 inches high by 0.010 inches thick. The pair of cathodes is located within the half cell structure in a pair of cathode wells. The space surrounding the cathode wells is anode space almost filled with ruffled metal anode plates. The anode plates are supported and separated from walls by ceramic insulators. All the anode plates are electrically connected and each group of plates (such as the center group and the two outside groups) are physically connected together but not to each other. The individual anode sections are removed separately even though they are connected electrically. A clamp is removed from the terminal of each section before removing the total anode from its location. The cathode cover rests on the main support housing. The unit half cell is clamped to the main support housing from the bottom side and through a half cell insulator. The cathode well and the main half cell housing is sealed to the ceramic insulator with omega seals. The construction of the half cell is such that when the cathode cover is removed, the cathode plates come out with it and when the half cell support screws are removed, the housing, the anode, the cathode wells and the insulator are removed from the main support housing as a unit. At the lower section of the cell, there are two sets of bubble screens: a vertical set and an angled set.

THIS PAGE IS BLANK

PRECEDING PAGE BLANK NOT FILMED.



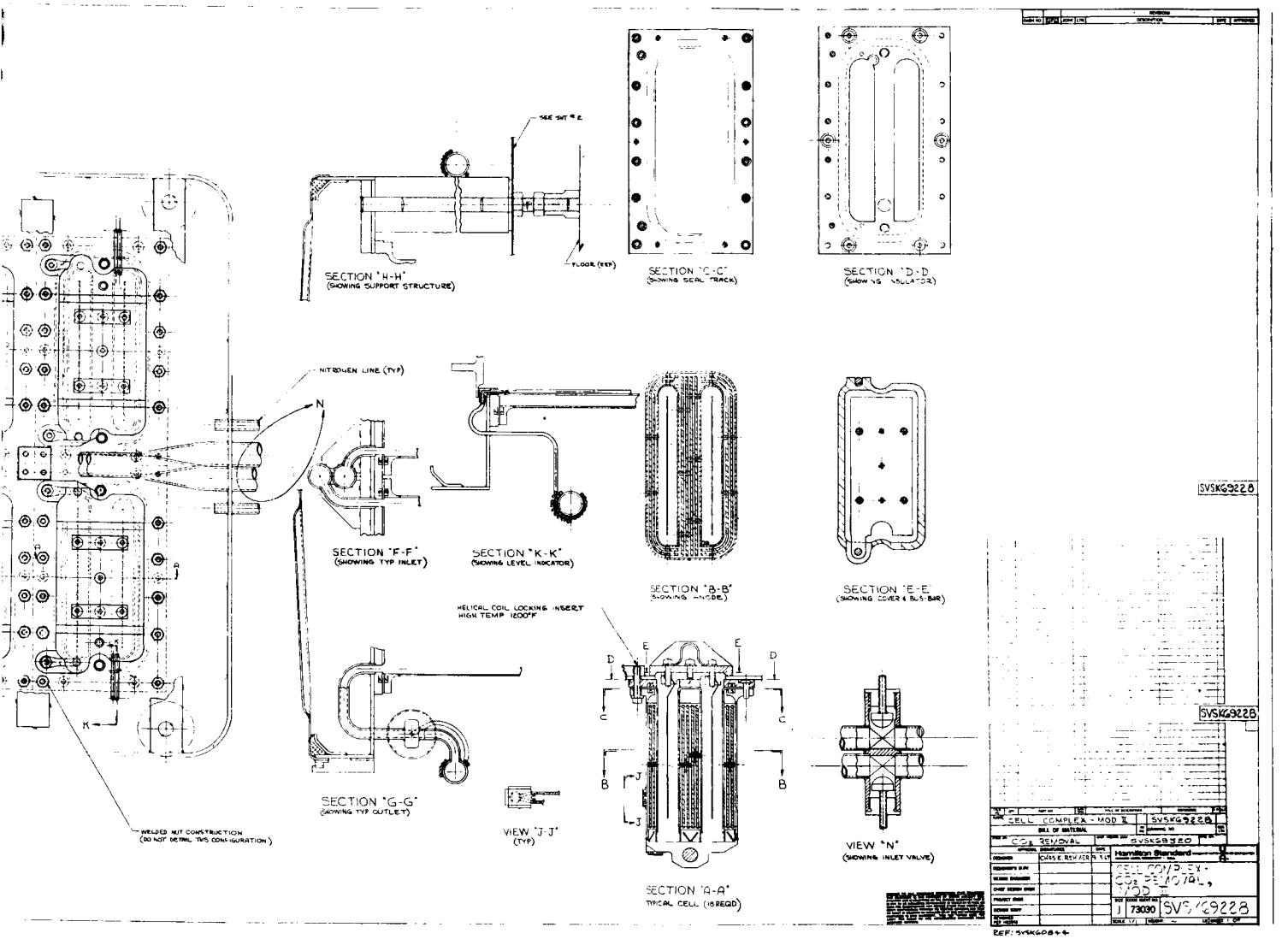
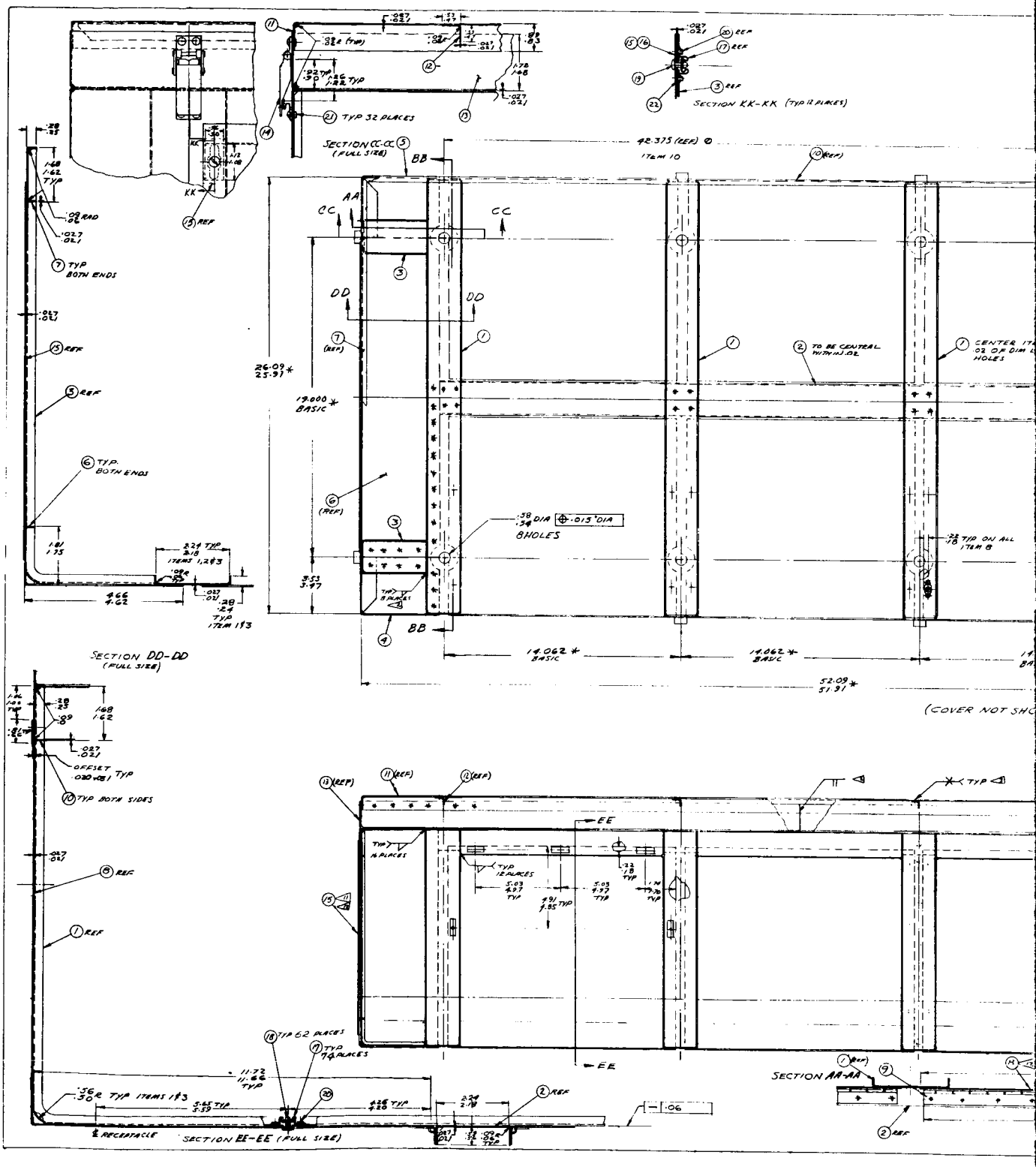


FIGURE 13–1. CELL COMPLEX CO_2 REMOVAL MOD. II (SHEET 1 OF 2)


SECTION CC-CC (FULL SIZE)
SECTION KK-KK (TYP 12 PLACES)
SECTION DD-DD (FULL SIZE)
SECTION EE-EE (FULL SIZE)
SECTION AA-AA
42.375 (REF) @ ITEM 10
26.09 * 25.91
19.000 * BASIC
14.062 * BASIC
14.062 * BASIC
52.09 * 51.91
.38 DIA .34 8HOLES
.013 DIA
TO BE CENTRAL WITH DIM .02
TYP BOTH ENDS
TYP BOTH SIDES
OFFSET .030 +.01
TYP 32 PLACES
TYP 62 PLACES
TYP 14 PLACES
TYP 12 PLACES
TYP 4 PLACES
TYP ON ALL ITEM B
ITEMS 1,2 & 3
RECEPTACLE
(COVER NOT SHO

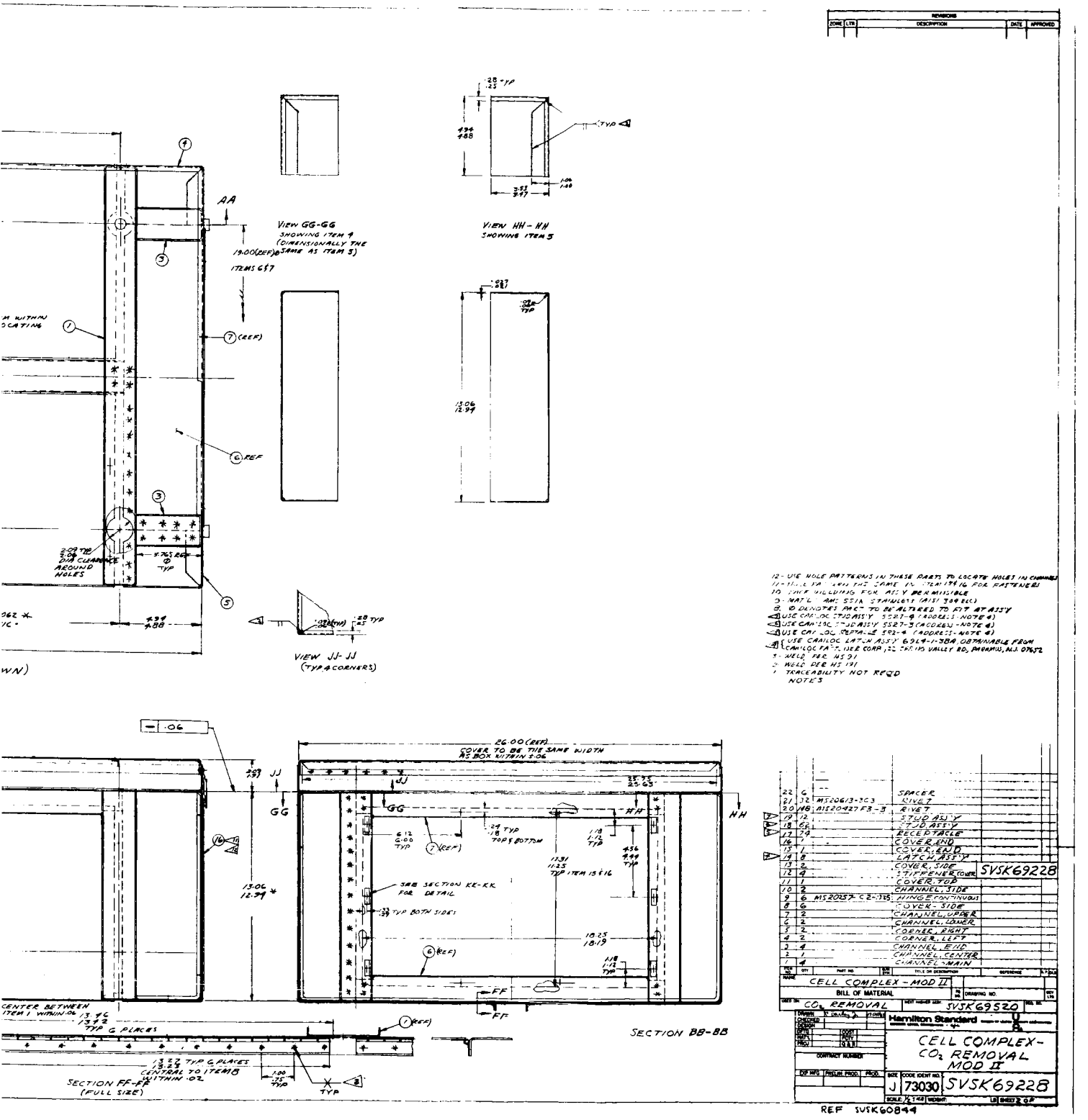


FIGURE 13–1. CELL COMPLEX CO_2 REMOVAL MOD. II (SHEET 2 OF 2)

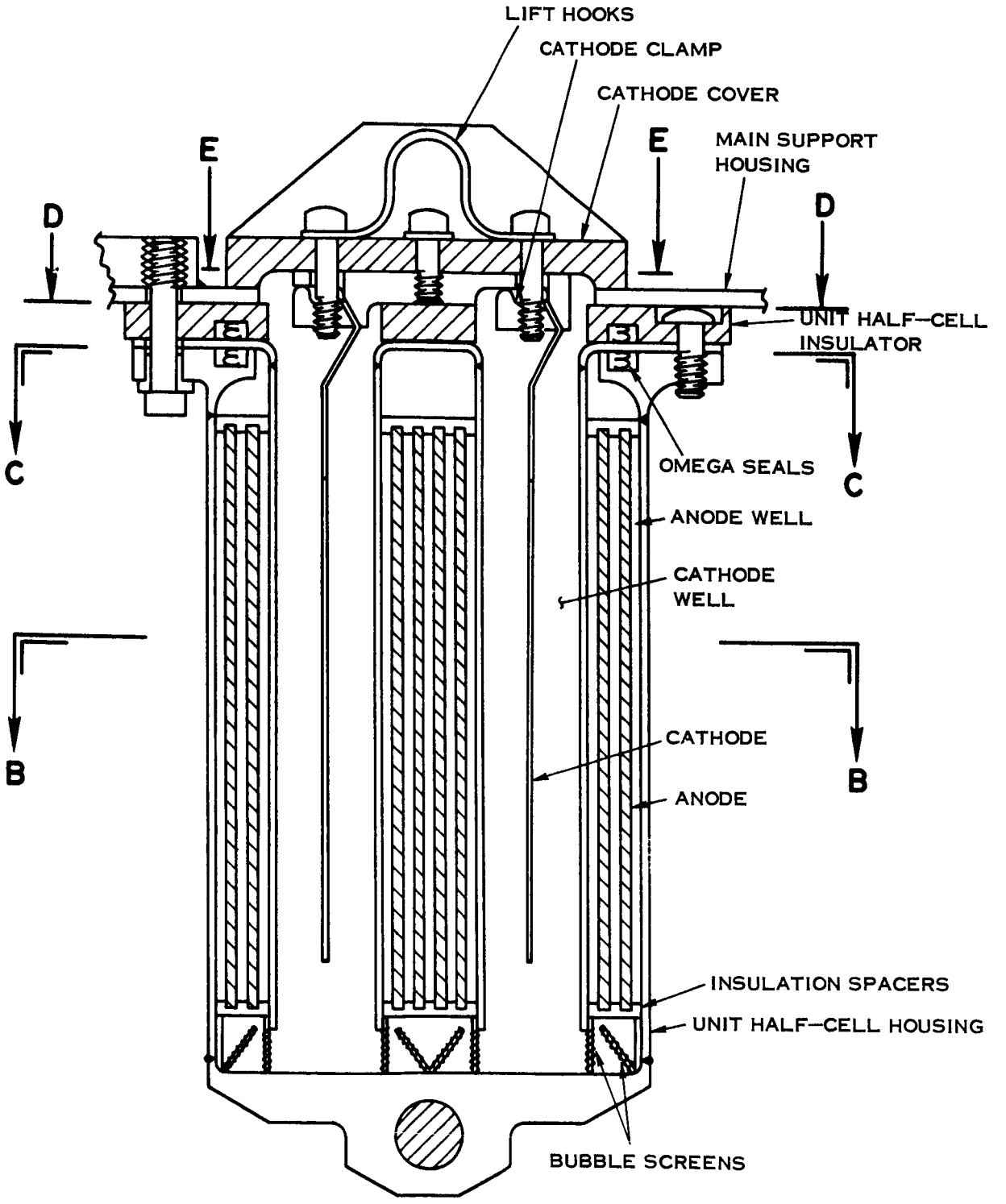


FIGURE 13-2. TYPICAL CELL (18 REQD)

13.1 (Continued)

The vertical set tends to be an absolute screen while the angular set tends to reduce the amount of bubbles that can get to the vertical set. In addition, it serves as a trap for loose material. The purpose of the bubble screens is to prevent the migration of oxygen bubbles into the cathode region. The anode plates are used as a combination anode for the electrolysis process, the upper portion being used as a scrubber. The plates are wetted by the cyclic action of the electrolyte and then exposed to the incoming air. The cyclic action of the electrolyte not only wets the scrubber but also permits the release of oxygen bubbles growing on the anode plate during the electrolysis action. The bottom of the half cell is a heavy structure which contains the unit heater. The heater is used to originally melt the salts and to maintain a proper temperature during the operation of the unit. Two temperature sensors are located on the outside of the half cell: one at the bottom of the cell next to the heater, and the other on the side of the cell opposite the low point of anolyte excursion.

The electrolyte is caused to move up and down in a preset frequency of excursion. The frequency of that excursion is determined by the melt quality controls. In the cathode region, the electrolyte moves approximately 4 1/2 inches from its upper to its lower level. In the anode region, the electrolyte moves approximately 3 inches between its high and low level. The excursion of the electrolyte and the quantity of electrolyte originally included in the cell is such that the cell does not fill completely to the cover, so that there is no danger of overflow of electrolyte into the cathode ullage space.

There are both high level and low level sensors (see figure 13-3). These sensors are small hollow tubes connected to a fluidic sensing and control system. The function of these sensors is to detect the level by a cutoff of the gas of the ullage space (a low pressure flow of nitrogen gas). The tubes give discrete and unique signals by means of each tube having an opening at a different level. The high level tube has an opening at the point at which the upward excursion of the catholyte should be reversed, and the low level sensor has an opening at the point where the downward excursion should be reversed. In operation, the catholyte level is maintained by a small oscillatory motion about the end of the selected sensor - whether high or low depending on the cycle of excursion. Also indicated in figure 13-3 is the auxiliary cathode probe, a ceramic armored metal cathode placed to contact the anolyte at the high level of its excursion. Its function is to pass a small amount of current between the end of this probe and the anode so that the quality of the melt may be detected and controlled.

Figure 13-4 is a horizontal section of the unit half cell just below the cathode cover. The cathode cover is shown as a surrounding cross-hatched outline, having at one end the cathode terminal which feeds current into the bus bar and then into the cathode plates. At the other end is a guide pin which serves to index enplacement of the cathode cover to assure proper orientation.

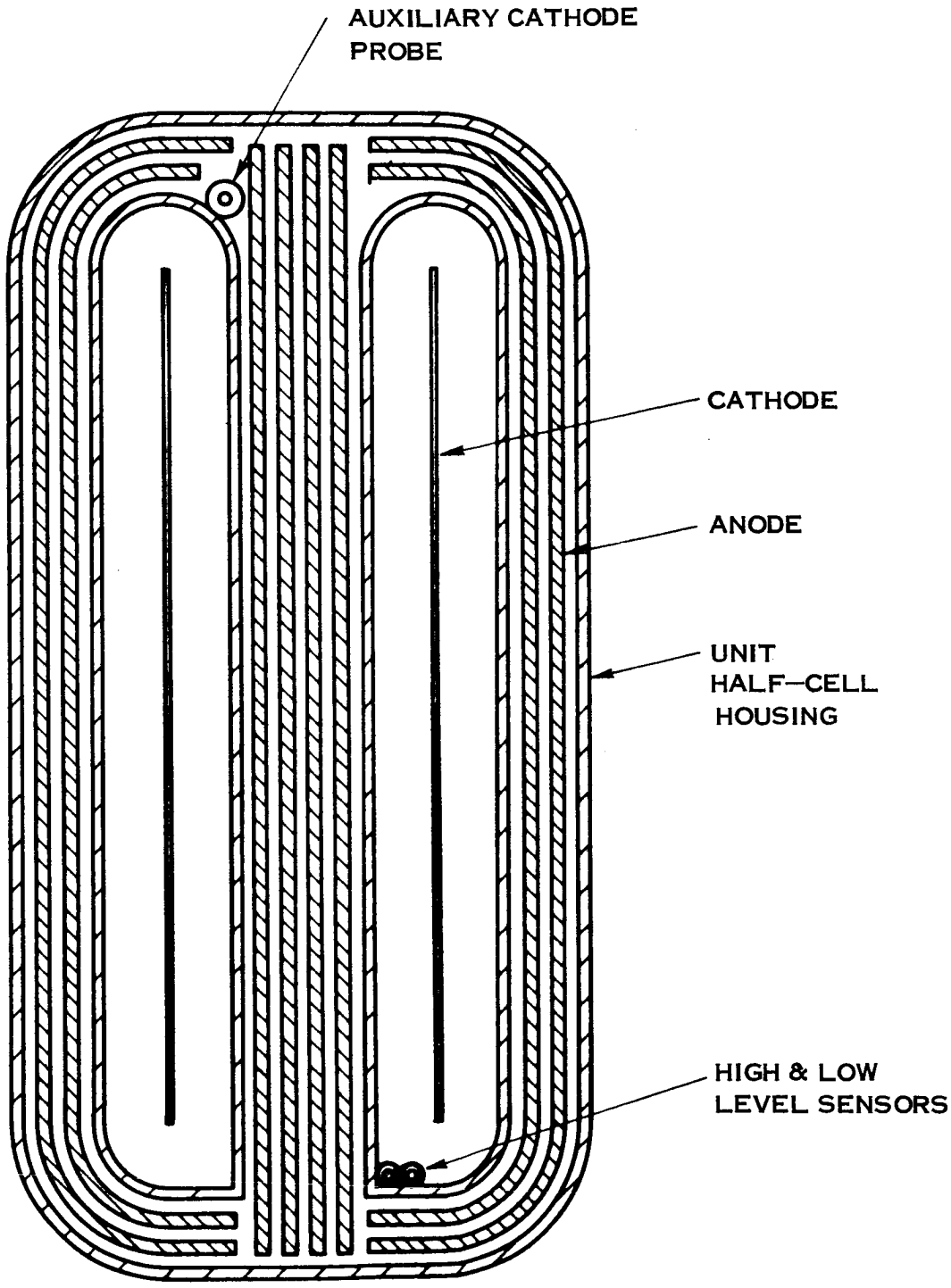


FIGURE 13-3. ANODE

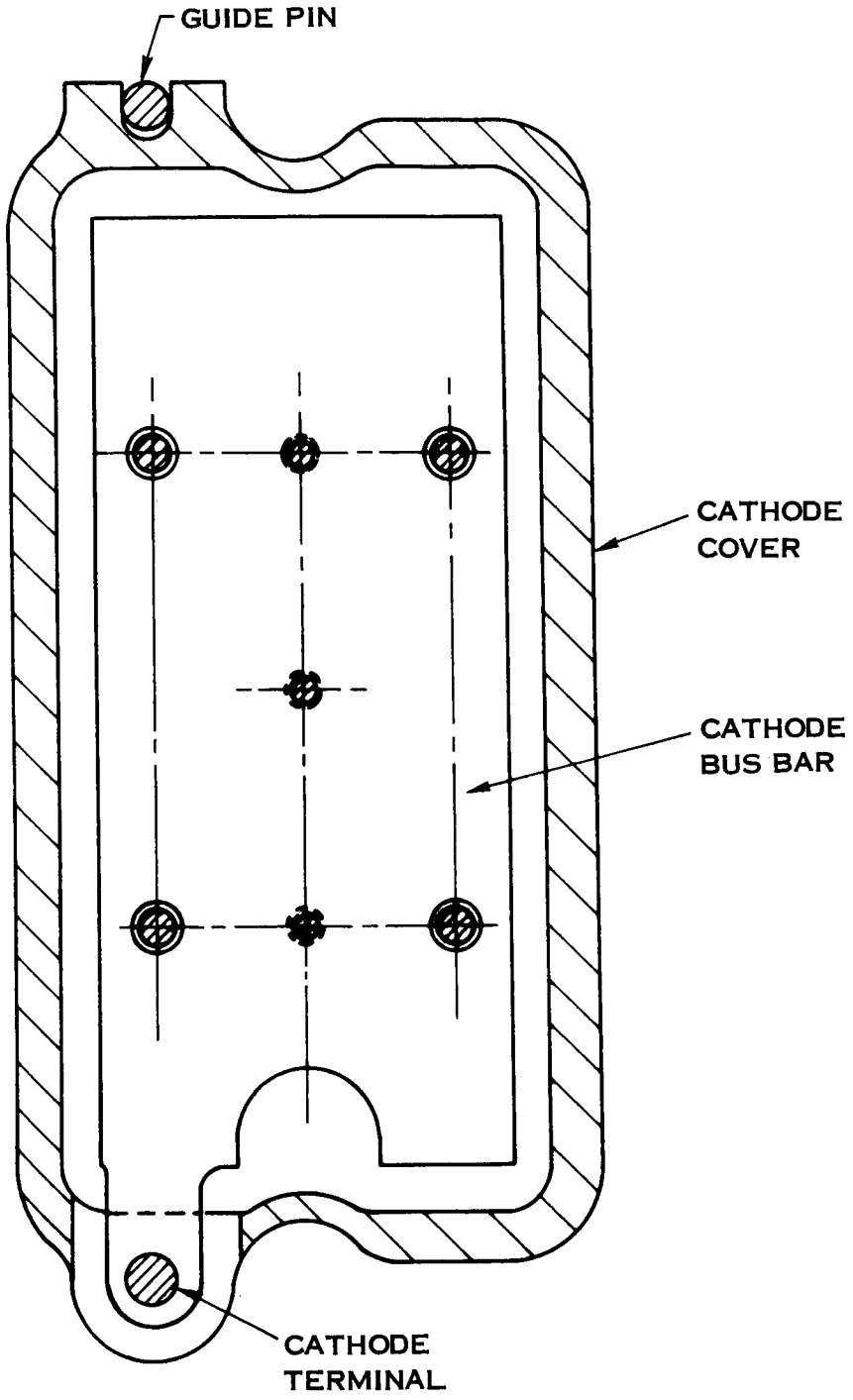


FIGURE 13–4. COVER & BUS BAR

3.1 (Continued)

Figure 13-5 shows a section that includes the air from the cabin manifolding. Two manifold tubes are run the length of the cell complex one over the other. Smaller tubes go to each unit half cell from the manifolds. The manifold is split into two sections so that the balance valves outside of the cell complex can adjust and balance the flow to each bank of half cells. The electrolyte excursion is controlled so that the electrolyte within half of the cells of the complex is raised in the cathode while the other half has the electrolyte depressed in the cathode space. The electrolyte excursion is caused by cyclic change in pressure in the air manifolds. The pressure in each bank of the air manifolds is cycled by the control of the servo-throttling valve in the outgoing portion of each cell circuit. The servo-throttling valve is shown in Figure 13-6. The servo-throttling valve consists of a housing around a bellows that is responsive to very low pressure outputs of the fluidic control system. The other end of the bellows, which also has the throttling vane, reflects the pressure of the air inside of the particular half cell. The position of the throttling vane is controlled by the action of the level sensors. When it is desired to lower the electrolyte in the cathode space, the throttling vane is withdrawn. This reduces the pressure drop in the particular half cell to a minimum, in turn permitting the gas pressure in the ullage space to push the electrolyte down in the cathode space and up in the anode space. When it is desired to raise the level of the electrolyte in the cathode space, the pressure in the anode space is increased by closing the throttling valve. The servo throttling valve is self-energizing from the pressure within the unit half cell. As the electrolyte level reaches the high level sensor, a reversing signal is given to the servo-throttling valve. The throttling valve is withdrawn until the pressure starts to drop and the electrolyte in the cathode space goes down below the end of the level sensor. At this point, the procedure is reversed. Thus, as long as the signal is present to maintain the high level position, the electrolyte will oscillate about the end of the high level sensor.

The entire complex, emphasizing support and insulation, is shown in Figure 10-7. The cell complex consisting of 18 unit half cells is supported by a series of 8 ceramic legs. These ceramic legs are insulated from the unit half cells, as they transmit heat at a greater rate than the outer insulation. The insulating legs are hollow to accept the ends of the leveling screws to permit setup, shipping, leveling and final location. The insulation is enclosed in a protective sheet metal housing which presents a pleasing business-like appearance as well as protecting the thermal insulation. It will be noted that there are no dynamic seals used in any portion of this cell complex. The only moving portion of the whole cell complex is the electrolyte which is driven by difference in gas pressure. Containment and control of electrolyte under one-sixth g is strictly by configuration control. In other words, capillary passages are provided to control the levels of the liquids at all points by employing the surface tension characteristics of the fluid.

The excursion of the electrolyte is such that the cathode is completely exposed when the electrolyte is at its lowest level, and the cathode is exposed to the cathode ullage gas. The half cells in each bank are so connected in a cycle such that the passage of

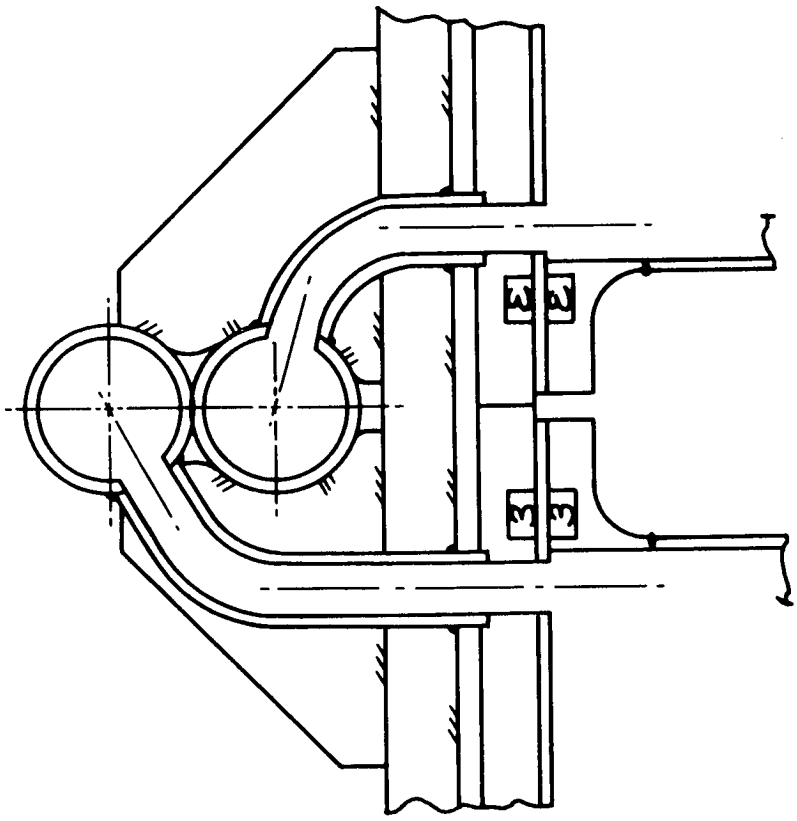


FIGURE 13–5. TYPICAL INLET

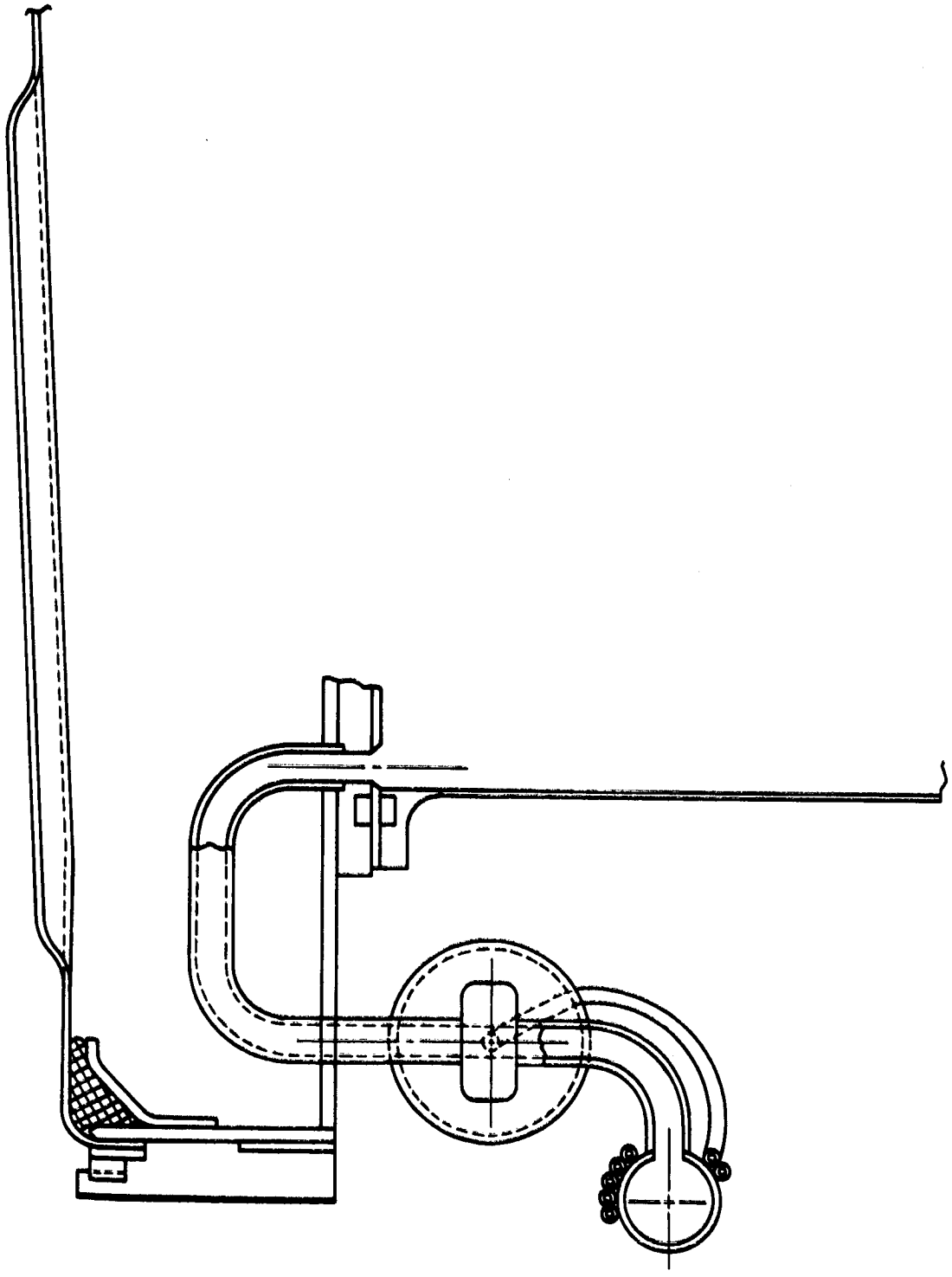


FIGURE 13–6. TYPICAL OUTLET

13.1 (Continued)

current through the complex is continuous, while in one bank of half cells the cathodes are completely exposed (having broken the current passage). The other bank of half cells has the cathodes completely immersed and is carrying the full load current. Continuous action at all times, therefore, exists to remove and reduce carbon-dioxide.

13.2 Considerations and Discussion of Description

The anode plates are so formed and are of such dimensions that they act both as anodes on the portion of the electrolyte that is always immersed and as a scrubber on the portion that is only immersed during the high anolyte excursion. This construction simplifies the design of the cell, while performing the desired functions without penalty due to size or configuration. The ruffled anode plates consist of 0.004 inch thick, 82% gold, 18% nickel sheet ruffled into a form that has a projection of 0.080 inch high. This arrangement gives approximately 2 square inches of anode surface for every square inch of projected area. The configuration of the ruffles, in addition to extending the area within the given space, also tends to give a certain amount of turbulence to the air flowing through the passages.

The cathode is a simple flat plate which helps control the buildup of carbon. The space allowed from the cathode to the cathode well wall is 3/8 inch. Based on an assumed 1/4 inch carbon growth, 1/8 inch of clearance is allowed. This would account for possible uneven growth of carbon at local spots. The cathode cover is designed so that a spare set of covers can be provided. The spare set may be stored, ready for cathode change. It is recommended that all cathodes be changed at the same t to avoid opening the ullage cover space, so as not to add to the burden of ullage gas carried for a mission. Dry nitrogen is planned for use as the ullage gas. During the time of changing cathodes, melt makeup can be accomplished by dumping pre-measured quantities of the electrolyte in pellet form or components thereof as necessary into each cell. The cathode cover uses a guide pin and the cathode terminal as a guide so that a quick and easy replacement of the cathodes can be accomplished by merely lifting the cathode cover (with its cathodes) out of the cell and replacing it with a previously prepared cover with fresh cathodes.

The servo valves used to throttle and change the air pressure in the half cell were designed to use the cell effluent gas flow as the means for achieving electrolyte oscillation. Each servo valve senses the pressure in the cell on one end of the bellows and is biased in the opposite direction by the servo valve control, which responds to the actual level of the electrolyte as selected by the main control. The individual servo valve concept is included to provide for individual level control so that the differences in electrolyte levels in any given half cell would not adversely affect the operation. Sizable variations in quantity of melt can be accommodated and still have the cell function properly by having the cell individually controlled according to the level within its own cathode well. The level sensors were described in paragraph 13.1 and were designed to function in the gaseous environment within the unit half cell.

13.2 (Continued)

The high temperatures and the corrosive atmosphere present difficulties in accomplishing an accurate and rapid sensing of the level itself. The small tubes, which always have a tendency to leak ullage gas, appeared to be a proper solution. The tubes are made of a compatible material and can stand the temperatures and the atmosphere without deterioration. The flow of gas out of the ends of the tubes, in addition to their being at the temperature of the cell, prevent clogging that would cause stoppage of their control function. The level sensors are repeated in each unit half cell. They are the elements that control the functioning of the servo valve to maintain the selected high or low level.

The current is distributed to the half cells in two banks. The total voltage drop across each bank is approximately 27 volts, presuming a drop of three volts per cell. The two cell banks are wired in parallel so that one bank is always passing current even though the other has the cathode out of the electrolyte. This cycling is beneficial to favorable carbon growth in the cathode well. The series parallel arrangement maintains the electrolysis current at a reasonable level of 50 amps and three volts per cell. Increased capacity of this unit can be rather easily acquired by adding additional unit half cells to the end of this complex. Various portions of the unit half cells are insulated from each other and from the main support housing to control the flow of electric current through the cathode - anode path or to prevent short circuiting by electrolyte to various cell housings.

Two temperature sensors are attached to each unit half cell. The sensor on the bottom of the cell prevents local overheating. When the heaters are turned on, heat flows from the bottom block, up the walls of the half cell, and from the top side of the heater block. When the salt pellets have poor contact, the bottom block heats up more rapidly than the heat can be transferred away by the pellets. In this case, the bottom temperature sensor acts as an overtemperature device by cutting off the current to the heater when the temperature exceeds approximately 1400°F. When the temperature drops considerably below 1400°F, the heater is re-energized - thus giving time for the passage of heat from the heater into the salt pellets. The second temperature sensor, on the side of the unit half cell, acts as a safety device to prevent final overheating after the half cell has been running at temperature. When the process power would add more heat to the electrolyte than is carried away through insulation (on through the air, or if there should be a low supply of electrolyte subject to abnormal heating) this upper sensor would detect the overtemperature and shut down the unit and sound an alarm.

The auxiliary cathode probe is a sensing device used to help control the quality of the melt. It is used in a circuit with the anodes to detect what corresponds to oxide ion content. The process decreases the current when the oxide ion rises, making a corrective action. Between this auxiliary cathode probe system and the carbon dioxide content detection system in the outgoing air, the quality of the melt can be maintained within certain desirable limits. The carbon dioxide content is corrected by changing

13.2 (Continued)

the frequency of electrolyte excursion. The greater the carbon dioxide content, the greater the frequency of excursion. For proper control and operation of the unit over large periods of time, both the oxide ion content and the CO_2 content of the outgoing air (which indicates the quality of the melt) should be kept within a narrow range.

The cells were constructed in the form of 18 unit half cells to 1) prevent short circuit of the anode/cathode currents by supplying the required insulation between each half cell and the adjacent cells and 2) to facilitate ease of service. Each unit half cell can be removed without affecting any of the other cells on the main support housing. To change a unit half cell, a section of outer cover of the total complex would be removed, removing blocks of insulation to expose the cell to be changed. With an extended handle wrench, the unit half cell support screws are removed permitting the cell to drop out of its position. The new cell may then be inserted and fastened in the same place with the screws so that the process may proceed when the melt is properly conditioned. In the event that it is necessary to permit the electrolyte to solidify, the cathode cover is so constructed that the cell may be disassembled without damage to the adjacent parts. The cathode clamping screws are loosened completely and the cover lifted off. Then the unit half cell may be removed from the bottom side of the main supporting housing. The initial charge of electrolyte is to be in pellet form requiring approximately 4.8 pounds of electrolyte per unit half cell. The initial charge of electrolyte can be placed in the unit half cell before assembly on the main support housing. Additions and replenishments of melt can be done through the cathode cover opening.

To protect people and equipment in the vicinity of the CO_2 removal system while it is operating, a leak detection system is incorporated. It is believed that such a safety device is worthwhile, especially in the state of knowledge about materials of construction and cell operation. A small amount of leakage dripping down to the ceramic containers immediately below each unit half cell would short the alarm wires and start an alarm system and shut down the unit so corrective action could be taken.

The total design indicated in the figures shown above is predicated on using tested systems and equipment where possible to avoid extensive development programs in construction of the early units.

The repetitive use of common shapes throughout the cell complex facilitates the basic objective of the one-sixth 'g' cell design by favoring moderate fabrication cost.

13.2 (Continued)

The configuration of the cathode and cover would allow some flexibility on the subsequent recovery of the cathode for re-insertion, or could further allow complete discarding of the used cathode.

The areas of electrode surfaces employed in the configuration result in a current density of 97 milliamperes per square centimeter and 22 milliamperes per square centimeter maximum for the cathode and anode surfaces, respectively.

One favorable consideration in increased anode life associated with the oscillating electrolyte configuration will be the positive effect of cyclically scrubbing oxygen gas formed at the anode surfaces to the extent of freeing these surfaces for active ion exchange at the electrode. This and the agitation of the electrolyte within each half cell should increase anode life.

13.3 Expected Performance

Pending the outcome of concurrently running tests and experiments concerning material controlled parameters, the goal of the present design is to provide support for 4 men on a 300 day mission. This is predicated on the removal of 9 lbs of carbon dioxide per day at a partial pressure of 3.8 mm Hg. abs. in a 14.7 psia oxygen/nitrogen mixture. The total expected air flow through the complex is 10.8 standard cubic feet of air per minute, assuming 100% scrubbing efficiency. Since the aforementioned flow is ideal it has been considered that compensation could be made for departure from the ideal efficiency by increasing the flow through the complex. A reasonable increase in flow is possible with this design. The anticipated operating pressure within the unit half cell is approximately 20 inches of water column above the ambient atmosphere. This pressure should be adequate to pump the air through the cell complex as well as cause the electrolyte excursions.

The theoretical length of time between cathode changes is approximately 10 days, based on the uniform buildup of carbon (1/4 inch) on each side of the cathode and extending over the entire active surface of each cathode.

The total amount of carbon discarded with each 300 day mission is approximately 732 lbs, which would normally occupy 5.25 cubic feet if totally pure. On the basis of 85% purity of carbon, approximately 150 lbs of melt would be inadvertantly removed (by inclusion within the carbon) during the mission. The salts required for replenishment would occupy approximately 1.3 cubic feet. To summarize, the total carbon and melt removed during a 300 day mission would weigh about 880 lbs and would occupy approximately 6.5 cubic feet. Regarding performance of the unit, at this point in time, a carbon purity of 80% and a cathode current efficiency upwards of 95% would be anticipated for the complex.

13.4 Possible Problem Areas Associated with the One-Sixth Gravity/Four Man Design

Introduction

The reference one-sixth gravity cell-complex design, as developed during this phase, has 'pushed' the state-of-the-art. Specific questions concerning the performance of this unit will require verification/development before initiating fabrication of the cell complex during the forthcoming phase of this contract. The purpose of this paragraph is to define the specific areas which should be investigated early in the follow-on phase of NAS 1-4154 prior to fabrication of the complex. This will give assurance that the cell hardware fabricated in the latter half of Part IIB will function satisfactorily.

Problems

(1) Materials: At the present time, no material has yet been defined which will endure for unlimited life in the corrosive cell ullage gas environment. Material specifications, where given on the detail drawings, largely represent the best materials known at present, but in certain cases are subject to reservations even in terms of limited life.

(2) CO_2 Scrubber Configuration: The areas and detailed configuration of the individual cell CO_2 scrubbing surfaces, as defined in the detailed drawings, have not yet been proven with respect to scrubbing efficiency or acceptable melt-carryover characteristic.

(3) Cathode Deposit Uniformity: As discussed in an earlier section a considerable question does exist with respect to the uniformity and consequent acceptability of the deposit upon the flat-plate cathode. The design constraints necessitate that a method be determined for achieving some degree of deposit thickness uniformity, to minimize cathode change frequency.

(4) Anode Life: Phase IIA experience has shown anode life to be limited. In testing to date, eight hundred hours has constituted the longest operating period achieved. Frequently, corrosion of 'lead-in' wiring within the cell ullage volume has resulted in anode failure significantly shorter than the aforementioned number. As reported elsewhere in this test, possible reasons contributing to this problem have been investigated and specific remedial action proposed. A considerable question regarding anode life will remain until configuration tests confirm the prolonged workability of the design.

(5) Electrolyte Volume: Ion transfer through the electrolyte of the proposed 1/6 g cell-halves will represent a significant increase of current density in the bulk electrolyte over levels used in laboratory test articles to date. The ionic

13.4 (Continued)

current density for the cell complex, as designed, involves an increase of approximately thirty-fold, with consequent uncertainties as to effects upon basic cell performance, e.g., inter-electrode mass transport.

Future Planning

To solve the aforementioned 'problems' (by attempting certain courses of action cited within various sections - particularly section 10.0 of this report) it is tentatively planned to run extensive tests during the first half of the follow-on contract part. These tests (and analyses where applicable) will tentatively be accomplished through the early construction of two half-cells (as designed) together with such modification of test equipment as may be required for effective testing.

APPENDIX A
DEFINITIONS

1. CO_2 Scrubbing Efficiency
2. Anode Current Efficiency
3. Cathode Current Efficiency

1. CO_2 SCRUBBING EFFICIENCY

Carbon dioxide scrubbing efficiency, where referred to in this report, is defined by:

$$\eta = \frac{pCO2_{in} - pCO2_{out}}{pCO2_{in}} \times 100$$

Where pCO_2 in = Partial pressure of carbon dioxide at inlet, mm. Hg.
pCO_2 out = Partial pressure of carbon dioxide at outlet, mm. Hg.
η = CO_2 scrubbing (removal) efficiency

2. ANODE CURRENT EFFICIENCY

Anode efficiency is the ratio of gaseous oxygen liberated at the anode compared to the theoretical oxygen released at that electrode as defined by Faraday's Law.

Oxygen theoretically generated is:

$$Q_{O_2} = \frac{60\,I}{F}\ \frac{\text{gm-equiv.}}{\text{min}} \times \frac{22,400}{4}\ \frac{\text{scc}}{\text{gm-equiv.}} = 3.48\,I\ \frac{\text{scc}}{\text{min}}$$

Where Q_{O_2} = Oxygen flow, scc/min, theoretical

I = Current, amperes

n = 2.0, valence of oxygen

F = 96,487 coulombs/gm-equivalent (Faraday's number)

Anode efficiency (η_a) can then be obtained -

$$\eta_a = \frac{\text{Actual measured oxygen flow scc/min}}{Q_{O_2}} \times 100$$

Note: When anode oxygen generated is not at standard temperature and pressure conditions, the numerator of the anode efficiency equation must accordingly be adjusted.

3. CATHODE CURRENT EFFICIENCY

Cathode current efficiency as used in part I of this report is the ratio of carbon recovered from the cathode,* compared with the theoretical carbon deposit as defined by Faraday's Law.

The theoretical weight of carbon deposited, as expressed by Faraday's Law states that during electrolysis 96,487 coulombs reduce or oxidize one gram-equivalent of a substance $\left(\text{i.e., } \frac{\text{gram atomic weight}}{\text{valence change}}\right)$.

Current efficiency can then be calculated:

$$\eta_C = \frac{\text{Weight of carbon deposit on cathode}}{W_C} \times 100$$

Where η_C = Cathode current efficiency (orientated to carbon deposition), %

I = Current, amperes

t = Total elapsed time, hours

M = 12.01, atomic weight of carbon

n = 4.0, valence of carbon

F = 96,487 coulombs/gram equivalent, Faraday's number

W_C = Theoretical carbon deposit, grams $\quad W_c = \frac{M}{n} \times \frac{3600\ It}{F} = 0.1121\ It$

* The significance of calculating current efficiency based upon only cathode adherent carbon, is felt to be an obvious one. Achievement, for example, of a 100% cathode current efficiency, in which 50% of the carbon had spalled-off the electrode into the electrolyte, would constitute an unmeaningful engineering criterion because such non-adherent carbon would not be recoverable with periodic cathode removal.

APPENDIX B
PROCEDURES

1. Carbon Purity Chemical Analysis
2. Melt Chemical Analysis
3. Measurement of Electrolyte Moisture-Level Concentration (Dew Point)
4. Measurement of Electrolyte CO_2 Partial Pressure
5. Current Density
6. Conditioning of Melt
7. Cell Performance Test Techniques Typically Employed in Engineering Tasks

1. CARBON PURITY CHEMICAL ANALYSIS

Method

Carbon is determined as acid insolubles using hydrochloric acid and distilled water.

Apparatus and Material

1. Hydrochloric acid, reagent grade
2. Sintered glass Gooch crucible - 25 ml capacity - (medium sinter porosity)
3. Water-cooled condenser.
4. Other common laboratory apparatus.

Procedure

1. Extract cathode with its carbon deposit from the cell and allow to cool. Wash off surface salts from the deposit using tap water, exercising care to remove surface salts (not those imbedded in carbon deposit).

2. Bake cathode with deposit at 250°F for 3 hours to dry sample.

3. Weigh cathode with deposit.

4. Remove as much as possible of the deposit from the cathode.

5. Weigh deposit sample obtained.

6. Transfer the deposit to a 200 ml flask and add approximately 4 parts of reagent grade HCl to 1 part of distilled water (50-75 ml. total mixture).

7. Boil the flask and contents for 2-3 hours, employing a condenser to return liquid to the flask.

8. Clean, dry, cool, and weigh the glass sintered crucible.

9. Empty entire contents of flask (the HCl solvent plus acid insoluble solids), into the sintered crucible and flush with distilled water until only the acid insolubles remain.

10. Place the sintered crucible in a 250°F oven and bake for 3 hours.

1. CARBON PURITY CHEMICAL ANALYSES (CONT.)

11. Weigh the crucible containing the remaining cathode deposits and subtract initial sintered crucible weight.

12. The difference in weight, representing the HCl insoluble solids, is presumed to be 100% carbon, if minor constituents contained in the deposit and not leached by the HCl + H_2O are neglected.

2. MELT CHEMICAL ANALYSIS

INTRODUCTION

During phase IIA of the NAS 1-4154 program, the composition of the fused-salt electrolyte was chemically analyzed periodically to establish that it had the proper balance of carbonate and chloride. The following procedures document the chemical analyses methods employed.

I. Analysis of Lithium Carbonate and Lithium Oxide

The purpose of this procedure is to describe the method used for the quantitative analysis of lithium carbonate and lithium oxide in the lithium salt mixture. The lithium carbonate and lithium oxide are determined by neutralization with standard hydrochloric acid using a pH meter.

Apparatus and Materials

A. pH meter (or indicator) - capable of covering the pH range from 0 to 14.
B. HCl, 1.0 normal, standardized with reagent grade sodium carbonate.
C. Common laboratory apparatus.

Procedure

Dissolve approximately 0.5-1.0 grams of dry gound sample of the eutectic in 400 ml of distilled water. Place the pH electrodes in the sample solution. Add standard 1.0 N HC in increments of 0.2-5 ml until ph increases. Add smaller increments of 1.0 N HCl (this will occur at a ph of approximately 9.5 and again at 5.0). Continue titration with standard HCl to a pH of 2. Plot pH against volume of 1.0 N HCl added.

The first inflection point is caused by the neutralization of the hydroxide and of the carbonate to bi-carbonate as shown by the reactions:

1. $LiOH + HCl \longrightarrow H_2O + LiCl$
2. $Li_2CO_3 + HCl \longrightarrow LiHCO_3 + LiCl$

The second inflection point is due to the neutralization of the bicarbonate as shown by the reaction:

3. $LiHCO_3 + HCl \longrightarrow H_2O + CO_2 + LiCl$

Calculations

$$\% W(Li_2CO_3) = \frac{2\,(B-A) \times N \times 0.03695 \times 100}{W}$$

Calculations (Continued)

$$\% W(LiOH) = \frac{A - (B-A) \times N \times 0.02395 \times 100}{W}$$

$$\% W(Li_2O) = \frac{A - (B-A) \times N \times 0.01494 \times 100}{W}$$

Where A = Volume of HCl required to neutralize the hydroxide and the carbonate to bi-carbonate, milliliters.

B = Volume of HCl required to neutralize the bi-carbonate to CO_2 and H_2O, milliliters.

N = Normality of HCl in gram equivalents per liter

W = Weight of sample in grams

II. Analysis of Lithium Chloride

The purpose of this procedure is to describe a method for the quantitative analysis of lithium chloride in the fused salt electrolyte. Lithium chloride is determined by the Volhard method, where the solution containing the chloride is titrated in excess with standard silver nitrate. The excess silver nitrate is then determined by titrating with standard potassium thiocyanate using ferric alum as the indicator.

Apparatus and Materials

1. Silver nitrate, 0.1 N

2. Sodium chloride - reagent grade

3. Potassium thiocyanate - dissolve 5.5 g. reagent grade potassium thiocyanate in 500 ml distilled water. Determine the ratio of $AgNO_3$ to KCNS by placing 50 ml silver nitrate solution in a 250 ml Erlenmeyer flask and adding 1 ml of ferric alum solution. Titrate with the KCNS solution until the pink color produced is permanent for 1-2 minutes.

4. Ferric alum indicator - acidify 25 ml of distilled H_2O with 1 ml conc. HNO_3 and to this solution add 2 g. $Fe(NH_4)(SO_4)_2 \cdot 12\ H_2O$.

Procedure

Dissolve a weighed sample of the melt (about 0.5 g) in a 250 ml Erlenmeyer flask with 50 ml distilled water. Acidify to litmus paper with conc. HNO_3 and

Procedure (Continued)

add 3 ml pure nitrobenzene. Titrate with silver nitrate, shaking the flask vigorously to coagulate the AgCl precipitate. Continue the titration until no silver chloride appears and add 2-3 ml silver nitrate in excess. Back titrate the excess silver nitrate with the standard KCNS solution with the ferric alum indicator according to the procedure in the standardization.

Calculations

$$\% \, W(LiCl) = \frac{(A - B \times R) \times N \times 0.0424 \times 100}{W}$$

Where A = total volume of silver nitrate, milliliters
B = volume of potassium thiocyanate, milliliters
R = ratio of silver nitrate to potassium thiocyanate
N = normality of silver nitrate, gm equivalents per liter
W = weight of sample, grams

3. MEASUREMENT OF ELECTROLYTE MOISTURE-LEVEL CONCENTRATION (DEW POINT)

It is customarily required to measure and control the partial pressure of the water vapor within the fused salt. Unless otherwise stated, whenever values of the 'melt' dew point (water vapor) have been tabulated for tests described within this report, the procedures to obtain the dew point values were as follows:

1. All influent flow to the electrolytic cell, except for that flow which subsequently came in intimate contact with the melt, was interrupted.

2. The effluent gaseous flow from the cell was thereafter assured to contain a moisture level in equilibrium with the moisture level within the melt.

3. Water vapor within the resultant effluent gaseous flow would then be monitored in a dew point measuring device (an Alnor or Cambridge).

4. MEASUREMENT OF ELECTROLYTE CO_2 PARTIAL PRESSURE

As with moisture concentrations, whenever it becomes necessary to define the partial pressure of CO_2 within the fused salt, the following procedure (similar to moisture determination) was employed, unless otherwise stated:

1. All influent flow etc. (as with water procedure).

2. The effluent gaseous flow from the cell was thereafter assumed to contain a CO_2 level in equilibrium with the CO_2 concentration within the melt.

3. CO_2 concentration (partial pressure) within the resultant effluent gaseous flow would then be monitored by means of a CO_2-sensitive infra-red gas analyzer.

5.0 CURRENT DENSITY

Current density is the current per unit of active electrode surface area.* This report consistently expresses current density in the units, milliamperes/cm^2.

*Once a test is initiated, the electrode surface area becomes indeterminate. Where current density values are given for specific tests in this report, the value is based upon the initial and determinable electrode area.

6. CONDITIONING OF MELT

To insure proper operating conditions of the fused salt electrolyte an acceptable water vapor and carbon dioxide equilibrium must be insured.

Water Vapor Equilibrium

For proper conditioning of the molten fused salt, it is necessary to maintain a -20°F to -40°F dew point in the electrolyte. To achieve this level, approximately 400 ml/min of CO_2 is bubbled through a 1/8-inch I.D. alumina tube for 16 hours. Thereafter, an inert gas such as Argon is bubbled through the scrubber at 400 ml/min for two hours. At this point a dew point reading is taken. If the dew point is too high, this process is repeated until an acceptable level is obtained.

Carbon Dioxide Equilibrium

To insure proper operating conditions, the fused salt carbon dioxide concentration should be of the order of 0.07 to 0.20 mm. Hg. Abs. To achieve this, add 4 grams of dry Li_2O to the electrolyte. If the CO_2 count is still high, more Li_2O may be added; however, close monitoring of the composition is advisable. If excessive Li_2O is added, it may become necessary to add LiCl to the fused salt to maintain the proper Li_2CO_3/LiCl ratio.

NOTE: Also see paragraph 10.1.5.1 (Carbon deposit purity), discussed under General Results and Interpretation of Engineering Test Program.

7. CELL PERFORMANCE TEST TECHNIQUES TYPICALLY EMPLOYED IN ENGINEERING TESTS

NOTE: The following test procedure assumes that the electrolyte has been properly 'conditioned' per procedure number 6.

Step	Action
1.	Select desired cathode current density.
2.	Calculate 'active' (A) area of cathode selected for test.
3.	Calculate cell electrolytic current to be employed in test (in consideration of number 1 and number 2 above).
4.	Define approximate value of influent stream CO_2 partial pressure to be employed.
5.	Establish total scrubber volumetric influent flow rate from figure C-1.
6.	Initiate electrolysis by applying cell current in the amount calculated in step number 3 above.
7.	Initiate carrier-gas flow through the cell 'scrubber' in the amount established in step number 5 above.
8.	Increase CO_2 partial pressure in the amount established in step number 4 above.
9.	Adjust CO_2 partial pressure in the influent flow as necessary to maintain CO_2 outlet pressure at a desirable level. Note: Necessary because of non-ideal cell CO_2 'scrubbing' efficiencies.

(A) When employing oscillating electrolyte configuration, with associated cyclic variation in current flowing through each cathode (zero to maximum with each excursion of electrolyte) it is the general practice to assume one cathode fully immersed and the other cathode not immersed in the selection of the cathode area.

APPENDIX C
CONFIGURATION OF TEST HARDWARE

C-1. Electrolytic Current As a Function of Influent Flow Rate
C-2. Cell Configuration (Tests 19-27)
C-3. Oscillating Electrolyte Double Cathode Control Subsystem (W/O Ullage Pressure Compensation)
C-4. Cathode Configurations 1-5
C-5. Cathode Configurations 6-8
C-6. Cathode Configurations 9-12
C-7. Cathode Configurations 13-14
C-8. Anode No. 1 Crossectional View
C-9. Anode No. 2
C-10. Anode No. 3
C-11. Anode No. 4 Centrifugal Anode
C-12. Anode No. 5
C-13. Anode No. 6
C-14. Anode No. 7
C-15. Anode No. 8
C-16. Scrubber Configuration 1-3

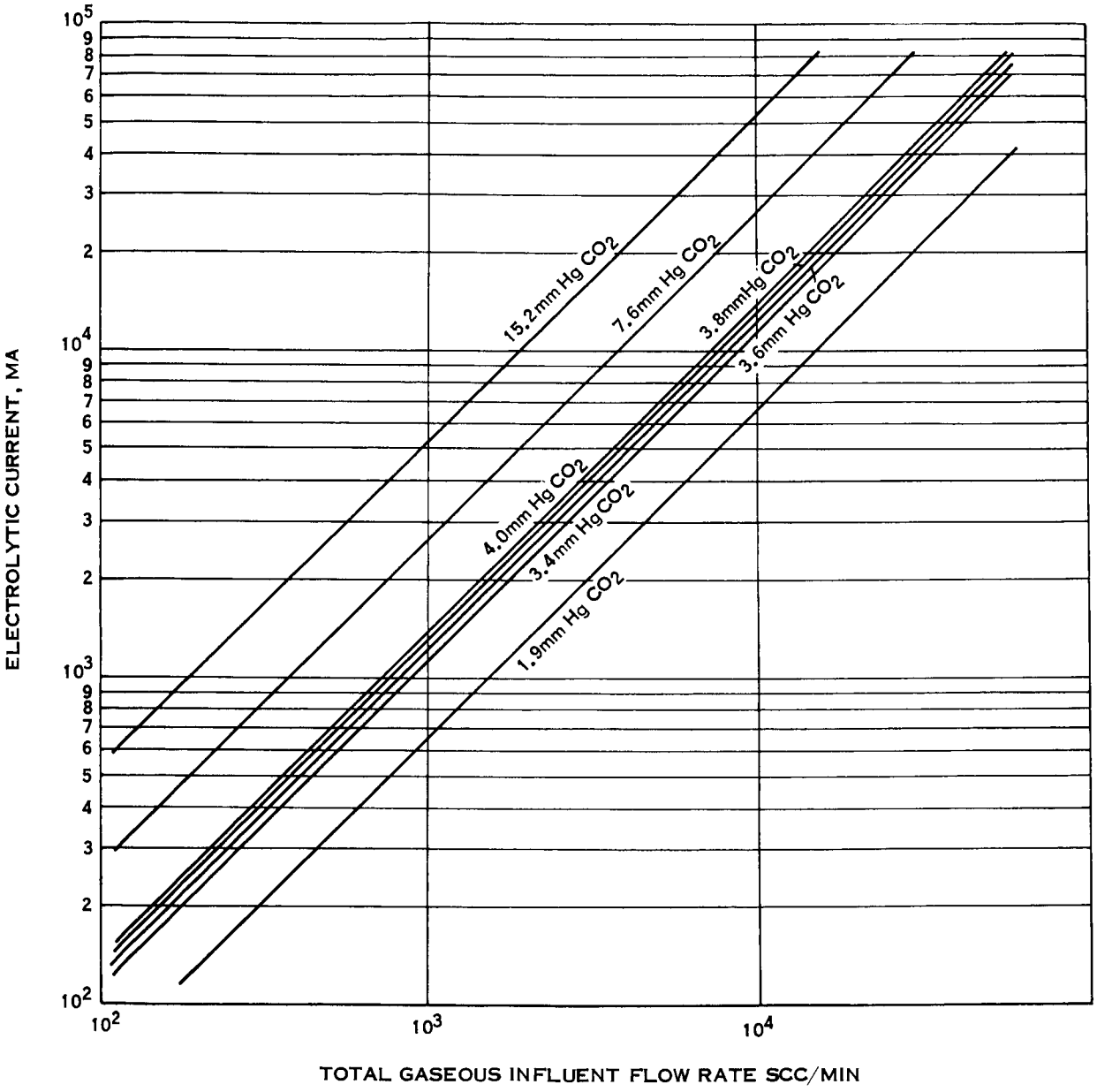


FIGURE C–1. ELECTROLYTIC CURRENT AS A FUNCTION OF INFLUENT FLOW RATE

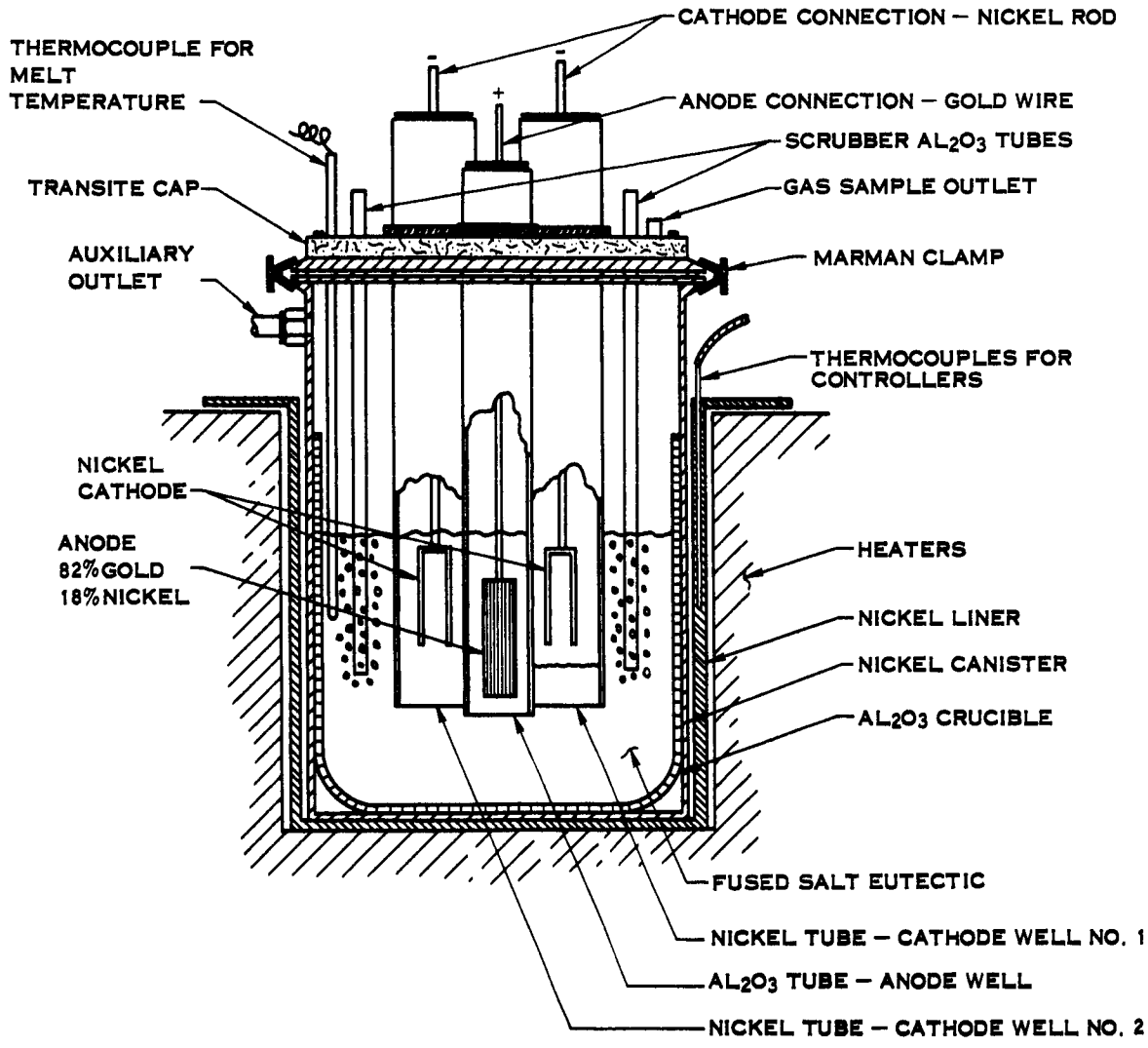


FIGURE C–2. CELL CONFIGURATION (TESTS 19 – 27)

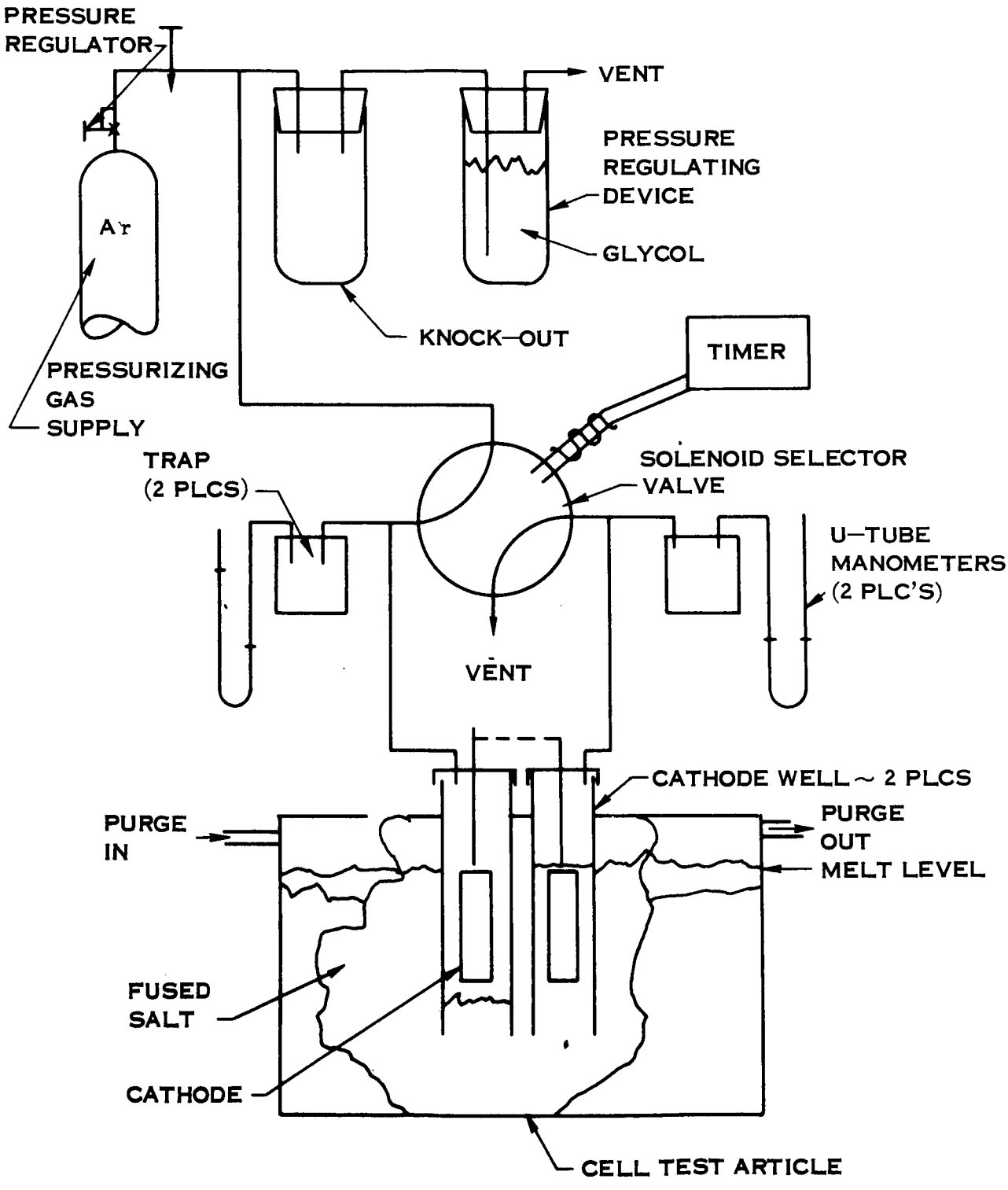
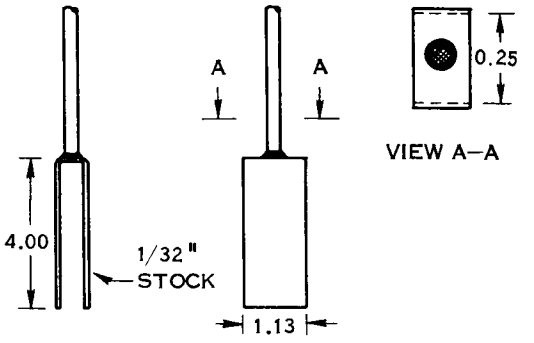


FIGURE C—3. OSCILLATING ELECTROLYTE DOUBLE CATHODE CONTROL SUB—SYSTEM (W/O ULLAGE PRESSURE COMPENSATION)

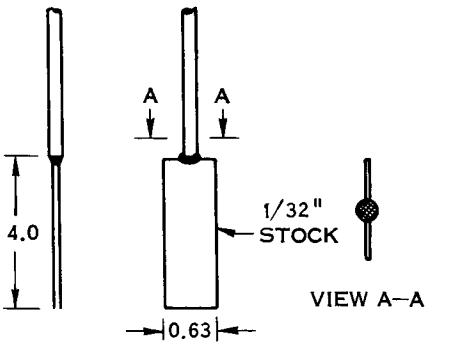
NUMBER 1 & 2



TOTAL SURFACE AREA = 129.0CM^2

MATERIAL: NICKEL 201 – 0.030 THICK

NUMBER 3



TOTAL SURFACE AREA = 32.3 CM^2

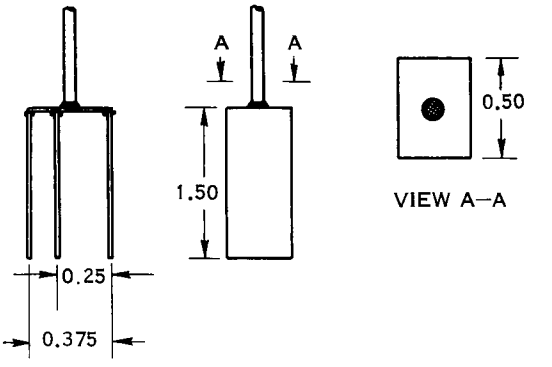
MATERIAL: NICKEL 201 – 0.030 THICK

NUMBER 4 – A, B, C, D

SAME SHAPE AS NO. 3, EXCEPT :

A. TOTAL SURFACE AREA = 25.8 CM^2
B. TOTAL SURFACE AREA = 32.2 CM^2
C. TOTAL SURFACE AREA = 13.15 CM^2
D. TOTAL SURFACE AREA = 16.10 CM^2

NUMBER 5

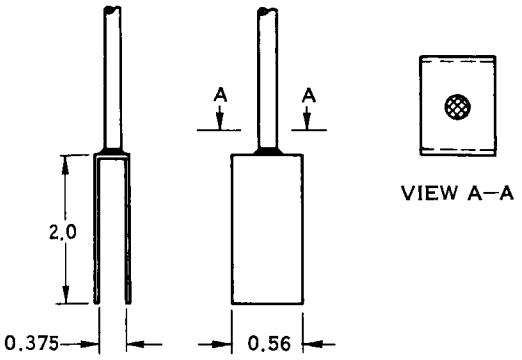


TOTAL SURFACE AREA = 31.6 CM^2

MATERIAL: NICKEL 201 – 0.030 THICK

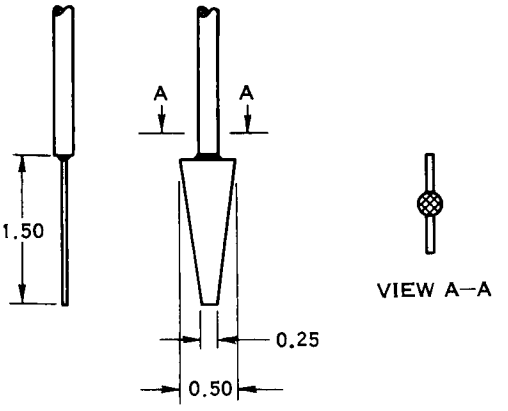
FIGURE C–4. CATHODE CONFIGURATIONS 1 – 5

NUMBER 6



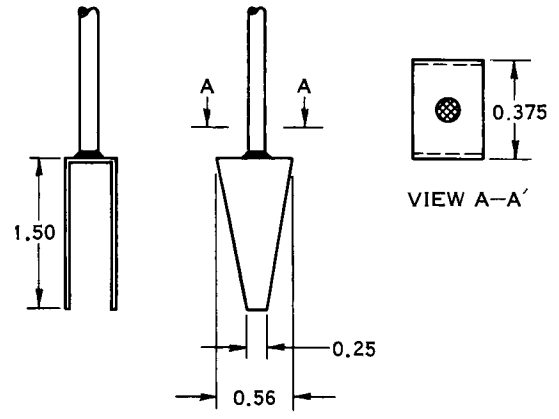
TOTAL SURFACE AREA = 91.9 CM^2
MATERIAL : NICKEL 201 – 0.030 THICK

NUMBER 7



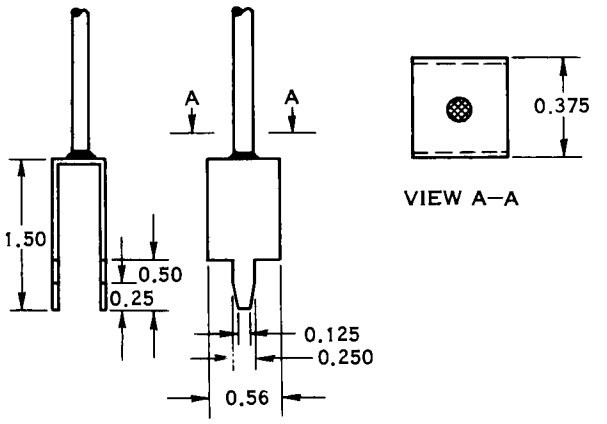
TOTAL SURFACE AREA = 7.25 CM^2
MATERIAL : NICKEL 201 – 0.030 THICK

NUMBER 8–A



TOTAL SURFACE AREA = 18.40 CM^2
MATERIAL : NICKEL 201 – 0.030 THICK

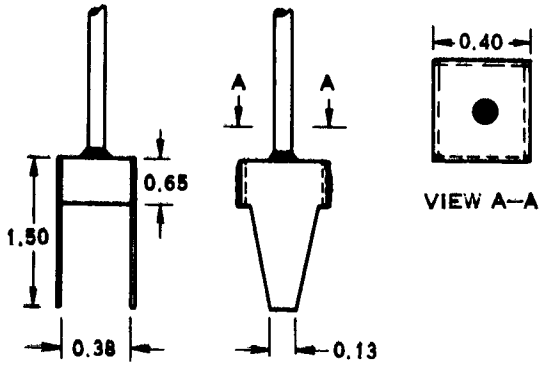
NUMBER 8–B



TOTAL SURFACE AREA = 20.45 CM^2
MATERIAL:NICKEL 201 – 0.30 THICK

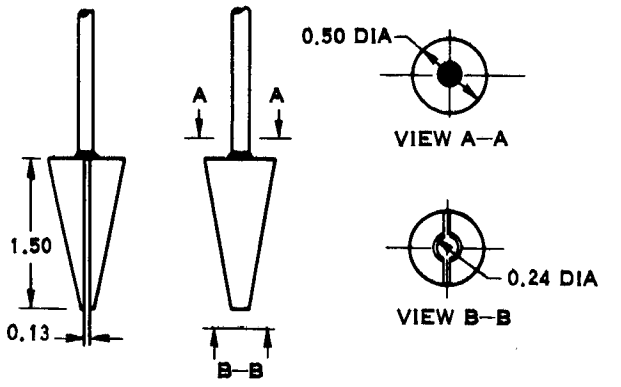
FIGURE C–5. CATHODE CONFIGURATIONS 6 – 8

NUMBER 9



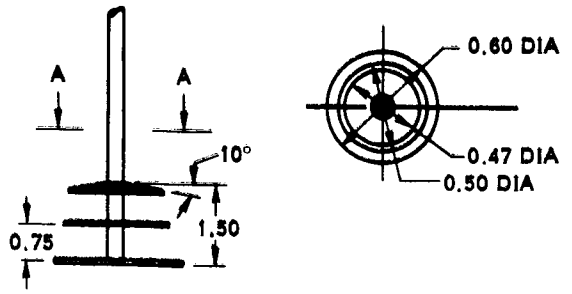
TOTAL SURFACE AREA = 18.4 CM^2
MATERIAL: NICKEL 201 – 0.030 THICK

NUMBER 10



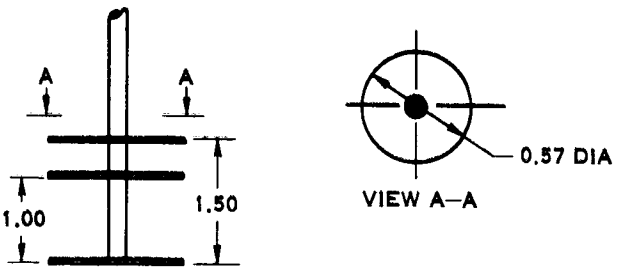
TOTAL SURFACE AREA = 20.50 CM^2
MATERIAL: NICKEL 201 – 0.030 THICK

NUMBER 11



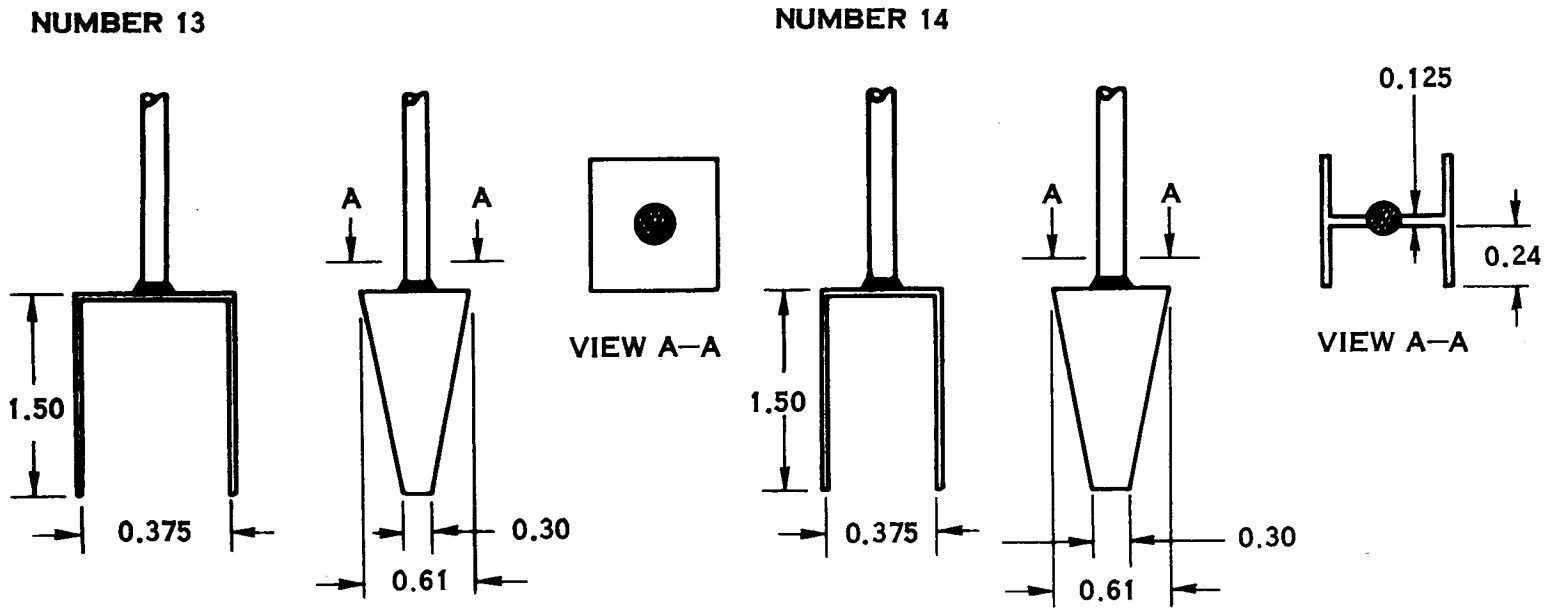
TOTAL SURFACE AREA = 14.28 CM^2
MATERIAL: NICKEL 201 – 0.030 THICK

NUMBER 12



TOTAL SURFACE AREA = 14.28 CM^2
MATERIAL: NICKEL 201 – 0.030 THICK

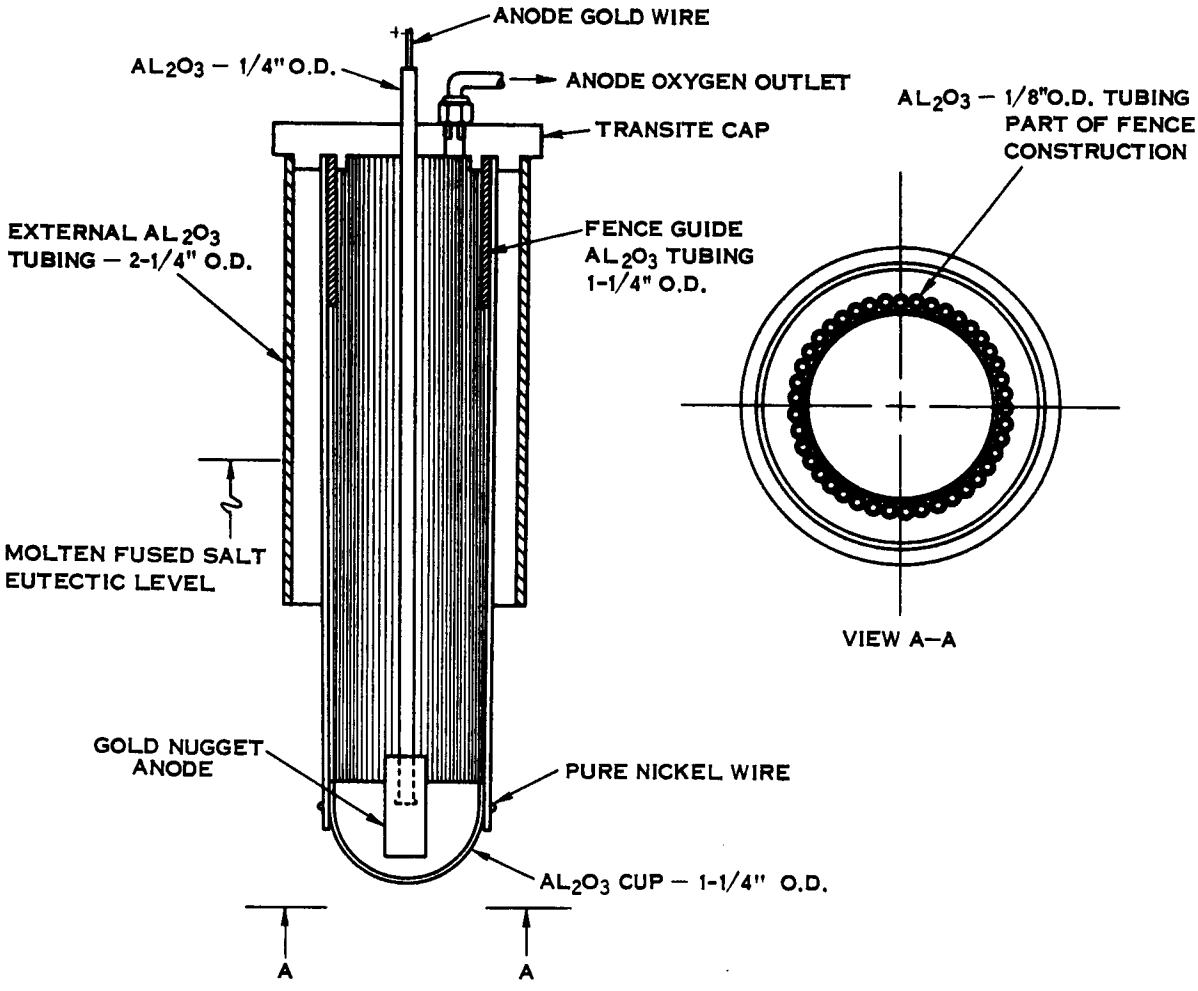
FIGURE C–6. CATHODE CONFIGURATIONS 9 – 12



TOTAL SURFACE AREA = 20.56 CM^2
MATERIAL: NICKEL 201 – 0.030"THICK

TOTAL SURFACE AREA = 19.20 CM^2
MATERIAL: NICKEL 201 – 0.030"THICK

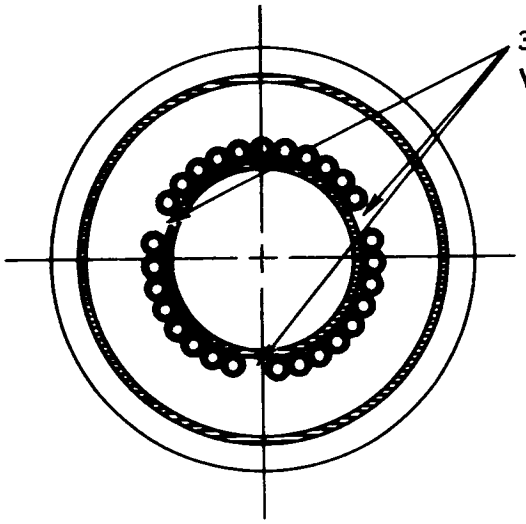
FIGURE C-7 CATHODE CONFIGURATIONS 13 – 14



INITIAL EXPOSED GOLD SURFACE AREA = 6.66 CM^2

FIGURE C–8. ANODE NO. 1 CROSSECTIONAL VIEW

IDENTICAL IN ALL RESPECTS TO ANODE NO. 1 EXCEPT FOR THE FOLLOWING ALTERATION:



BOTTOM VIEW OF ANODE

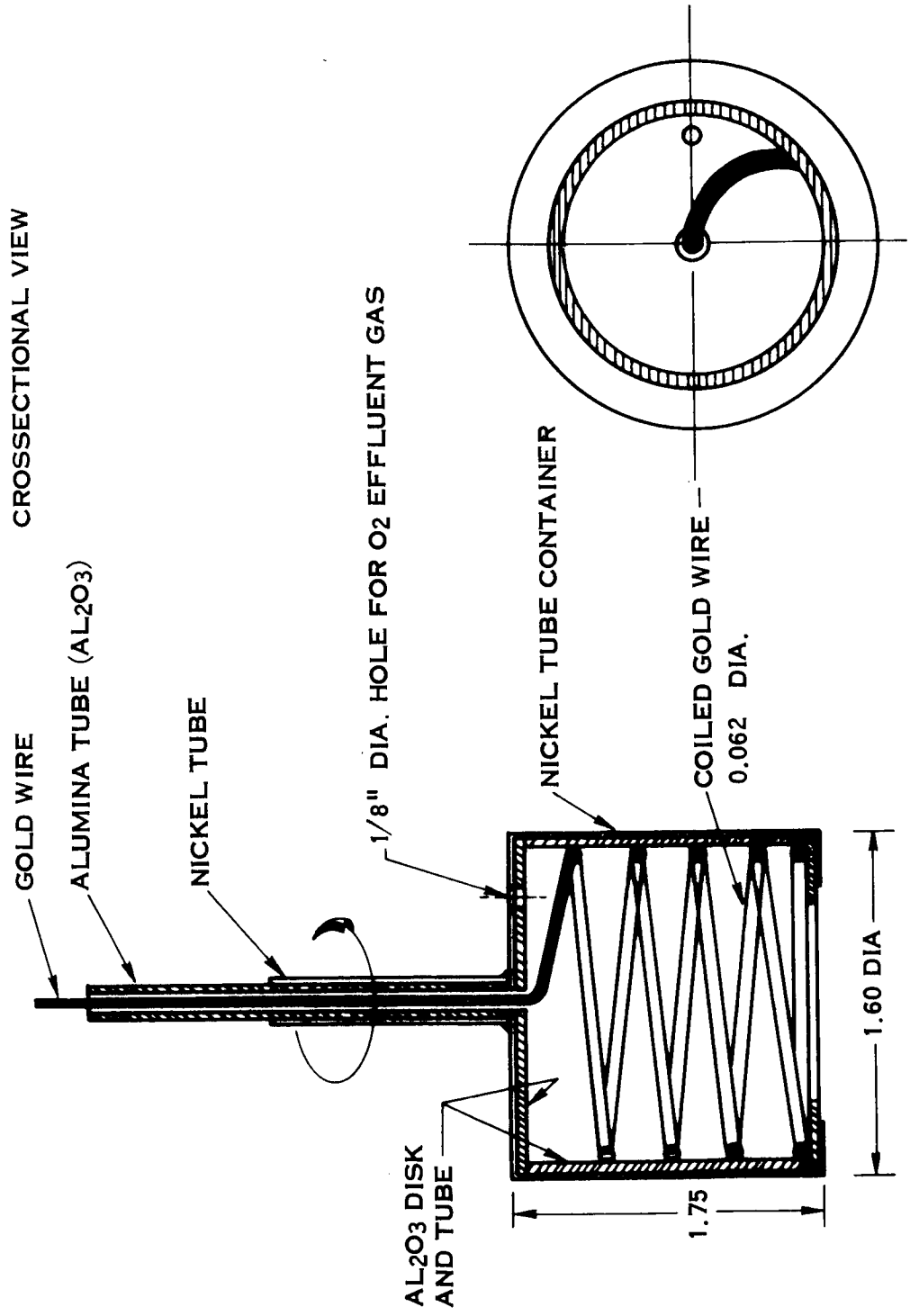
FIGURE C—9. ANODE NO. 2

IDENTICAL IN ALL RESPECTS TO ANODE NO. 1 EXCEPT FOR THE FOLLOWING ALTERATION:

FENCE CONSTRUCTION CONSISTS OF ALTERNATING 1/8" O.D. TUBES WITH SPACES BETWEEN EQUIVALENT TO TWO 1/8" O.D. TUBES

BOTTOM VIEW OF ANODE

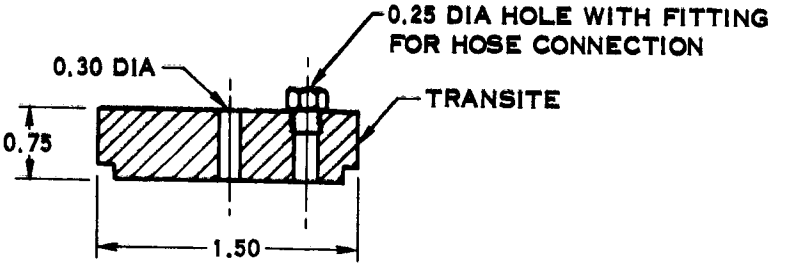
FIGURE C-10. ANODE NO. 3

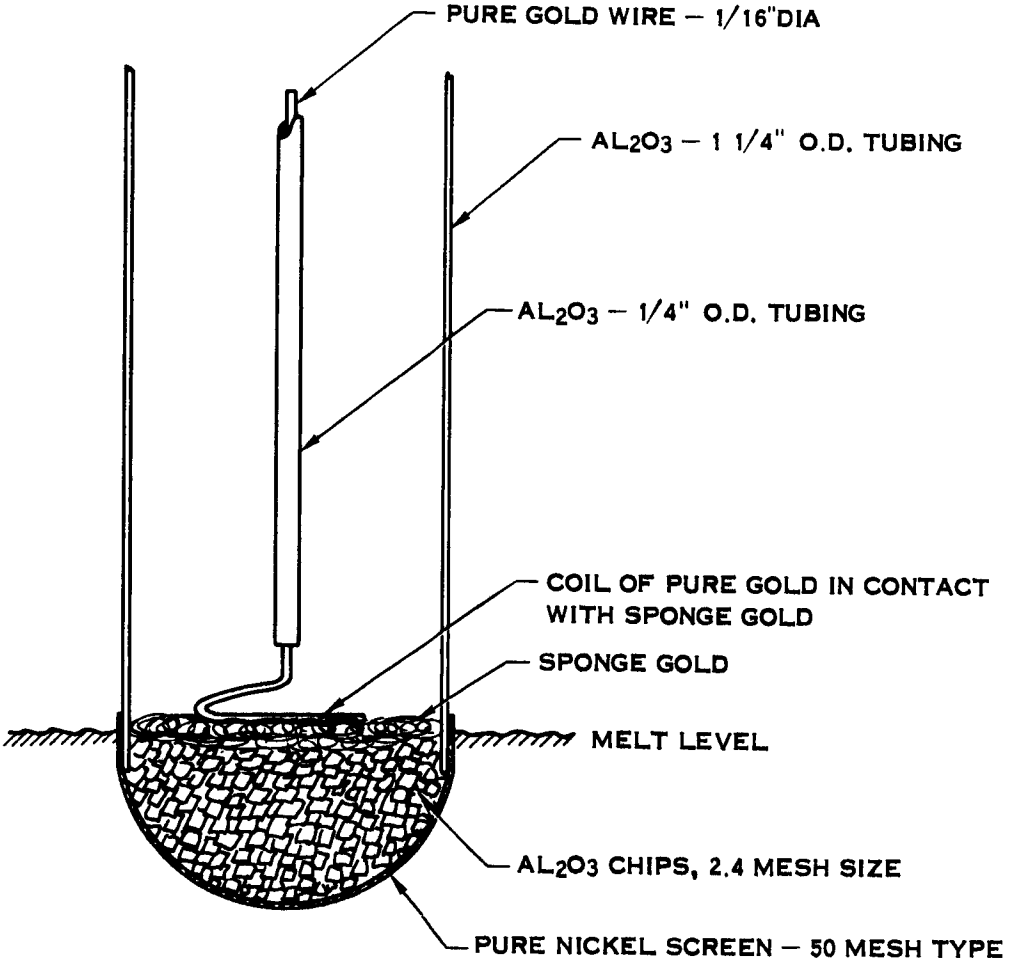


TOTAL EXPOSED ANODE SURFACE AREA: 32.9 CM^2

FIGURE C-11. ANODE NO. 4 CENTRIFUGAL ANODE

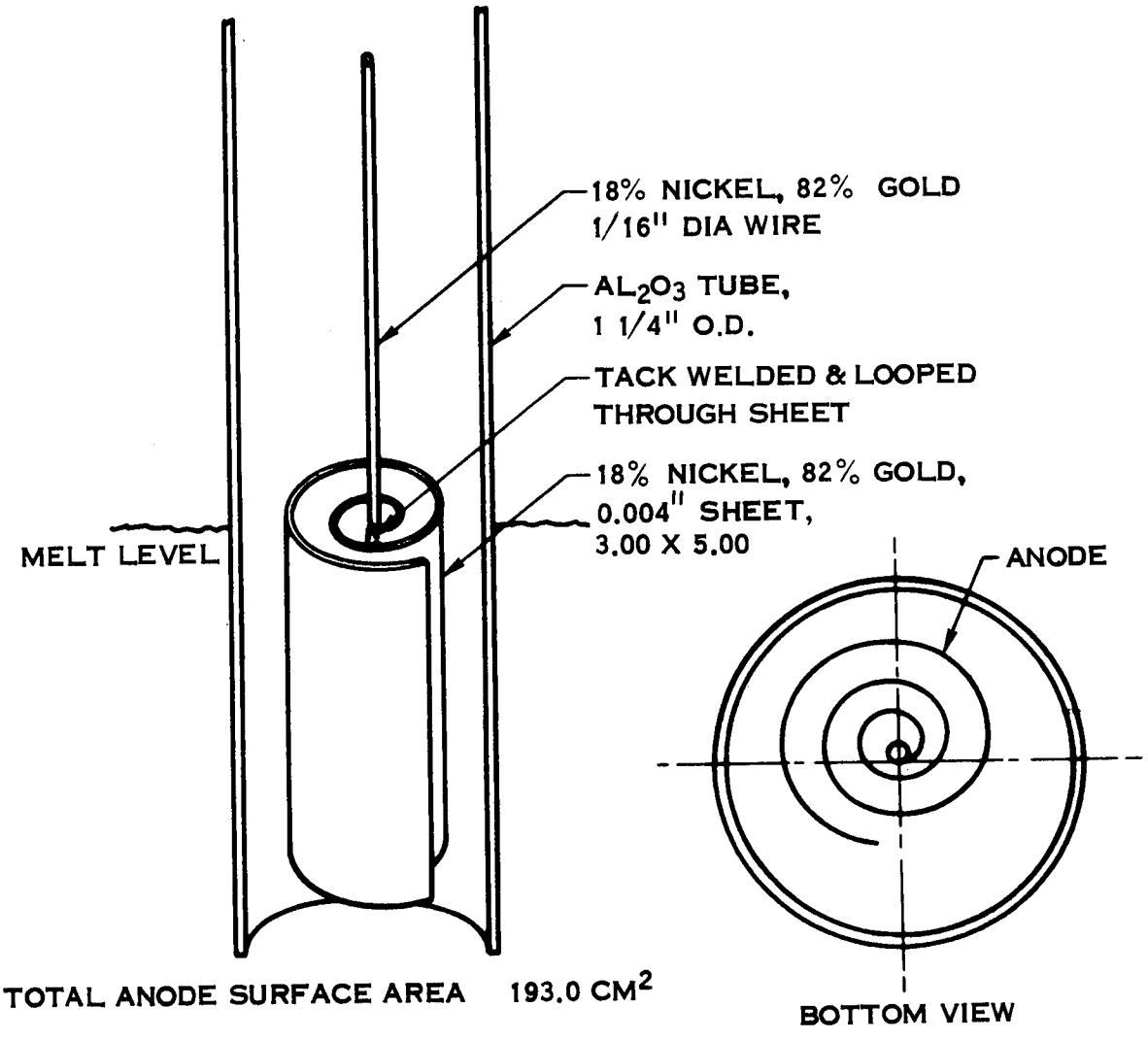
ANODE ASSEMBLY CAP:





TOTAL ANODE SURFACE AREA: UNDETERMINED

FIGURE C–12. ANODE NO. 5

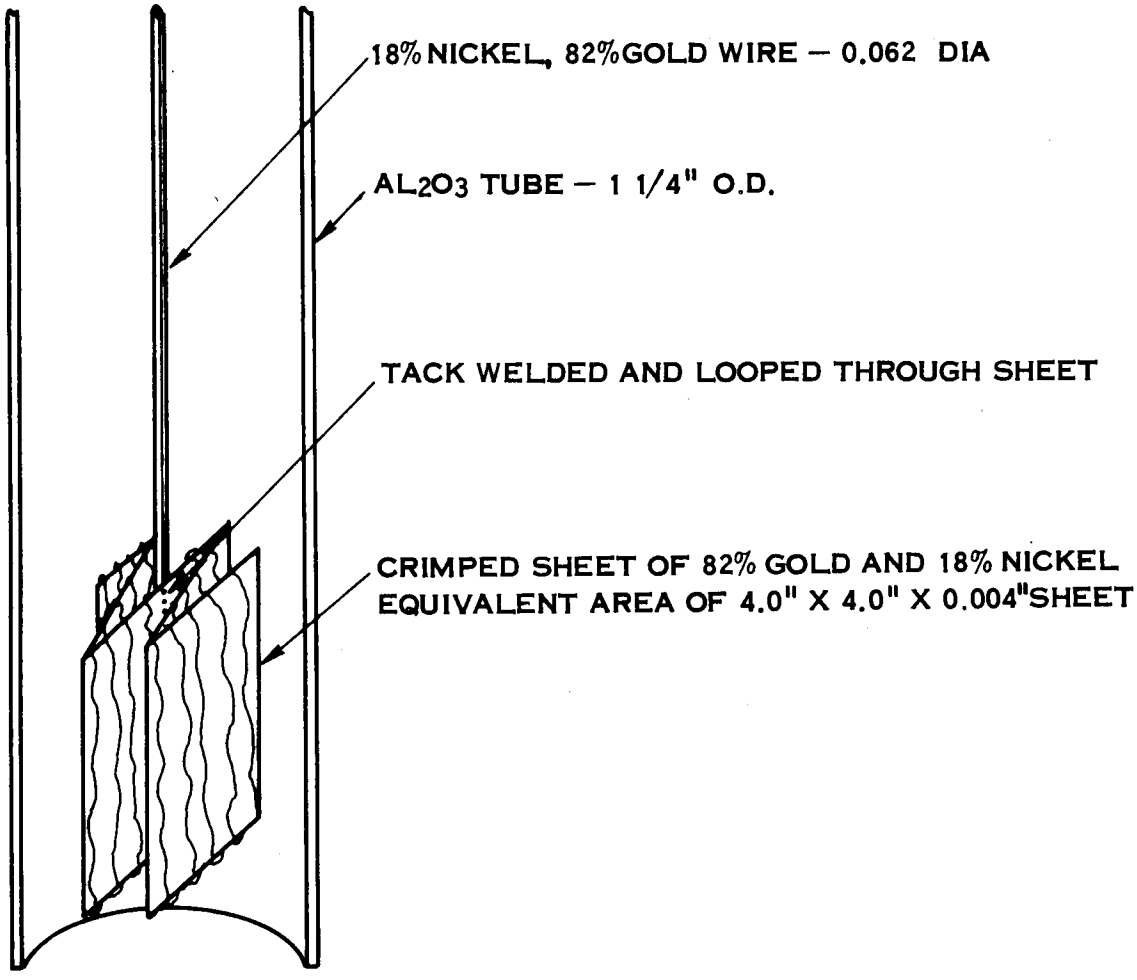


ANODE ASSEMBLY CAP SAME AS THAT OF ANODE NO. 5

FIGURE C–13. ANODE NO. 6

IDENTICAL IN ALL RESPECTS TO ANODE NO. 6 EXCEPT THAT ANODE SHEET (82%AU, 18%Ni) IS 4.0" X 4.0" AND ITS TOTAL SURFACE THEREFORE IS 206.4 CM^2

FIGURE C—14. ANODE NO. 7



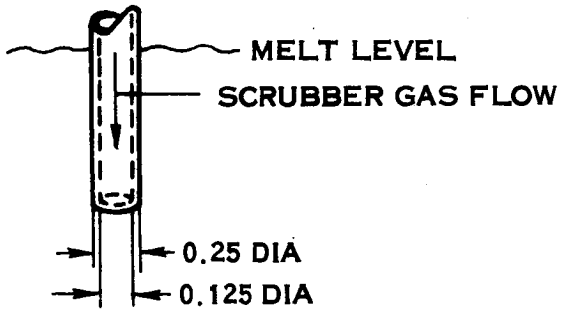
TOTAL ANODE SURFACE AREA: 206.4 CM^2

ANODE CAP SAME AS THAT OF ANODE NO. 5

FIGURE C–15. ANODE NO. 8

SCRUBBER NO. 1

ONE ALUMINA STANDPIPE IMMERSED INTO THE EUTECTIC



SCRUBBER NO. 2

TWO ALUMINA STANDPIPES IMMERSED INTO THE EUTECTIC
DIMENSIONS SAME AS SCRUBBER NO. 1

SCRUBBER NO. 3

TWO ALUMINA STANDPIPES IMMERSED INTO THE EUTECTIC

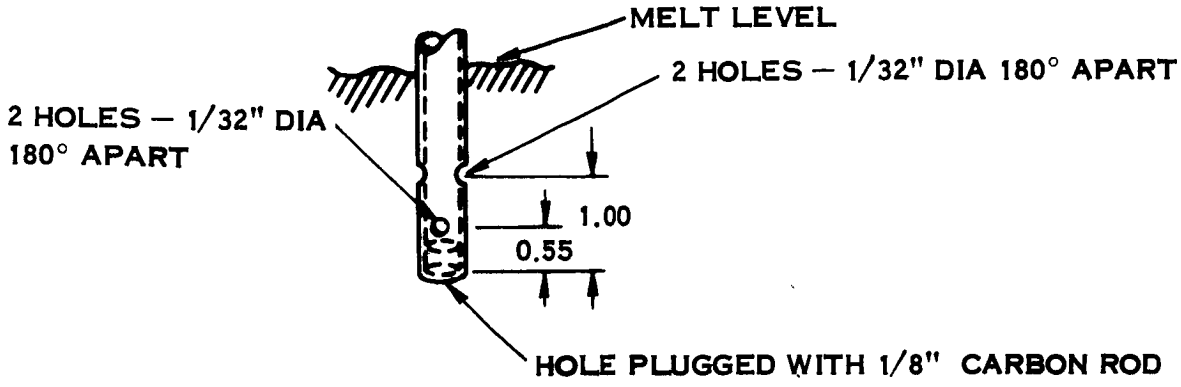


FIGURE C–16. SCRUBBER CONFIGURATION 1 — 3